Castle, Ryan M. (2012) *A radio and infrared investigation of Seyfert galaxies in the local universe.* Masters (Research) Thesis, James Cook University.

https://doi.org/10.25903/jrbr%2D0b36

A Radio and Infrared Investigation of Seyfert Galaxies in the Local Universe

Thesis submitted by

Ryan M. Castle, M.Sc.

in August 2012

for the degree of M.Sc.

from the Centre for Astronomy

in the School of Engineering and Physical Sciences

James Cook University

THE CONTRIBUTION OF OTHERS

David Blank, my one-time supervisor, suggested the initial research project of constructing a southern-sky sample of Seyferts and investigating their large-scale radio properties using the data from the SUMSS.

Zhixin Peng, Department of Astronomy at Nanjing University, Nanjing, China, contributed to this work by providing a copy of an auxiliary computer file used (and described) in Chapter 3.

ACKNOWLEDGEMENTS

I would like to thank my dear wife Karen for putting up with my diverted attention during my studies at JCU.

ABSTRACT

Presented here are the results of an investigation of a newly constructed sample of local ($z < 0.0303$), southern-sky Seyfert galaxies. Data from the 843 MHz Sydney University Molonglo Sky Survey (SUMSS) was used, as well as near and mid/far-infrared data from the *IRAS* and 2MASS surveys, respectively.

The first goal of this research was to construct a complete sample of southern-sky Seyferts for use in an ongoing study of this type of AGN in the local universe. The next and main research goal in this study was to search for any previously unidentified large-scale radio emission from the Seyferts - taking advantage of the good sensitivity and (u, v) plane coverage of the Molonglo Observatory Synthesis Telescope (MOST) used in the SUMSS. This was a search for extended radio emission that could perhaps identify past epochs of activity from the nucleus. In addition, this research enables another test the unified scheme for this type of AGN by carrying out several conventional two-sample statistical tests. Radio contour maps of all sample objects are presented as well as the distances, galactocentric recession velocities, and the 843 MHz, NIR (1.25, 1.65, 2.17 μm), and MID/FIR (12, 25, 60, 100 μm) luminosities. The IR data for this sample were also used to compute several spectral indices and the spectral energy distributions (SEDs) for the sample objects, as well as to investigate the global radio-FIR correlation known to exist among all galaxies.

The most significant of the new results reported here include the identification of six radio-excess Seyferts, heretofore not identified as such in the literature, as well as a newly identified "radio-loud" type-2 Seyfert. Evidence for significant radio variability over a span of twenty years was also found for five of the sample objects by comparing data from the SUMSS to that from an earlier, smaller study using the MOST. In addition, the 2MASS K_s - band images of several of the closest type-2 Seyfert were decomposed into disk, bulge, and nuclear components in a study of the NIR properties of this type of active galaxy, increasing by nearly 50% the number of local Seyferts for which this type of analysis has been published.

TABLE OF CONTENTS

LIST OF TABLES

LIST OF FIGURES

1. INTRODUCTION: A REVIEW OF THE LITERATURE

1.1. THE NATURE OF SEYFERT GALAXIES

Carl Keenan Seyfert was not the first researcher (e.g., Fath 1908; Slipher 1917) to notice broadened emission lines originating from the nucleus of some spiral nebulae. He was however the first to systematically investigate a sample of such objects (Seyfert 1943) with the knowledge that they constitute a special type of galaxy. Since then, what we now call Seyfert galaxies have become some of the most extensively studied type of extragalactic object.

Seyferts galaxies are usually some type of spiral galaxy, though elliptical, irregular, interacting pairs, etc, are also found, and contain an Active Galactic Nucleus (AGN). Hence, what Seyfert galaxies have in common with radio galaxies and quasars - which is also what sets them apart from "normal" galaxies - is the fact that their nuclei are very luminous, contain a large amount of gas, and have unique spectral properties (Pogge & Martini 2002). Taniguchi (1999) reported that only about 10% of Seyferts have companion galaxies while another study (Schmitt et al. 2001a) suggests that the number is between ~ 19 to 28%. The nuclei are so luminous that they can appear almost indistinguishable from stars, something first pointed out by Humason (1932) in a study of NGC 1275. Another example would be NGC 7213 (a type 1.5 Seyfert), seen in Figure 1.1 below at 843 MHz.

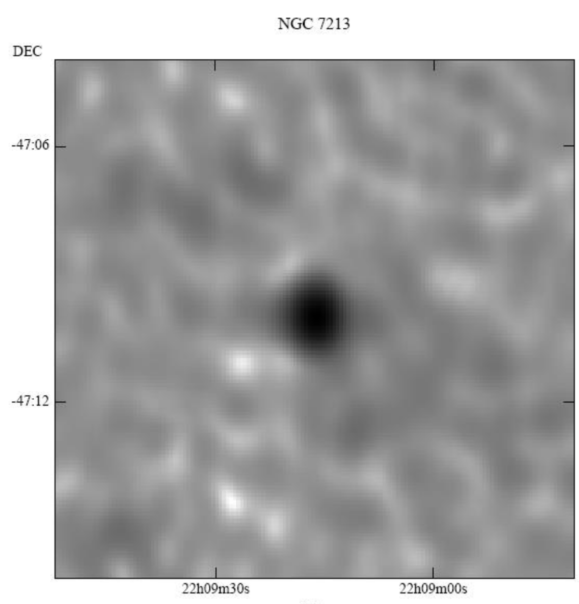

FIG 1.1.- An 843 MHz image of the (type 1.5) Seyfert galaxy NGC 7213. The peak & total flux densities measured were 98.0 $\pm$ 3.1 mJy/beam & 119.6 $\pm$ 3.4 mJy, respectively (SUMSS Catalogue Ver. 2.1, 2008).

Today we call such galaxies Active Galaxies, and say that they contain an Active Galactic Nuclei (AGN). The energy source of an AGN is almost universally thought to be the accretion disk formed by the infall of gas and dust into a super-massive black hole (SMBH). Until fairly recently it was thought that such objects typically had masses on the order of 10^6 to 10^9 M_{SOL} (Ho 1999; Wu & Han 2001). Greene & Ho (2004) have though recently identified a previously unknown population of (type 1) Seyfert galaxies that contain BHs with masses in the range $M_{BH} \approx 8 \times (10^4 - 10^6)$ M_{SOL}, providing more evidence that our understanding of the evolution of galaxies is far from complete.

There is a (log-linear) correlation between the black hole mass and the stellar velocity dispersion of the central bulges of AGNs, the so-called $M_{BH} - \sigma_*$ relation (Kormendy & Richstone 1995; Magorrian et al. 1998; Nishiura & Taniguchi 1998; Ferrarese & Merritt 2000). It is thought that perhaps the relation "is established during the active galactic nucleus (AGN) phase of a galaxy's life-cycle, since energy emitted by the BH may simultaneously limit the gas supply for building both the bulge and the BH itself" (Greene & Ho 2006). In Ferrarese & Merritt a tight correlation was observed, giving the relation $M_{BH} \propto \sigma^{\alpha}$, for $\alpha = 4.8 \pm 0.5$. The line of best fit for the data was computed to be $\log M_{BH} = 4.80(\pm 0.54)\log \sigma_c - 2.9(\pm 1.3)$ with M_{BH} in units of solar mass (M_{SOL}), and σ_c in units of km s^{-1}. The sample consisted of 12 galaxies for which reliable BH masses were available. They were a mix of normal galaxies (including the Milky Way) and those with AGN.

Nelson et al. (2004), a study of the $M_{BH} - \sigma_*$ relation for (16 type 1) Seyfert galaxies, reported a similar result; in the relation given above a slope of 4.1 ± 0.5 was obtained. Both of those studies have been of the local universe. Robertson et al. (2006), an investigation of how this relation might evolve over time, suggest that out to higher redshifts, "the slope is consistent with being constant near the locally observed value of $\beta \sim 4$."

Wu & Han (2001) is one study among others (e.g., Laor 2001) that suggests a relation between M_{BH} and the mass of the bulge of the galaxy, M_b. In a sample of 82 galaxies (37 Seyferts, 15 quasars, and 30 normal galaxies) the relation observed was $M_{BH} \propto M_b^{1.74 \pm 0.14}$. Such a relation is not unexpected considering the well-known $M_{BH} - \sigma_*$ relation mentioned above as well as the longer known relationship between the bulge luminosity and σ_* (Faber & Jackson 1976).

Seyfert galaxies in general are, in most aspects, similar to quasars and have traditionally been thought to be lower-luminosity versions of them; the high luminosity (type 1) Seyferts and low-luminosity quasars being essentially the same, usually an optical magnitude cut-off used in the classification (Schmidt & Green 1983). However, more recent work (Floyd et al. 2004) shows more significant differences, even if the underlying SMBH paradigm is the same. The results of that study, of 17 quasars with z ~ 0.4 using imaging from the Hubble Space Telescope (HST), show that all radio-loud quasars in the sample, and all the radio-quiet quasars (RQQSOs) with $M_v < -24$ reside in giant elliptical host galaxies. In contrast, Seyferts in the local universe usually reside in a spiral host (only ~ 5% of the new sample presented in this thesis, as discussed in §2.1, reside in E type host galaxies).

Pacholczyk & Weymann (1968) is an important early paper describing what was then known (and postulated) about Seyferts and their relation to quasars. The paper is the published proceedings of a major conference on Seyferts and related objects that was held at Steward Observatory in 1968. Weedman (1977) is a comprehensive review of what was known about Seyferts about decade later.

The traditional definition of a radio-loud AGN is a “large” radio to optical ratio, usually defined as the logarithm of the ratio of radio and optical fluxes; R = $\log_{10}(S_{6cm}/S_{Bband})>1.3-1.8$ (Sramek & Weedman 1980; Visnovsky et al. 1992; Roy & Norris 1997). The percentage of Seyferts that are radio loud have been estimated to be < 10% (Rush et al. 1996), which is about half of the value for quasars. Radio-loud AGN are very rare in late-type spirals (Brunthaler et al. 2005). In general, radio-loud AGN tend to reside in elliptical galaxies, radio-quiet AGN in spirals (Véron-Cetty & Woltier 1990; Roy & Norris 1997). The work of Ho & Peng (2001) casts doubt on this conventional view however, at least for Sy1, if the relevant luminosities are properly measured for just the nuclear components. This is important because there is a "tremendous range of brightness contrast between the nucleus and bulge" at optical wavelengths. Similarly, significant radio emission is known to come from synchrotron emission of the disk of the host galaxy. In fact, normal early-type spirals generally have 20 cm (log) luminosities in the range 20 - 22 (W/Hz), comparable to that observed globally. Ho & Peng (2001) reported that more than 60% of the 45 nearby Sy1 in their sample have values R > 10. They also conclude that the "physical origin underlying the radio-optical correlations may be a close link between the disk accretion rate and the generation of relativistic radio jets."

In the late 1990s a new intermediate radio-type (between radio-quiet and radio-loud) of AGN was identified (Roy & Norris 1997). Five of the twelve example objects were Seyferts (four "type-2" and 1 "type-1", the distinction between type is discussed below). All twelve objects had typical 6.3 cm radio luminosities between $10^{22.1}$ and $10^{25.4}$ W Hz^{-1}, almost two orders of magnitude more than the radio luminosity of the average Seyfert. The term “radio-excess” is often used to describe this type of AGN. Three of the radio-excess Sy identified in Roy & Norris (1997) are in the sample investigated in the later chapters of this thesis and are discussed there (particularly in §3.7 and

Chapter 4). Several new radio-loud candidates in this new sample constructed for the research reported in this thesis are identified in §3.7.

1.2. SEYFERT TYPES

In the small initial study by Seyfert it was noted that "profiles of the emission lines show that all the lines are broadened, presumably by Doppler motion, by amounts up to 8500 km/s". The distinction between the two main types of Seyfert galaxies (type-1 and type- 2; from here on in this thesis the notation Sy1 and Sy2 will often be used) is based on the width of the observed emission lines (Khachikyan & Weedman 1971, 1974; see also Osterbrock 1977, 1981 and discussion in Roy et al. 1994). Broadened emission lines are detected in Sy1 but not in Sy2 - that is *one of the defining characteristics* of Sy2. Permitted emission lines are observed from broad line regions (BLRs). The narrow line emission, from the so-called NLRs, includes many forbidden lines, indicating that the gas density is much lower than in BLRs. For example, the doublet (often referred to that way, it is actually a triplet but one is on the order of 10^3 weaker than the others) emission line of O [III] (doubly ionized oxygen), is only observed when gas densities are $< \sim 10^8$ cm^{-3} (Kawakatu et al. 2008).

It came apparent that the classification System for Seyferts, into the types Sy1 and Sy2, was too general because as more Seyferts were investigated it was observed that there is a continuum of the emission-line properties that define these galaxies. Osterbrock (1977) added the intermediate types 1.2, 1.5, and 1.8 "on the basis of the appearance of its Hβ profile". The sample of 36 Seyferts in that study by Osterbrock consisted of those from Khachikian & Weedman (1974), as well as (those listed as probable) Seyferts in Markarian & Lipovetsky (1973). The imaging was done at the Lick Observatory using the 120 inch telescope. This work built on earlier results (Osterbrock et al. 1976), an investigation of the emission line profiles and relative intensities for four Sy1 (3C 227, 382, 445, 390.3).

In Osterbrock (1977), the classification of type 1.5 (NGC 4151 is given as a good example) was defined to be intermediate between typical type 1 and 2 Seyferts, "with an easily apparent narrow Hβ profile superimposed on broad wings". Type 1.8 and 1.2 would then be defined to be Seyferts with relatively stronger and weaker narrow Hβ components, respectively, as compared to Sy1.5.

A few years later (Osterbrock 1981), type 1.9 was added as a result of the investigation of the emission line properties of five Seyfert galaxies (Mrk 423, 516, 609, 1018, and V Zw 317). All of the objects were seen to have fairly strong narrow emission lines, in addition to weak Hα and sometimes Hβ components to the emission. The difference between type 1.8 and 1.9 was defined to be "depending on whether or not broad Hβ emission can be seen in the scans…".

The classification of galaxies in general is based primarily on morphology and especially on spectral properties for more distant, higher-redshift galaxies (Madgwick et al. 2003; Bromley et al. 1998). Principle component analysis, which is a method of using orthogonal basis functions to investigate the significant spectral components of a galaxy, is a particularly useful and powerful way of classification (Connolly et al. 1995; Francis et al. 1992; for application to quasars see Mittaz et al. 1990).

1.3. UNIFIED SCHEME

In the unified view of AGN today, it is thought that intense UV radiation originating from a central engine (SMBH) is the dominant cause of photoionization and the cause of the observed broad line emission. The difference between Sy1 & 2 is thought to be due primarily to the angle of inclination, with respect to our line of sight, of a central torus of obscuring gas and dust. When viewed edge on, it is thought that the torus obscures the broad line emission detected in Sy1.

The first significant evidence for this was given by Antonucci & Miller (1985) when polarized broad emission lines were detected in the nuclear spectrum of the Seyfert galaxy NGC 1068. "The polarized flux plot reveals the presence of very highly polarized, very broad (~ 7500 km s^{-1}) symmetric Balmer lines and also permitted Fe II. This plot closely resembles the flux spectra of Seyfert type 1 nuclei". The polarization appeared to be due to scattering, and it was suggested that this was due primarily to free electrons. More evidence followed a few years later in Miller & Goodrich (1990). In that spectropolarimetric study of a sample of Sy2s, "evidence for a hidden BLR, visible only in the polarized flux spectrum" was found. Some Sy2, however, do not display broad emission lines in their polarized flux spectra (Tran 2003a,b ; Matt 2000) indicating that some other factor may be involved, some aspect of the geometry not understood, or perhaps even a genuine lack of BLRs in some Sy2. This in itself does not necessarily threaten the unified scheme; likely it is suggesting some added complexity.

The full history and details of the development of the unified scheme for Seyferts is beyond the scope of this thesis. However the results reported in the next two chapters do, in particular several two-sample statistical tests (§2.6), add to the existing evidence supporting the unified schemes. More generally, the unified scheme is obviously important when considering the processes generating, and the components of, radio and infrared emission which is of interest in this thesis.

Lawrence (1987) is a thorough, early review of AGN unification in general. There have been several, slightly differing (in most cases) models (Blanford & Königl 1979; Wilson 1981, 1982; Pedlar et al. 1985; Wilson & Ulvestad 1987) put forth to explain the relationship between nuclear nonthermal radio sources and the narrow line regions (NLRs) in Seyfert galaxies. Most models have in common the idea that there is a central source of ionizing radiation in the nucleus and the interaction of it with surrounding ambient gas produces the observed spectral features. Over the ensuring years there have been, and continue to be, more studies on the unified scheme (e.g., Antonucci 1993; Dultzin-Hacyan 1999; Cappi et al.1999; Schmitt et al. 2001a; Alexander 2001; Delgado 2002; Bian & Zhao 2002; Lutz et al. 2002; Ogle et al. 2003; Deluit & Courvoisier 2003; Lal 2000, 2004; Taniguchi et al. 1999, 2003; Bianchi et al. 2004; Rhee & Larkin 2005). Although there is still general agreement that all AGN are essentially the same creature, many of the details are still unknown.

1.4. RADIO JETS IN AGN

An in-depth discussion of the physics of radio jets is beyond the scope of this thesis however a brief discussion of their general (particularly radio) properties, as related to Seyferts, is in order.

Good treatments of the physical theory of jets and beams in astrophysics are the books by Hughes (ed. 1991) & Burgarella et al. (ed. 1993). Laing (1993) is a chapter in the latter book and focuses on the physics of large-scale jets. The information is relevant to Seyferts since the basic SMBH-accretion disk-beam paradigm is thought to apply to all AGN. Chapter 3 (Witta 1991) of the book by Hughes covers jets in the context of AGN more generally. See Gallimore, Baum & O'Dea (1996) (and references therein) for a detailed study of jets in particular Seyferts and a proposed model of jet interaction with the central regions of the nucleus.

It has been theorized for many years that some sort of beaming mechanism could be powering observed radio jets (Morrison 1969; Longair, Ryle & Scheuer 1973; Blanford & Rees 1974; Hargrave & Ryle 1974; Scheuers 1974) emanating from very near the postulated SMBH. Although many of the details are still uncertain "there are many indirect arguments…which justify the conventional assumption that jets are fairly direct tracers of well-collimated, continuous, outflowing beams of material" (Lainge 1993).

The power and extent of radio jets varies considerably from one class of AGN to another, from usually very modest ones for Seyferts, to massive relativistic jets in quasars and giant radio galaxies (Boyce 2000).

The evolutionary track for active galaxies is not a settled question, nor the question of any connection between such large scale emission seen in radio giants and more sedate AGN observed today. One of the primary goals of the research being reported on in this thesis is to look for any large-scale, relic radio emission representing any such earlier stages.

Although we can now, with the VLBI, observe the central regions of AGNs down to scales ~ 0.1 pc, much about what initiates the jets is unclear, as it is thought that the critical processes involved occur on scales at least a couple of orders of magnitude smaller still (Witta 1991). It has been known for some time (Fanaroff & Riley 1974) that for extended nonthermal radio structures emanating from the nucleus, the brightness tends to be at a maximum either close to or far away from the nucleus, depending on whether it is a high or low power source, respectively. For example, excluding emission from the central most regions, emission with 1.4 GHz power greater than ~ $10^{24.5}$ W Hz^{-1} tends to have peak brightness at more than half way out from the nucleus (Lainge 1993). “The synchrotron lifetimes of the relevant electrons in these ‘hot spots’ seems to be shorter than the light travel time from the galaxy, suggesting that the electron supply is being continually replenished” (Blanford & Rees 1974). As described in Witta (1991) there are competing models for beam production. Two broad classes are the so-called hydrodynamic and the magnetohydrodynamic models, depending on how significant a role played by magnetic fields.

Radio jets have been observed in Seyfert galaxies for many years, and are thought to exist as part of the basic SMBH scheme for all AGNs. Radio sources in Seyferts (typical cm radio powers of ~ 10^{23} W Hz^{-1}) are not as strong as in other types of AGN, nor are they usually of significant size or extent (typically < .5 kpc) (Ulvestad & Wilson 1989; Ulvestad et al. 1999a). The latter paper was a 15 GHz VLBA investigation of two Seyferts, the Sy1 Mrk 231 and the Sy2 Mrk 348. It is noted that measurements of jet speeds in Seyfert cores are rare, and so the study was designed to do just that. Some of the few other published results on jet speeds were those in Ulvestad et al. (1998), which reported measurements of NGC 4151. Velocities with upper limits of 0.14c and 0.25c were measured, on scales of 7 and 36 pc, respectively. The work of Ulvestad, Neff, & Wilson (1987) and Roy et al. (1998a) seem to show an upper velocity limit of ~ 0.5c for components separated by about 20 pc. The VLBI results reported in Falcke et al.(1999), a radio investigation of III Zw 2, a Sy1, seem to imply subparsec scale speeds < 0.2c or so.

1.5. RADIO JETS AND RADIO VARIABILITY

Several of the Seyferts in the sample being investigated in this thesis were imaged back in the 1980s at 843 MHz using the MOST (Subrahmanya & Harnett 1987). Those results were compared (Chapter 4) to the new ones being reported in this thesis in a search of any variability of the radio emission. Variability, over various time-scales, has been observed (at not just) radio frequencies for different types of active galaxies.

For example, the radio continuum counterpart to the optical BLR of the Sy1 NGC 5548 was found to be photometrically variable (8.4 GHz using the VLA) by 52% $\pm$ 5% over a time span of 4.1 yr and 33% $\pm$ 5% over just 41 days (Wrobel 2000). At 4.9 GHz (VLBA) the variation over 41 days was only 19% $\pm$ 5%. An inverted spectrum (spectral index $\alpha \sim 0.3 + 0.1$) between 4.9 GHz and 8.4 GHz was reported. Another interesting result of Wrobel was that "the nucleus is astrometrically stable at 8.4 GHz to an accuracy of 15 pc between VLA observations separated by 4.1 yr and to an accuracy of 0.95 pc between VLBA observations separated by 3.1 yr". This supports the idea that a SMBH is likely the "ultimate energy source for the BLR". Ulvestad et al. (1998) reported upper limit values of 0.14*c* and 0.25*c* for the speed of two nuclear components, at distances of 7 and 36 pc respectively, from the nucleus in the type 1.5 Seyfert NGC 4151. The observations were at 6 & 18 cm using the VLBA.

Brunthaler et al. (2005), a follow up study of Falcke et al. (1999), is a VLBA multi-epoch (41 observations spaced roughly 1 month apart from September 1998 to September 2001) study of the radio flares in the Sy1 III Zw 2. The dynamics and variability observed reveal "a textbook example of a synchrotron self-absorbed jet". There is no evidence for large scale interactions being the cause of the observed variability.

Until the new results reported in this thesis, the galaxy III Zw 2 is one of the few galaxies in which long term (20+ years in this case) radio variability data are available. It was not until the work of Dent (1965) that extragalactic radio variability was established. The results of Aller et al. (1985) show that in just four years the core of III Zw 2 can undergo a twenty-fold increase in radio flux density. It has now been shown that major flares, resulting in a nearly 30-fold increase in flux density, have occurred within just two years. Such flares "occur roughly every five years with sub-flares on shorter time scales" (Brunthaler et al 2005). III Zw 2 is also variable at optical and X-ray wavelengths (Lloyd 1984; Clements 1995 and Kaastra & de Korte 1988, respectively). For IR variability in AGNs see Enya et al. (2002) and references therein.

Blank et al. (2005) was a 8.4 GHz investigation of the Sy1.5 NGC 7213 using the Australian Long Baseline Array. NGC 7213 is one of the rare Seyferts with observed radio power that is found to be intermediate between traditional radio-loud and radio-quiet AGN. The galaxy was chosen from the sample of this new type of AGN first reported in Roy & Norris (1997). Blank (1999) observed NGC 7213 at 1.4 GHz & 2.4 GHz using the Australian Telescope Compact Array (ATCA) and at 843 MHz using the Molonglo Observatory Synthesis Telescope (MOST). A value of $P_{1.4}$ = 3×10^{22} W Hz^{-1} was reported. The observations revealed extended radio structures usually only found in radio-loud objects. The large scale structures in the 1.4 GHz and 843 MHz images are "strongly suggestive of jet-fed radio lobes". The MOST observations showed variability of up to 30% on a time scale of just weeks.

The three milliarcsec 8.4 GHz images in Blank et al. (2005) revealed an unresolved point source. The total & peak flux densities measured were 57 $\pm$ 1.3 mJy and 57.1 mJy, respectively. It is observed that the core is < 3 mas across with a minimum brightness temperature of $T_b \approx 1.5\times10^8$ K. The core size results were predicted in Blank & Harnett (2004), based on the previously observed variability at lower frequencies. With the results of Blank et al. it can now be seen that NGC 7213 "has decreased in flux density by nearly a factor of 6 during the period from 1988 to 2000". As the authors point out, few long-term variability studies for Seyferts exist. However on the timescales involved in this study, the variability observed in NGC 7213 seems to be uncommon.

NGC 7213, mentioned above, is an object contained in the newly constructed sample investigated in this thesis in later chapters. It is a radio-excess object (Roy & Norris 1997), discussed in §3.7, one of nine identified in this new sample. The variability observed for NGC 7213 in previous studies is also indicated in some of the objects in this new sample, as discussed in Chapter 3.

The importance of determining the direction/orientation of the radio jets in AGNs is of obvious importance, especially when investigating extended radio emission. There are several studies (e.g., Nagar & Wilson 1999; Schmitt et al. 1997; Brindle et al. 1990; Ulvestad & Wilson 1984b) which indicate that radio jets in Seyferts are not generally at right angles with the disk of the host galaxy, but are in fact randomly distributed. The reasons for such a distribution are not known but could be caused by radiation-induced warping of the accretion disk around the SMBH (on such warping see Pringle 1996, 1997; Maloney, Begelman & Pringle 1996), or perhaps it is caused by the so-called Bardeen-Petterson effect (Kumar & Pringle 1985; McKernan & Reynolds 2004). Similarly, nuclear bars in some Seyferts appear to be randomly oriented with respect to the host galaxy bar (e.g., Martini et al. 2001).

The paper by Kinney et al. (2000) builds on Clarke et al. (1998) by investigating a more complete sample, one based on some isotropic properties - namely the 60 μm flux and warm infrared colors. This resulted in a sample of 88 Seyferts, 29 Sy1 and 59 Sy2. The general results are consistent with the other studies on jet orientation mentioned.

A result of Kinney et al. relevant to this thesis (though larger-scale emission is being searched for in Chapter 2, as the data used is more global in nature) is that 33 (8 Sy1 and 25 Sy2) of the Seyfert galaxies showed extended emission and none are thought to be in interacting Systems.

1.6. EXTENDED RADIO EMISSION FROM SEYFERTS

One of the research goals in this thesis is to look for large-scale, extended radio emission from the sample objects. I will be analyzing the 843MHz radio data from the SUMSS. Therefore I will briefly discuss some of the major research results of the last few decades on extended radio structures around Seyfert galaxies. It is important to note that because of the global nature of the data from the SUMSS, the emission searched (e.g., when creating radio contour maps in §2.3) would be on very large scale, meaning in size comparable to the Seyfert host galaxy, as we see in even larger scale (relic or otherwise) in radio galaxies (Boyce 2000). For optical investigations of extended gas in Seyferts see Fraquelli et al. (2003) and references therein. For NIR see Storchi-Bergman et al. (1999) & Winge et al. (2000). Prieto (2000) is an investigation of extended X-ray emission in a radio-loud Sy1.

In a series of papers Nagar et al. (1999) investigate 47 early-type Seyfert galaxies. That paper discusses the results from an investigation of the radio structures of the Seyfert sample, using the VLA at 3.6 and 20 cm. The paper also discusses some statistical results of the sample and how it all fits into the unified scheme for Seyferts. The sample of Seyferts investigated has been built up over the years. The paper by Mulchaey et al. (1996) discusses more of the details of the sample as well as a discussion of its completeness. The galaxies in the sample are of type 1.0, 1.2, 1.5, and 2.0. All have recessional velocities < 7000 km s^{-1} and total visual magnitude < 14.5. Emission line ([O III] and H_α + [N II]), as well as green and red continuum imaging results, were presented in Mulchaey et al. (1996).

There were several significant results in Nagar et al. (1999). For example, the mean 20 cm radio luminosities were similar for Sy1 and Sy2; $10^{22.72}$ W Hz^{-1} for type 1 and $10^{22.75}$ W Hz^{-1} for type 2.

The radio luminosity of the Seyferts also appears to be independent of the morphological type of the host galaxy. In agreement with some earlier results (Ulvestad and Wilson 1989; Colbert et al. 1996b), the fraction of resolved radio sources was higher for Seyfert 2 galaxies (93%) than for Seyfert 1 galaxies (64%). However it was found that the mean radio extent of sources was not statistically significant.

Probably the most significant result of Nagar et al. (1999) was that the Seyfert galaxies which showed the largest radio extent, defined to be structures larger than 1.5 kpc, all were Sy1.2. "This result implies that… the Seyfert intermediate-type classification depends on some factor other than the angle between the axis of the obscuring torus and the line of sight". Further, it is argued that this factor affects an important flux ratio (R, see below) and that the factor is correlated with the observed radio extent of the galaxies. Among the other types of Seyfert in the sample, a distribution consistent with the unified scheme was observed. Even though Sy1 have a lower fraction of resolved radio sources, the Sy1 with the observed extended structures makes the mean radio extent for Sy1 (1.2 $\pm$ 0.4 kpc) larger than the mean for Sy2 (0.6 $\pm$ 0.1 kpc). This is consistent with the unified models for Seyferts.

Ulvestad and Wilson (1989) discounted much of the differences previously (Ulvestad & Wilson 1984b) observed in the strength and size of radio sources between Sy1 and Sy2. Yet there still remained an "only marginally statistically significant" tendency for Sy2 to have stronger and larger radio sources. Nagar et al. (1999) commented on this, noting that with their discovery of the extended radio structures in Sy1 (described above) such remaining differences vanish, with the mean Sy1 radio extent now greater than that for Sy2. But to be consistent with the unified scheme, we would expect to observe a larger mean projected radio extent in Sy2, since we would be observing the central obscuring torus more edge-on.

To investigate this further Nagar et al. (1999) had to construct a larger sample of Seyfert galaxies because the size of the early-type sample being discussed was too small. So to the above discussed early-type sample, Nagar et al. (1999) "added to it all Seyfert galaxies from the literature that show extended radio structure". Such galaxies are listed in table 1 (type 1.0, 1.1, 1.2, 1.5), table 2 (type 1.8 & 1.9), and table 3 (type 2.0) in Nagar & Wilson (1999), a paper describing the results of an investigation of the distribution of β, the angle between the nuclear accretion disk with respect to the disk of the host galaxy. The significant results from Nagar & Wilson (1999) were that there was "no evidence that the β distribution of Seyfert 1s and 2.0s are different from each other or that either one is significantly different from a random distribution"

These Seyferts, forming a “radio-excess Seyfert sample”, consists of 74 Seyferts (26 Sy1, 9 Sy1.8 and Sy1.9, and 40 Sy2). Forty-six of these came from Schmitt et al. (1997) and were obtained from the literature. They all had high-resolution maps published and they all displayed linear or slightly resolved radio structures. The definition of these types of radio structures (linear, slightly resolved, etc.) were taken from Ulvestad & Wilson (1984_a). Schmitt et al. (1997) presented the results of a study in which the authors used “the radio axis as an indicator of the orientation of the obscuring torus in Seyfert galaxies and analyze the difference between the position angles of extended radio structures and host galaxy major axis Seyfert 1 and 2 galaxies”. This sample of 46 Seyfert galaxies consisted of 15 Sy1 and 31 Sy2.

All five of the most extended radio structures (extent $\geq$ 1.5 kpc) Sy1.2 in Nagar et al. (1999) described above had a computed R value confined within the relatively narrow range $-0.4 < R < 0.7$, and it seems as though the unknown factor responsible for the classification of Seyfert galaxies as Sy1.2 (discussed above) also effects R.

If one was to delete the extended Sy1.2, “the distribution of the other Seyfert galaxies…appears consistent with the expectations of the unified scheme”. Although the number of Sy1.8 and Sy1.9 in the Nagar et al. (1999) sample was too small to make any statistical inferences, it is noted that all of them are extended, the 1.9s more than the 1.8s, and that “the Seyfert 1.9’s appear to be among the most radio-extended objects in the sample, even though their [O III] and H_β luminosities are not significantly different from those of Seyfert 2.0’s”. No correlation was found between radio extent and R for Sy2.

Many Seyferts (36 of 88) in the 60 μm sample used in many of the papers mentioned so far (de Grijp 1987, 1992; Schmitt et al. 2001a) displayed extended radio emission when imaged at 3.6 cm (Kinney et al. 2000, a study on β discussed above).

The “radio-excess” AGN, many of which are Seyferts, as described by Roy & Norris (1997) and discussed earlier, was also a sample chosen for their IR flux at 60 μm (among other criteria). The reason for the 60 μm selection criteria is due to the fact that it is thought to be an isotropic property. e.g., see de Grijp (1985, 1987). As suggested in the torus model put forth in Pier & Krolik (1992), it is thought that circumnuclear torus is thought to radiate very nearly isotropically at this wavelength.

As the objective of this thesis is to try and identify all known Sy in the local universe (as well as estimate the true mean values for distances and luminosity, see §2.7), in the volume of space defined below in §2.1, many of the objects from the above mentioned 60 μm samples are included in this new, thesis sample. As described in §2.1 many other sources were also used in constructing this new sample.

The so-called radio-excess Seyferts identified by Roy & Norris (above) are potential candidates for having extended radio emission simply because they have such above average IR emission and most have some linear radio structure identified. As discussed in Chapter 4, nine Sy in the sample investigated in this thesis are, for the first time, identified as being radio-excess galaxies though none have any extended emission of the scale investigated by the SUMSS.

1.7. THE RADIO-FIR CORRELATION

The standard explanation for the observed global FIR-radio correlation observed among all galaxies is that the FIR and radio emission are both due to star formation and death. Emission from high-mass stars heats nearby dust, which is then reradiated at FIR wavelengths.

The correlation is thought to come about due to the same high-mass stars; when the giant stars end their lives as supernovae they produce relativistic electrons which generate the observed (non-thermal) synchrotron radio emission (Vlahakis et al. 2007).

This FIR-radio correlation was investigated (§3.7) for the sample of Seyferts in this thesis using the SUMMS 843MHz data and the four bands covered by *IRAS* bands (12, 25, 60, and 100 μm). NIR data from the 2MASS was also used to investigate any correlation (with the SUMSS radio data).

Most of the luminous extragalactic sources of far infrared (FIR) radiation are dust clouds opaque to visible light. However, these are fairly transparent to radio waves, making such identifications of infrared sources unbiased (Condon & Broderick 1986). A large FIR luminosity observed in an AGN is an indicator of large dust masses (Roy & Norris 1997). It is still unclear, however, if the (*IRAS*, discussed in detail in §3.7) mid & far IR emission from Seyferts is dominated by large-scale disk emission or emission by the circumnuclear torus (Thean et al. 2001b and references therein).

The first study to establish a (global) linear correlation between radio and IR luminosity in spiral galaxies was by van der Kruit (1971).The sample (eight of which were Seyferts), consisted of all of the galaxies listed in Seyfert (1943) with $\delta > +10°$. The radio observations were made with the WRST at 1415 MHz and the resulting data was compared with 10 μm data from Kleinman & Low (1970a,b), which were infrared observations of galaxies between 1 – 25 μm using the three

Cassegrain telescopes at the Catalina Observing Station of the University of Arizona. A strong correlation for all of the spiral galaxies in van der Kruit (1971) was observed.

Dickey & Salpeter (1984) investigated the Hercules galaxy cluster (A2151) near 1.4 GHz with the VLA (D configuration). Comparing the fluxes of the 65 detected sources with *IRAS* (60 μm) data from Young et al. (1984) for the same sources, a strong 60 μm – 1.4 GHz correlation was found.

de Jong et al (1985) investigated a rather heterogeneous sample of 91 galaxies at 6.3 cm using the 100 m radio telescope at the Max Plank Institute for Radio Astronomy. This sample included normal spirals, active galaxies, irregulars, and dwarf galaxies. The collected radio data (detection rate of 95% for all galaxies with flux density S > 1 Jy) were compared to published *IRAS* 60 μm data and a very strong correlation was found; the computed line of best fit was found to be $\log S(6.3cm) = (0.94 \pm 0.06)\log S(60\,\mu m) - (2.34 \pm 0.06)$.

In a follow-up study, Wunderlich et al. (1987) used much of the data from de Jung et al. The data set was slightly expanded, mainly by adding some measurements at 2.8 cm. The total number of (mostly spiral) galaxies in this inhomogeneous sample was brought up to 99. Most significantly, in this paper "the calculation of flux densities…utilizes a more careful data analysis resulting in a largely reduced scatter in the correlation…" The results are striking, as seen in Figure 1.3 below which was taken from Wunderlich et al. (1987).

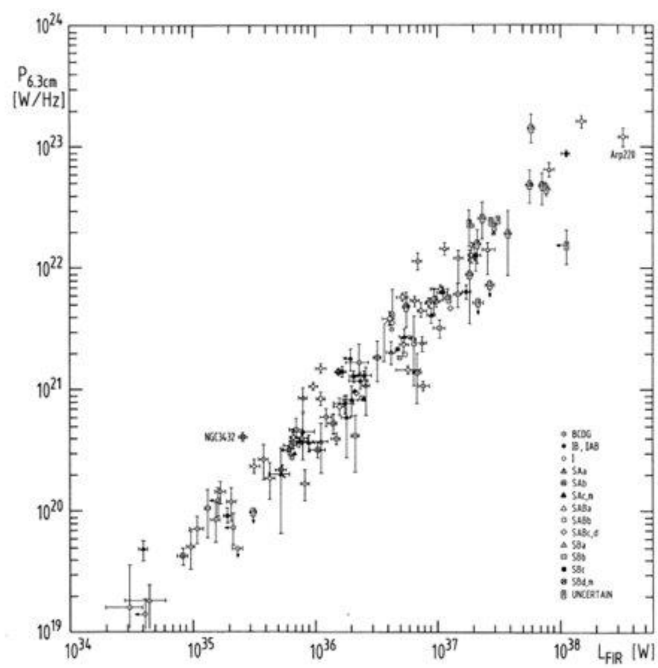

FIG. 1.3.- A plot of the radio vs. FIR luminosities (or powers) for a large collection of spiral galaxies taken from Wunderlich et al. (1987).

It was reported that almost all of the cooler ($S_{60\mu} > S_{12\mu}$) high latitude *IRAS* sources are extragalactic (a large majority of which are spirals) and that their IR and radio fluxes are strongly correlated. These 490 sources (with the additional constraint $S_{12\mu m} \geq 2$ Jy) had a 1400 MHz flux-density distribution with a median value of $\langle S_{1400} \rangle = +37 \pm 4$ mJy. This was fitted by a quantity q given by $q \equiv -0.474 + \log\left[\frac{2.58 S_{60\mu m} + S_{100\mu m}}{S_{1400}}\right]$ that has a Gaussian distribution with median $\langle q \rangle = +2.35$ and dispersion $\sigma_q \leq 0.3$. Only 9 out of the 2840 *IRAS* sources with 1400 MHz flux that had $S_{60\mu m} \geq S_{12\mu m}$ and $2 > S_{60\mu m} > 0.5$ Jy were matched with any of the ~3000 radio sources stronger that 0.20 Jy at 14000 MHz. "Thus even though the radio and infrared fluxes of most *IRAS* sources are tightly correlated, complete samples of strong radio and infrared fluxes of most *IRAS* extragalactic sources are almost completely disjoint, with ≤ 1% of the infrared sources being radio sources and ≤ 1% of the radio sources being infrared sources".

The FIR-radio correlation displayed by Seyfert galaxies are generally more scattered compared to normal spirals. Indeed, in the study of Sanders and Mirabel (1985), *after* the bright, compact, nuclear radio-components (smaller than 100 pc in extent) from the Seyfert galaxies in the sample were subtracted from the total flux, the FIR / 21 cm flux ratios of the Seyfert lined up with the other spirals in the sample. The resulting line of best fit then had a slope of 1.06 ± 0.6 (with r = 0.97). The six Seyferts in the sample that had bright radio components subtracted were NGC 3227, 5506, 3628, 3504, 1068, and 7469. The central 15" of NGC 1968 was also subtracted.

FIR emission from Seyfert AGN is thought to be thermal in origin, coming primarily from nuclear dust heated by the UV continuum from the central engine. Investigations in the 1980s (e.g., Rodríguez-Espinosa et al. 1987) seemed to show that FIR emission in Seyferts is mainly from disk star formation activity, relegating the AGN contribution to heating to a minor role. But some studies have indicated that many Seyfert do in fact seem to have considerable nuclear FIR.

"On larger scales, their (Baum et al. 1993) Seyferts sometimes displayed small-scale versions of the lobes of powerful radio galaxies, occurring on larger scales up to ~ 5 pc" (as described in Roy et al. 1998). The results of Baum et al. (1993), a study of kpc-scale radio emission in Seyferts, indicate that these lobes could be what are displaying the normal radio-FIR correlation. The extra-nuclear lobes are "diffuse, sometimes 'bubble-like' radio emission in these sources which aligns preferentially with the projected minor axis of the galaxy disk" (Baum et al. 1993). In that study, thirteen Seyfert were investigated at 20 cm using the WSRT. Twelve of the thirteen Seyfert displayed the extended, extra-nuclear radio emission described above. It is hypothesized this emission is caused by cosmic-ray electrons generated by circumnuclear starburst activity (see also Forbes & Norris 1998; Hill et al. 2001).

Roy & Norris (1997) investigated the increase scatter of Seyferts in the radio-FIR correlation. It is noted that those galaxies showing the most deviation from the correlation are those that are more radio-loud than normal (spiral) galaxies with the same FIR luminosity. These objects were termed "radio-excess", to differentiate them from traditional radio-loud galaxies, and are now considered to be examples of a new intermediate-radio-power class of AGN. It was shown (e.g., Sanders & Mirabel 1985) that the excess emission originates on sub-kpc nuclear regions.

Special selection criteria in Roy & Norris were defined. These included detection at 60 μm, several methods of excluding stars, detection in the Parkes-MIT-NRAO survey at a level stronger than 70 mJy at 6.3 cm, and $\left(S_{6.3cm}/Jy\right)/\left(S_{60\mu m}/Jy\right) > \frac{1}{55}$, or $\left(S_{6.3cm}/Jy\right)/\left(S_{60\mu m}/Jy\right) < \frac{1}{875}$ to retain those objects that lie outside 3σ radio-FIR correlation displayed by normal spirals.

The above selection criteria proved to work well for selecting radio-excess AGN and were used in §3.7 to search for radio-excess objects in the newly constructed sample being reported on in this thesis.

Ultimately twelve objects were found to satisfy these criteria. Five of these were Seyfert, four of which were Sy2, the other Sy1 – a common bias for FIR selected samples (de Grijp et a. 1992). The five had radio luminosities between $10^{22.1}$ and $10^{25.4}$ W Hz^{-1} which is almost two orders of magnitude more than the radio luminosity of the average Seyfert (Ulvestad & Wilson 1989), and is to be expected considering the selection criteria mentioned above. Two of the Seyfert (*IRAS* 00182-7112 and PKS J1557-7913) were also radio-loud, rare for Seyferts.

All 12 of the selected radio-excess galaxies displayed a significant scatter in the radio-FIR correlation; they all fell well outside the $\pm$ 3σ bounds displayed by normal galaxies (de Jong et al. 1985), validating the selection criteria defined above.

In a related, follow-up study, Roy et al. (1998b) (see also Bransford et al. (1998) for a similar study of southern-sky Seyferts using the same sample) investigated a sample of 149 Seyfert and radio-quiet quasars at 13 cm by both the 6 km Australian Telescope and the 275 km PTI. The PTI is sensitive to structures < 0.1 arcsec in extent, corresponding to about 20 up to 200 pc, when considering the redshift range of the sample.

It was found that Seyfert without strong, compact radio cores exhibited the radio-FIR correlation seen in normal spirals. Those deviating from the normal correlation being “more radio-loud than normal spirals with the same FIR luminosity”. An interesting result, differing from some earlier work mentioned above, was that subtracting off the 2.4 GHz emission from the core detected by the PTI did not result in a larger *r* value; the radio-FIR plot did not fall back in line with the normal spiral correlation. The median and scatter values computed did not change significantly. The important results in Roy et al. were summarized as follows.

1. Many Seyferts display a correlation between the total nonthermal radio continuum and thermal FIR emission (selection effects ruled out)
2. Seyferts that lack compact radio cores display the normal FIR/radio ratio.
3. Seyferts that harbor compact radio cores depart from the normal correlation, tending to be more radio-loud than spirals. These “radio-excess” [see Roy & Norris (1997), above] Seyferts constitute a little recognized population of radio-loud AGNs with spiral hosts that may represent a stage in the formation of powerful radio galaxies or radio-loud quasars.
4. The relatively poor radio-FIR correlation displayed by Seyferts that harbor compact radio cores was not improved by subtracting off the core radio component. Thus, it seems that the radio-FIR correlation breaks down in Seyferts at a scale larger than 100 pc from the AGN. Although the extra-nuclear radio emission is powered by starburst activity, the nuclear emission, it seems, is not.

As this introduction has shown, relatively little is known about the large-scale radio structures of Seyferts. So among the primary goals of this study are to first construct a new sample of southern-sky Seyferts (§2.1) and then use appropriate radio data to search for any previously unidentified, large-scale radio emission, relic or otherwise (§2.3), as well as looking at the general (including radio) properties of the sample (§2.5), including distances, recession velocities, and luminosities. Several two-sample statistical tests are performed (§2.6) to test the unified view of AGN discussed above.

In Chapter 3 the (mostly global) infrared (IR) properties of this new sample of local southern-sky Seyferts are considered at seven wavelengths (or more precisely, bands centered on that wavelength), covered by two all-sky surveys. One pioneering survey was famously carried out in the 1980s by the *Infrared Astronomical Satellite* (*IRAS*) in the mid and far-infrared (MIR/FIR - all but the 12 μm usually considered FIR). The other, more modern-day, near IR (NIR) survey at J, H, K_s bands (centered at, approximately, 1.25, 1.65, and 2.17μm, respectively) is the *Two-Micron All Sky Survey* (2MASS). The advantage of using data from the former is that it allows the results to be compared to those from many previous published studies (of different, mostly smaller, samples) found in the literature.

For the latter, very little has been done with the 2MASS data as it relates to Seyferts. In fact, at the time of this writing only Peng et al. (2006) has given any results from the (K_s -band) 2MASS data as it relates to Seyferts. So in this thesis (§3.8), the 2MASS K_s -band images of several of the Sy2 in the newly constructed southern-sky sample described in §2.1 are decomposed into the bulge, disk, and nuclear IR components. This increases by nearly 50% the number of such objects for which this analysis has been done (published).

Some of the main, relevant specifications and characteristics of both surveys are discussed in more detail below in §3.2. The main NIR and FIR properties of the sample objects are given in §3.3. After upper limits for the censored objects in the sample, in both surveys, are derived and discussed in §3.4, the main results for the sample are given in §3.5. This includes an investigation of the luminosities at all seven wavelengths. The spectral energy distribution and several spectral indices for the sample are also computed and summarized, and plots given for all of the wavelengths covered. These include two in the optical, blue and red, or at approximately .44 and .64μm, for 61 of the Sy2 and 24 of the Sy1 (79% and 57% of each type, respectively, or ~71% of the total sample).

In §3.6 the results of the relevant survival-analysis tests (defined and discussed in §2.7) are given, as well as the results of the correlation statistical tests performed. In §3.7 the well-known, global, radio-IR correlation is investigated for this sample, including plots and lines of best fit for each of the seven IR wavelengths covered, broken down by type. The 843MHz data from the previous chapter is used.

In chapter 4 there is a discussion of the main results obtained in this study and how they compare overall to what is found in the literature, and how they might contribute to the unified view of AGN. Finally, in Chapter 5, a summary of this work is given, as well as an outline of several possible follow-up research projects using this newly constructed sample.

2. A SOUTHERN-SKY SEYFERT SAMPLE & ITS 843 MHz RADIO PROPERTIES

2.1 THE SAMPLE

Tables 2.1 and 2.2 below summarize some of the main properties of the sample, by type. The sample is homogeneous and distance limited, with $0.00145 < z < 0.03029$. It was constructed by compiling a list of all of the known Seyferts (denoted by Sy1 and Sy2 for type-1 and type-2 objects generally) with the above redshift restriction, in the southern sky with $\delta < -30°$ and $|b| > 10°$, which comprises the part of the sky covered by the SUMSS and MGPS-2 (§2.2). The cutoff value for z was chosen so as to reduce the effects of Malmquist bias. This is where only more and more luminous objects are detected the farther out into the universe one looks, since no other objects are luminous enough to be detected. Hence the larger the volume surveyed, the more weaker sources missed. In past studies of local Seyferts, many of them discussed in §2.2, it has been shown that beyond $z \sim 0.03$ fainter Seyferts start to be missed, enough to bias a sample appreciably. The precise cut-off value is though somewhat arbitrary. I extended the distance for this sample to just a small amount beyond $z = 0.03$ to include the little studied Sy2 LEDA 088648.

Initially a list of all AGN classified as Sy1 or Sy2 (within the above stated restrictions) were obtained from NED and SIMBAD databases. Then two main sources were consulted, Lipovetsky (1988) and Veron-Cetty & Veron (2001). In the Notes on Individual Objects (§2.4), these two sources are listed as [1] and [2], respectively. Most of the objects in this sample were listed in one of these two sources, though a few were not and were instead found in the literature (published papers and catalogs). In §2.4 these are referred to as [3] (de Grijp et al. 1987), [4] (Paturel et al. 2005), [5] (Maia et al 2003), and [6] (Shu et al. 2007). There were a few objects listed in [1] and/or [2] that were not in the two databases consulted and were added to the sample. If the specific Sy1 subclassification (Sy1.0 - Sy1.9) in [1] and [2] conflicted, and there were no other (more recent) results in the literature contradicting it, the listing in [2] was adopted.

This selection process resulted in a sample consisting of 119 Sys in all, with 77 Sy2 and 42 Sy1. Several of the main properties of the sample objects are given in Tables 2.1 & 2.2. Whenever the sample is broken down by type, all Sy1 are grouped together, including types 1.8 and 1.9. Some authors (e.g., Deo et al. 2007) list them separately in their analysis of the objects. In this sample there are only seven such objects (five Sy1.8 and two Sy1.9), a number too small for meaningful statistical inferences to be drawn. A total of 63 Sy2 and 27 Sy1 were detected in the SUMSS imaging (a detection rate of ~ 82% and ~ 64%, respectively). When an object is said to be 'censored' it is meant simply that its emission fell below the detection limit of the telescope.

Upper-limits (values for flux density for censored objects, so an upper-limit on luminosity can be estimated) are derived for all censored objects. A further discussion of the completeness of the sample is given in §2.7, including the results of several tests for correlation between recession velocity and the (log) 843 MHz luminosity.

Of the 77 Sy2 in the sample, two (LEDA 087391, LEDA 093365-censored) have no host galaxy morphological classification listed in NED. However, as commented upon on an individual basis in §2.4, some morphologies are suggested in various published images, as well as in the maps created from the SUMSS images (§2.3). Two (LEDA 166339, WKK 3546) are listed as elliptical, and two (LEDA 141858, PGC 059124) as E-S0 (intermediate elliptical/lenticular). Three (IC 4518, NGC 0454, AM 0426-625) are actually interacting pairs (of various types). Four (LEDA 088648, PGC 044167, ESO 383- G018, PGC 052101) are listed primarily as lenticular (S0). The Sy PGC 070458 is listed as peculiar. The remaining 63 (~82%) of the Sy2 are classified, at least primarily, as residing in some type of spiral host galaxy (see column (9) in Table 2.1).

Of the 42 Sy1, seven (PKS 0056-572, PMN J0133-5159, PGC 050427-censored, ESO 399-IG 020, PGC 064989-censored, CTS 0109-censored, and [VV2003c]J224704) have no host galaxy morphological classification listed in NED. As with the Sy2, in §2.4 some of these morphologies are suggested by inspecting various published images. Two are interacting pairs of spirals (ESO328- G036 and PGC 073028). Three are ellipticals (PKS 1521-300, *IRAS* 01089-4743, PGC 047969), though PGC 047969 is listed as an elliptical/lenticular (E-S0). Five are listed as lenticular (S0). The remaining 25 (~60%) of the Sy1 are classified, at least primarily, as residing in some type of spiral host galaxy (see column (9) in Table 2.1).

Unless otherwise stated, by 'distance' (as in Tables 2.1 and 2.2) what is meant is the luminosity distance, D_L. The angular distance of an object, defined as $D_A = length/angle$, with length being the (true or absolute) linear extent of an object, and angle being the angle the object subtends in the sky, is probably the most commonly used type of distance. That is just the standard "small-angle" distance formula. But for extragalactic objects the luminosity distance is most often used. It is related to angular distance by $D_L = D_A(1 + z)^2$ (Wright 2006) and is predicted by certain cosmological models; in this paper an open universe cosmology with $H_0 = 71$ km/s/Mpc, $\Omega_M = 0.27$, and $\Omega_{vac} = 0.73$, was adopted. Ω_M is the fraction of the energy density of the universe in the form of ordinary baryonic plus hypothesized 'dark matter'. Ω_{vac} is the so-called 'dark energy' which the dominant cosmological theories posit is the bulk of the energy density of the universe, though, like dark matter, has not been identified yet. The luminosity distances as well as the scale lengths given in column 4 in Tables A.1 and A.2 (Appendix A) in units of kiloparsecs per arcsecond (kpc/"), are based on the assumed above mentioned adopted cosmology (Wright 2006). Because the Sy in this sample under investigation are in the local universe, the difference between luminosity distance and angular distance is fairly small, less than 5% in all cases for this sample. But it is the luminosity distance that is properly used to compute luminosities (843 MHz luminosities in §2.5.3 and several infrared luminosities in Chapter 3), and to analyze the completeness of the sample (§2.7).

TABLE 2.1
Seyfert 2

	Name (1)	Alias (2)	R.A. (J2000) (3)	Decl. (J2000) (4)	Type (5)	z (6)	GCVel (km/s) (7)	D (Mpc) (8)	Host Classification (9)
	LEDA 087391	2MASX J00231403-5358239	00 23 13.91	-53 58 25.7	2	0.02929	8698	127	
	NGC 0424	ESO 296- G 004	01 11 27.46	-38 05 01.5	2	0.01176	3474	50	(R)SB(r)0/a
!	LEDA 093365	PDS J011153.5-455846	01 11 53.50	-45 58 46.0	2	0.02601	7661	112	
	PGC 004440	IC 1657	01 14 06.90	-32 39 02.1	2	0.01195	3546	51	(R')SB(s)bc
	NGC 0454	ESO 151-IG 036	01 14 24.57	-55 23 53.6	2	0.01216	3541	52	Pec/inter. pair
	PGC 004569	FAIRALL 0294	01 15 55.20	-50 11 19.4	2	0.02435	7209	105	(R_1)SB(l)o/a
	PGC 005696	ESO 353- G 009	01 31 50.29	-33 07 12.1	2	0.01649	4911	71	SB(r)bc:
	PGC 006078	ESO 297- G 018	01 38 37.24	-40 00 44.0	2	0.02520	7484	109	Sa: sp
	PGC 006351	ESO 353- G 038	01 43 37.30	-33 42 10.0	2	0.02955	8803	128	SB0^0^: pec
	PGC 008012	ESO 153- G 020	02 06 03.12	-55 11 38.6	2	0.01974	5795	85	(R'_1)SB(rs)ab
!	NGC 0824	PGC 008068	02 06 53.20	-36 27 11.0	2	0.01938	5760	83	SB(rs)b
	PGC 009634	IC 1816	02 31 51.05	-36 40 16.4	2	0.01695	4990	73	(R'L)SA:(s:)a
	PGC 010665	IC 1859	02 49 03.99	-31 10 21.6	2	0.01956	5778	84	Sb
	PGC 010705	ESO 299- G 020	02 49 33.95	-38 46 10.9	2	0.01666	4888	71	(R'_1)SB(rs)a
!	PGC 011104	ESO 417- G 006	02 56 21.50	-32 11 08.0	2	0.01629	4792	70	(R)SA0/a?
	PGC 012759	ESO 116- G 018	03 24 53.39	-60 44 19.8	2	0.01850	5386	79	(R)SAB(r)0^+
	NGC 1386	ESO 358- G 035	03 36 46.06	-36 00 00.3	2	0.00290	744	12	SB(s)0+
	PGC 014702	ESO 420- G 013	04 13 49.64	-32 00 27.5	2	0.01191	3435	51	SA(r)a?
	AM 0426-625	SGC 0426-629	04 27 12.27	-62 47 36.1	2	0.01831	5309	78	2 S0 pec
	PGC 015172	ESO 202- G 023	04 28 04.63	-47 54 17.5	2	0.01650	4778	71	(PR?)SB(rl)
	NGC 1672	ESO 118- G 043	04 45 42.27	-59 14 48.9	2	0.00444	1146	19	(R'_1:)SB(r)bc
!	PGC 016072	ESO 119- G 008	04 48 56.70	-57 39 33.0	2	0.02294	6693	99	(R')SB(rs)a
	PGC 016357	ESO 033- G 002	04 56 00.13	-75 32 29.2	2	0.01810	5240	78	SB0
	NGC 1808	ESO 305- G 008	05 07 42.33	-37 30 45.2	2	0.00332	823	14	(R'_1)SAB(s:)b
!	PGC 016873	ESO 362- G 008	05 11 09.10	-34 23 36.0	2	0.01575	4552	67	Sa;HII?
!	PGC 017768	ESO 306- G 025	05 45 51.10	-39 29 39.0	2	0.02500	7304	108	(R)SA(r)0/a
*	LEDA 096373	PMN J0726-3554	07 26 26.26	-35 54 24.1	2	0.02940	8597	127	S
	PGC 021057	IC 2202	07 27 54.08	-67 34 25.6	2	0.01201	3387	51	SAB(s)bc
	PGC 023573	ESO 018- G 009	08 24 07.55	-77 46 56.3	2	0.01782	5140	76	SA(s)c
	PGC 028144	ESO 434- G040	09 47 39.89	-30 56 53.8	2	0.00849	2325	36	(RL)SA(l)0^0
	PGC 028147	IC 2510	09 47 43.47	-32 50 18.3	2	0.00935	2581	40	(R)SAB(r)a
	PGC 029778	ESO 374- G 044	10 13 19.68	-35 58 57.4	2	0.02845	8310	123	(R'_2)SB(s)ab
	PGC 029993	IC 2560	10 16 18.59	-33 33 49.5	2	0.00976	2708	42	(R':)SB(r)bc
	PGC 030984	ESO 436- G 029	10 30 23.00	-30 23 26.4	2	0.01371	3900	59	SAB(rs)c:
	NGC 3281	ESO 375- G 055	10 31 51.86	-34 51 13.0	2	0.01067	2985	46	SAB(rs+)a
!	LEDA 088648	IRAS 12323-3659	12 35 03.80	-37 15 31.0	2	0.03020	8878	131	S0
	NGC 4507	ESO 322- G 029	12 35 36.65	-39 54 34.2	2	0.01180	3359	50	SAB(s)ab
	PGC 042504	IC 3639	12 40 52.85	-36 45 21.3	2	0.01092	3103	47	SB(rs)bc
*	WKK 1263	2MASX J12412572-5750038	12 41 25.25	-57 50 07.3	2	0.02443	7132	105	[[Sa]]
!	PGC 043779	ESO 323- G 032	12 53 20.30	-41 38 08.0	2	0.01600	4622	68	(R)SAB(l)0^
	NGC 4785	ESO 219- G 004	12 53 27.36	-48 45 00.8	2	0.01227	3496	52	(R')SAB(r)ab
!	PGC 044167	ESO 269- G 012	12 56 40.50	-46 55 34.0	2	0.01672	4835	72	S0
	NGC 4903	ESO 443- G 030	13 01 23.30	-30 55 59.9	2	0.01646	4782	70	SB(rs)c
	NGC 4945	ESO 219- G 024	13 05 27.41	-49 28 06.3	2	0.00188	385	8	SB(s)cd: sp
	ESO 383- G 018	2MASX J13332607-3400529	13 33 25.92	-34 00 48.3	2	0.01241	3579	53	S0-a
*	Circinus	ESO 097- G 013	14 13 09.25	-65 20 20.7	2	0.00145	266	6	SA(s)b:
!	LEDA 141858	2MASX J14212135-7250207	14 21 21.30	-72 50 21.0	2	0.02620	7684	113	E-S0
	NGC 5643	ESO 272- G 016	14 32 40.57	-44 10 27.6	2	0.00400	1068	17	SAB(rs)c
	PGC 052101	2MASX J14344546-3250326	14 34 45.37	-32 50 37.9	2	0.02540	7509	109	*+S0

TABLE 2.1
Continued

	Name (1)	Alias (2)	R.A. (J2000) (3)	Decl. (J2000) (4)	Type (5)	z (6)	GCVel (km/s) (7)	D (Mpc) (8)	Host Classification (9)
!	LEDA 166339	WKK 3262	14 35 14.90	-69 44 00.0	2	0.02586	7585	111	[[E]]
	IC 4518	IRAS F14544-4255	14 57 41.36	-43 07 53.4	2	0.01573	4598	67	Sc/Inter. pair
!	WKK 3646	HIPASS J1504-67	15 04 39.40	-68 00 07.0	2	0.01479	4278	63	[[E:]]
*	PGC 058547	ESO 137- G 034	16 35 13.87	-58 04 47.4	2	0.00914	2630	39	S?
*	PGC 059124	ESO 138- G 001	16 51 20.49	-59 14 03.6	2	0.00914	2631	39	E/S0
*	NGC 6221	ESO 138- G 003	16 52 47.33	-59 12 58.7	2	0.00500	1390	21	SB(s)bc pec
	NGC 6300	ESO 101- G 025	17 16 59.77	-62 49 09.3	2	0.00370	997	16	SB(rs)b
	PGC 060594	ESO 139- G 012	17 37 39.10	-59 56 19.3	2	0.01702	5004	73	(R':)SA(rs)bc
	PGC 062134	FAIRALL 0049	18 36 58.23	-59 24 08.9	2	0.02023	5982	87	Sa
	PGC 062174	ESO 103- G 035	18 38 19.85	-65 25 37.7	2	0.01329	3880	57	SA0^0
!	PGC 062218	IC 4729	18 39 56.40	-67 25 32.0	2	0.01481	4330	63	SAB(rs)bc
	PGC 062428	ESO 104- G 011	18 47 44.29	-63 09 22.8	2	0.01512	4440	65	SB(rs)bc
	PGC 062440	IC 4777	18 48 11.44	-53 08 51.2	2	0.01853	5497	79	(R_1)SB0^+
	NGC 6810	ESO 142- G 035	19 43 34.54	-58 39 22.0	2	0.00678	1961	29	SA(s)ab:sp
	PGC 063874	ESO 339- G 011	19 57 37.48	-37 56 08.5	2	0.01920	5769	82	Sb
	NGC 6890	ESO 284- G 054	20 18 18.02	-44 48 27.2	2	0.00807	2407	34	(R')SA(r:)ab
	PGC 064491	IC 4995	20 19 59.10	-52 37 19.1	2	0.01609	4782	69	SA0^0^ pec?
!	PGC 064537	ESO 462- G 009	20 21 51.50	-31 17 23.0	2	0.01928	5822	83	(R'_1)SB(rl)a
	PGC 065600	IC 5063	20 52 02.09	-57 04 06.7	2	0.01135	3342	48	SA(s)0+:
	NGC 7130	IC 5135	21 48 19.28	-34 57 03.8	2	0.01615	4868	69	Sa pec
	NGC 7172	ESO 466- G 038	22 02 01.89	-31 52 07.4	2	0.00868	2639	37	Sa pec sp
	PGC 068122	ESO 404- G 032	22 08 27.94	-34 06 24.4	2	0.01466	4422	63	S
	PGC 068198	IC 5169	22 10 09.95	-36 05 24.3	2	0.01037	3128	44	(R_1)SAB(r)0+
	FAIRALL 0357	2MASX J22273122-7023159	22 27 31.73	-70 23 18.5	2	0.02885	8536	125	SB?
	PGC 070458	ESO 469- G 011	23 05 49.22	-30 36 37.0	2	0.02837	8530	123	Pec
	NGC 7496	ESO 291- G 001	23 09 47.00	-43 25 38.0	2	0.00550	1625	23	(R':)SB(rs)bc
	NGC 7582	ESO 291- G 016	23 18 23.49	-42 22 12.5	2	0.00525	1553	22	(R'_1)SB(s)ab
	NGC 7590	ESO 347- G 033	23 18 54.95	-42 14 17.7	2	0.00526	1553	22	S(r?)bc

Note. - Basic properties of the Sy2 in the sample used in this study. Column (1) is the primary object name used in this paper and (2) an alternate name often found in the literature. The object coordinates in columns (3) & (4) are taken from SUMSSCAT v.2.1 and indicate the center of the fitted (as described in §2.2) region. AGN classification in column (5) is taken from NED or in some cases by the sources described above (§2.1) and §2.4. Redshifts listed in column (6) are taken from NED. See §2.5.1 for a definition of the recession velocity listed in column (7). Column (8) is the luminosity distance, defined in the previous paragraph. The host galaxy morphologies listed in column (9) are taken from NED. The presence of * next to the object name in column 1 indicates that the object was covered by the MGPS-2 survey, and ! indicates the object was censored at 843 MHz.

TABLE 2.2
Seyfert 1

	Name (1)	Alias (2)	R.A. (J2000) (3)	Decl. (J2000) (4)	Type (5)	z (6)	GCVel (km/s) (7)	D (Mpc) (8)	Host Classification (9)
	LEDA 087392	2MASX J00391586-5117013	00 38 54.35	-51 17 21.2	1.0	0.02800	8315	121	[[S?]]
	PGC 002450	ESO 012- G 021	00 40 45.42	-79 14 24.0	1.5 '	0.03002	8847	130	N galaxy
	PKS 0056-572	SUMSS J005846-565912	00 58 46.57	-56 59 12.3	1.0 '	0.01800	5293	77	
	PGC 003864	ESO 113- G 010	01 05 17.28	-58 26 15.0	1.8	0.02570	7596	111	(R_1)SB(rl)0/a
	IRAS 01089-4743	[VCV2001] J011109.7-472735	01 11 09.50	-47 27 45.1	1.0	0.02430	7205	105	E
	PGC 004822	ESO 244- G 017	01 20 19.85	-44 07 41.7	1.5	0.02350	6970	101	(R:)SB(r)a
	NGC 526A	IRAS 01216-3519	01 23 54.55	-35 03 53.8	1.9	0.01910	5676	82	S0pec?
	PMN J0133-5159	PKS 0131-522	01 33 05.62	-52 00 05.7	1.0	0.02000	5894	86	
!	ESO 080- G 005	2MASX J01473933-6609475	01 47 39.30	-66 09 47.0	1.8	0.02695	7941	116	S
	NGC 1097	ARP 077	02 46 19.08	-30 16 27.8	S1.0	0.00424	1190	18	(R'_1:)SB(r'l)b
!	PGC 011706	ESO 031- G 008	03 07 35.30	-72 50 03.0	1.2 '	0.02800	8228	121	Sa
	NGC 1365	ESO 358- G 017	03 33 36.40	-36 08 26.0	1.5 "	0.00546	1514	23	(R')SBb(s)b
	NGC 1566	ESO 157- G 020	04 20 01.21	-54 56 13.6	1.5 '	0.00502	1331	21	(R'_1)SAB(rs)bc
	PGC 017103	ESO 362-G018	05 19 35.51	-32 39 34.0	1.5	0.01245	3561	53	S0/a
!	FAIRALL 0265	IRAS 06563-6529	06 56 29.80	-65 33 38.0	1.2 '	0.02950	8631	128	Sa
*	LEDA 096433	IRAS 09026-3817	09 04 32.69	-38 29 05.6	1.0	0.01603	4576	69	S
!	PGC 027468	ESO 373- G 013	09 38 20.40	-33 51 46.0	1.0	0.00901	2477	38	S0/a? sp
!	PGC 029148	LEDA 623230	10 03 04.00	-37 25 50.0	1.0 '	0.02360	6852	102	[[Sb]]
!	PGC 029151	ESO 374- G 025	10 03 23.60	-37 23 45.0	1.0	0.02367	6874	102	S
!*	PGC 033084	ESO 215- G 014	10 59 19.10	-51 26 33.0	1.0	0.01901	5480	82	SB(rs)b
!	PGC 034101	ESO 377- G 024	11 12 34.00	-36 25 41.0	1.0	0.00977	2722	42	SA(rs)c: pec
	PGC 036002	ESO 216- G 024	11 37 44.78	-49 10 38.1	1.9	0.01691	4862	72	(R'_2)SAB(s)bc
	NGC 3783	ESO 378- G 014	11 39 01.70	-37 44 19.1	1.5 '	0.00973	2718	41	(R')SB(r)a
	LEDA 096527	IRAS 12288-4741	12 31 35.24	-47 57 54.0	1.0	0.02765	8101	119	S
	PGC 045371	ESO 323-G 077	13 06 25.89	-40 24 53.2	1.2	0.01501	4335	64	(R)SB(l)0^0
	PGC 047969	ESO 383- G 035	13 35 57.93	-34 20 10.2	1.5 '	0.00775	2182	33	E-S0
	PGC 049051	IC 4329A	13 49 19.23	-30 18 30.5	1.2	0.01605	4688	69	SA0+: sp
	PGC 050427	2MASX J14080674-3023537	14 08 06.80	-30 23 54.0	1.5 '	0.02355	6944	101	
	ESO 328- G036	[VCV2001] J151450.7-402023	15 14 44.78	-40 21 15.6	1.8 '	0.02370	7003	102	S0 + S0 pair
	PKS 1521-300	LEDA 141885	15 24 33.27	-30 12 24.2	1.0 '	0.01960	5806	84	Elliptical
*	LEDA 2793282	WKK 6092	16 11 51.40	-60 37 55.0	1.5 '	0.01564	4563	67	[[Sba]]
	PGC 062346	ESO 140- G 043	18 44 54.31	-62 21 51.2	1.5 '	0.01418	4163	61	(R'_2)SB(rs)b
	PGC 062554	ESO 025- G 002	18 54 41.73	-78 53 57.2	1.0	0.02888	8515	125	(R:)SAB(r)b
	ESO 399-IG 020	AM 2003-344	20 06 57.69	-34 32 42.7	1.0 '	0.02495	7508	107	
	NGC 6860	ESO 143- G 009	20 08 46.78	-61 05 57.2	1.5 '	0.01488	4385	64	(R')SB(r)ab
!	PGC 064989	MC 2031-307	20 34 31.35	-30 37 28.8	1.0	0.01900	5742	81	
!	ESO 235- G 059	[VCV2001] J210633.5-491308	21 06 33.70	-49 13 10.0	1.8	0.02490	7436	107	S0
!	CTS 0109	6dF J2132022-334254	21 32 02.20	-33 42 54.0	1.2	0.02929	8813	127	
!	PGC 067075	ESO 287- G 042	21 38 07.90	-42 36 17.0	1.8 '	0.01867	5593	80	S0
	NGC 7213	ESO 288- G 043	22 09 16.14	-47 10 00.9	1.5	0.00584	1725	25	SA(s)0^0
	[VV2003c] J224704.	311041.5	22 46 58.68	-30 55 21.3	1.0 '	0.01400	3030	43	
!	PGC 073028	AM 2354-304	23 57 28.00	-30 27 40.0	1.2	0.03029	9087	131	Sb pair

Note. - Basic properties of the Sy2 in the sample used in this study. Column (1) is the primary object name used in this paper and (2) an alternate name often found in the literature. The object coordinates in columns (3) & (4) are taken from SUMSSCAT v.2.1 and indicate the center of the fitted (as described in §2.2) region. AGN classification in column (5) is taken from NED or in some cases by the sources described above (§2.1) and §2.4. Redshifts listed in column (6) are taken from NED except for [VV2003c] J224704.9-305502 which is taken from Veron-Cetty & Veron (2001). See §2.5.1 for a definition of the recession velocity listed in column (7). Column (8) is the luminosity distance, defined in the previous paragraph. The host galaxy morphologies listed in column (9) are taken from NED. The presence of * next to the object name in column 1 indicates that the object was covered by the MGPS-2 survey, and ! indicates the object was censored at 843 MHz.

2.2 THE SUMSS

Bock et al. (1999) is a thorough discussion of the goals, design, and instrumentation of the SUMSS. For the sake of completeness I will review some of the details of the SUMSS catalog. However the reader is urged to read Mauch et al. (2003) for a full picture of that endeavor, including catalog completeness and reliability.

The Sydney University Molonglo Sky Survey (SUMSS) is a southern-sky ($\delta < -30°$ as well as $|b| > 10°$) survey at 843 MHz (~35.6 cm) using the Molonglo Observatory Synthesis Telescope (MOST) which is located near Canberra, Australia, and operated by the School of Physics at the University of Sydney. The MOST was constructed through a major modification of what was known as the One-Mile Mills Cross telescope. It consists of two 778 m x 12 m cylindrical paraboloids in an East-West alignment with a separation of 15 m.

The current version of the SUMSS catalog (SUMSSCAT 2008) is v.2.1. The SUMSS was completed in 2007. Each MOST observation in the SUMSS is a 12-hour synthesis covering a region with diameter 160' x 160cosec(|δ|)'. The images are then combined to produce the 4.3° x 4.3° mosaics. The resolution is 45" x 45cosec(|δ|)". Regions of the sky with $-50° < \delta < -30°$ are labeled as "northern", while the "southern" regions are defined as those with $\delta < -50°$.

The SUMSS has a limiting peak brightness of 6 mJy/beam for $\delta < -50°$ and 10 mJy/beam for $\delta > -50°$. The position accuracy in the SUMSS catalog is good to within 1-2 arcsec for those sources with peak brightness $A_{843} > 20$ mJy/beam and always within 10 arcsec for all other sources.

The internal flux density scale for the survey is accurate to within 3%. The median rms noise of the mosaics at $\delta < -50°$ is 1.27 mJy/beam and, as there is more scatter at $\delta > -50°$, the median rms is larger in such regions, approximately 1.9 mJy/beam. For the censored objects in the sample, as described further below, a total flux density of three times the above median rms noise is used.

The sources imaged in each mosaic are fitted with elliptical Gaussians using the VSAD routine in AIPS. This returns the following parameters, used in the catalog: α, δ (both J2000, in degrees), A_{843} (peak flux), S_{843} (total flux density), the FWHM fitted major & minor axes θ_M, θ_m, and the position angle P.A. The fitting uncertainties listed in the SUMSS catalog are computed using the relevant equations in Condon (1997). "All uncertainties calculated in the catalog are a combination of both fitting and calibration uncertainties of the MOST" (Mauch et al. 2003). In general though, it is the fitting uncertainties that tend to dominate. The errors for S_{843} are given in table 2.3 and 2.4 below.

Figure 2.1 below is taken from Mauch et al. (2003) and shows the distribution of the rms noise of the MOST as used in the SUMSS.

The SUMSS does not cover the region of sky near our galactic plane, |b| > 10°. This region was instead covered by a sister-project to the SUMSS, the second epoch Molonglo Galactic Plane Survey (MGPS-2). The same instrumentation was used as with the SUMSS, and resulted in a similar catalog. The primary reference paper on the MGPS-2 is Murphy et al. (2007). For the sample under study in this paper, the 843 MHz data for six Sy2 and three Sy1 were obtained from the MGPS-2 catalog (MGPSCAT 2007) because of their location in the sky. In Tables 2.1 and 2.2 above, in column (1) next to the objects name, * is used to denoted those objects covered by MGPS-2 and ! is used for those objects censored (not detected because their 843 MHz flux fell below the instrument sensitivity) in the SUMSS. One of the nine sample objects, PGC 033084, in the region of the sky covered by MGPS-2 was censored.

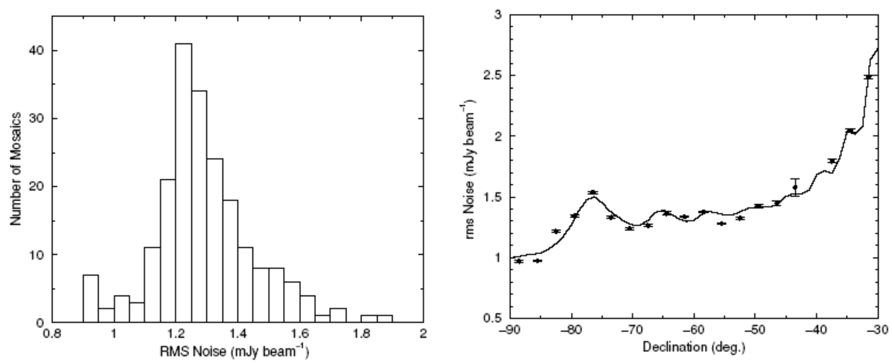

FIG. 2.1 - Analysis of the rms noise of the MOST, by count and declination. Taken from Mauch et al. (2003).

This thesis is in part an investigation of very large-scale extended radio emission of Seyferts using the data obtained from the SUMSS. The good sensitivity and (u, v)-plane coverage of the telescope (MOST) used to conduct the survey makes it an ideal instrument for such investigations. The data from the SUMSS is also of interest because it is at the largely unexplored wavelength ~ 35.6 cm. This unique view adds to what we already know about this type of AGN by filling in the gaps in wavelength coverage. For example, consider the Sy PGC 063874 (cz = 5756, with luminosity distance of 82.3 Mpc in a Sb host galaxy). The 843 MHz flux density contributes appreciably to the coverage of this Seyfert which is little studied at radio frequencies (Figure 2.2).

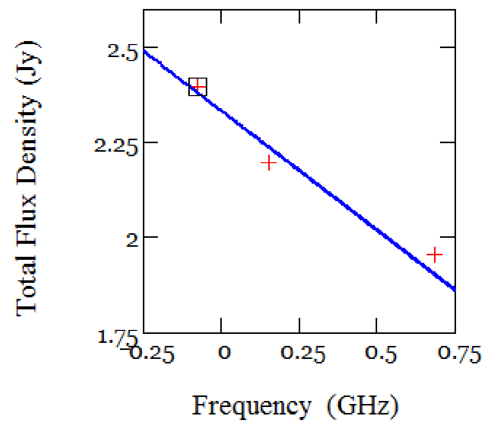

FIG. 2.2. – A log-log plot of all of the published radio total flux densities, in Jy, for the Sy2 PGC 063874. The value at 843 MHz is boxed. Using the Levenberg-Marquardt method for minimization (Marquardt 1963), the two parameter curve of best fit (shown in log scale) was computed to be $S(\nu) = 215.31\ \nu^{-0.623}$.

2.3 RADIO MAPS AND SUMSS DATA FOR THE SAMPLE

Figures A.1 - A.20 in Appendix A contain the 843 MHz radio contour maps for the entire sample (Sy2 shown first, in Figures A.1 - A.13). The images used are part of the relevant mosaics from the SUMSS. No additional processing was done. Negative contours (result of imaging cleaning, to help identify all true sources) are in blue and each image is centered on the coordinates given in Tables 2.1 and 2.2. Maps of the area around censored objects are also given. The brown ellipse on each map is the beam size of the MOST. The software application *kvis*, contained in the *Karma* package (ver. 1.7.25) was used to create the maps. The maps were created from the full SUMSS (or MGPS-2 as the case may be) mosaics, each being 4.3° x 4.3° in size with each (square) pixel covering 1 arcsec^2.

Tables A.1 and A.2 (Appendix A) give the contour levels for the radio maps contained in Figures A.1 - A.20. The contour levels are in multiples of the median rms error of the *processed SUMSS mosaics*, which as described §2.2, is taken to be 1.27 mJy ($\delta < -50°$) or 1.9 mJy ($\delta > -50°$). The median rms error value for each particular object is given in the tables, immediately following the highest contour level listed. Tables A.1 and A.2 also list the figure number in which a given map is located.

Tables 2.3 and 2.4 below contain the 843 MHz data for the sample, by type. Columns 2-7 were taken from SUMSSCAT v2.1, whereas columns 8-9 were derived from that data. The upper limits for the censored objects in the sample are conspicuous by the less-than symbol following the given total flux density vales in the tables.

The luminosities given in Tables 2.3 and 2.4 are computed from the total flux densities, $S_{843.}$ The luminosity values and their associated errors as discussed further in §2.5.3.

Following Tables 2.3 and 2.4, in §2.4, are some notes on individual objects, listed under the primary name given in Tables 2.1 and 2.2. This includes the primary sources used for identification and classification, comments on the published wavelength coverage for the object as listed (primarily) in NED, as well as details of any interesting aspects of the objects as revealed in the data and contour maps. Chapter 4 contains further discussion on any such noteworthy details noted in the maps.

Because of the resolution of the MOST, and the weak radio emission of Sys generally, most objects in the sample show up as essentially point-sources. Thirty of the 77 Sy2 in the sample (~39%) and 12 of the 42 Sy1 (~29%) have their 843 MHz flux density values listed in NED. However almost all of those are what are referred to in §2.4 as the "uncorrected SUMSS" value, as they are from one of the earlier releases of SUMSSCAT (before and including v.1.6) which had some significant fitting errors. The errors were fixed as of v.1.7. As noted earlier, SUMSS catalog 2008 v.2.1 is used for all analysis in this thesis.

A total of 63 Sy2 and 27 Sy1 of the 119 objects in the full sample were detected in the SUMSS (a detection rate of ~ 82% and ~ 64% by type, respectively). Of the 90 Sy detected, the majority (70 or ~78%) show up in the SUMSS as point sources. The remaining 20 objects (13 Sy2 and 7 Sy1) display morphologies that fall into two main categories which I will refer to as type A and B. The Sy1.2 Fairall 0265 is located (apparently) near a bright source and is thus obscured in the SUMSS mosaic.

Type-A are nearly point sources but with a "wing" at the 2-3*rms contour levels. An example would be PGC 005696 (Figure A.2, Appendix A). These all seem to be due either to 1) the bar or disk of the host galaxy (for the closest Sy), 2) other sources in the sky that happen to be near (apparently or literally) the Sy, or 3) a host galaxy that is actually an interacting pair of galaxies. Of the five Sy2 and two Sy1 displaying Type-A morphology, all but one (the Sy1.2 PGC 049051, host galaxy SA0+) are in barred spiral host galaxies or an interacting pair, and one (the Sy1 PMN J0133-5159) resides in an unknown type of host galaxy (no classification found in the literature).

Type-B morphology is observed almost exclusively in the closest Sy, particularly with a face-on or nearly face-on orientation of the host galaxy. The outer contours are not circular but rather distorted in a wavy pattern, primarily due to the fact that the host galaxies are so close to us; we are seeing a lot of emission from the disk and/or spiral arms of the host galaxy in addition to the central sources due to the AGN. An example of this type would be Circinus (Figure A.8, Appendix A). Of all eight of the Sy2 and five of the Sy1 that display this morphology, all close-by and have redshifts $z < 0.009$ with the exception of the Sy1 PKS 0056-572, which resides in an unknown/unpublished type of host galaxy at $z \sim 0.018$.

TABLE 2.3

SUMSS Data for the Seyfert 2

Name (1)	Peak Flux (mJy/b) (2)	err	Flux Density (mJy) (3)	err	a (arcsec) (4)	b (arcsec) (5)	b/a (6)	P.A. (deg.east) (7)	L (W/Hz) (8)	err	Log(L) (W/Hz) (9)
LEDA 087391	31.1	1.3	32.5	1.4	54.3	47.3	0.871	102.6	6.22E+22	2.68E+21	22.79
NGC 0424	22.4	1.2	22.4	1.2	76.6	50.1	0.654	57.2	6.73E+21	3.60E+20	21.83
LEDA 093365			5.7	<					8.57E+21	<	21.93
PGC 004440	41.5	2.2	46.2	2.4	94.0	45.9	0.488	3.5	1.43E+22	7.44E+20	22.16
NGC 0454	46.6	1.6	51.3	1.8	54.3	51.9	0.956	57.2	1.65E+22	5.78E+20	22.22
PGC 004569	12.0	0.8	13.7	0.9	62.7	48.0	0.766	156.3	1.80E+22	1.18E+21	22.26
PGC 005696	41.2	1.9	46.0	2.1	84.9	70.1	0.826	30.4	2.74E+22	1.25E+21	22.44
PGC 006078	51.9	1.9	53.9	2.0	70.0	50.1	0.716	118.1	7.59E+22	2.82E+21	22.88
PGC 006351	14.0	0.0	14.0	1.6	84.9	50.8	0.598	57.4	2.73E+22	3.12E+21	22.44
PGC 008012	10.8	0.9	10.9	0.9	54.3	46.0	0.847	110.9	9.33E+21	7.71E+20	21.97
NGC 0824			5.7	<					4.71E+21	<	21.67
PGC 009634	39.5	1.6	39.5	1.6	76.6	45.2	0.590	84.7	2.48E+22	1.01E+21	22.40
PGC 010665	26.4	1.9	26.4	2.0	84.9	46.1	0.543	174.9	2.22E+22	1.68E+21	22.35
PGC 010705	28.5	1.7	30.2	1.8	70.0	47.7	0.681	88.1	1.84E+22	1.09E+21	22.26
PGC 011104			5.7	<					3.31E+21	<	21.52
PGC 012759	20.9	1.1	20.9	1.1	52.0	45.1	0.867	85.5	1.57E+22	8.28E+20	22.20
NGC 1386	42.8	2.3	42.8	2.3	76.6	45.6	0.595	77.9	7.75E+20	4.16E+19	20.89
PGC 014702	84.8	3.0	84.8	3.0	84.9	51.3	0.604	168.9	2.62E+22	9.26E+20	22.42
AM 0426-625	17.0	1.2	19.0	1.4	55.6	45.2	0.813	11.5	1.40E+22	1.03E+21	22.15
PGC 015172	136.8	4.2	152.9	4.7	60.6	51.4	0.848	74.4	9.12E+22	2.80E+21	22.96
NGC 1672	186.2	5.8	291.7	12.8	61.5	59.8	0.972	109.7	1.23E+22	5.41E+20	22.09
PGC 016072			3.8	<					4.42E+21	<	21.65
PGC 016357	10.6	1.0	10.6	1.0	46.4	45.0	0.970	83.0	7.62E+21	7.19E+20	21.88
NGC 1808	671.6	20.2	805.3	24.2	76.6	67.2	0.877	141.6	1.92E+22	5.76E+20	22.28
PGC 016873			5.7	<					3.09E+21	<	21.49
PGC 017768			5.7	<					7.90E+21	<	21.90
LEDA 096373	243.2	7.5	247.0	7.7	76.6	46.1	0.602	100.1	4.77E+23	1.49E+22	23.68
PGC 021057	11.3	0.9	19.3	2.7	82.6	45.1	0.546	177.4	6.05E+21	8.47E+20	21.78
PGC 023573	28.1	1.3	30.3	1.4	49.3	45.1	0.915	28.3	2.11E+22	9.75E+20	22.32
PGC 028144	27.6	1.7	31.3	1.9	95.4	46.2	0.484	5.2	4.88E+21	2.96E+20	21.69
PGC 028147	10.5	1.3	12.3	1.5	99.1	45.5	0.459	3.7	2.33E+21	2.84E+20	21.37
PGC 029778	89.4	3.1	89.5	3.1	76.6	46.0	0.601	5.0	1.61E+23	5.59E+21	23.21
PGC 029993	37.4	1.7	37.8	1.8	84.9	49.4	0.582	170.5	7.79E+21	3.71E+20	21.89
PGC 030984	12.0	2.3	19.0	3.6	91.2	76.9	0.843	137.5	7.78E+21	1.47E+21	21.89
NGC 3281	90.8	3.2	90.9	3.2	76.6	45.0	0.587	91.5	2.25E+22	7.93E+20	22.35
LEDA 088648			5.7	<					1.16E+22	<	22.07
NGC 4507	68.7	2.3	89.1	3.0	75.0	55.9	0.745	112.8	2.70E+22	9.08E+20	22.43
PGC 042504	97.2	3.2	110.0	3.6	76.6	58.0	0.757	52.9	2.90E+22	9.47E+20	22.46
WKK 1263	21.3	1.1	21.7	1.1	54.8	45.9	0.838	167.3	2.87E+22	1.45E+21	22.46
PGC 043779			5.7	<					3.19E+21	<	21.50
NGC 4785	56.4	2.0	82.1	2.9	63.6	62.4	0.981	93.2	2.69E+22	9.49E+20	22.43
PGC 044167			5.7	<					3.50E+21	<	21.54
NGC 4903	11.9	1.9	14.7	2.3	84.9	72.3	0.852	145.1	8.72E+21	1.36E+21	21.94
NGC 4945	5386.0	161.6	5549.0	165.5	60.6	53.2	0.878	35.0	4.14E+22	1.24E+21	22.62
ESO 383- G 018	10.5	1.5	12.0	1.7	85.0	48.5	0.571	9.7	4.02E+21	5.69E+20	21.60
Circinus	1019.0	30.6	1640.0	65.7	60.7	59.8	0.985	100.5	7.30E+21	2.93E+20	21.86
LEDA 141858			3.8	<					5.80E+21	<	21.76
NGC 5643	67.1	2.3	203.5	8.5	97.0	91.3	0.941	86.5	6.95E+21	2.90E+20	21.84
PGC 052101	11.0	1.6	11.0	1.6	84.9	67.1	0.790	27.8	1.58E+22	2.29E+21	22.20

TABLE 2.3 - Continued											
SUMSS Data for the Sy2											
Name (1)	Peak Flux (mJy/b) (2)	err	Flux Density (mJy) (3)	err	a (arcsec) (4)	b (arcsec) (5)	b/a (6)	P.A. (deg.east) (7)	L (W/Hz) (9)	err	Log(L) (W/Hz) (10)
LEDA 166339			3.8	<					5.64E+21	<	21.75
IC 4518	203.9	6.2	245.3	7.5	64.8	55.5	0.856	108.1	1.33E+23	4.05E+21	23.12
WKK 3646			3.8	<					1.82E+21	<	21.26
PGC 058547	99.7	3.2	111.9	3.6	52.0	51.1	0.983	128.4	2.03E+22	6.52E+20	22.31
PGC 059124	44.1	1.8	51.0	2.1	52.2	51.8	0.992	82.1	9.23E+21	3.80E+20	21.97
NGC 6221	168.0	5.1	420.0	15.0	80.0	73.7	0.921	29.9	2.26E+22	8.07E+20	22.35
NGC 6300	24.6	1.2	102.1	6.1	109.9	85.5	0.778	118.2	3.01E+21	1.80E+20	21.48
PGC 060594	11.5	1.3	17.3	2.0	68.4	51.6	0.754	52.4	1.10E+22	1.27E+21	22.04
PGC 062134	264.4	8.0	270.3	8.2	52.0	46.9	0.902	110.9	2.44E+23	7.39E+21	23.39
PGC 062174	32.8	1.6	34.7	1.7	50.1	47.7	0.952	78.4	1.33E+22	6.54E+20	22.13
PGC 062218			3.8	<					1.82E+21	<	21.26
PGC 062428	46.4	1.8	59.7	3.5	56.4	51.7	0.917	151.2	2.98E+22	1.75E+21	22.47
PGC 062440	28.1	1.2	28.1	1.2	57.1	45.5	0.797	8.6	2.12E+22	9.05E+20	22.33
NGC 6810	147.2	4.5	201.4	9.1	64.7	49.6	0.767	169.1	2.00E+22	9.03E+20	22.30
PGC 063874	218.0	6.7	247.4	7.6	70.0	56.6	0.809	124.7	2.00E+23	6.16E+21	23.30
NGC 6890	29.5	1.3	38.7	1.7	67.8	59.0	0.870	127.7	5.45E+21	2.39E+20	21.74
PGC 064491	13.5	0.9	13.5	0.9	57.1	46.5	0.814	165.2	7.65E+21	5.10E+20	21.88
PGC 064537			5.7	<					4.65E+21	<	21.67
PGC 065600	1930.0	57.9	1975.0	59.3	54.3	46.6	0.858	73.6	5.51E+23	1.66E+22	23.74
NGC 7130	205.3	6.4	225.0	7.0	76.6	53.4	0.697	60.6	1.29E+23	4.00E+21	23.11
NGC 7172	45.6	1.7	45.6	1.7	84.9	45.9	0.541	177.5	7.43E+21	2.77E+20	21.87
PGC 068122	11.8	1.7	11.8	1.7	76.6	62.8	0.820	31.0	5.53E+21	7.97E+20	21.74
PGC 068198	26.3	1.6	28.1	1.7	76.6	55.6	0.726	128.7	6.57E+21	3.97E+20	21.82
FAIRALL 0357	12.3	1.0	16.5	1.3	62.2	46.0	0.740	39.6	3.07E+22	2.41E+21	22.49
PGC 070458	36.2	1.9	36.2	1.9	84.9	51.4	0.605	169.0	6.50E+22	3.41E+21	22.81
NGC 7496	30.4	1.3	39.9	1.7	64.8	62.7	0.968	126.0	2.59E+21	1.10E+20	21.41
NGC 7582	323.5	9.8	395.3	12.0	67.5	56.4	0.836	146.3	2.35E+22	7.14E+20	22.37
NGC 7590	50.6	2.3	78.0	3.5	73.4	65.2	0.888	41.7	4.64E+21	2.08E+20	21.67

Note. - Radio properties of the Sy2 in the sample.

TABLE 2.4

SUMSS Data for the Sy1

Name (1)	Peak Flux (mJy/b) (2)	err	Flux Density (mJy) (3)	err	a (arcsec) (4)	b (arcsec) (5)	b/a (6)	P.A. (deg.east) (7)	L (W/Hz) (9)		Log(L) (W/Hz) (10)
LEDA 087392	276.5	8.3	278.6	8.4	57.1	46.3	0.811	167.7	4.86E+23	1.47E+22	23.69
PGC 002450	26.7	1.2	28.8	1.3	48.4	45.9	0.948	69.2	5.81E+22	2.62E+21	22.76
PKS 0056-572	463.6	13.9	479.4	14.4	54.3	48.5	0.893	34.4	3.41E+23	1.02E+22	23.53
PGC 003864	13.9	1.0	13.9	1.0	52.0	48.4	0.931	140.2	2.04E+22	1.47E+21	22.31
IRAS 01089-4743	10.1	1.0	13.9	1.3	78.2	49.7	0.636	26.1	1.82E+22	1.70E+21	22.26
PGC 004822	10.2	1.1	11.8	1.3	64.8	56.1	0.866	58.0	1.44E+22	1.59E+21	22.16
NGC 526A	13.6	1.3	15.4	1.5	86.0	46.4	0.540	174.8	1.24E+22	1.20E+21	22.09
PMN J0133-5159	351.9	10.6	366.4	11.0	57.1	49.4	0.865	59.4	3.23E+23	9.69E+21	23.51
ESO 080- G 005			3.8	<					6.14E+21	<	21.79
NGC 1097	277.4	8.6	344.4	10.6	84.9	56.7	0.668	101.3	1.34E+22	4.11E+20	22.13
PGC 011706			3.8	<					6.65E+21	<	21.82
NGC 1365	534.0	16.1	641.2	19.3	77.1	54.2	0.703	78.0	4.09E+22	1.23E+21	22.61
NGC 1566	57.4	2.0	299.5	11.7	131.4	98.6	0.750	145.0	1.63E+22	6.35E+20	22.21
PGC 017103	20.1	2.0	20.1	2.0	84.9	67.1	0.790	27.4	6.78E+21	6.75E+20	21.83
FAIRALL 0265			3.8	<					7.39E+21	<	21.87
LEDA 096433	13.2	2.2	15.8	2.6	70.0	59.9	0.856	144.4	8.87E+21	1.46E+21	21.95
PGC 027468			5.7	<					1.00E+21	<	21.00
PGC 029148			5.7	<					7.03E+21	<	21.85
PGC 029151			5.7	<					7.07E+21	<	21.85
PGC 033084			3.8	<					3.02E+21	<	21.48
PGC 034101			8.0						1.66E+21	0.00E+00	21.22
PGC 036002	29.7	1.3	34.5	1.5	66.4	48.2	0.726	12.1	2.16E+22	9.41E+20	22.34
NGC 3783	54.0	1.9	58.4	2.1	76.6	53.9	0.704	122.5	1.20E+22	4.31E+20	22.08
LEDA 096527	38.7	1.6	48.0	1.9	64.3	55.0	0.855	137.9	8.17E+22	3.24E+21	22.91
PGC 045371	48.0	1.9	48.0	1.9	70.0	45.9	0.656	5.2	2.37E+22	9.37E+20	22.37
PGC 047969	110.1	3.8	110.1	3.8	76.6	56.7	0.740	20.6	1.43E+22	4.92E+20	22.15
PGC 049051	79.7	3.0	79.7	3.0	84.9	64.5	0.760	32.2	4.50E+22	1.69E+21	22.65
PGC 050427			5.7	<					7.00E+21	<	21.85
ESO 328- G036	11.8	1.3	15.0	1.6	72.3	56.2	0.777	70.5	1.86E+22	1.99E+21	22.27
PKS 1521-300	176.9	5.6	177.0	5.6	84.9	54.8	0.645	13.5	1.49E+23	4.73E+21	23.17
LEDA 2793282			3.8	<					2.03E+21	<	21.31
PGC 062346	14.7	1.1	15.8	1.2	50.1	49.0	0.978	117.9	6.92E+21	5.26E+20	21.84
PGC 062554	9.2	1.3	11.6	1.6	57.3	45.2	0.789	146.4	2.16E+22	2.98E+21	22.33
ESO 399-IG 020	12.7	1.3	14.3	1.5	76.6	52.2	0.681	107.7	1.97E+22	2.07E+21	22.30
NGC 6860	17.9	1.1	18.8	1.2	52.0	48.8	0.938	135.7	9.10E+21	5.81E+20	21.96
PGC 064989			5.7	<					4.52E+21	<	21.66
ESO 235- G 059			5.7	<					7.84E+21	<	21.89
CTS 0109			5.7	<					1.09E+22	<	22.04
PGC 067075			5.7	<					4.36E+21	<	21.64
NGC 7213	98.0	3.1	119.6	3.4	61.3	54.6	0.891	78.5	8.80E+21	2.50E+20	21.94
[VV2003c] J224704	86.2	3.5	88.3	3.6	84.9	65.1	0.767	146.4	1.92E+22	7.82E+20	22.28
PGC 073028			5.7	<					1.17E+22	<	22.07

Note. - Radio properties of the Sy1 in the sample.

2.4 NOTES ON INDIVIDUAL OBJECTS

LEDA 087391

Point source in the SUMSS, though at the 2*rms contour there appears to be a faint source extending off to the west. Extent is approximately 106 pixels = 106". At 0.579 kpc/" this gives a length of ~61.4 kpc. Emission looks to be due to another close (apparently) to the galaxy. This Sy2, listed in [2] and [4], is near the redshift cutoff for this sample, with z = 0.02929. No morphological classification for the host galaxy has been published that could be found, though the published optical (468 nm) and 2MASS J-H-K_s composite and images in NED suggests what is perhaps a large bar. However the resolution of both is fairly low and the observed structure could the result of a disturbed/interacting system. No *IRAS* IR data listed in NED but there is a value from 2MASS. It is a weak IR source, S_{Jtot} ~ 0.00575 Jy. The only radio data listed is the (uncorrected) value from the SUMSS.

NGC 0424

Point source in the SUMSS. This is a long and frequently studied galaxy (127 references in NED going back to 1974), though mostly at IR and X-ray wavelengths. The only radio data in NED other than from the (uncorrected) SUMSS is at 1.4 GHz. This object is a warm IR Seyfert (de Grijp et al. 1987). Also listed in [2], [3], and [4].

LEDA 093365

Non-detection in the SUMSS. The only other data points for this Seyfert in NED are two optical and one radio (1.4 GHz ATCA). No published morphological classification for host galaxy could be found, though the one published image found in NED (optical at 468 nm) suggests a disturbed system/ interacting pair of galaxies. Listed in [2], and [4].

PGC 004440

Point source in the SUMSS. This object, listed [1], [4] and [5], shares a 2*rms contour with the (apparently) nearby spiral galaxy ESO-LV 3520242. This is a well-studied Sy but mostly just optical and IR measurements published. Only two other radio measurements other than the (uncorrected) SUMSS are listed in NED.

NGC 0454

Slight deviation from point source morphology at 843 MHz; slightly extended emission to south-east. This is because the host galaxy is a merging/interacting pair of galaxies. Several published studies on this point and on the spectroscopy of the system. Listed [1], and [4]. Little photometric data listed in NED; only those from *IRAS* and two data points at optical wavelengths.

PGC 004569

Point source in the SUMSS. This Sy2 is a weak radio source, with a total flux density at 843 MHz of just 13.7 mJy (~3.5 times the upper limit of 3.8 mJy). No other radio data listed in NED, however there are several optical and IR photometric data points. Host is (SB) ring galaxy. Listed in [1], [2], and [3].

PGC 005696

Type-A morphology in the SUMSS. This Sy2, listed in [1], [2], [4], and [5], is in a barred spiral host galaxy that is relatively close (z ~ 0.016). The bar of the host galaxy is evident here with extended emission running from the southwest to the northeast, with largest linear extent (at 2*rms) of 240 pixels = 240". At 0.332 kpc/" this gives a length of ~79.7 kpc. Only one radio point (1.4 GHz) other than the (uncorrected) SUMSS listed in NED, though it has been studied quite extensively, mainly optical and IR.

PGC 006078

Point source in the SUMSS. This Sy2 is listed in [2], [4], and several other (X-ray and optical) galaxy catalogs. Several IR and optical photometric data points in NED, but only one radio data point (1.4 GHz).

PGC 006351

Point source in the SUMSS. This Sy, at z = 0.02955, is near the z cutoff limit for the sample and is a weak radio source (S = 14.0 mJy). Only one radio point (1.4 GHz) published, aside from the (uncorrected) SUMSS, though several optical and IR photometric data points listed in NED. Listed in [1], [4], and [5], among others.

PGC 008012

Point source in the SUMSS. This Sy2 is one of the five weakest radio sources in the sample (10.9 mJy). Listed in [2], [3], and [4]. Several optical and IR photometric data points in NED and one radio, the (uncorrected) value from SUMSS.

NGC 0824

Non-detection in the SUMSS. A well-studied Sy2. Listed in [2], [4], and [5]. Only one radio point (1.4 GHz), those from 2MASS in the IR, and a few at optical wavelengths, are listed in NED.

PGC 009634

Point source in the SUMSS. SIMBAD lists this AGN as Sy1, due to Koulouridis et al. (2006). But [1] - [3] and several others list it as Sy2 and that classification has been adopted. *IRAS*, 2MASS, a few optical, and one radio (1.4 GHz) data point listed in NED.

PGC 010665

Point source in the SUMSS. A fairly well studied Sy2, listed in [1], [2], and [4], among others. Other than at IR wavelengths there are only a few optical and only one radio, the (uncorrected) SUMSS data point, listed in NED.

PGC 010705

Point source in the SUMSS. This Sy2 is listed in [1], [2], [4], and [5], among several others. This object has been studied quite a bit in the IR. There are however no other photometric data points listed in NED aside from a few at optical wavelengths.

PGC 011104

Non-detection in the SUMSS. The weakest Sy in the sample at 60 microns (S = 184.3 mJy). A fairly well studied Sy2, it is in [1], [2], [4], and [5]. Also a sample object in Nagar et al. (1999), an important radio study of Sy often referenced in this paper. No radio data in NED, only those from the 2MASS and *IRAS* in the IR, and a few at optical wavelengths.

PGC 012759

A fairly weak, point source in the SUMSS. This Sy2 has no radio data listed in NED other than the (uncorrected) SUMSS. Listed in [1], [2], [3], and [4] among others.

NGC 1386

Point source in the SUMSS. This nearby (*z* ~ .0029) AGN is one of the most extensively studied Sy2 with over 240 references in NED as of the time of this writing. Among many others, it is listed in [1], [2], [3], [4], and [5]. Over 90 photometric data points listed in NED with fairly thorough coverage from X-ray to radio. Five of the latter, in addition to the (uncorrected) SUMSS, though the points are all clustered around 20 and 6 cm. This object is the second least luminous Sy2 in this sample at 843 MHz , with log L ~ 20.89 W/Hz.

PGC 014702

Point source in the SUMSS. This Sy2 is listed in [2], [4], and [5], among others. Good IR coverage listed in NED, though only a few optical and two radio data points (around 21 cm).

AM 0426-625

Apparent extended region (at 2 and 4*rms) in the SUMSS from an otherwise point source; this object is actually an interacting pair of S0 peculiar galaxies. Very little is published on this pair. Listed in SIMBAD (from [2]) as Sy2. That database also lists one optical point (V = 13.0 mag). There are no photometric data points or spectra listed in NED.

PGC 015172

In the SUMSS this Sy2 (also known as the Carafe Nebula) displays a double lobe-type morphology (at 2,4,8,12 and 16*rms), extending down to the southeast and southwest from the central point source emission. Rifatto et al. (2001) suggest this interesting morphology, previously thought to be due to an asymmetric bar, is actually a result of a merger between two AGN. Max length measured from SUMSS radio map (from 2*rms contour across to 2*rms contour) is ~176 pixels = 176''. At 0.331 kpc/'' this gives a length of ~58.3 kpc. Only IR and optical data points listed in NED, though it is a fairly well studied AGN. It is found in [1], [2], [3], and [4], among others.

NGC 1672

Type-B morphology in the SUMSS. This nearby (*z* ~ 0.004) Sy2 is in a nearly face-on barred spiral host galaxy. Extensively studied (220 references in NED) at most of the commonly observed wavelengths from X-ray to radio, including the (uncorrected) SUMSS. Listed as Sy2 in [1], [2], [3], among many others. Sosa-Brito et a. (2001) argue for LINER classification. Considered an ultraluminous at X-ray wavelengths (Liu & Bregman 2005). This object was observed using the

MOST before (Subrahmanya & Harnett 1987), with a reported flux density of 350 mJy, a value 16.7% higher than reported in the SUMSSCAT v2.1. See Table 4.1.

PGC 016072

Non-detection in the SUMSS. This Sy2 is listed in [1], [2], and [4]. A nearly face-on barred spiral host galaxy with two major, very tightly wound, arms. Few photometric data points listed in NED; only 2MASS and a few optical, aside from one HI line measurement (1.42 GHz).

PGC 016357

Point source in the SUMSS. This Sy2 is weak at 843 MHz (S = 10.6 mJy). Listed in [1], [2], [3], and [4]. Optical, IR and a couple of X-ray data points listed in NED, along with the (correct) SUMSS value.

NGC 1808

Type-B morphology in the SUMSS. This nearby (z ~ 0.008) Sy2 resides in a barred spiral host galaxy. At 2*rms the longest contiguous extended region of radio emission is ~560 pixels = 560". At .068 kpc/" that gives ~ 38 kpc. Strong in the IR; *IRAS* 60 micron total flux density is 87.81 Jy, fourth strongest Sy2 in this sample at 843 MHz. One of the most studied objects in this sample, with 345 references in NED going back 50 years, not counting the NGC catalog from Dreyer (1888). Listed in [1], [2], [3], and [4], among many others. As quoted from Eskridge et al. (2002) ; "Very bright nuclear point source embedded in a short, faint bar that is further embedded in a boxy bulge, with a short, faint bar. At high surface brightness, bulge has a "lemon" morphology. At lower surface brightness, the bulge becomes strongly boxy..."

PGC 016873

Non-detection in the SUMSS. Listed in [1], [2], [3], and [4], among others. Several optical and IR data points in NED but only one other radio point (1.4 GHz).

PGC 017768

Non-detection in the SUMSS. This Sy2 is listed in [2] and [4]. Close to the redshift cut-off, with z = .025. Several optical and IR data points listed in NED but only one other radio point (1.4 GHz).

LEDA 096373

Point source in the MGPSCAT (b ~ -9.076232), though shares 2, 3 and 4*rms contours with several (apparently) nearby, fairly strong point sources. This Sy2, listed in [2] and [4]. is the eighth strongest sample object at 843 MHz and the third farthest (z = .0294). No optical, two (non-SUMSS) radio, and several IR (2MASS and *IRAS* data), are the only data points listed in NED.

PGC 021057

Point source in the SUMSS. This Sy2 is listed in [2] and [4]. Not listed as Sy in NED. Weak at 843 MHz (S = 19.3 mJy). *IRAS* and 2MASS data points listed in NED, along with a few optical points.

PGC 023573

Point source in the SUMSS. This Sy2 is listed in [1], [2], [3], and [4]. No radio points listed in NED aside from the (uncorrected) SUMSS. Very few optical, but both *IRAS* and 2MASS in the IR.

PGC 028144

Point source in the SUMSS, though the 2*rms contour level is shared by nearby source. Listed in [1], [2], [5], and Nagar et al. (1999) among many others. A well-studied Sy2, with over 89 photometric data points in NED, though most are in the IR (no *IRAS*) and X-ray, along with two radio points, at 6 and 20 cm. This AGN is bright at X-ray wavelengths, and variable; Mattson & Weaver (2004) have recorded a factor of six change in the 2-10 keV flux over a span of several months, from ~2×10^{-11} ergs cm^{-2} s^{-1} (low state) to more than 12×10^{-11} ergs cm^{-2} s^{-1}.

PGC 028147

Point source in the SUMSS. This Sy2 is a weak radio source at 843 MHz (S = 12.3 mJy). Listed in [1], [2], and [4]. 2MASS data points are listed in NED, along with a few optical. No *IRAS* or points at other wavelengths except for a HI line measurement (21 cm line).

PGC 029778

Nearly a point source in the SUMSS. This Sy2 is in a well-defined, barred-spiral host galaxy and one of the most distant (z ~ 0.028), and fifth most luminous (Log L ~ 23.21 W/Hz) Sy2 in the sample. There is a ~ 65 pixel = 65" (at 0.563 kpc/" this gives a length of ~36.6 kpc) extended region to the south-west at just 2 and 3*rms which appears to be unrelated background source(s). Listed in [2] and [4]. Only *IRAS* and 2MASS IR data points, in addition to a few in the optical, listed in NED.

PGC 029993

Point source in the SUMSS. This fairly-well studied Sy2 (73 references in NED) is listed in [1], [2], and [3] among others. Several optical and IR (*IRAS* and 2MASS) data points in NED, along with one radio (HI 21cm line).

PGC 030984

Non-point source in the SUMSS. This barred, ringed host galaxy (Sab(rs), $z \sim 0.014$), is listed in SIMBAD (from Bonato & Pastoriza (1997)), as ESO 436- G 09 but that was a typo; at the given coordinates we really find ESO 436- G 029. The apparent extended region to the south-east seems to be due to the one dominant spiral arm of the host galaxy. Also listed in [4], and de Vaucouleurs et al. (1991), the RC3 catalog. *IRAS*, 2MASS, several optical, and one radio point (HI 21cm line) listed in NED.

NGC 3281

Point source in the SUMSS. This well-studied Sy2 is listed in [1], [2], [3], [4], and [6], among many others including the RC3. There are 153 photometric data points listed in NED, most in the IR (both *IRAS* and 2MASS) and several others at optical and X-ray wavelengths. Only two (non-SUMSS) radio points listed though, a 1.4 GHz and HI 21cm line measurement.

LEDA 088648

Non-Detection in the SUMSS. This is the most distant ($z = 0.03020$, luminosity distance ~130.6 Mpc) Sy2 in the sample and second most distant Sy overall in this sample. Listed in [2] and [4]. *IRAS* and 2MASS IR and few X-ray data points listed in NED, but no optical or radio.

NGC 4507

Point source in the SUMSS. This is a well studied Sy2, with 82 data points (wide coverage though only the HI 21cm line measurement at radio wavelengths) and 232 references in NED. Listed in [1], [2], [3], [4], and [6] , among many others.

PGC 042504

Point source in the SUMSS, though the 2 and 4*rms contour levels are shared with the barred spiral galaxy ESO 381- G 009 which is slightly in front of (relative to us), and just to the north-east of, PGC 042504. This is a fairly well-studied Sy2, with over 132 references and 62 photometric data points in NED. The coverage is good from X-ray through IR. However only H1 (21cm line) and 1.4GHz data at radio wavelengths. Listed in [2], and [3], among many others.

WKK 1263

Point source in the SUMSS. This Sy2, listed in [2], has little data in either NED or SIMBAD. The only photometric data points listed are the 2MASS in the IR and one X-ray (17-60 keV from INTEGRAL). Since b ~ 5.011534, the 843 MHz data are from MGPSCAT.

PGC 043779

Non-detection in the SUMSS. This Sy2 is listed in [2], [3], [4], and the RC3 among several others. The only data points listed in NED are *IRAS* and 2MASS in the IR, and several optical.

NGC 4785

Point source in the SUMSS. This Sy2 is listed in [2], [4], and RC3 among others. In NED there are *IRAS* and 2MASS data points, and several optical. At radio wavelengths only HI 21cm line and (uncorrected) SUMSS.

PGC 044167

Non-Detection in the SUMSS. However, the upper limit used must be very close to actual flux density, as this Sy2 does barely show up in SUMSS mosaic at 1, 2, and 3*rms. Listed in [2], [4], and RC3 among others.

NGC 4903

Point source in the SUMSS. This Sy2 is listed in [2], [3], [4], and the RC3 among others. Faint (S = 19.3 mJy) radio source at 843 MHz. Several optical and IR (both *IRAS* and 2MASS) data points listed in NED but that is all, except for HI 21cm line measurement.

NGC 4945

Type-B morphology in the SUMSS; lots of detail in SUMSS radio map due to the disk of the host galaxy. This Sy2, a large barred spiral host galaxy, is the second closest Sy (z ~ 0.0019) in the entire sample, with luminosity distance of ~7.9 Mpc (The Sy2 Circinus, at 6.1 Mpc, is the closest). This object has the largest flux density in this sample (at 843 MHz), S = 5549 mJy, and is comparatively fairly luminous with Log L ~ 22.6 W/Hz. As discussed in Goulding & Alexander (2009), at optical wavelengths this galaxy has been identified as a starburst galaxy; only Mid-IR spectroscopy reveals the AGN activity. Extensively studied (388 references and 76 photometric data points) in NED, with pretty good wavelength coverage; seven radio points in addition to earlier measurements at 843 MHz from the MOST. Listed in [2], [3], and many others. The modern, published, research on this galaxy goes back to the 1950s. This object was observed using the MOST before (Subrahmanya & Harnett 1987), with a reported flux density of 8300 mJy; a value 33.1% higher than reported in the SUMSSCAT v2.1. See Table 4.1.

ESO 383- G 018

Point source in the SUMSS. Listed in [2], and [3]. A weak (S = 12 mJy) radio source at 843 MHz. Not much coverage in NED; no radio, one X-ray, a few optical, however both *IRAS* and 2MASS coverage in the IR.

Circinus

Type-B morphology in the MGPSCAT (b ~ -3.807809). This Sy2 is the closest to the Milky Way (z ~ 0.00145 which gives luminosity distance of ~ 6.1 Mpc) in this sample. Extensively studied galaxy, with over 286 references and 98 photometric data points (good coverage from X-ray to radio) in NED at the time of this writing. Listed in [2], [4], RC3 and many others. Third strongest 843 MHz source (flux) in this sample (behind NGC 4945 and IC5063), as would be expected for a large galaxy so close to us. Largest 2*rms measure (NE to SW) is ~620 pixels = 620". At .03 kpc/" this gives ~18.6 kpc. This object was observed using the MOST before (Subrahmanya & Harnett 1987), with a reported flux density of 2300 mJy, a value 28.7% higher than reported in the SUMSSCAT v2.1. See Table 4.1.

LEDA 141858

Non-detection in the SUMSS (though it must be fairly close detection limit, as it does show up at 1 and 2*rms contours). This Sy2 is listed in [2], and [4]. It has not been extensively studied; only 11 references in NED and the only photometric data points listed are from *IRAS* and 2MASS in the IR.

NGC 5643

Type-B morphology in the SUMSS. This Sy2, listed in [1], [2], [4], and RC3 among many others, resides in a large, nearby (z ~ .004) barred spiral; much of the disk shows up in SUMSS image. Well studied galaxy with 227 references in NED and 79 photometric data points, with good coverage from X-ray to radio.

PGC 052101

Point source in the SUMSS, and faint (S = 11.0 mJy). This Sy2 is listed in [2], [3], and [4], among a few others. The only photometric data points listed in NED are from *IRAS* and 2MASS.

LEDA 166339

Non-detection in the SUMSS. This Sy2 is listed in [2], and [4]. The only photometric data points listed in NED at from 2MASS.

IC 4518

Nearly a point source in the SUMSS. This Sy2 is actually composed of an interacting pair of Sc peculiar galaxies, causing the slightly distended morphology observed at 843 MHz. It is not listed in any of the databases, catalogs, or papers used for the rest of the sample. The classification as Sy2 is due to Beckmann et al. (2006), and references therein, which is study of the hard X-ray (20-40 keV, as measured by INTEGRAL) AGN luminosity function in the local universe (z < 0.022). In fact the only data points listed in NED for this galaxy aside from the INTEGRAL values are those from *IRAS*, and one radio point (VLA 1.425 GHz). A bright source in SUMSS (S = 245.3 mJy) and sixth most luminous in the sample at 843 MHz, with log L ~ 23.12 W/Hz.

WKK 3646

Non-detection in the SUMSS. Listed as Sy2 in [2], also investigated in Fairall et al. (1998). Only five other references, and few optical, and one radio (HI 21cm line) data point listed in NED.

PGC 058547

Type-B morphology in the MGPSCAT (b ~ -7.096980) ; lots of detail in SUMSS radio map due to the disk of the host galaxy. This Sy2, z ~ 0.009, resides in a barred spiral host galaxy. It is listed in [1], [2], and RC3 among others. Fairly thorough coverage in NED; photometric data points from X-ray through IR, though only one radio point (HI 21cm line).

PGC 059124

Point source in the MGPSCAT (b ~ -9.439839). This Sy2 is listed in [1], [2], [4], and RC3 among others. The 2*rms contour level is shared with two background sources to the east and west of the center of the object. A few X-ray and optical data points listed in NED, along with those from *IRAS* and 2MASS in the IR and two radio (HI 21cm line and 1.4 GHz).

NGC 6221

Type-B morphology in the MGPSCAT (b ~ -9.573205). The traditional classification of this nearby AGN (z ~ 0.005) as a Sy2 was by Veron et al. (1981) because there is no detectable broad optical emission. But the true nature of this object is not so clear-cut. Levenson et al. (2001) uses this galaxy as an example of what could be called a "X-ray loud composite" galaxy. They argue that it would be classified as Sy1 if our line of sight was such that we were not viewing it through a starburst region. It is listed in [1], [2], [3], and RC3, among many others, as Sy2. I follow those as well as Peng et al. (2006) and keep the Sy2 classification. It is an extensively studied AGN, with 175 references in NED along with 89 photometric data points, mainly in the optical and IR (both 2MASS and *IRAS*), along with a few at radio wavelengths. At 2*rms, from NE to SW, a max measurement of ~295 pixels = 295" is found. At .102 kpc/" this gives ~30 kpc. This object was observed using the MOST before (Subrahmanya & Harnett 1987), with a reported flux density of 420 mJy, a value unchanged than reported in the SUMSSCAT v2.1 (420.0 $\pm$ 15.0 mJy). See Table 4.1.

NGC 6300

Type-B morphology in the SUMSS. This Sy2 is the fifth closest (z = 0.0037, luminosity distance of 15.7 Mpc) in the sample and is listed in [1], [2], [3], [4], and RC3 among many others. A very well studied object, with 183 references and 72 photometric data points listed in NED. For the latter, the coverage is good from X-ray to radio (four points of the latter), including both 2MASS and *IRAS* in the IR. Longest measurement found on SUMSS mosaic is ~265 pixels = 265" from SE to NW. At 0.075 kpc/", this gives ~19.9 kpc. This object was observed using the MOST before (Subrahmanya & Harnett 1987), with a reported flux density of 116 mJy, a value 12.0% higher than reported in the SUMSSCAT v2.1. See Table 4.1.

PGC 060594

A weak (S = 17.3 mJy) point-source in SUMSS. This Sy2 is listed in [1]. [2], [4], and RC3 among a few others. *IRAS* and 2MASS data points listed in NED, along with a few optical and two radio (the uncorrected SUMSS and a HI 21cm line measurement). The 2*rms contour level on the map is shared with what appears to be an unrelated, apparently nearby point source.

PGC 062134

Point source in the SUMSS. This Sy2 is listed in [2], and [3] among several others. Sixth strongest source in the SUMSS (S = 264.4 mJy), though at z ~ 0.020 (86.8 Mpc) it is third most luminous

Sy2 in the sample with Log L ~ 23.39 W/Hz. The only photometric data points listed in NED are at X-ray, IR (both 2MASS and *IRAS*) and two radio (uncorrected SUMSS and 4.85 GHz) wavelengths. The 2*rms contour level is shared by two (apparently) nearby, unrelated sources.

PGC 062174

Point source in the SUMSS. Added from Peng et al. (2006). This Sy2 is listed in [1],[2],[3],and [4] among many others. No radio points other than the (uncorrected) SUMSS listed in NED, though good IR (2MASS and *IRAS* included), optical, and X-ray coverage.

PGC 062218

Non-detection in the SUMSS. This Sy2 is listed in [2], [3], [4], and RC3 among others. Limited wavelength coverage; several optical, IR (both *IRAS* and 2MASS), but just one radio point (HI 21cm line) listed in NED.

PGC 062428

Point source in the SUMSS. This Sy2 is listed in [1], [2], [4], RC3 and many others. Fairly well studied galaxy (59 references and 39 photometric data points listed in NED). Coverage in the latter from X-ray to radio (uncorrected SUMSS and a HI 21cm line measurement) including both *IRAS* and 2MASS in the IR.

PGC 062440

Point source in the SUMSS. This Sy2 is listed in [1] - [4], RC3, among others. Aside from the (uncorrected) SUMSS, there are IR (both *IRAS* and 2MASS) and several optical photometric data points listed in NED.

NGC 6810

Point source in the SUMSS. The classification of this object as Sy2 comes not from [1]-[3] but from Rush et al. (1993). See also the recent paper by Buchanan et al. (2006) for Spitzer IR analysis of this and several other local Sys. Fairly extensive coverage from X-ray through radio, though in the latter only two points (HI 21 cm line and 4.85 GHz).

PGC 063874

Point source in the SUMSS. This Sy2 is listed in [2], and [4], among a few others. Good IR coverage (*IRAS* and 2MASS) in NED, but the only other points listed are a few optical and two radio (1.425 and 4.85 GHz). This is the fourth most luminous Sy in the sample at 843 MHz, with log L ~ 23.30 W/Hz.

NGC 6890

Point source in the SUMSS. A well-studied Sy2, with 107 references and 64 photometric data points in NED with good wavelength coverage from X-ray through IR, but only one radio point (a HI 21cm line measurement). Listed in [1], [2], [3], [4], and RC3 among many others.

IC 4995

Weak point source (*S* = 13.5 mJy) in the SUMSS. Listed in [1], [2], [3] among others. Some X-ray and optical points in NED, and good IR coverage (2MASS and *IRAS*), but that is it.

PGC 064537

Non-detection in the SUMSS. This Sy2 is listed in [1], [2], and RC3 among a couple of others. Only 2MASS, *IRAS*, and a few optical data points listed in NED.

PGC 065600

Point source in the SUMSS. However the SUMSS mosaic has a lot of noise and artifacts around the object, most significantly the bright radio source SUMSS J205132-570351 (alias MRC 2047-572). This extensively studied Sy2 is listed in [1] - [4], and RC3 among many others. It is the second strongest 843 MHz source in this sample, with *S* = 2041.5 mJy, but the most luminous with Log L ~ 23.74 W/Hz. NED lists 273 references and 107 photometric data points. Good wavelength coverage published, from X-ray to radio (eight of the latter including two at 843 MHz (using the MOST) - the (uncorrected) SUMSS value and one from Jones & McAdam (1992).

NGC 7130

Point source in the SUMSS. A well-studied Sy2, listed in [1] - [6], RC3, and many others. NED lists 79 references and 179 photometric data points; good wavelength coverage, except for radio where there is just a HI 21cm line measurement and one data point at 1.4 GHz, in addition to the (uncorrected) SUMSS value. Sixth most luminous Sy2 in the sample; log L ~ 23.11 W/Hz.

NGC 7172

Point source in the SUMSS. This Sy2 is listed in [1], [2], [5], [6] among many others. NED lists 240 references and 83 photometric data points; good wavelength coverage, except for radio where there is just one at 1.4 GHz, and the (uncorrected) SUMSS value.

PGC 068122

A faint point source (S = 11.8 mJy) in the SUMSS. The Sy2 is listed in (and gets its Sy classification from) [5]. Also listed in [4]. Not a very well-studied galaxy, with only *IRAS*, a few optical, and the (uncorrected) SUMSS listed in NED.

PGC 068198

Point source in the SUMSS. This Sy2 is listed in [1], [2], and [4] among several others. The only data points in NED are several optical, 2MASS and *IRAS* in the IR, and the (uncorrected) SUMSS value.

FAIRALL 0357

Weak (S = 16.5 mJy) point source in the SUMSS. This Sy2 is listed in [1], [2], and [3]. Aside from 2MASS and *IRAS* data points, only one optical and the (uncorrected) SUMSS points listed in NED.

PGC 070458

Point source in the SUMSS. The classification of this AGN as Sy2 comes from Kirhakos & Steiner (1990). Also listed in [4], and RC3 among a few others. 2MASS and *IRAS* data points in NED, along with a couple of optical, and two at radio wavelengths (HI 21cm line and uncorrected value from SUMSS).

NGC 7496

Point source in the SUMSS. This Sy2, listed in [1] - [4] among many others, is a very well-studied AGN with 159 references and 64 photometric data points in NED. Fairly good coverage of the latter from X-ray to radio (HI 21cm line, 1.49 GHz, and 8.46 GHz, in the latter wavelengths).

NGC 7582

Point source in the SUMSS. This Sy2 is one of the most extensively studied objects in this sample, with 405 references and 171 photometric data points listed in NED. Listed in [1] - [4], among many others. Good wavelength coverage in NED, though concentrated at X-ray and IR wavelengths.

NGC 7590

Point source in the SUMSS. This Sy2 is listed in [1] - [4] among many others. Extensively studied, with 166 references and 68 photometric data points in NED. Fairly good wavelength coverage, though only two radio points (HI 21cm line and 1.49 GHz).

TYPE 1:

LEDA 087392

Point source in the SUMSS. This Sy1 is listed in [2], among just a few other publications. The most luminous Sy1 in the sample, with log L = 23.69 W/Hz, at 843 MHz. The luminosity distance of the AGN is 121 Mpc. The only photometric points listed in NED are from the 2MASS in the IR and two at X-ray wavelengths (0.3-10.0 keV).

PGC 002450

A fairly weak point source in the SUMSS. This Sy1 is listed in [1] - [4], RC3, among a few others. The only data points in NED are from the 2MASS and *IRAS* in the IR, a few optical, and the (uncorrected) SUMSS value.

PKS 0056-572

Type-B morphology in the SUMSS. $z \sim 0.018$. This Sy1 (listed in SIMBAD but not in NED) gets its classification from the newest version of [2] (12th ed. 2006). Second strongest source in SUMSS (S = 479.4 mJy), and second most luminous Sy1 in this sample overall, with Log L = 23.53 W/Hz. No morphological classification published however the 843 MHz contour map for the object (Figure A.14) is consistent with a nearly face-on spiral with three prominent arms. The only photometric data points listed in NED are at (seven different) radio wavelengths, including the (uncorrected) SUMSS. Three different possible extended regions of 843 MHz emission at 2 and 4 and 8*rms contour levels. Appears to be emission from the disk of the (unknown type of) host galaxy.

PGC 003864

A weak point source in the SUMSS. This Sy1.8 is listed in [2], [4], and RC3. The 2MASS, *IRAS*, and a few optical data points are the only ones listed in NED.

IRAS 01089-4743

A weak point source (S = 13.2 mJy) in the SUMSS. One of the few elliptical host galaxies in the sample. This Sy1 is listed in [2]. The only data points listed in NED are one optical, those from *IRAS*, and the uncorrected SUMSS.

PGC 004822

A weak (S = 11.8 mJy) point source in the SUMSS. This Sy1.5 is listed in [1], [2], RC3, and a few others. Only the *IRAS*, 2MASS, and several optical data points listed in NED.

NGC 526A

A weak point source in the SUMSS. This Sy1.9 is listed in [1], [2], [3], [5] among many others. A well-studied AGN with 156 references and 57 data points listed in NED. Good coverage of the latter though only two radio points (uncorrected SUMSS and 1.4 GHz). *IRAS* values not listed in NED; obtained from *IRAS* Point Source Catalog (v.2). NED classifies this AGN as Sy1.5, the classification used in this work is taken from [2].

PMN J0133-5159

Type-A morphology in the SUMSS. Faint extended emission to the SW and NE (of an otherwise nearly point source) at 2 and 4*rms contours, possibly from disk of host galaxy. No morphological classification has been published, however the SUMSS contour map (Figure A.15) shows a strong, nearly point source with outer contours suggesting a barred spiral host. Maximum extent measured (end to end of 2*rms contour at each end of apparent extended regions) is ~237 pixels = 237". At 0.400 kpc/" this gives a distance of 94.8 kpc. The classification of this AGN as Sy1 comes from [2] (and that has not made its way into NED). The third most luminous Sy1 in this sample, with Log L = 23.51 W/Hz at 843 MHz. Of the 15 data points listed in NED, 14 are at radio wavelengths, including the (uncorrected) SUMSS value. The other being X-ray (0.1-2.4 keV ROSAT). The 2MASS magnitudes from 2MASS PSC directly (not listed in NED).

ESO 080- G 005

Non-detection in the SUMSS. Classification from [2]. Not a very well-studied Sy1.8, with only two optical and the 2MASS IR data points listed in NED.

NGC 1097

Type-B morphology in the SUMSS, $z \sim 0.004$. Large scale disk contributions obvious from the large, nearly face-on barred spiral host galaxy. This Sy1, listed in [1], [3], [5] and many others, is an extensively studied AGN in this sample with 491 references (going back to 1925, not including the 1888 NGC listing by Dreyer) and 164 photometric data points. Wide coverage of the latter, from X-ray through radio. Strong radio source in the SUMSS.

PGC 011706

Non-detection in the SUMSS. This Sy1.2, listed in [2], is not very well studied, with only the 2MASS and a few optical data points (and thirteen references) listed in NED.

NGC 1365

Type-B morphology in the SUMSS, $z \sim 0.005$. Large scale disk contributions obvious from the large, nearly face-on spiral host galaxy. This AGN is listed in NED (from [2]) as Sy1.8 but the classification of Sy1.5 by Joguet et al. (2001) has been adopted here because it is based on a newer observation; their higher resolution spectral analysis showing the object had been misclassified in [2]. Listed in [1] - [5] and many others; the most studied object in this sample, with 619 references going back over 50 years, not including the NGC catalog from Dreyer (1888), as well as 170 data points listed in NED. This Sy is the strongest radio source among the Sy1 in this sample (641.2 mJy), though only the sixth-most luminous.

NGC 1566

Type-B morphology in the SUMSS, $z \sim 0.005$. Large scale disk contributions obvious from the nearly face-on spiral host galaxy. This AGN, listed in [1]-[3] among many others, is the nearest Sy1 in the sample (luminosity distance ~21 Mpc) and well-studied, with 394 references and 158 data points listed in NED, with good wavelength coverage of the latter. This object was observed using the MOST before (Subrahmanya & Harnett 1987), with a reported flux density of 310 mJy, a value essentially unchanged (3.4% higher) than reported in the SUMSSCAT v2.1. See Table 4.1.

PGC 017103

A weak point source in SUMSS. This Sy1.5 is listed in [1]-[4]. The only photometric data points listed in NED are those from the 2MASS and *IRAS* in the IR, and a couple at optical wavelengths.

FAIRALL 0265

Non-detection in the SUMSS. This Sy1.2 is listed in [1]-[3]. The only data points in NED are from the 2MASS and *IRAS*.

LEDA 096433

Point source in the MGPS (b ~ 5.650294). This Sy1 is listed in [2], and [4]. The only data points listed in NED are from the 2MASS and *IRAS*.

PGC 027468

Non-detection in the SUMSS. This Sy1 is listed in [1], [2], and [4]. The only data points listed in NED are from the 2MASS in the IR.

PGC 029148

Non-detection in the SUMSS. This Sy1 is listed in [1] and [4]. The only data points listed in NED are those from the 2MASS in the IR and one at radio wavelengths (HI 21cm line measurement).

PGC 029151

Non-detection in the SUMSS. This Sy1 is listed in [1], [2], and [4]. The only data points listed in NED are those from the 2MASS and a few at optical wavelengths.

PGC 033084

Non-detection in the MGPS (b ~ 7.648160). This Sy1 is listed in [1]-[4]. The only photometric data points listed in NED are from the 2MASS, a few optical, and one radio (HI 21cm line). The *IRAS* values were taken from *IRAS* Point Source Catalog directly.

PGC 034101

Though technically a non-detection in the SUMSS, this Sy1, which is listed in [2]-[4], does show up in the SUMSS mosaic at 1, 2, and 3*rms. So in an effort to obtain the most accurate flux density measurement for this object at 843 MHz, a value was computed directly from the SUMSS mosaic. A value of approximately 8 mJy was obtained and adopted in this study. Photometric data points from the 2MASS, *IRAS*, one radio (HI 21cm line), as well as a few at optical wavelengths, are listed in NED. The procedure used here to obtain the flux density value of the object that was used for all analysis in this study, adapted in part from Hardcastle (2005), is as follows.

First an image of the region of the space around (and centered upon coordinates given in NED) the object was obtained from the SUMSS Postage Stamp Server, the field size of the image being 0.2° x 0.2°. The FITS viewer *fv*, created and distributed by the High Energy Astrophysics Science Archive Research Center (HEASARC) at NASA, was used to manually fit an ellipse around PGC034141, as can be seen below in Figure 2.3. The pixels in the image are square, 5 arcsec per side, or a pixel area PA = 25 arcsec^2.

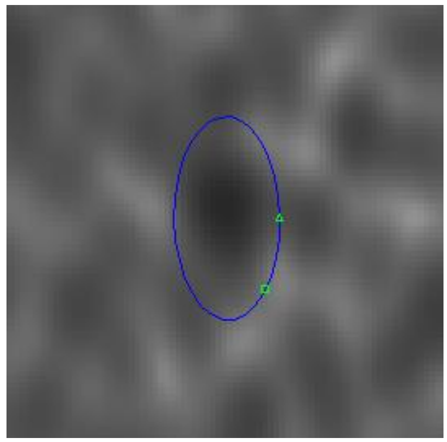

FIG. 2.3. - Fitted area around PGC 034101; obtained from manually fitting an ellipse using the software *fv*.

The total fitted flux was given by *fv* as $F \approx 1.2$ Jy/beam. Next the declination of the object had to be converted to decimal format, as the size of the MOST beam area is a function of the declination, δ. This is done by taking the value of δ given in Table 2.2, which is in Degrees.Minutes.Seconds (*D.M.S.*) format, and converting to decimal using the relation

$$\delta = |D| + \frac{M}{60} + \frac{S}{3600}$$

For PGC034141, D = -36, M = 25, and S = 41. This gives the value $\delta \approx 36.43$. So now the beam area *BA* (the beam solid angle of the Gaussian restoring beam of the MOST) is be computed as

$$BA = \frac{\pi(FWHM)^2}{4ln2},$$

where the FWHM (Full Width Half Maximum) is the resolution given in §2.2, 45"x45cosec(|δ|)". So therefore we get

$$BA = \frac{\pi 45^2}{4ln2}\csc(|\delta|) \approx 3864 \text{ arcsec}^2$$

Next the number of pixels P (per beam area) is computed as $P = \frac{BA}{PA} \approx 155$ pixels. Now we can compute the total flux density (in units of mJy).

$$S = 1000 \frac{F}{P} = 1000 \frac{1.2}{155} \approx 8 \text{ mJy}$$

This value is just below the limiting peak brightness of the SUMSS (§2.2) of 10 mJy/beam.

PGC 036002

Point source in the SUMSS. This Sy1.9 is listed in [1] and [4]. The *IRAS*, 2MASS, a few optical, and the uncorrected SUMSS value are the only data points in NED.

NGC 3783

Point source in the SUMSS. This Sy1.5 is listed in [1]-[4], among many others. An extensively studied AGN with 575 references and 132 photometric data points in NED. For the latter, the coverage is extensive at IR wavelengths, but also good at optical and X-ray wavelengths. Only two radio points listed (HI 21 CM line and 6cm).

LEDA 096527

Point source in the SUMSS. This Sy1, listed in [2], is not a very well-studied AGN, with only nine references and five photometric data points, consisting of the values from *IRAS* and the uncorrected SUMSS value, are listed in NED. The fourth most luminous Sy1 in the sample with log L = 22.91 W/Hz.

PGC 045371

Point source in the SUMSS. This Sy1.2 is listed in [1], [2], and [4]. The photometric data points listed in NED are not extensive, with values from the 2MASS, *IRAS*, a few optical, and one radio (1.425 GHz).

PGC 047969

Point source in the SUMSS. This is a fairly well-studied Sy1.5, fourth closest Sy1 in the sample, and is listed in [1]-[4], among several others. There are 361 references and 96 photometric data points listed in NED, with good coverage of the latter from X-ray down through IR (including from the 2MASS and *IRAS*) wavelengths, but only two radio points (at 6 and 20 cm).

PGC 049051

Nearly a point source in the SUMSS; the 2 and 4*rms contours are shared with apparent extended region to the N/NW of length ~175 pixels = 175". At 0.322 kpc/" this gives a length of ~56 kpc. This is likely unrelated background noise/emission, as the host galaxy diameter given in NED indicates (assuming the scale mentioned above) a size of only ~27 kpc. This Sy1.2, in a nearly edge-on spiral host galaxy, is listed in [1]-[4]. It is a well-studied AGN with 352 references and 118 photometric data points listed in NED, though all are in the IR (including from the 2MASS and *IRAS*), except for several at optical and X-ray wavelengths.

PGC 050427

Non-detection in the SUMSS. A little-studied AGN, this Sy1.5 is listed in [1], [2], and [4]. Only 10 references and 10 photometric data points listed in NED, the latter comprised of just the various 2MASS values. I could find no morphological classification for this AGN in the literature and all published images show a point source.

ESO 328- G036

A faint (*S* = 15 mJy) point source in the SUMSS. This Sy1.8, the host of which is actually a pair of interacting S0 galaxies, is one of the least studied AGN in this sample. Listed in [2]. A total of three references and no photometric data points listed in NED.

PKS 1521-300

Point-source in the SUMSS. This Sy1, listed in [2], is the fourth most luminous object in this sample among Sy1 of all types, with log L ~ 23.17 W/Hz. This AGN has 19 references in NED; the only data points listed there are from the 2MASS and five at radio wavelengths.

LEDA 2793282

Non-detection in the MGPS (b ~ -6.744355). This Sy1.5 is listed in [1] and [4]. Only 9 references and 11 data points listed in NED, the latter being just the values from the 2MASS along with one each at optical and X-ray wavelengths.

PGC 062346

A weak (*S* = 15.8 mJy), point-source in the SUMSS. This Sy1.5 is listed in [1]-[4] among several others. The photometric data points listed in NED give good coverage in the IR (including 2MASS and *IRAS*) and optical, but the only other points are two at radio wavelengths, the (uncorrected) SUMSS and HI 21cm line.

PGC 062554

Point source in SUMSS. This Sy1.0 is listed in [1], [2], and [4] and is the fourth most distant (and the weakest Sy1, with S = 11.6 mJy) Sy in the sample. A few optical and X-ray data points in NED, but good coverage in the IR (both *IRAS* and 2MASS) and one radio point, the (uncorrected) SUMSS value.

ESO 399- IG 020

A weak (S = 14.3 mJy) point-source in SUMSS. This Sy1, listed in [2], actually consists of two interacting galaxies, though no morphological classifications of them could be found. The only published image in NED (optical at 468 nm) clearly shows the disturbed morphology from the interacting hosts. This AGN has not been studied extensively; seven references in NED (note [2] not listed there) and the only data points are from *IRAS*.

NGC 6860

Point source in SUMSS. This Sy1.5 is listed in [1]-[4] among a few others. The only data points listed in NED are from the 2MASS and *IRAS* in the IR, a few optical, and the uncorrected SUMSS value.

PGC 064989

Non-detection in the SUMSS. This Sy1 is listed in [2]. Not an extensively studied AGN, with just 10 references listed in NED, and the only data points listed there are from the 2MASS and *IRAS*. No morphological classification for host galaxy could be found in the literature and the two published images (NIR and optical) in NED showing a point source.

ESO 235- G 059

Non-detection in the SUMSS. This Sy1.8 is listed in [2]. Not an extensively studied AGN, with just 8 references in NED, and the only data points listed there are from the 2MASS, *IRAS*, and a few at optical wavelengths.

CTS 0109

Non-detection in the SUMSS. This Sy1.2, listed in [2], has no data listed in NED. The 2MASS data taken from 2MASS PSC directly. *IRAS* non-detection. The upper limit used for the 843 MHz flux should be close to the actual value, as the object is just visible at 1 and 2*rms (.0019 and .0038 Jy, given the declination of the object). No host galaxy morphology could be found in the literature; the one published image in NED (468 nm) show several (apparently) nearby point sources. Morphology ambiguous.

PGC 067075

Non-detection in the SUMSS. This Sy1.8 is listed in [2] and [4]. There are 13 references and 17 data points in NED, the latter consisting of just a few at optical wavelengths, as well as the IR values from the 2MASS. SIMBAD, when queried for Sy, reports that one such object (with the *z* and declination restrictions defining this sample) is *NGC 7095* with coordinates 21 38 08.0 , -42 36 17. But that is an error. NGC 7095 has coordinates (from NED): 21 52 26.4, -81 31 51. PGC 067075 is the galaxy that is really at the coordinates given by SIMBAD.

NGC 7213

Type-B morphology in the SUMSS, $z \sim 0.005$. Large scale disk contributions obvious from the nearly face-on spiral host galaxy. This Sy1.5 is listed in [1]-[4], among many others. It is a well-studied AGN and one of the "radio-excess" Sy of Roy & Norris (1997). There are 292 references and 113 data points in NED. Good coverage of the latter from X-ray through IR wavelengths, as well as three radio points (at 4.85 GHz, 2.7 GHz, and HI 21cm line). This object was observed using the MOST before (Subrahmanya & Harnett 1987), with a reported flux density of 100 mJy, a value 19.6% lower than reported in the SUMSSCAT v2.1. See Table 4.1.

[VV2003c] J224704.9-305502

Point-source in the SUMSS. This Sy1.0 is from [2]. There are no references and no data points in NED except for one optical (B_J). The redshift value used is also from [2] (not listed in NED). No host galaxy morphology could be found in the literature and the only published image in is optical (468 nm) and is faint point source.

PGC 073028

Non-detection in the SUMSS. The classification of this AGN as Sy1.2 comes from Hewitt el at. (1991). Also listed in [4]. This Sy is the most distant in this entire sample, with $z = 0.03029$. Interacting Sb pair host galaxy. The only data points listed in NED are from the *IRAS*.

2.5 RESULTS

2.5.1 RECESSION VELOCITIES

The galactocentric recession velocities (galactic standard of rest) for this sample, which is derived from the objects (heliocentric) redshift, corrected for its motion around the center of the Milky Way, are the recession velocities given in Tables 2.1 and 2.2 and were computed using the NED Velocity Correction Calculator (NASA/IPAC). To convert a velocity from one reference frame to another the equation used is: $V_{convert} = V + V_{apex}[\sin(b)\sin(b_{apex}) + \cos(b)\cos(b_{apex})\cos(l - l_{apex})]$, where l and b are the longitude and latitude for the object and V is the unconverted velocity. The apices and galactic coordinates are given by de Vaucouleurs et al. (1991), for heliocentric to galactocentric conversion these are: $l_{apex} = 87.8°$, $b_{apex} = +1.7°$, and V_{apex} 232.3 km/sec.

The arithmetical mean, median, standard deviations, as well as the minimum and maximum values, are summarized below in Table 2.5.

TABLE 2.5

Recession Velocities (km/s)

	Median	Mean	σ	Min.	Max.
Both	4792	4890	2345	--	--
Sy2	4598	4514	2270	266	8878
Sy1	5709	5580	2349	1190	9087

Note. - Summary of recession velocities.

These results and how they compare to other, similar, samples in the literature from previous surveys is discussed in Chapter 4. The histograms of the recession velocities are given below in Figure 2.4. What is not apparent in Table 2.5, but can be clearly seen in Figure 2.5 below and in Figure 2.7 in §2.7 (as well as in the top histogram in Figure 2.4 below, however the bin values do not quite match), is the "gap" in the approximately 700 km/s range of $5982 < v < 6693$ km/s. Those two objects, defining this gap, both happen to be Sy2 (PGC 062134 and PGC 016072, respectively, the latter censored in the SUMSS). This range of recession velocities corresponds to the redshifts of $0.0202 < z < 0.0229$, and luminosity distances of $87 < D_L < 99$ (Mpc), approximately. As discussed further in Chapter 4 this apparent gap does not seem to be a peculiarity of this sample, as it has been observed before in samples in other parts of the sky.

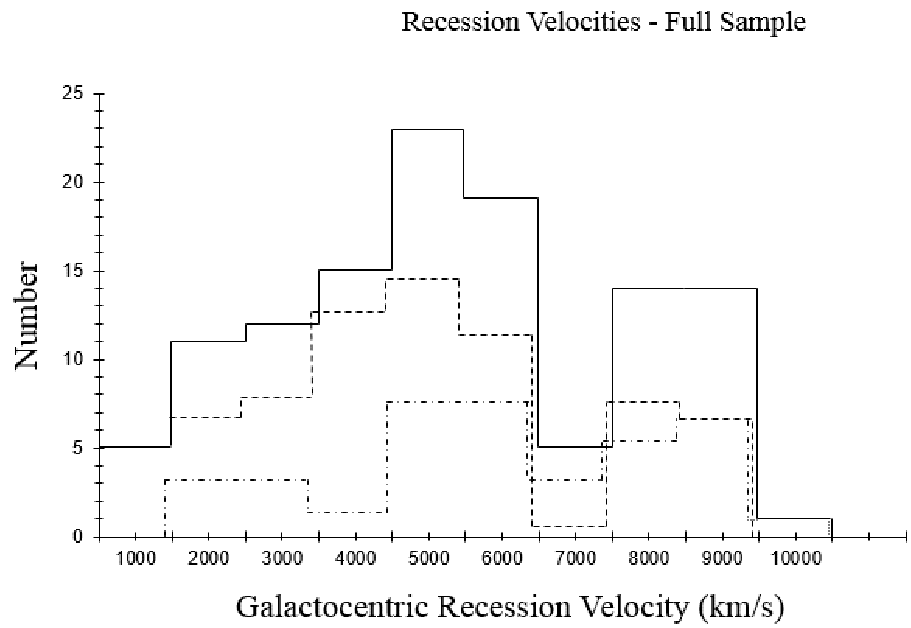

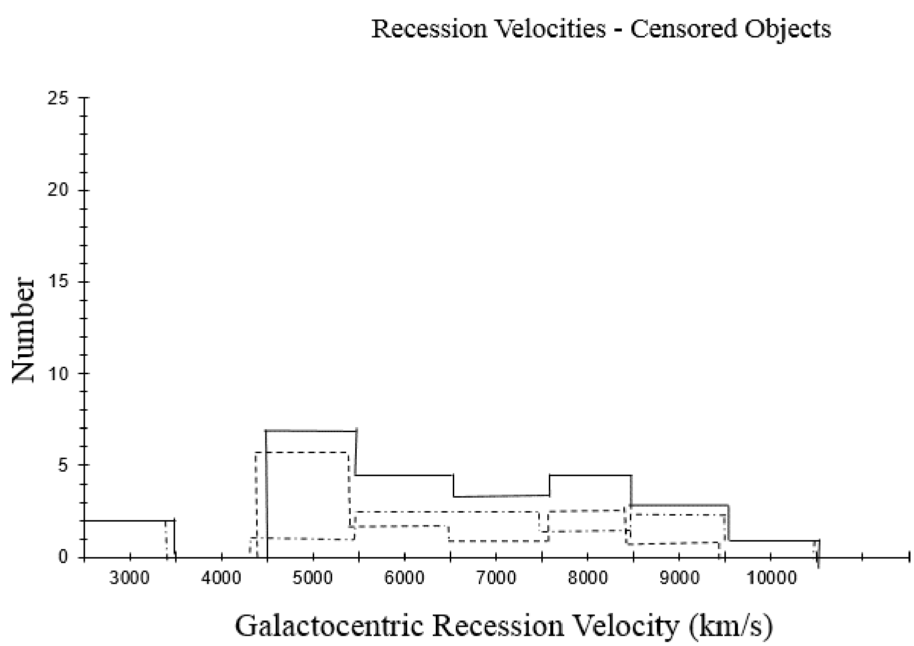

FIG. 2.4. - Recession velocities for the complete sample and for just the censored objects. All objects are shown with solid lines, Sy1 dash-dot lines, and Sy2 dashed lines

2.5.2 DISTANCES

The Seyferts in this sample have redshifts in the range $0.001448 < z < 0.030288$. All redshift values adopted for this study are taken from NED except for the value for [VV2003c] J224704.9-305502, as mentioned in (§2.1). The luminosity distances (defined in §2.1, and unless otherwise stated referred to simply as 'distance(s)', from now on) for the entire sample have an arithmetical mean of 72 Mpc and median of 70 Mpc. For Sy2 and Sy1, respectively, the arithmetical mean values are 66 Mpc and 82. The median values by type similarly show larger values for Sy1, with values of 67 and 82 Mpc reported. These (arithmetical) results are summarized in Table 2.6 below. As will be discussed in §2.7 (on the statistical tests performed), the results of some tests of correlation between distance and 843 MHz luminosity are "weakly significant" (as defined there) for the Sy2. Though inconclusive, along with these mean and median values there is some suggestion that perhaps we are missing some Sy2 in the volume of space sampled in this study. In Figure 2.5 below the histograms for distance, by type and combined, are shown, as well as for censored objects, also by type and combined.

Often the recession velocity / distance measure *cz* is given in the literature. In this sample of 119 local Sy the mean and median values of *cz* computed were 5015 and 4935 km/s, respectively. The minimum and maximum values were found to be 434 and 9080 km/s, respectively.

TABLE 2.6

Distances (Mpc)					
	Median	Mean	σ	Min.	Max.
Both	70	72	34	--	--
Sy2	67	66	33	6	131
Sy1	82	82	34	18	131

Note. - Summary of the luminosity distances for the sample

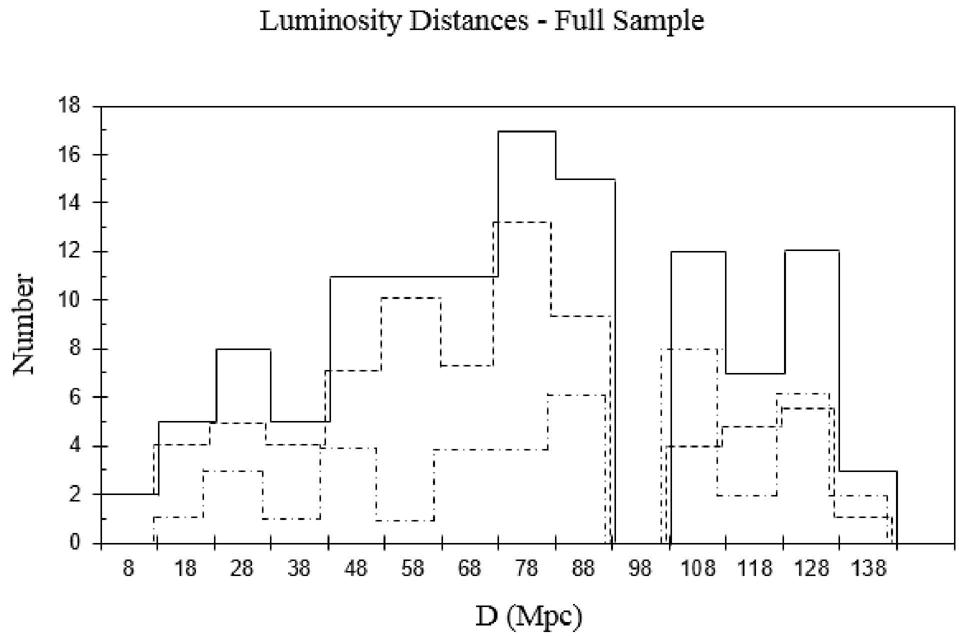

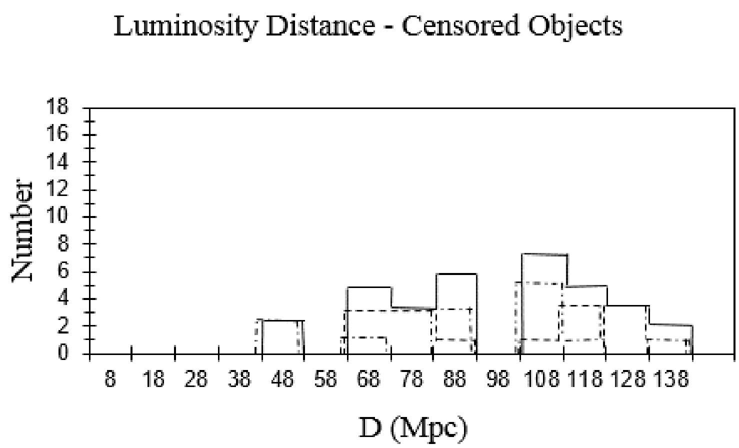

FIG. 2.5. - Recession velocities for the complete sample and for just the censored objects. All objects are shown with solid lines, Sy1 dash-dot lines, and Sy2 dashed lines.

2.5.3 THE 843 MHz LUMINOSITIES

Of particular interest in this investigation of the radio properties Seyferts are the (843 MHz) radio luminosities. Histograms of the luminosities for the sample (including censored objects), together and by type, are in Figure 2.6 below. Censored objects are the also plotted separately.

The radio luminosities reported here were computed in the conventional way (e.g., Edelson 1987), as $L = 4\pi Sd^2$, where S is the total flux density (in units of $\mathrm{Wm^{-2}Hz^{-1}}$) and d is the luminosity distance in meters. Not including the censored objects, the values for S are taken from the SUMSSCAT or MGPSCAT (as indicated in Table 2.1 and 2.2 above), except for the object PGC 034101 (ESO 377- G 024). The value for that object, as described in the notes for the object in §2.4, was determined by estimating the total flux density (Jy) directly from a SUMSS mosaic. A value of 8 mJy was estimated for the object and was used in all calculations in this paper, instead of the upper limit for objects with -50 < δ < -30, which is 3*rms = 5.7 mJy. No other censored objects in the sample were as visible in the SUMSS images, suggesting that the upper limits adopted for them are appropriate.

The errors associated with the luminosity values analyzed here (given in Tables 2.3 and 2.4) were computed using the standard theory of arithmetical error propagation for multiplication (e.g., ChemWiki, 2012). For a given sample object, the error associated with the luminosity propagates as $L\sqrt{\left(\frac{err}{S}\right)^2}$, where *err* is the error of the total flux density S_{843} and L the computed luminosity (all given in Tables 2.3 and 2.4). This assumes the only uncertainty is in the total flux density values. Due to the great sensitivity of the MOST, the errors associated with S_{843} are small, the arithmetical average being 5.2%.

The (arithmetical) median and mean values of the 843MHz log Luminosities (W/Hz) of the entire sample are computed to be 22.09 and 22.16, respectively. By type, the median values are 22.09 (all Sy1) and 22.13 (Sy2). For the mean the values computed were 22.17 (all Sy1), and 22.15 (Sy2). Table 2.7 below gives a summary of these values, along with the standard deviations and the minimum and maximum values of the sample.

TABLE 2.7

Log 843 MHz Luminosities (W/Hz)					
	Median	Mean	σ	Min.	Max.
Both	22.09	22.16	0.56	--	--
Sy2	22.13	22.15	0.56	20.89	23.74
Sy1	22.09	22.17	0.58	21.00	23.69

Note. - Summary of the 843 MHz luminosities for the sample

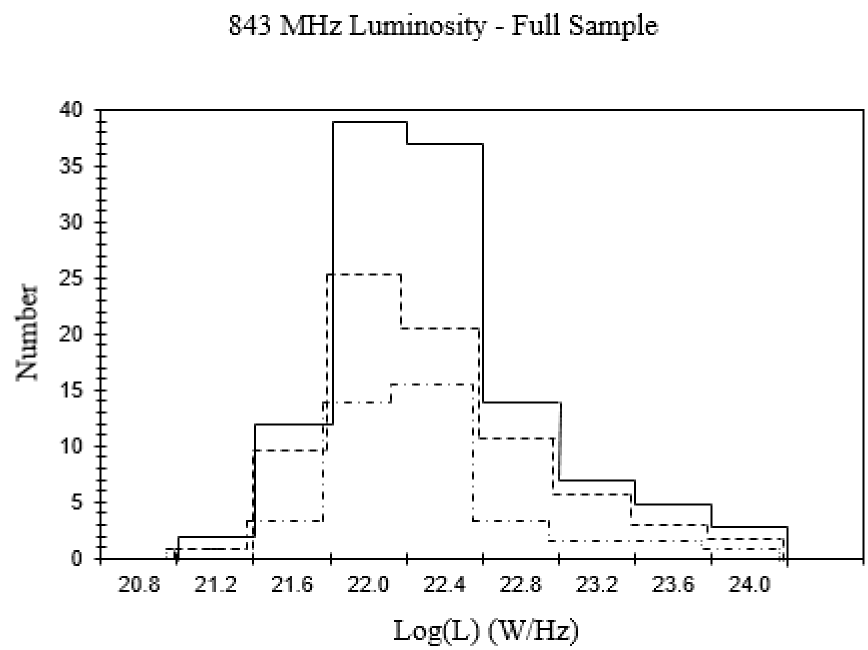

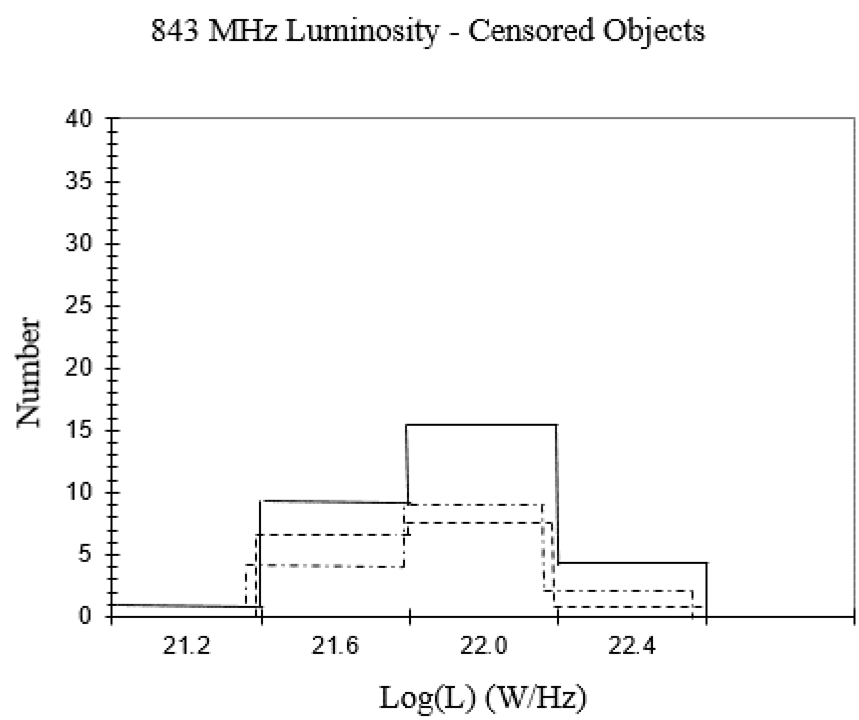

FIG. 2.6. - 843 MHz luminosities in units of W/Hz for the complete sample and for just the censored objects. Sy2 dashed line, Sy1 dash-dot line, full sample solid line.

2.6 ON THE COMPLETENESS OF THE SAMPLE

Plots of the galactocentric recession velocities and luminosity distances (how the latter were computed is described in §2.1) vs. the log 843 MHz luminosities for the sample are given in Figure 2.7.

Recession Velocity vs. 843 MHz Luminosity

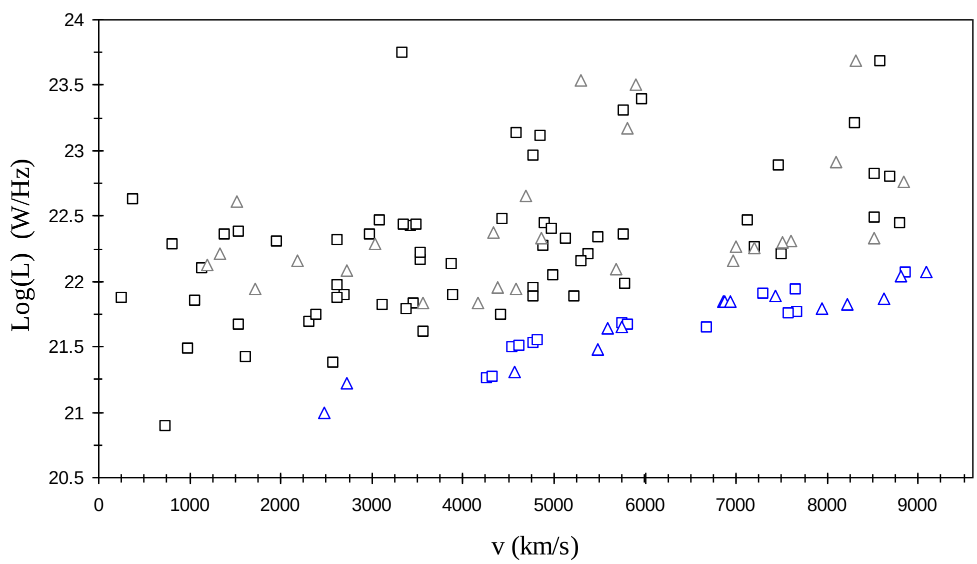

Luminosity Distance vs. 843 MHz Luminosity

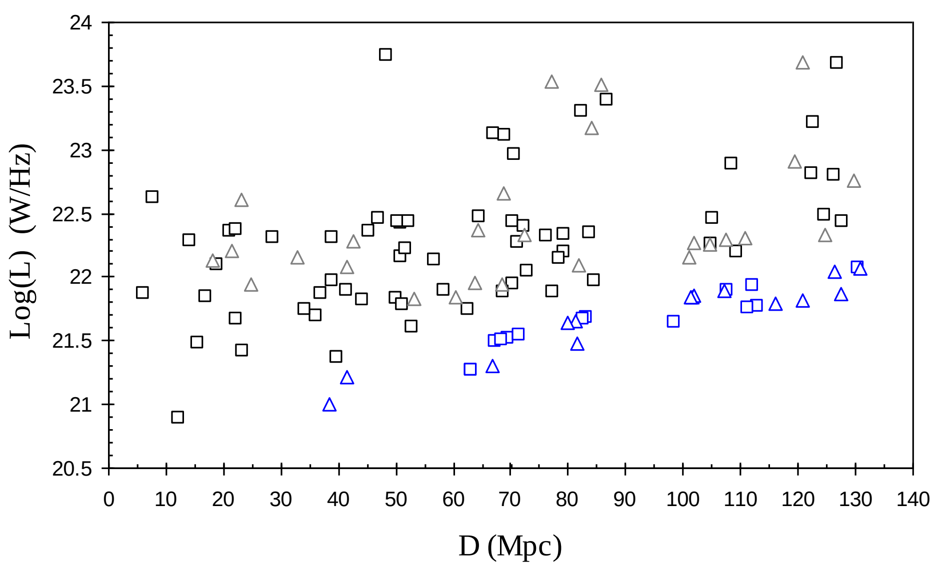

FIG. 2.7. - Boxes - Sy2. Triangles - Sy1. Censored objects in blue.

To test for a correlation between the parameters the Figure 2.7 plots, three tests were used as implemented in *ASURV*. The results are in Table 2.10.

TABLE 2.10

Tests for Correlation

		Cox	K. Tau	S. Rho
GCR Velocity				
	Both	0.9417	0.2303	0.2752
	Sy2	0.4096	0.0990	0.1138
	Sy1	0.4323	0.8573	0.8972
Luminosity Distance		0.5798	0.0861	0.1239
		0.1208	0.0200	0.0338
		0.4198	0.8838	0.9245

Note. - The results of the three bivariate tests for correlation with luminosity as implemented in *ASURV*. For each category, the top row gives the results for all such items in the sample.

The tests for correlation between luminosity distance and 843 MHz luminosity for the Sy2 in the sample were weakly significant (as defined in §2.7). However when testing galactocentric recession velocity, instead of distance, the results are much more mixed; the results do not meet the adopted criteria for being considered weakly significant. One of the test results (K. Tau) is less than 0.1 and the result from S. Rho is at 0.1138. However the result for the Cox Hazard test is much higher, at 0.4096. It could be that the volume of space being sampled contains low luminosity Sy2 that for some reason have not yet been identified, but these test results are inconclusive. No other results were significant, weakly or otherwise.

As is often seen in the literature, one way to help quantify the completeness of a sample is to compute what is called the V/V_{max} ratio, a parameter first formulated by Schmidt (1968) in an early study of the space distribution and luminosity functions of quasars. This is a ratio of (spherical) volumes. For a given object, two volumes of space are computed. The volume V is centered on the object and has as its radius the object's (observed) luminosity distance (Mpc). The volume V_{max} is the volume of space, still centered on the object, which represents the maximum volume of space over which the object would be observable. The radius of V_{max} is therefore the distance at which the flux density of the object would fall below the detection limit of the survey instruments. The radius used for V_{max} here is computed by assuming a 3*rms value for the flux density S (and the known luminosity L) in the luminosity equation in §2.5.3, and solving for the luminosity distance d. The ratio V/V_{max} is, then, a measure of the position of the object in the maximum observable volume. For a uniform distribution (from 0 to 1) in space, the values of V/V_{max} for the sample objects should have a mean value of 0.5. The value of unity is then obtained for censored objects since the flux density values used for them are exactly the 3*rms upper limit values as discussed above.

The arithmetical mean V/V_{max} value for all Sy2 in the sample is found to be 0.170 and for the Sy1, 0.283. For all 119 sample objects the arithmetical mean for V/V_{max} is 0.210. A summary of the results are given in Table 2.11 and the values of V/V_{max} for the individual objects are given in Table 2.12.

TABLE 2.11

V/V_{max}			
	Mean	Median	S.D.
Sy2	0.170	0.040	0.277
Sy1	0.282	0.125	0.336
All Sy	0.210	0.050	0.303

Note. - The average V/Vmax values for the sample, combined and by type.

As can be seen in Table 2.12 below, all *detected* objects have V/V_{max} values significantly less than 0.5. In fact only three Sy2 have values in the range $0.2 < V/V_{max} < 0.3$ while only one Sy1 has a value over 0.2, the Sy1.0 PGC 034101 (with a value of 0.327). Nine Sy2 and nine Sy2 have values in the range $0.01 < V/V_{max} < 0.02$. All other sample objects (97 in all) have values $V/V_{max} < 0.09$.

As discussed in more detail in Chapter 4, these results do not necessarily imply that the sample is incomplete. That is because in this sample, since we are dealing with Sy in the local universe ($z <$ 0.0303), one would not expect a uniform distribution; most Sy are strong enough radio sources to be detected within the volume of space surveyed. So we would expect the average values obtained to be less than 0.5.

TABLE 2.12

Name	V/V_{max}				
LEDA 087391	0.040	LEDA 141858	1.000	FAIRALL 0265	1.000
NGC 0424	0.070	NGC 5643	0.003	LEDA 096433	0.118
LEDA 093365	1.000	PGC 052101	0.203	PGC 027468	1.000
PGC 004440	0.024	LEDA 166339	1.000	PGC 029148	1.000
NGC 0454	0.020	IC 4518	0.002	PGC 029151	1.000
PGC 004569	0.146	WKK 3646	1.000	PGC 033084	1.000
PGC 005696	0.024	PGC 058547	0.006	PGC 034101	0.327
PGC 006078	0.019	PGC 059124	0.020	PGC 036002	0.037
PGC 006351	0.141	NGC 6221	0.001	NGC 3783	0.017
PGC 008012	0.206	NGC 6300	0.007	LEDA 096527	0.022
NGC 0824	1.000	PGC 060594	0.103	PGC 045371	0.022
PGC 009634	0.030	PGC 062134	0.002	PGC 047969	0.006
PGC 010665	0.055	PGC 062174	0.036	PGC 049051	0.010
PGC 010705	0.045	PGC 062218	1.000	PGC 050427	1.000
PGC 011104	1.000	PGC 062428	0.016	ESO 328- G036	0.128
PGC 012759	0.078	PGC 062440	0.050	PKS 1521-300	0.003
NGC 1386	0.026	NGC 6810	0.003	LEDA 2793282	1.000
PGC 014702	0.009	PGC 063874	0.002	PGC 062346	0.118
AM 0426-625	0.089	NGC 6890	0.031	PGC 062554	0.187
PGC 015172	0.004	PGC 064491	0.149	ESO 399-IG 020	0.137
NGC 1672	0.001	PGC 064537	1.000	NGC 6860	0.091
PGC 016072	1.000	PGC 065600	0.000	PGC 064989	1.000
PGC 016357	0.215	NGC 7130	0.002	ESO 235- G 059	1.000
NGC 1808	0.000	NGC 7172	0.024	CTS 0109	1.000
PGC 016873	1.000	PGC 068122	0.183	PGC 067075	1.000
PGC 017768	1.000	PGC 068198	0.050	NGC 7213	0.006
LEDA 096373	0.002	FAIRALL 0357	0.111	[VV2003c] J22470	0.009
PGC 021057	0.087	PGC 070458	0.034	PGC 073028	1.000
PGC 023573	0.044	NGC 7496	0.029		
PGC 028144	0.042	NGC 7582	0.001		
PGC 028147	0.172	NGC 7590	0.011		
PGC 029778	0.009	**Sy1:**			
PGC 029993	0.032	LEDA 087392	0.002		
PGC 030984	0.089	PGC 002450	0.048		
NGC 3281	0.009	PKS 0056-572	0.001		
LEDA 088648	1.000	PGC 003864	0.143		
NGC 4507	0.009	IRAS 01089-4743	0.143		
PGC 042504	0.006	PGC 004822	0.183		
WKK 1263	0.073	NGC 526A	0.123		
PGC 043779	1.000	PMN J0133-5159	0.001		
NGC 4785	0.010	ESO 080- G 005	1.000		
PGC 044167	1.000	NGC 1097	0.001		
NGC 4903	0.131	PGC 011706	1.000		
NGC 4945	0.000	NGC 1365	0.000		
ESO 383- G 018	0.178	NGC 1566	0.001		
Circinus	0.000	PGC 017103	0.082		

Note. - The V/V_{max} values for the entire sample.

2.7 STATISTICAL TESTS

The methods of survival analysis, as implemented in the package ASURV, were used to investigate the sample. The package ASURV "implements a suite of statistical methods for the analysis of censored data; i.e. data which are known to lie above or below some limit. It was written specifically to treat left-censoring arising in observational astronomy when objects are observed but sometimes not detected due to sensitivity limits. However, the methods can be useful to researchers in other disciplines, as the code includes techniques that are often omitted from commercial survival analysis packages" (Isobe, Feigelson, & Nelson 1986).

The theory and justification for the use of such methods is long established (Feigelson & Nelson 1985; Isobe, Feigelson, & Nelson 1986; LaValley, Isobe, & Feigelson 1990). While some of the routines in ASURV have been implemented in more modern software packages, ASURV is well tested and still used (e.g., Nagar et al. 1999; Thean et al. 2001; Buchanan et al. 2006). In Chapter 3 ASURV is used in the analysis of the infrared properties of this sample and more detail is given there on individual tests, as needed. ASURV Rev. 1.3 was used.

Several two-sample tests as implemented in ASURV were used to test the galactocentric recession velocities, distances, log 843 MHz luminosities, and fitted minor/major axis ratios. The results are in Table 2.8. The null hypothesis being tested is that the two populations are drawn from the same parent population. Following the methodology of Nagar et al. (1999), the results p(null) of all of the univariate two-sample statistical tests reported in this paper are considered significant only if all of the probabilities are less than 0.05. Results are considered "weakly" significant if all of the probabilities are less than 0.10, or if all but one is less than 0.05.

TABLE 2.8

Two Sample Tests

	Gehan 1	Gehan 2	Log Rank	Peto&Peto	PPW
Luminosity	0.6004	0.6021	0.3597	0.5285	0.5296
GCR. Velocity	0.3135	0.2948	0.3194	0.3406	0.3229
Luminosity Distance	0.2999	0.2810	0.2913	0.3218	0.3034
Minor/Major Fitted Axis*	0.1631	0.1693	0.1104	0.1631	0.1618

Note.-The first column contains the names of the (univariate) two-sample tests used. Gehan 1 is the Gehan's Generalized Wilcoxian test with permutation variance. Gehan 2 is the Gehan's Generalized Wilcoxian test with hypergeometric variance. The Peto & Peto test is the Peto & Peto Generalized Wilcoxian test and PPW is the Peto & Prentice Generalized Wilcoxian test. * indicates that only detected objects were tested.

"The two versions of the Gehan test in *ASURV* assume that the censoring patterns of the two samples are the same, but the version with hypergeometric variance is more reliable in case of different censoring patterns." (Feigelson & Nelson 1985). The logrank test requires the censoring patterns to be fairly similar, while the Peto-Prentice test is thought to be the test least affected by such differences. Less is known about the sensitivity of the Peto-Peto test to differing patterns of censoring. As summarized in Feigelson & Nelson (1985), these issues are discussed in great detail in Prentice and Marek (1979), Latta (1981) and Lawless (1982). The authors of Prentice & Marek (1979) suggest that "if the p-values differ significantly, then the Peto-Prentice test is probably the most reliable". However, as can be seen in Table 2.8, the tests all gave fairly similar results and so it seems likely that the distribution of the tested parameters for both type of Sy in this sample are similar and that the objects were drawn from the same parent population. None of the test results are significant, or even weakly significant, as defined above.

The Kaplan-Meier product-limit estimator, as implemented in *ASURV*, was used to calculate the mean and percentiles of the distances for the sample. This uses the distribution of censored objects to estimate the true value of the parameter. The results are in Table 2.9 below.

TABLE 2.9

Kaplan-Meier Product Estimator

		Percentiles			
		75th	50th	25th	Mean
Luminosity (W/Hz)					
	Both	21.63	22.09	22.38	22.04 +/- 0.07
	Sy2	21.68	22.11	22.43	22.08 +/- 0.08
	Sy1	16.54	22.08	22.32	21.95 +/- 0.12
GCR. Velocity (km/s)					
		2436	3846	5381	4135 +/- 64
		2503	3542	5144	3975 +/- 68
		1998	4366	5869	4468 +/- 98
Luminosity Distance (Mpc)					
		36	56	78	60 +/- 3
		36	51	75	57 +/- 4
		30	63	84	64 +/- 6
Minor/Major Fitted Axis*					
		0.017	0.718	0.856	0.576 +/- 0.034
		0.541	0.742	0.865	0.621 +/- 0.039
		0.000	0.681	0.811	0.495 +/- 0.062

Note. - Kaplan-Meier Product Estimator of the distribution of the parameters shown. This gives an estimate on the true distribution, considering the censored objects. * indicates that only detected objects were considered.

3. INFRARED PROPERTIES OF THE SAMPLE

3.1 SOME NOTES ON THE IR EMISSION OF SEYFERTS

As discussed in Chapter 1, in the prevailing unified framework for AGN it is thought that an optically thick, dusty, parsec-scale, torus surrounds a central engine (e.g., Pier & Krolik 1993; Mouri & Taniguchi 1992; Buchanan et al. 2006 and references therein). The dust in the torus absorbs and is heated by the optical, X-ray, and UV continuum from the accretion disk of the central engine (and are often thought to include heating from star bursts and SN remnants in the central regions of the galaxy), which is then reemitted, much of it in the IR. Many studies (e.g., Spinoglio et al. 1995; Krabbe et al. 2001; Spinoglio et al. 2008) have shown in fact that Sy are more luminous in the MIR than most non-Sy galaxies. Sy2 emission at wavelengths greater than 1µm account for at least 50% of the bolometric luminosity of the AGN and for Sy1 in general the percentage is closer to 10% (Li 2008). On a global scale, the host galaxies of most AGN are also a significant, usually dominant source of IR emission (Roy et al. 1998b).

MIR emission is the best indicator of the bolometric luminosity of AGN because as has been shown, for example by Spinoglio & Malkan (1989), from which Figure 3.1 below is taken, that at wavelengths between approximately 7-12 µm there is minimal scatter in the SED between most all AGN types; the percentage of the flux in the IR is nearly constant among AGN types. So we would expect, for example, the 12 µm flux density values to have a similar distribution. This is one reason that the "12 µm sample" of Rush et al. (1993) continues to be used in Sy investigations (e.g., Buchanan et al. 2006). Other examples include the Sy studies at 10µm by Giuricin et al. (1995), and 0.4-16µm by Alonzo-Herrero et al. (2003), to name just a few.

Recently a study (Peng at al. 2006) suggests that much could also be learned about AGN by looking at the K_s -band NIR (centered at approximately 2.17µm), from the 2MASS all-sky survey (details of the survey in §3.2). In that study a strong correlation was found between the nuclear K_s-band magnitudes and the [O III] λ5007 and hard X-ray luminosities. This approximately 2µm emission is thought to originate from the emissions of warm graphite grains in the central torus mentioned above.

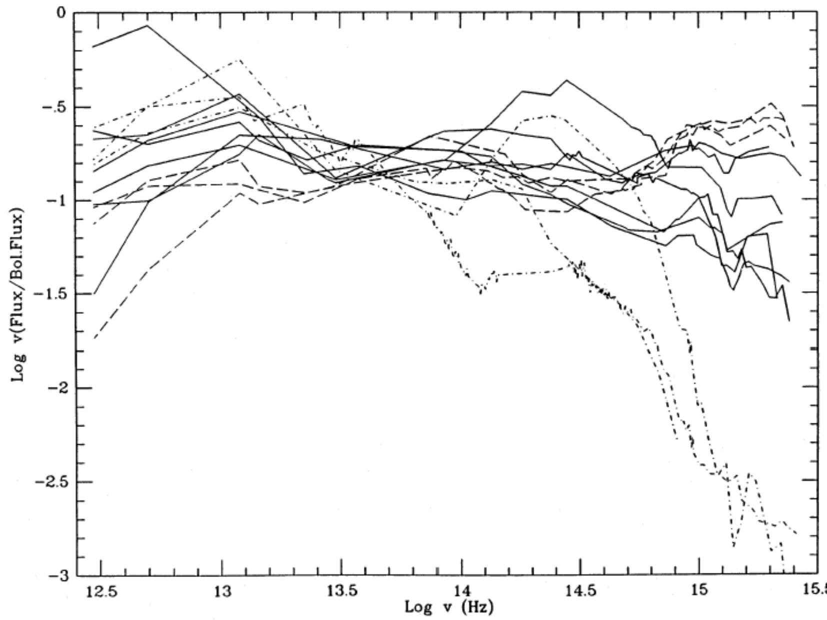

FIG. 3.1.- Taken from Spinoglio & Malkan (1989). The spectral energy distributions for 13 AGN. The "pinched" region has the least scatter around log ν = 13.4 - 13.6. Hence the best representation, for all AGN types, of the bolometric fluxes is at MIR wavelengths. The flux values here were normalized by the bolometric fluxes from 0.1 to 100 µm. The dashed lines, the bluest objects, are the Palomar Green Quasars (Green et al. 1986), the reddest are Sy1 from Edelson & Malkan (1986) and plotted as dash-dot.

The sources of the central far infrared (FIR) emission are thought to be essentially the same; the reradiation of energy by a dusty torus, as well as contributions from nonthermal emission from the nucleus (Mouri & Taniguchi 1992). Because the *IRAS* all-sky survey (details of the survey in §3.2) was an early, pioneering survey, Sy and AGN in general have been studied at that survey's instruments main bands (12, 25, 60, and 100 µm) for many years. One limitation is that *IRAS* was of fairly low resolution so FIR emission from starburst activity in the host galaxy can be a factor in the cataloged luminosities. Fortunately such emission in most local Sy is not significant in the *global* FIR total flux densities.

As outlined at the end of Chapter 1, in this chapter the M-FIR properties of the newly constructed sample (§2.1) are investigated, primarily using data from the *IRAS* and 2MASS all-sky surveys. Before this is done, following immediately below, a brief description of the two surveys is given.

3.2 THE SURVEYS

3.2.1 The *IRAS*

The *Infrared Astronomical Satellite* (*IRAS*) carried out what was, for many years, the only all-sky, FIR survey (12, 25, 60, and 100 µm) ever completed and so its results have been the focus of much of the (mainly global) MID & FIR research on Seyferts and AGN in general. The joint (US, UK, Netherlands) project was started in 1975 and the satellite was launched in January, 1983. Operations ceased several months later, in November, 1983.

The most comprehensive summary of the mission goals and instrumentation is to be found in the *IRAS* Explanatory Supplement (Beichman et al. 1988) which has more recently been revised and put online (Beichman et al. 2002).

The number of astronomical objects cataloged was dramatically increased, nearly 70%. Covering over 96% of the sky, over 350,000 objects were detected. The most significant data products that are the primary legacy of *IRAS* are the *Faint Source* and *Point Source Catalogs* (FSC and PSC, respectively). The PSC gives information on nearly 250,000 point sources, and the FSC some 20,000 extended sources (Beichman et. al 2002). These catalogs continue to play an important role in astrophysical research despite its somewhat lower resolution and sensitivity as compared to modern instruments of today.

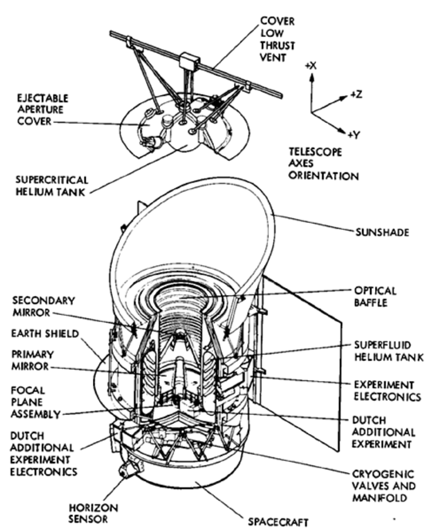

FIG. 3.2.- The telescope at the heart of the *IRAS*. Image taken from *IRAS* ES, chapter 2, C.

At heart of the *IRAS* optical system was a two-mirror Ritchey-Chretien telescope, constructed of beryllium, with a aluminum coated secondary mirror (Figure 3.2). The design goal, reached at all survey bands but 12 µm, was to obtain diffraction-limited optics. The primary mirror (eccentricity of 1.00569) had a diameter of 60 cm, with a (measured) system focal length of 545 cm. The effective collecting area of the *IRAS* telescope was 2019 cm^2, and the system F/number was 9.56. The measured plate scale at the focal plane was 1.585 mm per arcmin (*IRAS* ES, Chapter 2, C3). The positional accuracy of detected sources depended on several factors, namely the apparent size and luminosity of the object. In most cases this amounted to an accuracy < 20". In §3.4, a discussion on how upper limits for censored objects were derived, the sensitivity of the *IRAS* optical system is discussed in some more detail; in general the limiting flux density depended on sky location and bandwidth. For a detailed discussion of the optical system overall in *IRAS*, see Harned et al. (1981).

3.2.2 The 2MASS

This near infrared survey, started in 1997 (northern hemisphere, at Mt. Hopkins) and 1998 (southern hemisphere, at CTIO, Chile) and completed in just 2001, was ground-breaking in many ways. In it, the whole sky (or > 95% of the sky for galactic latitude |b|>10° and approximately 95% for |b|<10°, with no gaps > 200 deg^2) was scanned at bandwidths centered on 1.25, 1.65, and 2.17µm (J, H, K_s bands, respectively). The survey instruments detected and characterized point sources with flux density values greater than approximately 1 mJy in each of the three bands and obtaining a signal-to-noise ratio > 10 using a pixel size of 2.0" per side (Skrutskie et. al 2006).

The primary instruments for the 2MASS survey were two automated telescopes, located at the facilities mentioned above. Both had a three-channel camera, comprised of an array of mercury cadmium tellurium (HgCdTe) detectors of dimension 256 x 256 pixels which observed all three bands simultaneously (Figure 3.3).

FIG. 3.3- The three-band NIR camera (gold colored cylinder) mounted on the 2MASS telescope at Mt. Hopkins. Image taken from http://pegasus.astro.umass.edu/

Similar to the case of *IRAS*, two of the data products of 2MASS were both a point (PSC) and extended (ESC) source catalog. Unlike *IRAS*, the imaging capabilities were significant and a digital all-sky atlas has been completed. The primary paper describing the survey and its catalog and image data products is Skrutskie, et al. (2006).

For the PSC, the (designed) completeness requirement of > 0.99 at 10-σ sensitivity limit was met. A reliability of 0.9997 was achieved. For photometric sensitivity the requirement was for 10- σ at 15.8, 15.1, and 14.3 mag at J, H, and Ks bands (respectively), |b|>10°, and this was exceeded for most of the sky (Skrutskie et al. 2006).

In the ESC, the (designed) completeness requirement of > 0.90 for |b|>30° was met. A reliability of > 0.80 for 10°< |b|<20° and >0.99 for |b|>10° for was achieved. For photometric sensitivity the requirement of 10- σ at J < 15.0, H < 14.2, and Ks < 13.5 mag was met (Skrutskie et al. 2006).

Another way in which 2MASS was ground-breaking was the enormous challenges posed by the immense quantities of data that needed to be processed. Some issues in the automated pipeline have been found (Schombert 2007), mostly relating to the fitting of near-by, large galaxies with a lot of observed structure. As shown by Schombert (2007), for some near-by galaxies the 2MASS fits "consistently underestimate the amount of disk light per isophote". This can give rise to an error in the size of the galaxy, underestimating it by up to 50%. In general though, this is not an issue for this study of Seyferts as the majority of the objects in the sample are point sources. However, as discussed in §4.5, several are close-by and so an independent reanalysis of the 2MASS data seems to be in order.

3.3 THE DATA

In Tables 3.1 & 3.2 below the NIR and FIR flux densities for the sample are given. Also included are the flux density values at two optical wavelengths (blue and red), centered at approximately .44 and .64 µm. These data were available for 61 of the Sy2 and 24 of the Sy1 (79% and 57% of each type, respectively, or ~71% of the total sample). The data are from *The Surface Photometry Catalogue of the ESO-Uppsala Galaxies* (Lauberts & Valentijn 1989). The catalog uses the original plates, 407 blue and 407 red, which were from an earlier survey, the *ESO Quick Blue Schmidt Survey* (West & Schuster 1982). This older survey resulted in a catalog containing 14,155 galaxies with δ < -17.5° and a visual diameter > 1'. As discussed in Lauberts & Valentijn (1989), the newer catalog was derived by automating the process; scanning the original plates using a PDS microdensitometer. In the original survey the catalog information was obtained through visual inspection of the plates. Due to the method in which the catalog flux density values were obtained - directly from the plates - no attempt was made to compute the upper limits here for any object in this sample that was censored at these optical wavelengths.

IR flux density values in bold type are derived upper limit values. Bold and underlined values are upper limits taken from the literature. The derivation of the upper limits for all of the sample objects is discussed below in §3.4.

For each IR band, the associated errors for the total flux densities are given in tables 3.1 and 3.2. As can be seen, the errors on the 2MASS data are small, smaller in measure than achieved in the SUMSS, with an average of 2.8% (uncensored objects, J-band. The other two 2MASS bands having very similar errors). The *IRAS* error values are much larger which is to be expected of that much older instrumentation. At 100 µm the average of errors on the flux densities is 9.2%. This increases going to the lower bands, with an average of 12.9% at 12 µm.

TABLE 3.1

Optical and IR Flux Densities - Seyfert 2

			2MASS						IRAS							
Object	B_T .44 μm Jy	R_T .64 μm Jy	J 1.25μm Jy	err	H 1.65μm Jy	err	K_S 2.17μm Jy	err	12μm Jy	err %	25μm Jy	err %	60μm Jy	err %	100μm Jy	err %
LEDA 087391			0.00575	0.00046	0.00852	0.00074	0.01070	0.00082	**0.1700**	<	**0.4100**	<	**0.9900**	<	**1.2600**	<
NGC 0424	0.01330	0.03440	0.10000	0.00158	0.13000	0.00243	0.14900	0.00290	1.1010	5	1.7390	5	1.7960	7	1.8230	9
LEDA 093365			**0.00106**	<	**0.00169**	<	**0.00034**	<	**0.1800**	<	**0.1800**	<	**0.1800**	<	**0.3000**	<
PGC 004440	0.02320	0.04790	0.10800	0.00150	0.12800	0.00214	0.10700	0.00270	**0.2053**	<	0.2727	19	2.7680	7	7.4810	6
NGC 0454			**0.00026**	<	**0.00035**	<	**0.00012**	<	0.2129	24	0.4172	9	1.4760	12	2.8220	8
PGC 004569	0.00722	0.01760	0.03620	0.00081	0.04370	0.00102	0.03670	0.00131	**0.1131**	<	0.1051	27	0.6425	8	1.5790	10
PGC 005696	0.01430	0.04020	0.06330	0.00118	0.07540	0.00190	0.07060	0.00204	0.1812	25	0.3001	17	2.1630	11	5.7610	6
PGC 006078	0.00828	0.02010	0.05470	0.00102	0.07470	0.00181	0.06450	0.00199	**0.1735**	<	0.1664	24	0.6619	10	2.2080	9
PGC 006351	0.00766	0.02080	0.04030	0.00098	0.04810	0.00126	0.04390	0.00165	**0.1459**	<	0.1111	28	0.9909	8	1.7740	10
PGC 008012	0.01010	0.02630	0.05720	0.00171	0.07070	0.00198	0.06150	0.00260	0.0971	23	0.1954	11	0.8898	5	**3.0160**	<
NGC 0824	0.00939	0.02770	0.04040	0.00175	0.05090	0.00201	0.04610	0.00276	**0.0320**	<	**0.3200**	<	**0.3800**	<	**0.8500**	<
PGC 009634	0.01210	0.03770	0.07060	0.00131	0.08580	0.00168	0.07260	0.00204	0.1609	11	0.3926	6	1.3940	4	2.3350	8
PGC 010665	0.00834	0.02070	0.06080	0.00176	0.05820	0.00263	0.05220	0.00317	**0.1131**	<	**0.1240**	<	0.8276	6	2.2180	7
PGC 010705	0.00881	0.03030	0.05010	0.00093	0.06440	0.00132	0.05230	0.00137	0.0772	26	0.3285	8	4.4710	4	6.6770	4
PGC 011104	0.00821	0.01720	0.05330	0.00129	0.06400	0.00204	0.05360	0.00217	**0.1157**	<	**0.1577**	<	0.1843	22	**0.5872**	<
PGC 012759	0.00393	0.01190	0.04630	0.00121	0.05340	0.00175	0.04550	0.00162	0.1857	13	0.6383	4	1.4580	4	1.9790	11
NGC 1386	0.05830	0.15400	0.40900	0.00341	0.48200	0.00446	0.39600	0.00514	0.4927	6	1.4330	5	5.9200	1	9.6410	4
PGC 014702	0.02020	0.04310	0.10100	0.00149	0.11900	0.00210	0.10700	0.00250	0.5246	6	2.1350	5	14.1700	4	21.6100	4
AM 0426-625			**0.01267**	<	**0.01314**	<	**0.00067**	<	**0.4000**	<	**0.4000**	<	**0.4000**	<	**0.4000**	<
PGC 015172	0.01690	0.04900	0.09260	0.00207	0.12000	0.00302	0.10900	0.00407	0.0824	23	0.1963	11	1.8690	4	3.5760	5
NGC 1672	0.26200	0.47300	1.10000	0.02160	1.19000	0.02760	1.04000	0.02910	1.6740	4	5.2500	1	32.9600	4	69.8900	4
PGC 016072	0.00503	0.01020	0.02260	0.00070	0.02810	0.00116	0.01980	0.00126	**0.1300**	<	**0.1300**	<	**0.1300**	<	**0.3200**	<
PGC 016357	0.00610	0.01360	0.04810	0.00144	0.06910	0.00240	0.06500	0.00250	0.2075	8	0.4467	4	0.6777	5	**2.0790**	<
NGC 1808	0.20400	0.55500	1.40000	0.02210	1.65000	0.02760	1.45000	0.02830	4.4350	4	16.1400	4	87.8100	4	137.2000	4
PGC 016873	0.01510	0.03190	0.10100	0.00131	0.11900	0.00165	0.09930	0.00222	0.0660	27	0.1832	11	0.6444	6	**1.5010**	<
PGC 017768	0.00445	0.01190	0.02430	0.00075	0.02770	0.00104	0.02240	0.00131	**0.0867**	<	0.1144	17	0.1968	17	**0.7495**	<
LEDA 096373			0.05930	0.00155	0.08380	0.00227	0.07510	0.00289	0.2970	20	0.8700	7	1.5400	7	3.0280	7
PGC 021057	0.01500	0.02900	0.10700	0.00209	0.14000	0.00286	0.11100	0.00354	0.1680	9	0.2762	8	1.2620	5	4.2520	7
PGC 023573			0.03230	0.00162	0.03850	0.00257	0.03600	0.00300	**0.2790**	<	0.4530	14	1.3170	10	4.6470	16
PGC 028144	0.00979	0.03250	0.09750	0.00145	0.12600	0.00222	0.12100	0.00237	*0.3090*	<	*0.6830*	<	*2.5190*	<	*5.0325*	<
PGC 028147			0.05270	0.00168	0.07610	0.00235	0.04400	0.00267	**0.4200**	<	**0.4200**	<	**1.5800**	<	**2.6600**	<
PGC 029778	0.00406	0.00826	0.02640	0.00127	0.03350	0.00155	0.02950	0.00191	**0.1870**	<	0.2083	15	0.3800	13	**1.1210**	<
PGC 029993	0.04130	0.09750	0.21300	0.00297	0.26300	0.00416	0.22200	0.00517	0.2962	11	0.9435	6	3.2440	10	6.1090	6
PGC 030984	0.01750	0.03290	0.05450	0.00310	0.06290	0.00438	0.05030	0.00506	0.1541	20	0.1867	19	1.3780	7	3.3200	11
NGC 3281	0.03800	0.10500	0.30000	0.00417	0.36600	0.00612	0.31700	0.00737	0.8896	13	2.6330	7	6.8610	7	7.5120	7
LEDA 088648			0.02770	0.00099	0.03750	0.00112	0.03140	0.00136	**0.0767**	<	**0.1519**	<	0.5233	11	1.2180	20
NGC 4507	0.02810	0.06430	0.17100	0.00237	0.21400	0.00318	0.18900	0.00386	0.4566	10	1.3870	10	4.3100	7	5.3990	12
PGC 042504	0.02660	0.05480	0.09410	0.00148	0.10900	0.00182	0.09650	0.00234	0.6430	12	2.2620	7	7.5150	7	10.7300	9
WKK 1263			0.01940	0.00179	0.03710	0.00233	0.02780	0.00251	**0.1700**	<	**0.1700**	<	**0.2900**	<	**1.1700**	<
PGC 043779	0.01180	0.03740	0.09600	0.00170	0.12000	0.00200	0.10100	0.00273	0.1080	26	0.3054	13	0.9907	10	1.9120	20
NGC 4785	0.02200	0.06120	0.22600	0.00293	0.29500	0.00383	0.25000	0.00464	0.3085	12	0.4840	8	3.6400	6	10.4700	7
PGC 044167	0.00551	0.01390	0.01310	0.00116	0.06040	0.00198	0.01590	0.00173	**0.2000**	<	**0.2000**	<	**0.2000**	<	**0.9200**	<
NGC 4903	0.01360	0.03100	0.05830	0.00331	0.07920	0.00412	0.08220	0.00539	**0.1111**	<	0.2875	18	0.7686	13	2.3960	12
NGC 4945	0.80500	2.94000	9.18000	0.13600	11.90000	0.18700	10.70000	0.16900	23.6500	15	43.2800	15	625.4600	0	1415.5000	15
ESO 383- G 018	0.00326	0.00587	0.01570	0.00075	0.01830	0.00099	0.02070	0.00123	0.1360	21	0.4440	8	0.6164	9	**1.2220**	<
Circinus	0.18800	1.15000	5.10000	0.12400	7.40000	0.15800	6.77000	0.15800	18.8000	4	68.4400	4	248.7000	10	315.8500	10
LEDA 141858			0.01060	0.00073	0.01210	0.00105	0.01210	0.00117	**0.1090**	<	0.4186	6	1.6780	5	**2.1060**	<

TABLE 3.1 Con't.

Optical and IR Flux Densities - Seyfert 2

			2MASS						IRAS							
Object	B_T .44 µm Jy	R_T .64 µm Jy	J 1.25µm Jy	err	H 1.65µm Jy	err	K_S 2.17µm Jy	err	12µm Jy	err %	25µm Jy	err %	60µm Jy	err %	100µm Jy	err %
NGC 5643	0.16400	0.33100	0.93900	0.01830	1.06000	0.02380	0.90800	0.00870	1.0980	6	3.6470	6	19.4900	5	38.1600	5
PGC 052101			0.01220	0.00084	0.01440	0.00102	0.01440	0.12000	**0.0846**	<	0.2624	17	0.8256	7	**1.0710**	<
LEDA 166339			0.01750	0.00084	0.02420	0.00119	0.02550	0.05300	**0.1600**	<	**0.1600**	<	**0.1600**	<	**0.4400**	<
IC 4518			**0.00100**	<	**0.00023**	<	**0.00037**	<	0.3449	8	1.3080	6	7.6090	4	12.7600	6
WKK 3646			**0.00260**	<	**0.00098**	<	**0.00106**	<	**0.1800**	<	**0.1800**	<	**0.1800**	<	**0.4200**	<
PGC 058547	0.05630	0.14200	0.34500	0.00836	0.39100	0.01060	0.33200	0.03600	0.2900	7	0.7430	5	2.2770	5	**20.6200**	<
PGC 059124	0.00776	0.01910	0.06070	0.00187	0.08480	0.00238	0.08410	0.03200	0.4830	8	1.7580	8	2.6480	10	**2.3950**	<
NGC 6221	0.23200	0.41300	0.91300	0.01950	1.17000	0.02610	0.94500	0.02900	1.4930	6	5.2670	6	49.0700	0	86.0600	0
NGC 6300	0.18900	0.51400	1.14000	0.01800	1.35000	0.02390	1.13000	0.02000	0.9268	6	2.2720	5	14.6500	5	36.0300	7
PGC 060594	0.01530	0.02260	0.08970	0.00234	0.09980	0.00327	0.08720	0.03900	0.1217	22	0.1738	20	0.6557	10	1.6110	23
PGC 062134			0.03870	0.00068	0.06200	0.00104	0.09260	0.01500	0.6231	7	1.3850	6	3.2270	5	3.9050	9
PGC 062174	0.00536	0.01560	0.04480	0.00100	0.05720	0.00155	0.04930	0.03500	0.6121	7	2.3630	5	2.3140	5	1.0520	25
PGC 062218	0.01570	0.05650	0.08820	0.00356	0.09790	0.00537	0.10300	0.05300	0.1187	18	0.1559	26	1.4290	6	4.4850	7
PGC 062428	0.00984	0.02540	0.05170	0.00130	0.06230	0.00186	0.05800	0.03400	0.2320	12	0.7622	6	4.3760	5	8.1460	7
PGC 062440	0.00600	0.01280	0.03370	0.00123	0.04300	0.00186	0.03270	0.05900	**0.0933**	<	**0.1442**	<	0.6138	9	0.9646	22
NGC 6810	0.04950	0.16100	0.47700	0.00397	0.65600	0.00485	0.56500	0.00900	1.1010	5	3.4910	5	17.7900	5	34.5000	4
PGC 063874	0.00647	0.01660	0.06040	0.00107	0.07720	0.00187	0.06780	0.03000	0.3736	16	1.1750	10	6.0500	6	9.1390	9
NGC 6890	0.02550	0.07240	0.16100	0.00178	0.19300	0.00233	0.16300	0.01900	0.3422	11	0.6541	8	3.8550	6	8.1550	5
PGC 064491	0.00797	0.02250	0.05450	0.00132	0.06770	0.00215	0.05570	0.04000	0.0847	25	0.3294	9	0.8276	7	1.2540	16
PGC 064537	0.00577	0.01470	0.02670	0.00095	0.03210	0.00145	0.02680	0.06000	**0.1291**	<	**0.2122**	<	0.7513	8	1.3040	26
PGC 065600	0.02900	0.09270	0.20900	0.00271	0.25200	0.00374	0.21100	0.02000	1.0670	12	3.9100	5	5.3370	10	4.1680	8
NGC 7130	0.03050	0.07270	0.12900	0.00156	0.15700	0.00189	0.14000	0.01900	0.5882	6	2.1170	5	16.7100	0	25.5700	5
NGC 7172	0.03090	0.10700	0.26700	0.00471	0.34400	0.00671	0.31400	0.02300	0.4370	8	0.7612	7	5.7120	6	12.2900	5
PGC 068122	0.00365	0.00766	**0.00250**	<	**0.00009**	<	**0.00029**	<	**0.0972**	<	0.1478	22	0.9335	6	1.8780	8
PGC 068198	0.01320	0.03120	0.07480	0.00069	0.09400	0.00131	0.08200	0.02900	0.1982	14	0.4607	7	3.4040	5	6.7340	5
FAIRALL 0357			0.02200	0.00055	0.02660	0.00080	0.02340	0.04800	**0.0993**	<	0.0807	27	0.6686	10	1.5390	10
PGC 070458	0.00745	0.01610	0.03420	0.00080	0.04960	0.00139	0.03800	0.03900	0.1416	22	0.3514	13	2.9130	8	4.3680	7
NGC 7496	0.07280	0.12900	0.25500	0.00523	0.29800	0.00694	0.23100	0.04300	0.3473	17	1.6010	7	8.4580	9	15.5500	5
NGC 7582	0.18300	0.40900	0.72500	0.01140	0.87100	0.01460	0.79000	<	1.6200	6	6.4360	5	49.1000	6	72.9200	7
NGC 7590	0.06060	0.11600	0.30100	0.00279	0.34100	0.00379	0.28900	0.01700	0.5630	7	0.8312	8	6.9120	10	**23.7000**	<

Note. - Optical, NIR, MIR, and FIR total flux densities for the Sy2 in the sample, taken from the surveys described above.

In Tables 3.3 & 3.4 the optical, NIR, and M/FIR luminosities are given. These were computed the same was as described in §2.5.3 with the SUMSS 843MHz data. Values in bold type are computed by using the upper limit flux values from Tables 3.1 & 3.2, while the bold and underlined are computed by using the upper limits flux values taken from the literature, obtained through NED. The associated errors for the IR luminosities are given in Appendix C and are computed the same way as with the radio luminosity values (§2.5.3, page 68).

TABLE 3.2

Optical and IR Flux Densities - Seyfert 1

			2MASS						IRAS							
Object	B_T .44 µm Jy	R_T .64 µm Jy	J 1.25µm Jy	err	H 1.65µm Jy	err	K_S 2.17µm Jy	err	12µm Jy	err %	25µm Jy	err %	60µm Jy	err %	100µm Jy	err %
LEDA 087392			0.00732	0.00044	0.00818	0.00071	0.01120	0.00069	*0.0399*	<	*0.0692*	<	*0.1235*	<	*0.3171*	<
PGC 002450	0.00656	0.01300	0.02590	0.00063	0.03380	0.00098	0.03900	0.00109	0.1665	11	0.2531	7	1.4520	4	2.9810	6
PKS 0056-572			**0.00032**	<	**0.00008**	<	**0.00010**	<	**0.2300**	<	**0.2300**	<	**0.2300**	<	**0.3100**	<
PGC 003864	0.00598	0.01400	0.03050	0.00097	0.03390	0.00134	0.03720	0.00154	0.1698	21	0.2812	15	1.4710	11	2.3850	11
IRAS 01089-4743			**0.00718**	<	**0.00647**	<	**0.00064**	<	0.1327	18	0.1750	14	0.9569	7	2.1970	9
PGC 004822	0.00623	0.01820	0.04540	0.00149	0.05500	0.00259	0.04730	0.00255	**0.0880**	<	0.1115	26	0.5376	22	1.3860	12
NGC 526A	0.00532	0.01270	0.03650	0.00116	0.05590	0.00183	0.04460	0.00210	0.2450	12	0.5184	23	**0.4000**	<	**1.0000**	<
PMN J0133-5159			0.00040	0.00009	**0.00166**	<	**0.00055**	<	**0.1300**	<	**0.1300**	<	**0.0130**	<	**0.5800**	<
ESO 080- G 005	0.00162	0.00459	0.01230	0.00061	0.01820	0.00105	0.01310	0.00102	**0.1300**	<	**0.1300**	<	**0.1500**	<	**0.1900**	<
NGC 1097	0.43700	0.99700	2.14000	0.04380	2.56000	0.05950	2.10000	0.06700	1.9800	4	5.5090	5	44.5400	5	85.3400	4
PGC 011706	0.00385	0.00452	0.01830	0.00086	0.02480	0.00129	0.01850	0.00150	**0.1100**	<	**0.1100**	<	**0.1100**	<	**0.2400**	<
NGC 1365	0.31700	0.94000	1.81000	0.04380	2.07000	0.05990	1.88000	0.06350	3.3720	4	10.8200	5	76.1300	6	142.5000	4
NGC 1566	0.35600	0.64000	1.26000	0.02690	1.33000	0.03610	1.17000	0.03730	0.8310	7	1.2190	6	14.7100	5	46.3600	4
PGC 017103	0.01280	0.02500	0.05760	0.00102	0.07120	0.00139	0.06520	0.00201	0.2238	19	0.5699	6	1.3960	7	1.9930	8
FAIRALL 0265			0.01770	0.00058	0.02300	0.00093	0.02650	0.00102	0.0787	22	0.2033	9	0.6729	7	1.1620	18
LEDA 096433			0.04110	0.00123	0.05800	0.00146	0.05730	0.00171	**0.2500**	<	0.1640	18	1.2890	10	3.5550	12
PGC 027468			0.03650	0.00154	0.04680	0.00189	0.04010	0.00208	*0.1991*	<	*0.3452*	<	*0.6160*	<	*1.5811*	<
PGC 029148			0.03640	0.00085	0.04460	0.00129	0.03740	0.00151	**0.0700**	<	**0.0700**	<	**0.0700**	<	**0.0700**	<
PGC 029151	0.00400	0.00768	0.02410	0.00086	0.02770	0.00122	0.02330	0.00150	**0.1400**	<	**0.1400**	<	**0.1400**	<	**0.3800**	<
PGC 033084	0.00203	0.00411	0.02140	0.00185	0.02860	0.00250	0.02950	0.00252	**0.3210**	<	**0.2500**	<	0.3440	10	**8.6100**	<
PGC 034101	0.01630	0.04980	0.07480	0.00775	0.08290	0.01110	0.06930	0.01070	0.1278	28	0.2438	18	0.9976	14	2.9270	13
PGC 036002	0.01060	0.02810	0.08700	0.00260	0.11400	0.00385	0.10000	0.00395	0.1430	16	0.2354	10	1.3440	6	4.2520	11
NGC 3783	0.04400	0.09070	0.18600	0.00242	0.23600	0.00350	0.23100	0.00430	0.8396	7	2.4920	6	3.2570	6	4.8990	11
LEDA 096527			**0.00141**	<	**0.00035**	<	**0.00050**	<	0.1158	20	0.3261	8	1.1570	6	1.8280	19
PGC 045371	0.01570	0.04860	0.13100	0.00207	0.18500	0.00275	0.20100	0.00317	0.6828	6	1.2210	6	5.6590	5	8.7900	6
PGC 047969	0.01180	0.03300	0.07150	0.00086	0.09440	0.00140	0.09800	0.00155	0.3803	9	0.8088	7	1.0870	7	1.0960	20
PGC 049051	0.01280	0.04150	0.12800	0.00297	0.17100	0.00413	0.20000	0.00241	1.0820	5	2.2130	5	2.0300	5	1.6610	13
PGC 050427			0.00512	0.00032	0.00623	0.00046	0.00718	0.00058	**0.1800**	<	**0.1800**	<	**0.1800**	<	**0.5600**	<
ESO 328- G036			**0.00049**	<	**0.00025**	<	**0.00023**	<	**0.1700**	<	**0.1700**	<	**0.1700**	<	**0.5600**	<
PKS 1521-300			0.02800	0.00076	0.03710	0.00121	0.02880	0.00125	**0.0900**	<	**0.0900**	<	**0.0900**	<	**0.1300**	<
LEDA 2793282			0.04200	0.00272	0.02260	0.00044	0.05340	0.00303	**0.1400**	<	**0.1400**	<	**0.1400**	<	**0.9000**	<
PGC 062346	0.00938	0.02060	0.05300	0.00108	0.07030	0.00150	0.08690	0.00162	**0.4671**	<	1.0350	5	1.8440	8	2.7490	17
PGC 062554	0.00617	0.01800	0.04380	0.00148	0.05940	0.00228	0.04880	0.00230	0.0680	28	0.0911	20	0.3235	14	**2.3270**	<
ESO 399-IG 020			**0.00053**	<	**0.00010**	<	**0.00048**	<	0.1143	28	0.1667	25	0.5423	10	**1.4750**	<
NGC 6860	0.01410	0.04280	0.09200	0.00119	0.11800	0.00198	0.11700	0.00228	0.2397	12	0.3321	10	0.9538	8	2.4690	9
PGC 064989			0.04620	0.00077	0.05700	0.00138	0.05240	0.00147	**0.0903**	<	**0.1050**	<	0.3539	19	1.4780	28
ESO 235- G 059	0.00551	0.01530	0.03730	0.00080	0.04640	0.00126	0.04340	0.00117	**0.1057**	<	**0.0706**	<	0.3963	15	0.8110	22
CTS 0109			0.00569	<	0.00726	<	0.01049	<	**0.1000**	<	**0.1000**	<	**0.1800**	<	**0.6700**	<
PGC 067075	0.00398	0.01020	0.02530	0.00061	0.03080	0.00083	0.02320	0.00098	**0.0900**	<	**0.0900**	<	**0.0900**	<	**0.1400**	<
NGC 7213	0.17400	0.48200	1.04000	0.00862	1.18000	0.01200	1.02000	0.01520	0.6063	8	0.7421	6	2.6660	6	8.1770	5
J224704.9-305502			**0.00017**	<	**0.00026**	<	**0.00023**	<	**0.0700**	<	**0.0700**	<	**0.0700**	<	**0.0600**	<
PGC 073028			**0.00022**	<	**0.00032**	<	**0.00017**	<	**0.1609**	<	0.1201	36	0.3464	14	0.9323	21

Note. - Optical, NIR, MIR, and FIR total flux densities for the Sy1 in the sample, taken from the surveys described above.

TABLE 3.3

Log(Luminosity) (W/Hz) Seyfert 2

Object	.44μm	.64μm	1.25μm	1.65μm	2.17μm	12μm	25μm	60μm	100μm
LEDA 087391			22.04	22.21	22.31	**23.51**	**23.89**	**24.28**	**24.38**
NGC 0424	21.60	22.01	22.48	22.59	22.65	23.52	23.72	23.73	23.74
LEDA 093365			**21.20**	**21.41**	**20.71**	**23.43**	**23.43**	**23.43**	**23.65**
PGC 004440	21.86	22.17	22.52	22.60	22.52	**22.80**	22.93	23.93	24.37
NGC 0454			**19.92**	**20.05**	**19.59**	22.83	23.13	23.68	23.96
PGC 004569	21.98	22.36	22.68	22.76	22.68	**23.17**	23.14	23.93	24.32
PGC 005696	21.93	22.38	22.58	22.65	22.62	23.03	23.25	24.11	24.53
PGC 006078	22.07	22.45	22.89	23.02	22.96	**23.39**	23.37	23.97	24.49
PGC 006351	22.17	22.61	22.90	22.97	22.93	**23.45**	23.34	24.29	24.54
PGC 008012	21.94	22.35	22.69	22.78	22.72	22.92	23.22	23.88	**24.41**
NGC 0824	21.89	22.36	22.52	22.62	22.58	**22.42**	**23.42**	**23.50**	**23.85**
PGC 009634	21.88	22.37	22.65	22.73	22.66	23.01	23.39	23.94	24.17
PGC 010665	21.85	22.24	22.71	22.69	22.64	**22.98**	**23.02**	23.84	24.27
PGC 010705	21.73	22.27	22.48	22.59	22.50	22.67	23.30	24.43	24.61
PGC 011104	21.68	22.00	22.49	22.57	22.49	**22.83**	**22.96**	23.03	**23.53**
PGC 012759	21.47	21.95	22.54	22.60	22.53	23.15	23.68	24.04	24.17
NGC 1386	21.02	21.45	21.87	21.94	21.86	21.95	22.41	23.03	23.24
PGC 014702	21.79	22.12	22.49	22.57	22.52	23.21	23.82	24.64	24.82
AM 0426-625			**21.97**	**21.99**	**20.69**	**23.47**	**23.47**	**23.47**	**23.47**
PGC 015172	22.00	22.47	22.74	22.85	22.81	22.69	23.07	24.05	24.33
NGC 1672	22.04	22.30	22.67	22.70	22.64	22.85	23.35	24.14	24.47
PGC 016072	21.77	22.07	22.42	22.51	22.36	**23.18**	**23.18**	**23.18**	**23.57**
PGC 016357	21.64	21.99	22.54	22.70	22.67	23.17	23.51	23.69	**24.17**
NGC 1808	21.69	22.12	22.52	22.59	22.54	23.02	23.58	24.32	24.51
PGC 016873	21.91	22.24	22.74	22.81	22.73	22.55	23.00	23.54	**23.91**
PGC 017768	21.79	22.22	22.53	22.58	22.49	**23.08**	23.20	23.44	**24.02**
LEDA 096373			23.06	23.21	23.16	23.76	24.23	24.47	24.77
PGC 021057	21.67	21.96	22.53	22.64	22.54	22.72	22.94	23.60	24.13
PGC 023573			22.35	22.43	22.40	**23.29**	23.50	23.96	24.51
PGC 028144	21.18	21.70	22.18	22.29	22.28	*22.68*	*23.03*	*23.59*	*23.89*
PGC 028147			22.00	22.16	21.92	**22.90**	**22.90**	**23.48**	**23.70**
PGC 029778	21.86	22.17	22.68	22.78	22.73	**23.53**	23.57	23.84	**24.31**
PGC 029993	21.93	22.30	22.64	22.73	22.66	22.79	23.29	23.83	24.10
PGC 030984	21.86	22.13	22.35	22.41	22.31	22.80	22.88	23.75	24.13
NGC 3281	21.97	22.42	22.87	22.96	22.89	23.34	23.81	24.23	24.27
LEDA 088648			22.75	22.88	22.81	**23.19**	**23.49**	24.03	24.40
NGC 4507	21.93	22.29	22.71	22.81	22.76	23.14	23.62	24.12	24.21
PGC 042504	21.85	22.16	22.39	22.46	22.40	23.23	23.77	24.30	24.45
WKK 1263			22.41	22.69	22.57	**23.35**	**23.35**	**23.58**	**24.19**
PGC 043779	21.82	22.32	22.73	22.83	22.75	22.78	23.23	23.74	24.03
NGC 4785	21.86	22.30	22.87	22.98	22.91	23.00	23.20	24.08	24.53
PGC 044167	21.53	21.93	21.91	22.57	21.99	**23.09**	**23.09**	**23.09**	**23.75**
NGC 4903	21.91	22.26	22.54	22.67	22.69	**22.82**	23.23	23.66	24.15
NGC 4945	21.78	22.34	22.84	22.95	22.90	23.25	23.51	24.67	25.02
ESO 383- G 018	21.04	21.29	21.72	21.79	21.84	22.66	23.17	23.31	**23.61**
Circinus	20.92	21.71	22.36	22.52	22.48	22.92	23.48	24.04	24.15
LEDA 141858			22.21	22.27	22.27	**23.22**	23.81	24.41	**24.51**

TABLE 3.3 Con't.									
Log(Luminosity) (W/Hz) Seyfert 2									
Object	.44µm	.64µm	1.25µm	1.65µm	2.17µm	12µm	25µm	60µm	100µm
NGC 5643			22.51	22.56	22.49	22.57	23.10	23.82	24.12
PGC 052101			22.24	22.31	22.31	**23.08**	23.57	24.07	**24.19**
LEDA 166339			22.41	22.56	22.58	**23.38**	**23.38**	**23.38**	**23.82**
IC 4518			**20.73**	**20.09**	**20.30**	23.27	23.85	24.61	24.84
WKK 3646			**21.09**	**20.67**	**20.70**	**22.93**	**22.93**	**22.93**	**23.30**
PGC 058547	22.01	22.41	22.80	22.85	22.78	22.72	23.13	23.62	**24.57**
PGC 059124	21.15	21.54	22.04	22.19	22.18	22.94	23.50	23.68	**23.64**
NGC 6221	22.10	22.35	22.69	22.80	22.71	22.90	23.45	24.42	24.67
NGC 6300	21.75	22.18	22.53	22.60	22.52	22.44	22.83	23.64	24.03
PGC 060594	21.99	22.16	22.75	22.80	22.74	22.89	23.04	23.62	24.01
PGC 062134			22.54	22.75	22.92	23.75	24.10	24.46	24.55
PGC 062174	21.31	21.78	22.24	22.34	22.28	23.37	23.96	23.95	23.61
PGC 062218	21.88	22.43	22.63	22.67	22.69	22.76	22.87	23.84	24.33
PGC 062428	21.69	22.10	22.41	22.49	22.46	23.06	23.58	24.34	24.61
PGC 062440	21.66	21.98	22.41	22.51	22.39	**22.85**	**23.04**	23.67	23.86
NGC 6810	21.69	22.20	22.68	22.81	22.75	23.04	23.54	24.25	24.53
PGC 063874	21.72	22.13	22.69	22.80	22.74	23.48	23.98	24.69	24.87
NGC 6890	21.56	22.01	22.36	22.43	22.36	22.68	22.96	23.73	24.06
PGC 064491	21.65	22.11	22.49	22.58	22.50	22.68	23.27	23.67	23.85
PGC 064537	21.67	22.08	22.34	22.42	22.34	**23.02**	**23.24**	23.79	24.03
PGC 065600	21.91	22.41	22.77	22.85	22.77	23.47	24.04	24.17	24.07
NGC 7130	22.24	22.62	22.87	22.95	22.90	23.53	24.08	24.98	25.16
NGC 7172	21.70	22.24	22.64	22.75	22.71	22.85	23.09	23.97	24.30
PGC 068122	21.23	21.56	**21.07**	**19.63**	**20.13**	**22.66**	22.84	23.64	23.94
PGC 068198	21.49	21.86	22.24	22.34	22.28	22.67	23.03	23.90	24.20
FAIRALL 0357			22.61	22.69	22.64	**23.27**	23.18	24.09	24.46
PGC 070458	22.13	22.46	22.79	22.95	22.83	23.41	23.80	24.72	24.89
NGC 7496	21.67	21.92	22.22	22.29	22.18	22.35	23.02	23.74	24.00
NGC 7582	22.04	22.39	22.63	22.71	22.67	22.98	23.58	24.47	24.64
NGC 7590	21.56	21.84	22.25	22.31	22.24	22.53	22.69	23.61	**24.15**

Note. - Optical, NIR, MIR, and FIR luminosities for the Sy2 in the sample, computed from the survey data as described above.

TABLE 3.4

Log(Luminosity) (W/Hz) Seyfert 1

Object	.44µm	.64µm	1.25µm	1.65µm	2.17µm	12µm	25µm	60µm	100µm
LEDA 087392			22.11	22.15	22.29	*22.84*	*23.08*	*23.33*	*23.74*
PGC 002450	22.12	22.42	22.72	22.83	22.90	23.53	23.71	24.47	24.78
PKS 0056-572			**20.36**	**19.76**	**19.85**	**23.21**	**23.21**	**23.21**	**23.34**
PGC 003864	21.94	22.31	22.65	22.70	22.74	23.40	23.62	24.33	24.54
IRAS 01089-4743			**21.97**	**21.93**	**20.92**	23.24	23.36	24.10	24.46
PGC 004822	21.88	22.35	22.74	22.83	22.76	**23.03**	23.13	23.82	24.23
NGC 526A	21.63	22.01	22.47	22.65	22.55	23.29	23.62	**23.51**	**23.90**
PMN J0133-5159			20.55	**21.16**	**20.69**	**23.06**	**23.06**	**22.06**	**23.71**
ESO 080- G 005	21.42	21.87	22.30	22.47	22.33	**23.32**	**23.32**	**23.38**	**23.49**
NGC 1097	22.23	22.59	22.92	23.00	22.91	22.89	23.33	24.24	24.52
PGC 011706	21.83	21.90	22.51	22.64	22.51	**23.28**	**23.28**	**23.28**	**23.62**
NGC 1365	22.31	22.78	23.06	23.12	23.08	23.33	23.84	24.69	24.96
NGC 1566	22.29	22.54	22.84	22.86	22.80	22.65	22.82	23.90	24.40
PGC 017103	21.64	21.93	22.29	22.38	22.34	22.88	23.28	23.67	23.83
FAIRALL 0265			22.54	22.65	22.71	23.18	23.60	24.12	24.35
LEDA 096433			22.36	22.51	22.51	**23.15**	22.96	23.86	24.30
PGC 027468			21.81	21.91	21.85	*22.54*	*22.78*	*23.03*	*23.44*
PGC 029148			22.65	22.74	22.66	**22.94**	**22.94**	**22.94**	**22.94**
PGC 029151	21.70	21.98	22.48	22.54	22.46	**23.24**	**23.24**	**23.24**	**23.67**
PGC 033084	21.21	21.51	22.23	22.36	22.37	**23.41**	**23.30**	23.44	**24.84**
PGC 034101	21.53	22.01	22.19	22.23	22.16	22.42	22.70	23.32	23.78
PGC 036002	21.82	22.25	22.74	22.85	22.80	22.95	23.17	23.93	24.43
NGC 3783	21.96	22.27	22.58	22.68	22.68	23.24	23.71	23.82	24.00
LEDA 096527			**21.38**	**20.78**	**20.93**	23.29	23.74	24.29	24.49
PGC 045371	21.89	22.38	22.81	22.96	23.00	23.53	23.78	24.45	24.64
PGC 047969	21.18	21.63	21.97	22.09	22.10	22.69	23.02	23.15	23.15
PGC 049051	21.86	22.37	22.86	22.98	23.05	23.79	24.10	24.06	23.97
PGC 050427			21.80	21.88	21.95	**23.34**	**23.34**	**23.34**	**23.84**
ESO 328- G036			**20.78**	**20.49**	**20.46**	**23.32**	**23.32**	**23.32**	**23.84**
PKS 1521-300			22.37	22.50	22.39	**22.88**	**22.88**	**22.88**	**23.04**
LEDA 2793282			22.35	22.08	22.46	**22.87**	**22.87**	**22.87**	**23.68**
PGC 062346	21.61	21.96	22.37	22.49	22.58	**23.31**	23.66	23.91	24.08
PGC 062554	22.06	22.52	22.91	23.04	22.96	23.10	23.23	23.78	**24.64**
ESO 399-IG 020			**20.86**	**20.14**	**20.82**	23.20	23.36	23.87	**24.31**
NGC 6860	21.83	22.32	22.65	22.76	22.75	23.06	23.21	23.66	24.08
PGC 064989			22.56	22.66	22.62	**22.85**	**22.92**	23.45	24.07
ESO 235- G 059	21.88	22.32	22.71	22.80	22.78	**23.16**	**22.99**	23.74	24.05
CTS 0109			22.04	22.14	22.30	**23.28**	**23.28**	**23.54**	**24.11**
PGC 067075	21.48	21.89	22.29	22.37	22.25	**22.84**	**22.84**	**22.84**	**23.03**
NGC 7213	22.11	22.55	22.88	22.94	22.88	22.65	22.74	23.29	23.78
J224704.9-305502			**19.57**	**19.75**	**19.70**	**22.18**	**22.18**	**22.18**	**22.11**
PGC 073028			**20.65**	**20.82**	**20.54**	**23.52**	23.39	23.85	24.28

Note. - Optical, NIR, MIR, and FIR luminosities for the Sy1 in the sample, computed from the survey data as described above.

3.4 THE DETERMINATION OF UPPER LIMITS

Before any meaningful statistical analysis could be performed, on for example the NIR and M/FIR luminosities, flux density values for the objects in the sample that were too faint to be detected (censored) had to be obtained. The method by which this was done varied by survey. The processes followed, for each of the two IR surveys, are given below.

3.4.1 *IRAS* UPPER LIMITS

As discussed in (Beichman 1988) in regards to PSC and FSC, "These catalogs give the characteristics of some 250,000 point sources and 20,000 small extended sources down to a limiting flux density, away from confused regions of the sky, of about 0.5 Jy at 12, 25 and 60 µm and about 1.5 Jy at 100 µm for point sources, and about a factor of three brighter than this for small extended sources." Therefore all objects in the sample that are weaker IR sources than those limits were censored.

For 22 Sy2 and 10 Sy1 in the sample, the reported flux density values (Tables 3.1 & 3.2) for *one or more* of the *IRAS* bands (12, 25, 60, and 100 micron) are actually upper limits taken from the literature. These are in underlined bold type.

Another 11 Sy2 and 15 Sy1 had no *IRAS* flux density values in the literature and no values recorded in either the PSC or FSC. Of those objects, two Sy1 (LEDA 087392 and PGC 027468) and one Sy2 (PGC 028144) are located in one of the gaps in *IRAS* coverage and so no upper limits were obtained. In §3.4 estimates of the flux density values for these three objects are computed in a separate way. The remaining objects (10 Sy2 and 13 Sy1) are fully censored, so upper limit estimates for the total flux density values, for all four *IRAS* survey bands, needed to be obtained.

The technical limitations of *IRAS* were such that the background and instrumental noise was not kept track of as it varied over the sky. So to facilitate the process of determining upper limits, *Scanpi* (*IRAS* Scan Processing and Integration tool 2007) was used. This software was designed to measure the flux values from the *IRAS* survey images. The benefit of this is that all of the necessary processing and cleaning of the images is done automatically. The procedure used to compute the *IRAS* upper limits was as follows.

Of the censored objects all but one Sy1 and one Sy2 are in spiral host galaxies (they are in interacting S0/pec). As a starting point, a diameter of 60 kpc (just under 200,000 ly) for the host galaxy was assumed. Then for each object 60 kpc was converted into arcmin using the scale listed for each object, listed above in Tables 2.1 & 2.2 in chapter 2. The value obtained was the initial value used in *Scanpi* for the *Source Fitting Range* in *Scanpi*. Actually the parameter is +/- from the center, so 1/2 the initial value used is entered in *Scanpi* for the *Source Fitting Range*. As the name implies, *Source Fitting Range* is the area for which the integrated flux, or total flux density, was computed. Values between 1 and 30 arcmins were used as the *Local Background Fitting Range*. The other input value needed in the fitting process using *Scanpi* was the *Source Exclusion Range for Local Background Fitting.* The *Source Fitting Range* value, increased by 5-10 per cent, was used for the *Source Exclusion Range for Local Background Fitting* value. In general, the values ultimately used for any of the *Scanpi* parameters, was obtained through some trial and error.

Scanpi output

As can be seen in Figure 3.4 below, the following information is displayed when Scanpi is run for a given object and input parameters.

sigma: The rms deviation in mJy of the residuals after the baseline subtraction

snr: The signal-to-noise ratio (peak/sigma)

Scan: When Scanpi is run for an object, four scan values are given. These are

999: The weighted mean (weights of 1 for good scans or 0.5 for noisy ones)

1001: The straight (arithmetical) mean.

1002: The statistical median, formed at each point, of all the data scans averaged. If the number of scans is even, the average of the two middle data values is taken at each point.

1003: The noise-weighted mean scan. The weighting is as 1/SIGMA**2 where SIGMA is the root-mean-square residual after background subtraction.

peak: The maximum (in Jy) within the signal range specified.

fnu_t: An estimate of the total flux density (in Jy) from integration of the averaged scan between fixed points defining an integration range.

miss: The in-scan deviation of signal peak from the user-specified target position in arc minutes. The location of the peak is taken to be the center of the best-fitting template.

amp: The peak flux (in Jy) of the best-fitting point source template.

corr_coeff: The correlation coefficient characterizing the best fitting template. The range is 0 to 1.0; the higher the value, the better the fit. "It should be emphasized that this cannot be compared directly to the correlation coefficients in the *IRAS* Point Source Catalog (PSC). The coefficients produced by Scanpi run much higher than those in the PSC, mostly because of the larger number of points produced by over-sampling."

As a test to check the accuracy of values obtained for upper limits in the above described fashion, the total flux density was computed for all four *IRAS* bands for an object that was *not* censored, (listed in the PSC), for comparison. The example chosen at random was PGC 004440 (alias IC

1657). At a (luminosity) distance of 51 Mpc, a scale of .251 kpc per arcsec was used to obtain a *Source Fitting Range* of ~4 arcmin. The *Source Exclusion Range for Local Background Fitting* values used was then 4.2 arcmin. The 100 μm total flux density value for this object, as listed in the PSC, is 7.481 Jy. Using Scanpi with the above listed parameter values, the upper-limit value of 7.49 Jy was the best fit.

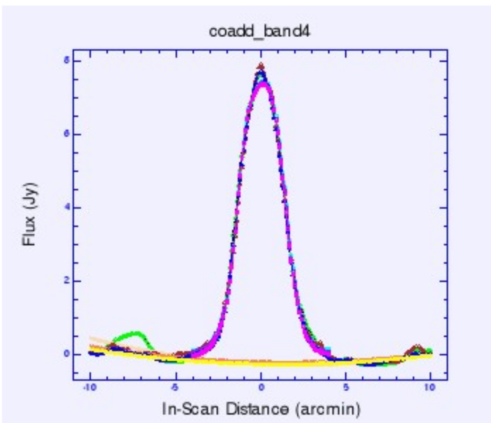

100 Microns Coadds Summary (Band 4)
User Input Source/Location: IC 1657

scan	sigma	snr	peak	fnu_t	miss	amp	corr_coeff
	mJy		Jy	Jy	arcmin	Jy	
999	184.87	42.68	7.73	7.72	0.07	7.28	0.99825
1001	184.87	42.68	7.73	7.72	0.07	7.28	0.99825
1002	96.08	84.12	7.92	7.51	0.12	7.24	0.99860
1003	60.57	131.30	7.79	7.49	0.09	7.30	0.99911

FIG. 3.4.- Scanpi output for IC 1657 at 100 μm

Table 3.5 shows the estimated upper limits computed as described above vs. the *IRAS* PSC values taken from NED. For IC 1647, Scan 1002 gives the best fit for all but the 12 μm flux. For that value, Scan 1001 gives a slightly better fit than the others.

TABLE 3.5

PGC 004440				
Band (μm)	100	60	25	12
PSC Value (Jy)	7.4810	2.7680	0.2727	0.2053
Est. Upper-Limit (Jy)	7.49	3.18	0.28	0.24

Note.- Comparison of flux density values from the PSC and from Scanpi

The upper limits for the 10 Sy2 and 13 Sy1 censored in the *IRAS* survey, computed as described above, listed in Appendix B along with all of the relevant *Scanpi* input and output. Only the adopted upper limits are included in Table 3.1 & 3.2. The scale factors (kpc / arcsec) from Tables 2.1 & 2.2 in chapter 2 are given again in Appendix B for convenience.

The strongest signal for each of the censored objects was usually observed at 100 µm. As discussed later, this is to be expected in many Seyferts and late-type galaxies (Spinoglio & Malkan 1989).

Unfortunately the signal for many of the censored objects in this sample, particularly at 12 and 25 µm, was often too weak to fit properly or even detect at all. In addition, the local noise often made it impossible to get a fit resulting in a correlation coefficient .995 or greater which was the goal in the fitting process. Also, the smallest value that can be used in *Scanpi* for the *Source Fitting Range* is +/1 arcsec from the center of the object, which is often too large and so makes an ideal fit impossible.

As a result, for all but one (the Sy2 LEDA 087391) of the censored objects, the 12 micron upper-limit adopted is the value obtained for the object at 25 or 60 µm, because only at those longer wavelengths could a signal with a "good enough" fit be obtained. Similarly, for all but four of the censored Sy2 (LEDA 087391, NGC 0824, PGC 028147, WKK 1263) and all but two of the Sy2 (ESO 080- G 005, and CTS0109), the 25 µm upper limit estimate adopted is the value obtained for the object at 60 or 100 µm. For all but one object (the Sy1 PGC 029148) a reasonably good fit was obtained, and an upper limit value adopted, for the 60 micron total flux density using *Scanpi*. For PGC 029148 the 60 µm upper limit adopted is the value obtained at 100 µm. For all of the censored objects an upper limit at 100 microns was obtained. A correlation coefficient of .95 or greater for the fit in *Scanpi* was the goal in each fit but was not always possible. In most all cases a fit of .90 or better was achieved.

Inevitably, sometimes of the object under consideration happened to be (apparently) located next to another bright IR source, thus making the upper limit estimate very difficult. This is particularly true at 100 µm. Figure 3.5 shows an example of this, LEDA 166339. In Appendix B, * is used to denote those objects for which this is an issue. Often a "fairly reasonable" fit can be obtained by adopting a small value for the *Local Background Fitting Range* in *Scanpi*. In the case of LEDA 166339 an upper-limit estimate of 0.44 Jy for the total flux density at 100 microns was obtained. The correlation coefficient of the fit, however, was only .93 (note that the fit resulting in that adopted upper limit is not the one shown below; the parameters used in the fit displayed in Figure 3.5 were chosen to highlight the obscuring bright source).

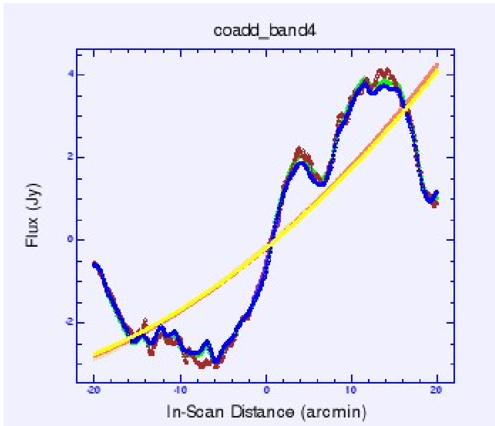

100 Microns Coadds Summary (Band 4)
User Input Source/Location: LEDA 166339

scan	sigma	snr	peak	fnu_t	miss	amp	corr_coeff
	mJy		Jy	Jy	arcmin	Jy	
999	1329.81	0.00	0.57	0.61	-99.00	-99.00	-99.00000
1001	1329.81	0.00	0.57	0.61	-99.00	-99.00	-99.00000
1002	1374.77	0.00	0.36	0.78	-99.00	-99.00	-99.00000
1003	1275.93	0.00	0.54	0.53	-99.00	-99.00	-99.00000

FIG 3.5.- Scanpi output for LEDA 166339 at 100 µm. Note the bright source, offset to the right, peaking at approximately 12 arcmin from the center of the censored objects location.

3.4.2 SAMPLE OBJECTS NOT COVERED BY *IRAS*

Three of the objects in this sample are located in the few gaps of the sky coverage of *IRAS*. There was one Sy2 (PGC 028144) and two Sy1 (LEDA 087392 and PGC 027468). To account for these objects in the statistical tests, upper limits for their flux density values needed to be obtained. Fortunately 2MASS data is available for all three of these objects, which enabled the method outlined below to be used to obtain the needed FIR upper limits.

In §3.5.3 below the spectral indices are computed and analyzed, by Sy type and all type combined. This is simply a calculation of the slope α of the line between two points.

The points are the (log) wavelength vs. the (log) total flux density; ($\log\lambda_1$, $\log S_1$) and ($\log\lambda_2$, $\log S_2$). The slope of the line segment connecting these two points is

$$\alpha_{1-2} = \frac{\log S_2 - \log S_1}{\log\lambda_2 - \log\lambda_1}, \quad \text{Eq. 3.1}$$

which, upon using the quotient rule for logarithms, can be written more concisely as

$$\alpha_{1-2} = \frac{\log\left(\frac{S_2}{S_1}\right)}{\log\left(\frac{\lambda_2}{\lambda_1}\right)} \quad \text{Eq. 3.2}$$

Setting λ_1 to 1.25 µm, the lowest IR wavelength obtained for the entire sample (from 2MASS), we can then for the three objects not covered by *IRAS* use their 2MASS 1.25 µm flux density values (in Jy) for S_1 and then solve for and compute S_2. This is done for S_2 = 12, 25, 60, and 100 µm.

Before that can be done though, a value of α_{1-2} is needed. The values used were the median values computed for the remaining 76 Sy2 and 40 Sy1 (all have *IRAS* data or upper limits)

That is, for all objects (by type), except for the three objects not covered by *IRAS*, the quantities $\alpha_{1.25-12}$, $\alpha_{1.25-25}$, $\alpha_{1.25-60}$, and $\alpha_{1.25-100}$ were computed using Equation 3.2. The median values computed in each case are listed below.

	Sy1	Sy2
1.25 - 12 μm	0.76	0.51
1.25 - 25 μm	0.75	0.65
1.25 - 60 μm	0.73	0.84
1.25 - 100 μm	0.86	0.90

The median values of $\alpha_{1.25-12}$, $\alpha_{1.25-25}$, $\alpha_{1.25-60}$, and $\alpha_{1.25-100}$ listed above are then used to compute S_2 for the three objects not covered by *IRAS*.

Solving Equation 3.2 for S_2 we get

$$S_2 = S_1 \left(\frac{\lambda_2}{\lambda_1}\right)^{\alpha_{1-2}} \quad \text{Eq. 3.3}$$

As an example, consider the Sy2 PGC 028144. The 2MASS 1.25 μm total flux density (listed in Table 3.1) is $S_{1.25} = 0.09750$ Jy. The median value of $\alpha_{1.25-100}$ (for the remaining 76 Sy2) from Table 3.5 is, rounded to two decimal places, 0.90. Hence, using Equation 3.3 we compute the 100 μm estimate for PGC 028144,

$$S_{100} = 0.09750 \left(\frac{100}{1.25}\right)^{0.90},$$

which is approximately 5 Jy.

In a similar way, estimates of S_{60}, S_{25}, and S_{12} are computed for PGC 028144, with the corresponding value of λ_2 and median value α_{1-2}. This process is then repeated for LEDA 087392 and PGC 027468. The flux density values computed in this way are listed in underlined italic in Tables 3.1 & 3.2.

3.4.3 2MASS UPPER LIMITS

There were only 13 censored Sy in the sample for which no upper limits were listed in the literature, 6 Sy2 and 7 Sy1. The process for obtaining the upper limits (in all three bands, J, H, K_s), based on 2MASS data, was as follows.

For a given censored object, the PSC was searched for other, nearby, objects that were censored *in just one or two* of the three survey bands. In such cases, a (97% confidence) upper limit (for the magnitude) is given for the band(s) for which there was non-detection(s). The search was done using *Gator* which is the NASA/IPAC *Infrared Science Archive catalog query engine*.

The object's primary name was entered along with the search radius ($\leq$ 15 arcmin was sufficient in all cases). *Gator* resolves the name, through NED, for the coordinates used as the center of the search. In Table 3.6 below the Sy coordinates are given (in degrees latitude and longitude, which is what is used in the PSC), along with the coordinates of the "nearby" object for which the upper limit was taken from the PSC. The table is sectioned by band.

The output of the search through *Gator* is a table which lists all of the objects within the specified search radius, along with their PSC entries. The *rd_flag* column lists for each object a three digit string, for J, H, K_s bands. A zero in the first, second, or third digit (or any combination of two zeros) signifies a non-detection in the J, H, K_s bands, respectively. If possible a nearby object with non-detections in two bands was used. Objects were chosen as close as possible to the censored Sy under investigation. Table 3.6 also gives a measure (the offset of the coordinates of the two objects, in degrees) of how close in the sky the partially-censored object is located to the censored Sy.

TABLE 3.6

	Lat. (deg)	Long. (deg)	Near Obj. Lat. (deg)	Near Obj. Long. (deg)	Diff. in Lat. (deg)	Diff. in Long. (deg)	**J (mag)**
				Seyfert 2			
LEDA 093365	17.972881	-45.979581	17.872383	-45.938732	0.100498	-0.040849	**15.444**
NGC 0454	18.593870	-55.398710	18.961615	-55.312981	-0.367745	-0.085729	**16.982**
AM 0426-625	66.804580	-62.787220	66.927364	-62.521152	-0.122784	-0.266068	**12.749**
IC 4518	224.428750	-43.131670	224.341974	-43.217510	0.086776	0.085840	**15.509**
WKK 3646	226.164378	-68.002061	226.053310	-68.089081	0.111068	0.087020	**14.469**
PGC 068122	332.117880	-34.106364	332.194375	-34.043648	-0.076495	-0.062716	**14.512**
				Seyfert 1			
PKS 0056-572	14.694088	-56.986519	15.153083	-56.824074	-0.458995	-0.162445	**16.748**
IRAS 01089-4743	17.790650	-47.460342	17.809359	-47.541019	-0.018709	0.080677	**13.366**
LEDA 096527	187.904167	-47.966944	187.984188	-47.964039	-0.080021	-0.002905	**15.136**
ESO 328- G036	228.696670	-40.359720	228.782022	-40.352581	-0.085352	-0.007139	**16.271**
ESO 399-IG 020	301.740420	-34.549440	301.921002	-34.213104	-0.180582	-0.336336	**16.187**
[VV2003c] J224704.9-305502	341.780484	-30.914226	341.675610	-31.192732	0.104874	0.278506	**17.448**
PGC 073028	359.363750	-30.460280	359.289044	-30.594826	0.074706	0.134546	**17.137**

Note.- "Nearest neighbors" used to determine upper limits for the censored objects in the 2MASS J-band.

TABLE 3.7

	Lat. (deg)	Long. (deg)	Near Obj. Lat. (deg)	Near Obj. Long. (deg)	Diff. in Lat. (deg)	Diff. in Long. (deg)	**H (mag)**
				Seyfert 2			
LEDA 093365	17.972881	-45.979581	17.871349	-45.938736	0.101532	-0.040845	**14.457**
NGC 0454	18.593870	-55.398710	18.606819	-55.321487	-0.012949	-0.077223	**16.156**
AM 0426-625	66.804580	-62.787220	66.927364	-62.521152	-0.122784	-0.266068	**12.229**
IC 4518	224.428750	-43.131670	224.510517	-43.066097	-0.081767	-0.065573	**16.645**
WKK 3646	226.164378	-68.002061	226.176878	-67.888474	-0.012500	-0.113587	**15.053**
PGC 068122	332.117880	-34.106364	332.156111	-34.073132	-0.038231	-0.033232	**17.615**
				Seyfert 1			
PKS 0056-572	14.694088	-56.986519	14.878220	-56.919155	-0.184132	-0.067364	**17.771**
IRAS 01089-4743	17.790650	-47.460342	17.809359	-47.541019	-0.018709	0.080677	**12.998**
LEDA 096527	187.904167	-47.966944	187.982520	-47.979420	-0.078353	0.012476	**16.156**
ESO 328- G036	228.696670	-40.359720	228.648949	-40.356808	0.047721	-0.002912	**16.512**
ESO 399-IG 020	301.740420	-34.549440	301.724020	-34.304291	0.016400	-0.245149	**17.572**
[VV2003c] J224704.9-305502	341.780484	-30.914226	341.717374	-30.711657	0.063110	-0.202569	**16.497**
PGC 073028	359.363750	-30.460280	359.380265	-30.334230	-0.016515	-0.126050	**16.248**

Note.- "Nearest neighbors" used to determine upper limits for the censored objects in the 2MASS H-band.

TABLE 3.8

	Lat. (deg)	Long. (deg)	Near Obj. Lat. (deg)	Near Obj. Long. (deg)	Diff. in Lat. (deg)	Diff. in Long. (deg)	**K_s (mag)**
				Seyfert 2			
LEDA 093365	17.972881	-45.979581	18.072353	-46.046848	-0.099472	0.067267	**15.745**
NGC 0454	18.593870	-55.398710	18.606819	-55.321487	-0.012949	-0.077223	**16.883**
AM 0426-625	66.804580	-62.787220	66.691222	-62.836266	0.113358	0.049046	**15.000**
IC 4518	224.428750	-43.131670	224.510517	-43.066097	-0.081767	-0.065573	**15.652**
WKK 3646	226.164378	-68.002061	226.176878	-67.888474	-0.012500	-0.113587	**14.496**
PGC 068122	332.117880	-34.106364	332.156111	-34.073132	-0.038231	-0.033232	**15.910**
				Seyfert 1			
PKS 0056-572	14.694088	-56.986519	14.878220	-56.919155	-0.184132	-0.067364	**17.096**
IRAS 01089-4743	17.790650	-47.460342	17.795695	-47.459412	-0.005045	-0.000930	**15.052**
LEDA 096527	187.904167	-47.966944	187.982520	-47.979420	-0.078353	0.012476	**15.321**
ESO 328- G036	228.696670	-40.359720	228.648949	-40.356808	0.047721	-0.002912	**16.147**
ESO 399-IG 020	301.740420	-34.549440	301.921002	-34.213104	-0.180582	-0.336336	**15.357**
[VV2003c] J224704.9-305502	341.780484	-30.914226	341.717374	-30.711657	0.063110	-0.202569	**16.135**
PGC 073028	359.363750	-30.460280	359.289044	-30.594826	0.074706	0.134546	**16.505**

Note.- "Nearest neighbors" used to determine upper limits for the censored objects in the 2MASS K_s-band.

The next step was to convert the upper limits obtained from magnitudes to total flux density values (in Jy). This is done through the magnitude relation

$$m = M_{zp} - 2.5\log(S) \qquad \text{Eq. 3.4}$$

where *m* is the apparent magnitude, which in this case is the upper limit values listed in Tables 3.6-3.8 above. M_{zp} is the zero-point magnitude. Table 3.9 below reproduces part of the table given in section VI.4a in Skrutskie et al. (2006).

TABLE 3.9

Band	Lambda (μm)	Bandwidth (μm)	S - zero mag (Jy)
J	1.235 $\pm$ 0.006	0.162 $\pm$ 0.001	1594 $\pm$ 27.8
H	1.662 $\pm$ 0.009	0.251 $\pm$ 0.002	1027 $\pm$ 20.0
K_s	2.159 $\pm$ 0.011	0.262 $\pm$ 0.002	666.7 $\pm$ 12.6

The information in Table 3.9 enables us to compute M_{zp}. Rearranging Equation 3.4 we get

$2.5\log(S) = M_{zp} - m$ or, since we are dealing with zero magnitude reference, just

$2.5\log(S) = M_{zp}$

So using the flux density values from Table 3.9 above, we compute M_{zp} for each band, obtaining

J: 2.5log(1594) ~ 8.006 mag

H: 2.5log(1024) ~ 7.526 mag

K_s: 2.5log(666.7) ~ 7.060 mag

Next we solve Equation 3.4 for S, getting

$$m = M_{zp} - 2.5\log(S)$$

$$\log(s) = \frac{M_{zp} - m}{2.5}$$

$$S = 10^{\frac{M_{zp} - m}{2.5}} \qquad \text{Eq. 3.5}$$

We can now easily compute the total flux density (in Jy) from Equation 3.5, for all three bands, for each censored Sy, using the upper limit values for *m* and the above derived values for M_{zp}. These are the total flux density values adopted for the censored objects in Tables 3.1 & 3.2, shown in bold.

3.5 THE IR RESULTS

3.5.1 FLUX DENSITIES & LUMINOSITIES

The mean total IR flux densities for J, H, & Ks bands for the sample as a whole were computed to be 0.2887, 0.3634, and 0.3225 Jy (with standard deviations of 1.0040, 1.3211, 1.1886 Jy), respectively.

At 12, 25, 60, & 100 µm the mean total flux densities for the entire sample were computed to be 0.7408, 1.9519, 12.5126, and 24.2809 Jy (with standard deviations of 2.7714, 7.5497, 62.3083, 133.6413 Jy), respectively.

As can be seen from these values, the mean 2MASS flux densities rise from J to H bands but then decrease going to K_s band. However for the four *IRAS* bandwidths the mean flux densities approximately doubles each time, going from 12 to 100 µm.

The NIR and M/FIR luminosities, in the same way as with the 843MHZ data in chapter 1, were computed for the sample at all seven of the bands covered by *IRAS* and 2MASS. The arithmetical mean and median values of the luminosities are given in Table 3.10.

The errors in the log luminosity values (given in Appendix C) for the sample objects are small, generally between 0.01 - 0.02 for the J, H, And K_s bands from 2MASS. While the median values for each type of Sy in each of these bands appear to be fairly similar, to really be able to say how the distributions of the luminosities compare, we must use the techniques of survival analysis (§3.6), which takes into account the censored objects, to give the probability that the two populations (Sy type) are drawn from the same parent population.

For the FIR data from *IRAS*, the difference in mean luminosities given in Table 3.10 below between Sy type at 60 and 100 µm stand out as more significant. Indeed in §3.6 it is those two bands that show a statistically significant difference, by Sy type. The errors in the log luminosity values (given in Appendix C) for the sample at these FIR bands, an average of about 0.06 at 12 micron and approximately 0.05 for 25, 60, and 100 micron, are larger than the errors for the 2MASS data by a factor of almost three.

In the unified view of AGN, in which Sy2 are defined primarily as being no different than Sy1 except that they are oriented such that the dusty central torus is obscuring the central engine, it follows that Sy2 should be more luminous in the IR in these FIR bands, as also can be seen from the scatter in Figure 3.1 above.

TABLE 3.10

Averages of 2MASS Log Luminosities (W/Hz)									
	J			H			Ks		
	All	Sy2	Sy1	All	Sy2	Sy1	All	Sy2	Sy1
Mean	22.31	22.40	22.16	22.37	22.47	22.21	22.31	22.39	22.18
Median	22.51	22.52	22.37	22.59	22.60	22.50	22.53	22.54	22.48
Min.	19.57	19.92	19.57	19.63	19.63	19.75	19.59	19.59	19.70
Max.	23.06	23.06	23.06	23.21	23.21	23.12	23.16	23.16	23.08
s.d.	0.63	0.51	0.80	0.74	0.63	0.89	0.75	0.66	0.90

Averages of *IRAS* Log Luminosities (W/Hz)												
	12μm			25μm			60μm			100μm		
	All	Sy2	Sy1	All	Sy2	Sy1	All	Sy2	Sy1	All	Sy2	Sy1
Mean	23.04	23.02	23.09	23.31	23.35	23.24	23.79	23.91	23.58	24.12	24.20	23.96
Median	23.06	23.01	23.17	23.28	23.30	23.26	23.82	23.88	23.60	24.15	24.19	24.02
Min.	21.95	21.95	22.18	22.18	22.41	22.18	22.06	22.93	22.06	22.11	23.24	22.11
Max.	23.79	23.76	23.79	24.23	24.23	24.10	24.98	24.98	24.69	25.16	25.16	24.96
s.d.	0.34	0.34	0.32	0.37	0.37	0.37	0.50	0.43	0.57	0.48	0.40	0.58

Note.- The arithmetical mean, median, and standard deviation of the IR luminosities.

The histograms showing the distribution of the luminosities are shown below in Figures 3.6 - 3.12. For each band there are two histograms. One shows the entire sample (119 objects) as well as a breakdown by type (Sy1 and Sy2). The other shows the distribution of just the censored objects, by type. This results in 14 histograms.

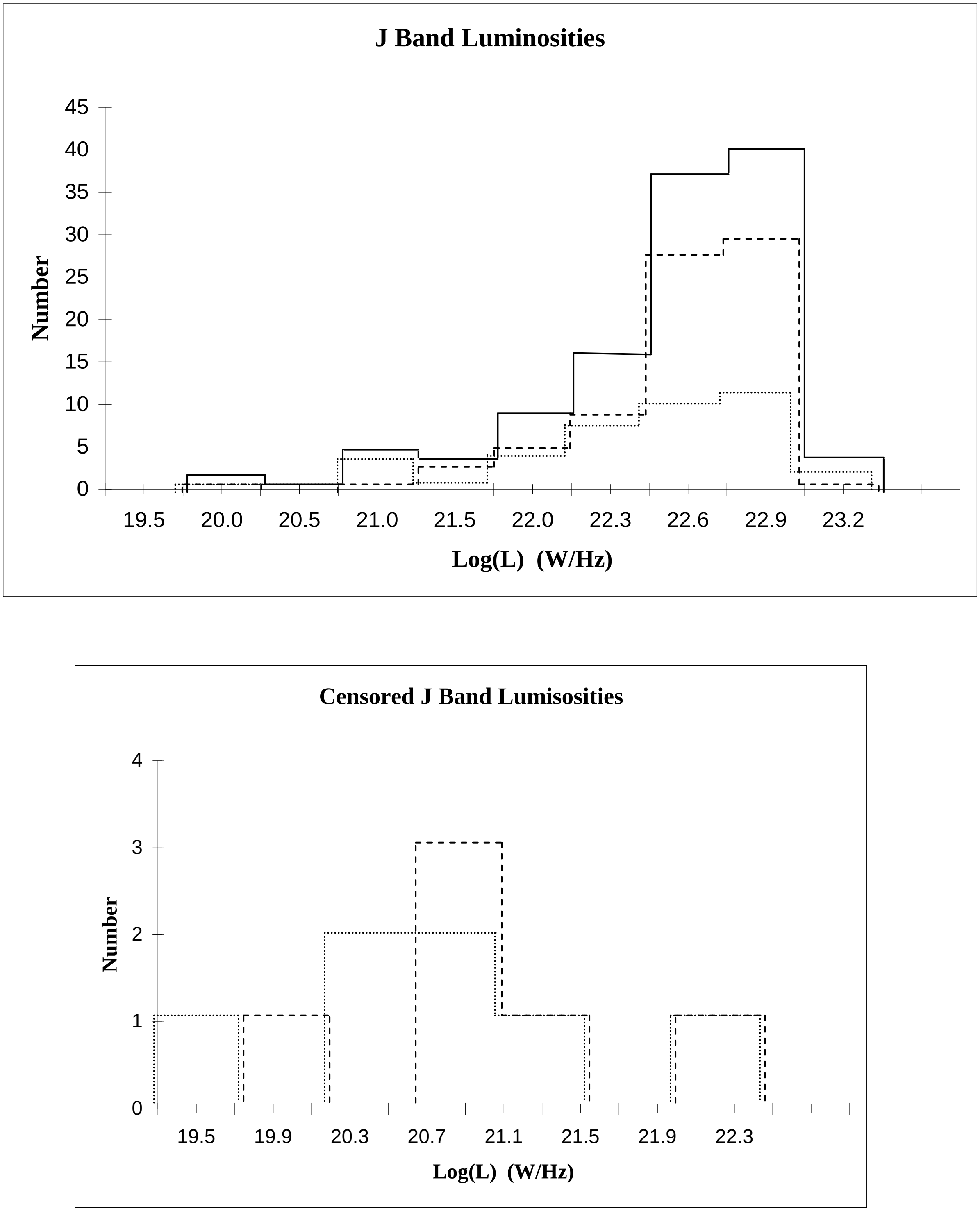

FIG. 3.6. - Log J band luminosities. *Top*: contains all objects (solid), and by type (dashed Sy2, dotted Sy1). Note the bin size changes from 0.5 to 0.3 starting with 22.0 W/Hz. *Bottom*: censored objects; dashed Sy2, dotted Sy1. Vertical lines on both are offset horizontally for clarity.

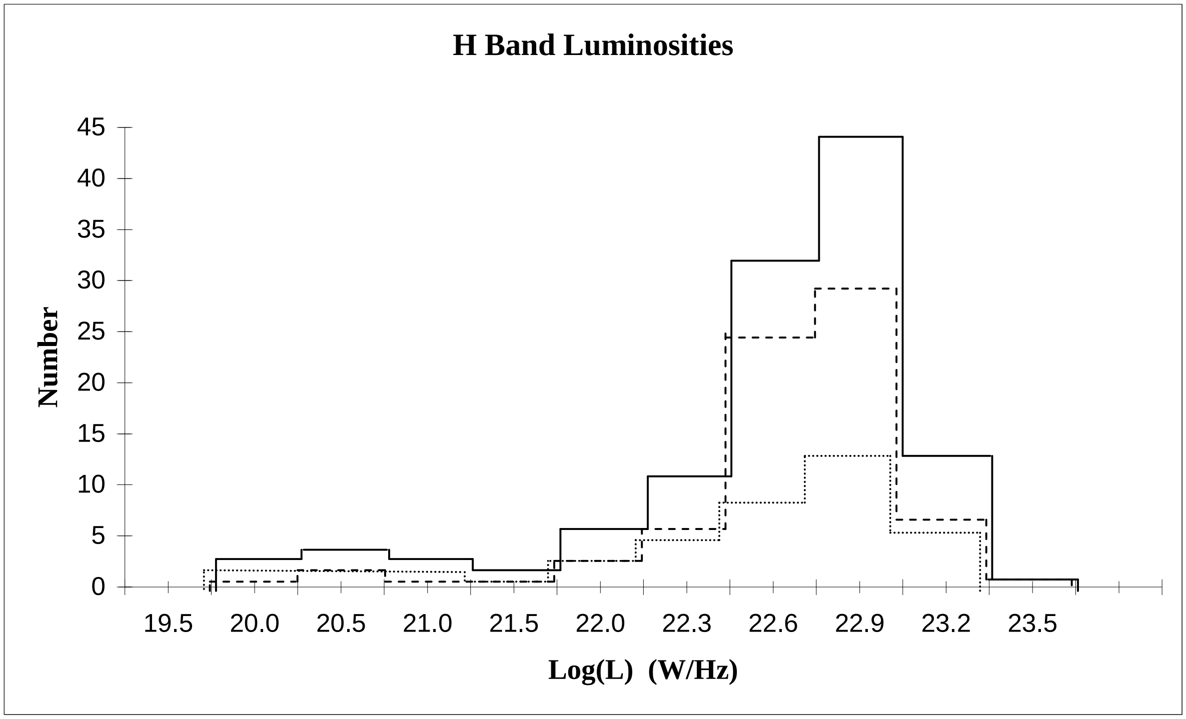

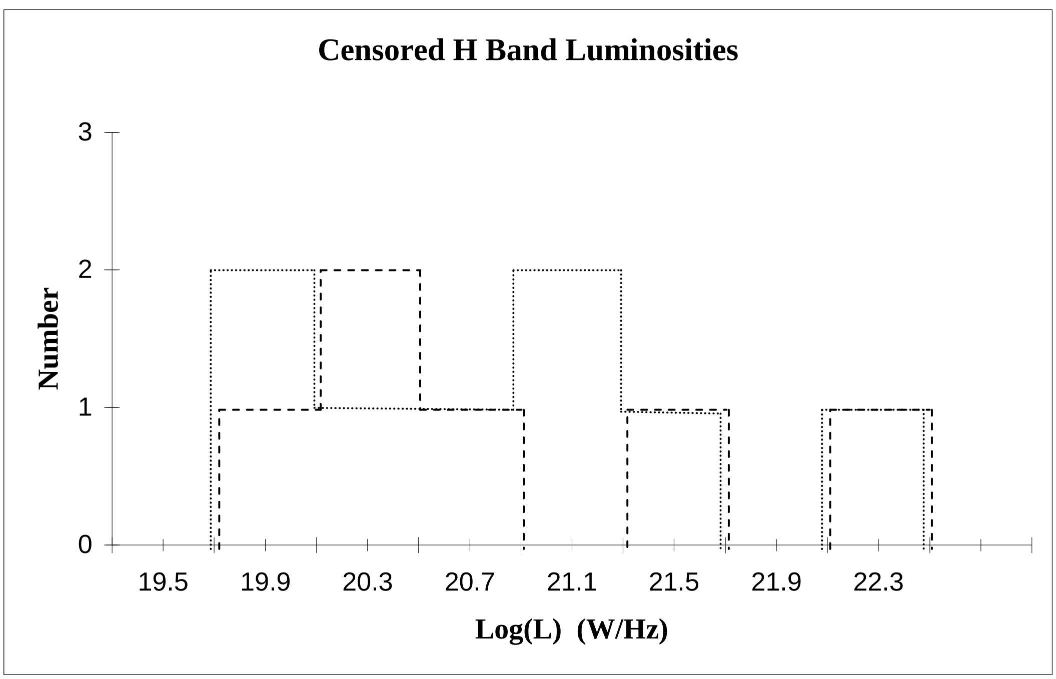

FIG. 3.7. - Log H band luminosities. *Top*: contains all objects (solid), and by type (dashed Sy2, dotted Sy1). Note the bin size changes from 0.5 to 0.3 starting with 22.0 W/Hz. *Bottom*: censored objects; dashed Sy2, dotted Sy1. Vertical lines on both are offset horizontally for clarity.

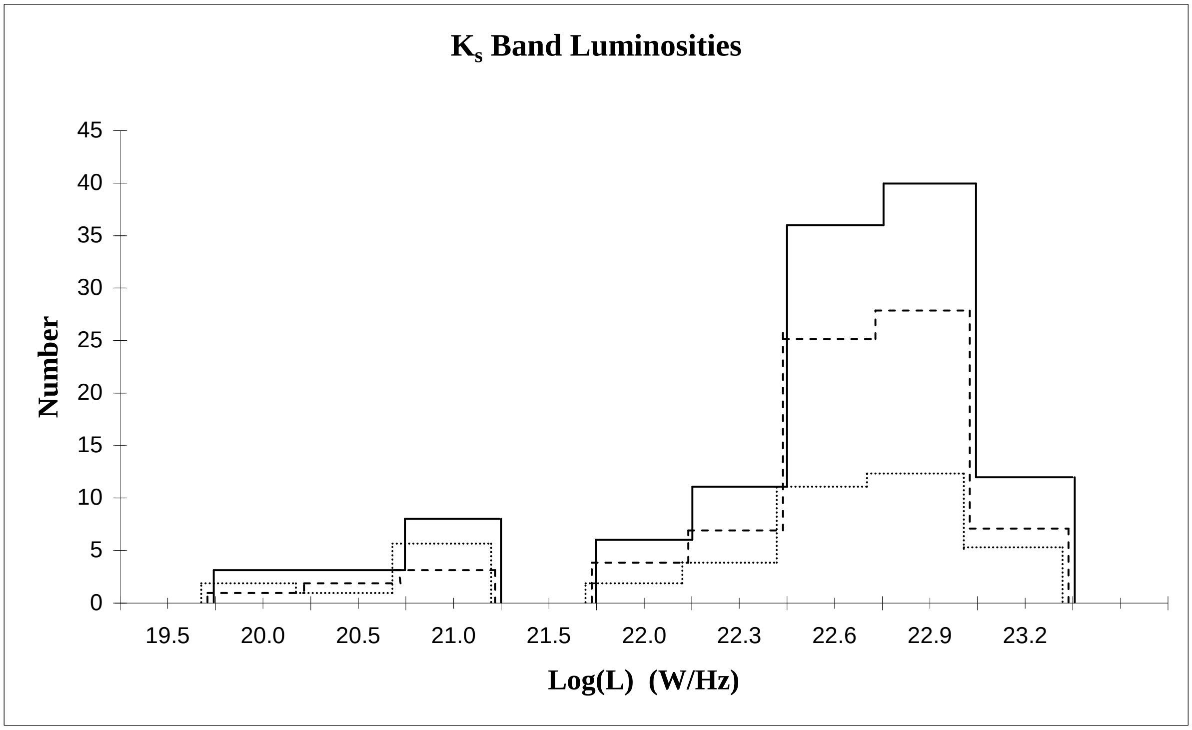

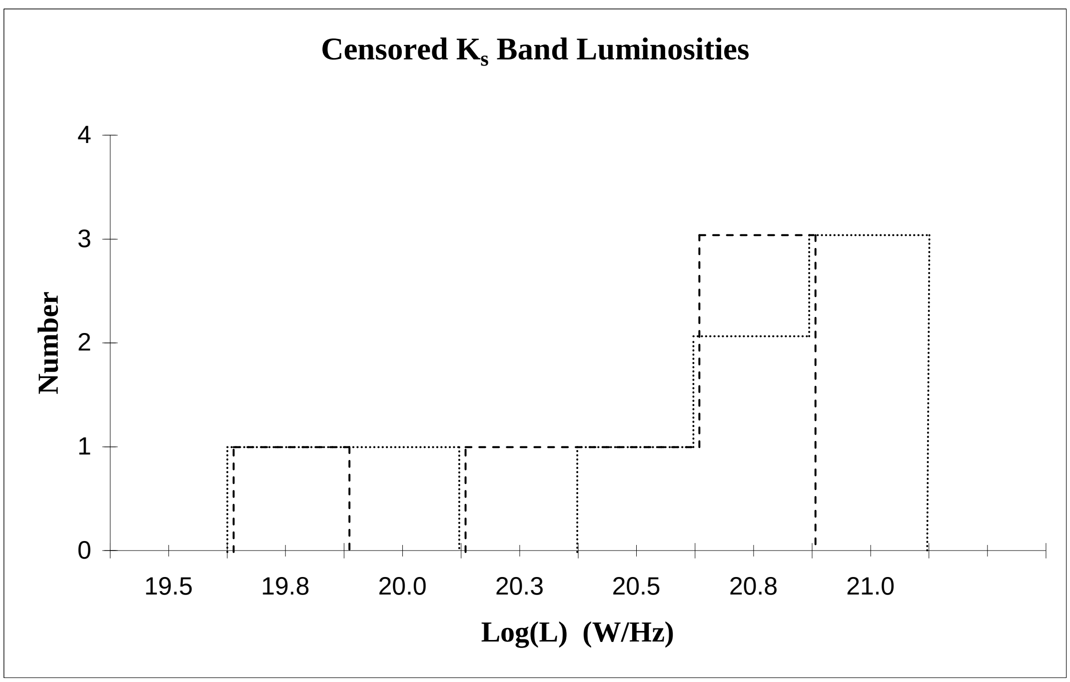

FIG. 3.8. - Log K_s band luminosities. *Top*: contains all objects (solid), and by type (dashed Sy2, dotted Sy1). Note the bin size changes from 0.5 to 0.3 starting with 22.0 W/Hz. *Bottom*: censored objects; dashed Sy2, dotted Sy1. Vertical lines on both are offset horizontally for clarity.

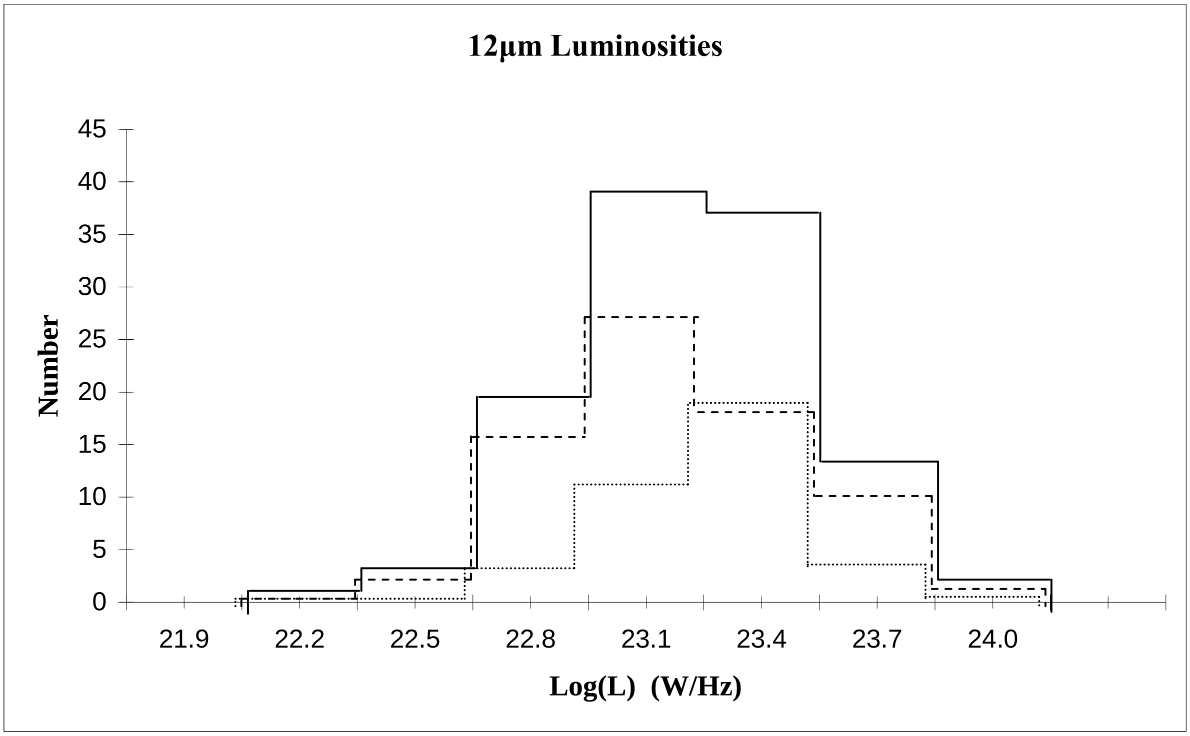

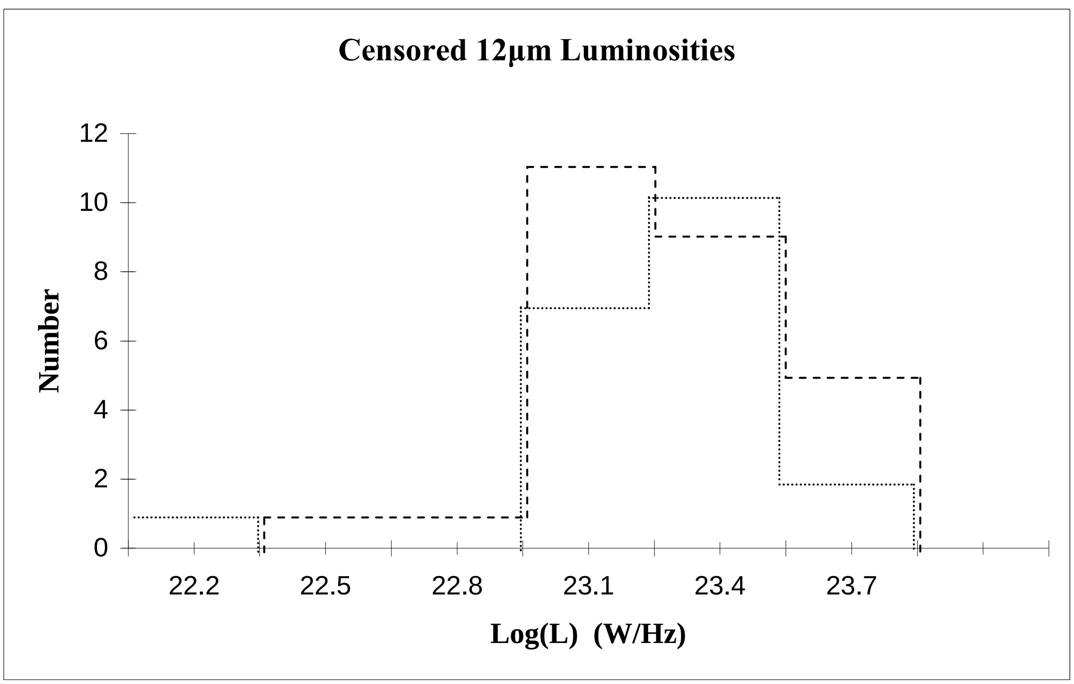

FIG. 3.9. - Log 12 μm luminosities. *Top*: contains all objects (solid), and by type (dashed Sy2, dotted Sy1). *Bottom*: censored objects; dashed Sy2, dotted Sy1. Vertical lines offset horizontally for clarity.

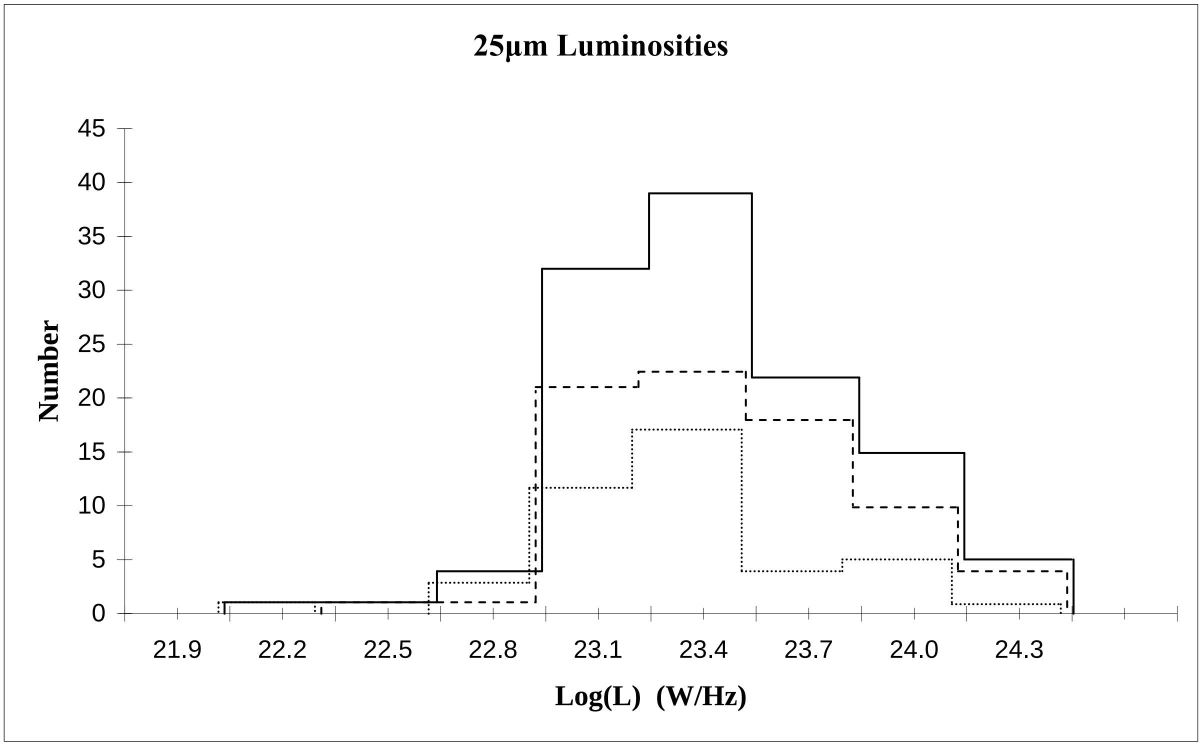

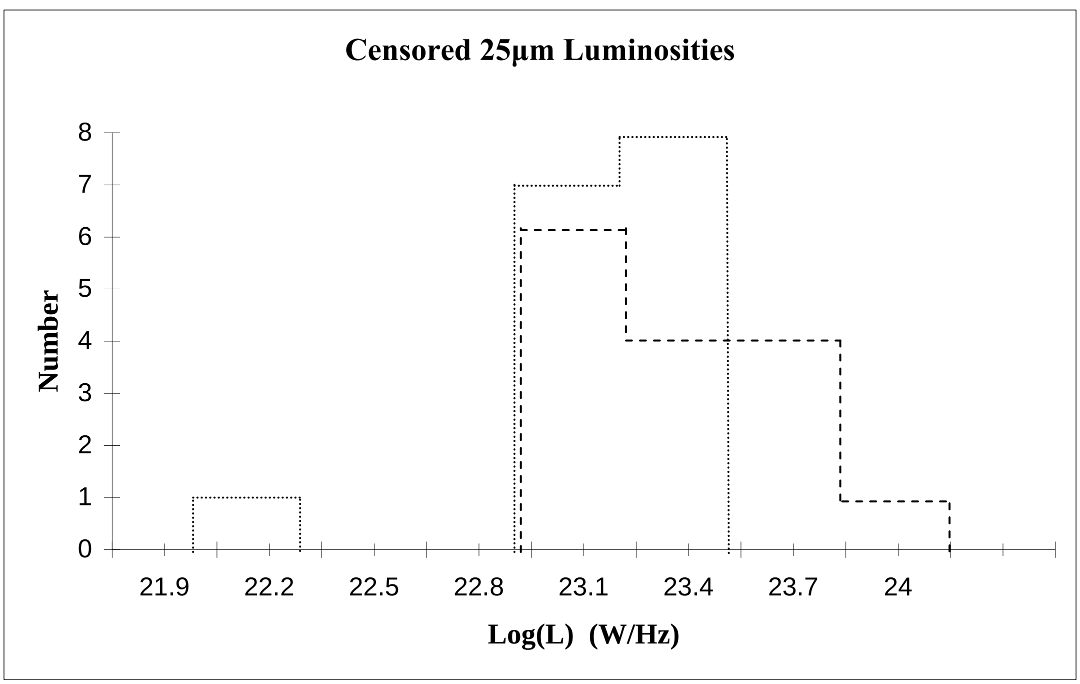

FIG. 3.10. - Log 25 µm luminosities. *Top*: contains all objects (solid), and by type (dashed Sy2, dotted Sy1). *Bottom*: censored objects; dashed Sy2, dotted Sy1. Vertical lines offset horizontally for clarity.

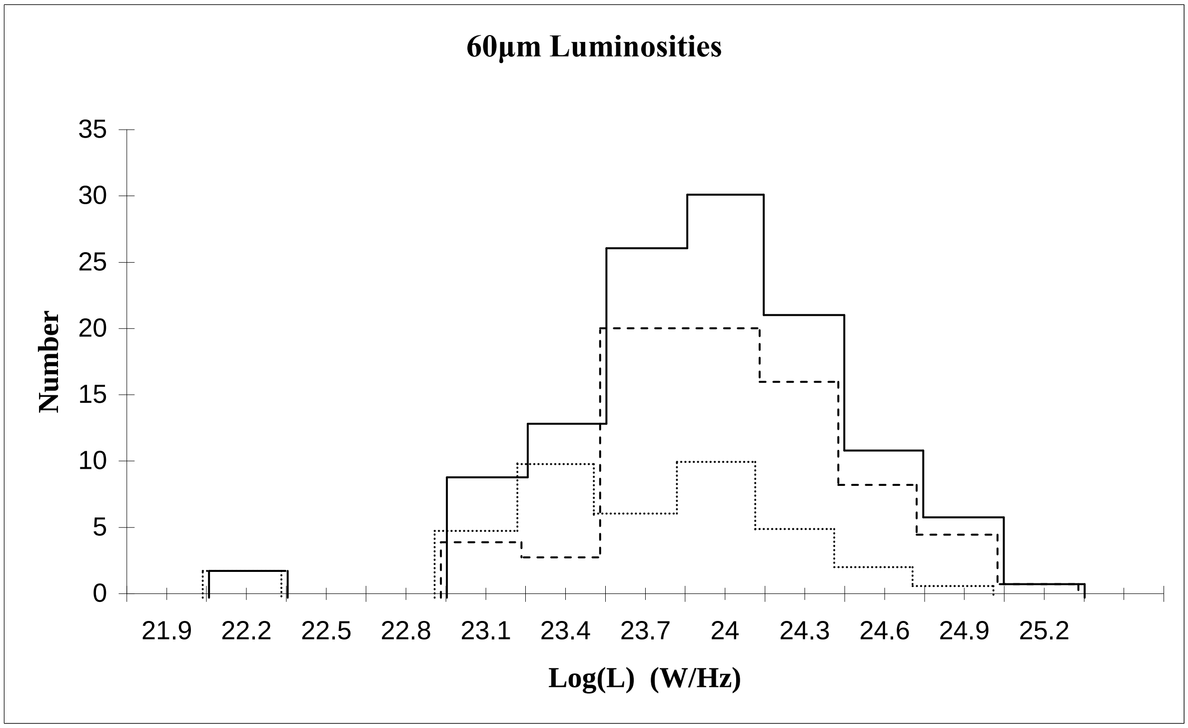

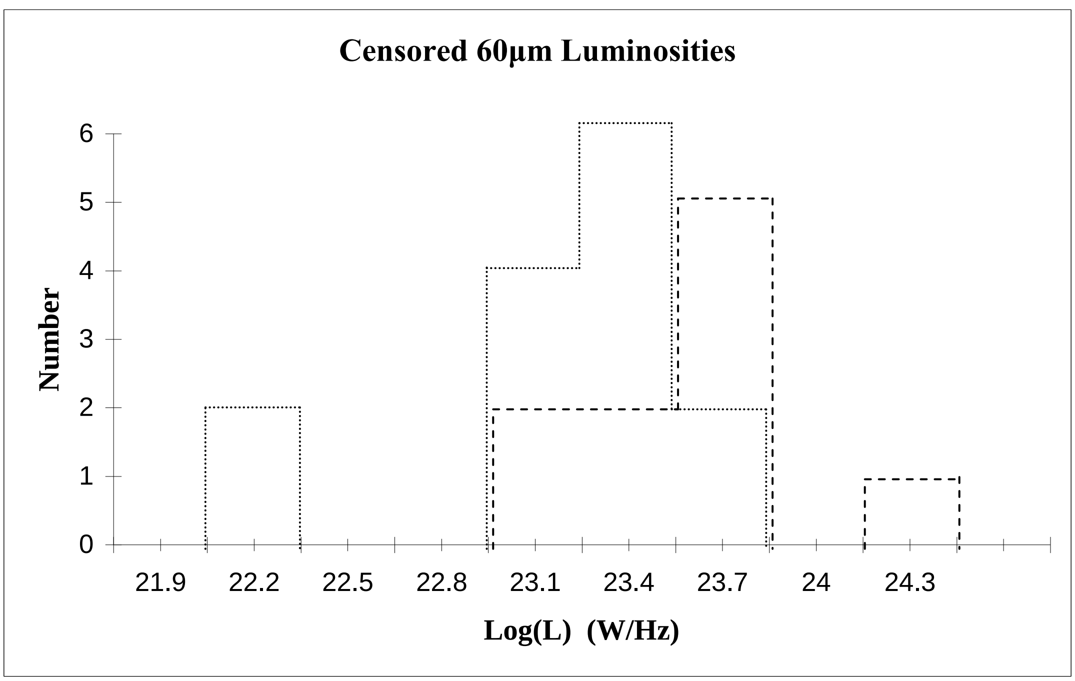

FIG. 3.11. - Log 60 µm luminosities. *Top*: contains all objects (solid), and by type (dashed Sy2, dotted Sy1). *Bottom*: censored objects; dashed Sy2, dotted Sy1. Vertical lines offset horizontally for clarity.

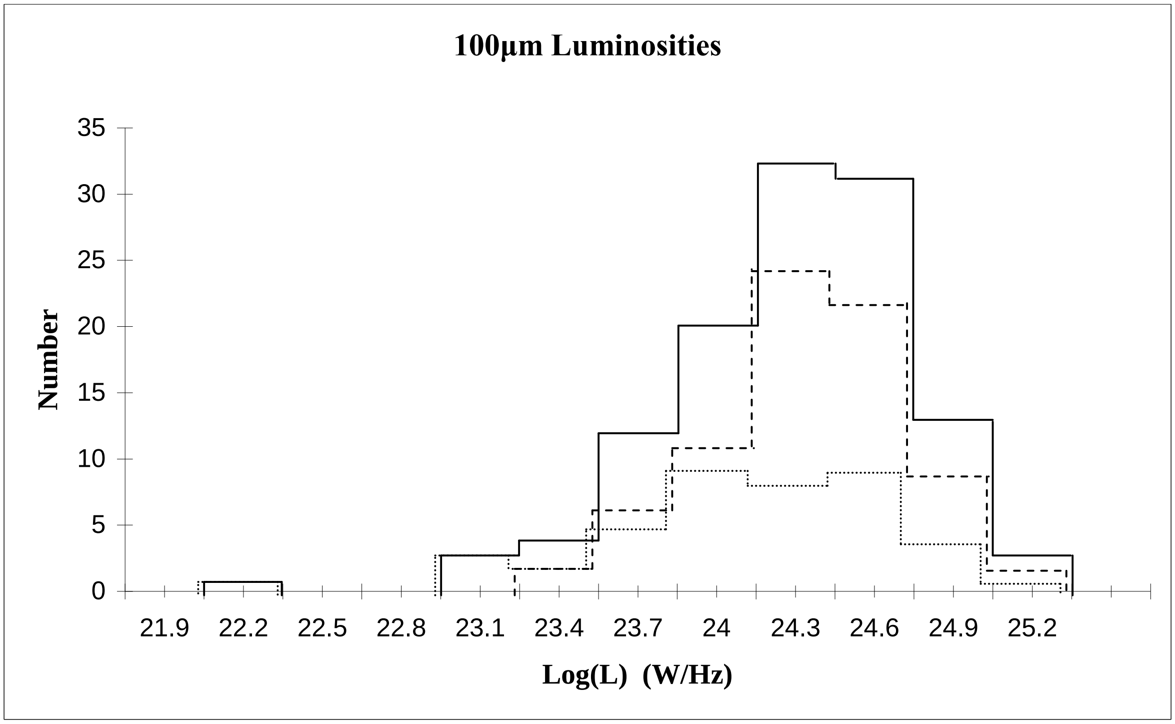

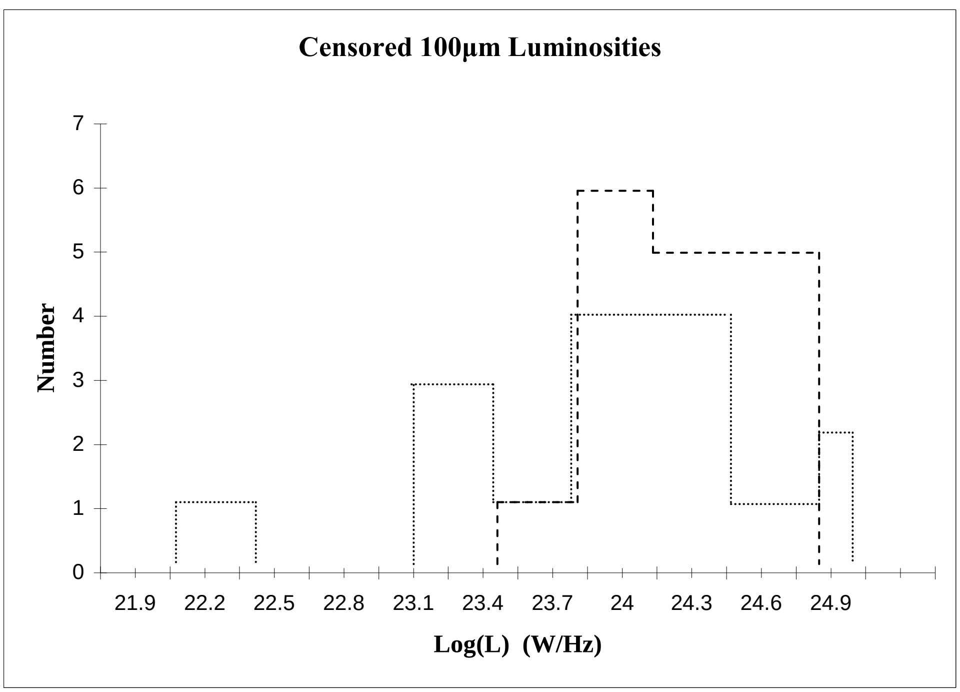

FIG. 3.12. - Log 100 μm luminosities. *Top*: contains all objects (solid), and by type (dashed Sy2, dotted Sy1). *Bottom*: censored objects; dashed Sy2, dotted Sy1. Vertical lines offset horizontally for clarity.

The median log luminosities (Jy) for the Sy2, at J, H, and K_s bands respectively, were computed to be 22.53, 22.60, and 22.54. For the Sy1 the values 22.37, 22.50, and 22.48 were obtained. For all 119 objects in the sample, the arithmetical median values of 22.51, 22.59, and 22.53 and mean values of 22.31, 22.37, and 22.31 were found. As with these mean luminosity values, the flux densities of most of the objects display this "H-band peak" as is shown in more detail in §3.52-3.53. Some possible explanations for this are given there as well.

It is hard to say much about the distribution of just the censored objects since their number is so small (6, 7, and 7 Sy1 and 6, 6, and 6 Sy2 in the J, H, and K_s bands, respectively). For these censored objects the Sy1 are slightly less luminous. For K_s band that seems to be reversed; the censored Sy2 seem to be slightly less luminous than the censored Sy1.

At 12 µm (MIR) the distributions show a similar shape by type but with the Sy2 perhaps slightly less luminous. The arithmetical mean and median values of 23.02 and 23.01 for the Sy2 and 23.09 and 23.17 for the Sy1. As will be seen below, when estimating the true mean and median values of the entire population using the Kaplan-Meier estimator, at 12 µm the Sy2 are seen to have a similar distribution; mean and median values of the former being 22.87 $\pm$ 0.05 and 22.82. For the later, the estimated values obtained were 22.89 $\pm$ 0.07 and 22.85.

At the remaining (FIR) bands the results show the Sy2 to be somewhat more luminous on average. The (arithmetical) mean and median values computed for the Sy2 at 25 µm were 23.35 and 23.30. At 60 µm, 23.91 and 23.88. At 100 µm, 24.20 and 24.19. For the Sy1 at 25 µm the mean and median values obtained were 23.24 and 23.26. At 60 µm, 23.58 and 23.60. At 100 µm, 23.96 and 24.03.

There were many more censored objects in the M/FIR bands (27, 15, 10, 22 Sy2 and 20, 16, 14, 17 Sy1 at 12, 25, 60, and 100 µm, respectively). The histograms of the log luminosities of these censored objects, by type, show that at 25, 60, and 100 µm the censored Sy2 are more luminous. At 12 µm the difference by type of the censored objects is much smaller, as would be expected based on the known, smaller scatter in the SED of AGN in the 7-12 µm range, as discussed in §3.1.

In the NIR bands the sample have ranges in their luminosities values that are fairly similar, by type. In J-band the Sy2 have max-min values of 23.06-19.92, in H-band the range is 23.21-19.63, and for K_s-band the values 23.16-19.59 were obtained. For the Sy1 the max-min values computed were 23.06-19.57, 23.12-19.75, and 23.08-19.70, in J, H, and K_s -bands respectively.

In the J-band the most luminous object was a Sy1.5 (NGC 1365) and least luminous object a Sy1.0 ([VV2003c] J224704.9-305502), with log luminosity values (in Jy) of 23.06 and 19.57 (upper limit) obtained. In H-band the most luminous object (LEDA 096373 and least luminous object (PGC 068122) were both Sy2, with log luminosity values of 23.21 and 19.63 (upper limit), respectively. In K_s-band the most luminous object (LEDA 096373) and least luminous object (NGC 0454) were again both Sy2, with log luminosity values of 23.16 and 19.59 (upper limit), respectively.

In the FIR bands the max-min values of the (log) luminosities for the Sy2 in the sample were computed to be 23.76-21.95, 24.23-22.41, 24.98-22.94, and 25.17-23.24 at 12, 25, 60, and 100 µm, respectively. For the Sy1 in the sample the ranges computed were 23.79-22.18, 24.10-22.18, 24.69-22.06, and 24.96-22.12 at 12, 25, 60, and 100 µm, respectively.

At 12 µm the most luminous object was a Sy1.2 (PGC 049051) and least luminous object was a Sy2 (NGC 1386) with log luminosity values of 23.79 and 21.95, respectively.

At 25 µm the most luminous object was the Sy2 LEDA 096373 - also the most luminous Sy in the K_s-band as mentioned above - and the least luminous object was the Sy1.0 [VV2003c] J224704.9-305502 - also the least luminous object in J-band as mentioned - with log luminosity values of 24.23 and 22.18 (upper limit), respectively.

At 60 µm the types were split again, with the most luminous object a Sy2 (NGC 7130) and least luminous object a Sy1.0 (PMN J0133-5159), with log luminosity values of 24.98 and 22.06 (upper limit), respectively. The same difference in type is seen at 100 µm, with the most luminous object again being the Sy2 NGC 7130 and the least luminous again (as in J-band and 25 µm) being the Sy1.0 [VV2003c] J224704.9-305502, with log luminosity values of 25.17 and 22.12 (upper limit), respectively.

3.5.2 THE SPECTRAL ENERGY DISTRIBUTION

In this section the spectral energy distributions (SEDs) for the sample are presented. For 61 of the 77 Sy2 in the sample (79%) there are data points at 9 wavelengths; .4 and .64µm in the optical (Cousins blue and red) and the 7 NIR & FIR bands that have been under investigation in this paper so far. This leaves 16 of the 77 Sy2 (21%) with data points at just the seven *IRAS* and 2MASS bands. The radio data for this sample was not used in the construction of the SEDs.

For the Sy1 in the sample, 24 of the 42 (57%) have data points at all 9 wavelengths, leaving 18 of the 42 Sy1 (43%) with data points at just the seven *IRAS* and 2MASS bands. Hence, 85/119 of the full sample (71%) have data points at all 9 wavelengths.

While the SEDs presented here are of a low resolution, being just seven or nine data points, compared to the continuous spectra being imaged with cutting-edge instruments such as the *Spitzer* space telescope (e.g., Buchanan et al. 2006), some general patterns are clearly visible and are of sufficient resolution to make comparisons with the results of previous studies, as will be done in Chapter 4. In addition, these results are useful because, despite their low resolution, proper upper limits were used and overall such wavelength coverage is rare in the literature for this type of sample. The SEDs are shown below in Figures 3.13 - 3.22.

The SED are plots of the form: log wavelength (µm) versus $\nu \cdot S_\nu$, which are in the units of erg cm^{-2} s^{-1}. These units result when multiplying frequency and the units of the flux densities, Jy. Since 1 Jy = 10^{-26} W m^{-2} Hz^{-1} = 10^{-23} erg cm^{-2} s^{-1} Hz^{-1}, multiplying by frequency (Hz), (and the factor 10^{-23}), results in erg cm^{-2} s^{-1} for the plot, which just gives the total energy flux independent of frequency. The plots below are given in the following order. First, Sy2 with data points at all 9 wavelengths are given (in order of the objects number in the sample), then the plots of the Sy2 without the two optical data points. Then the plots for the Sy1 in the sample are presented in the same way.

A few forms of the SEDs stand out. At the optical wavelengths, a moderate to large positive slope in the SED for all Sy2 was observed except for PGC 060594. The SED for that object is essentially flat, with $\nu \cdot S_\nu$ = 1.0419 x 10^{-10} at .4µm and 1.0577 x 10^{-10} at .64µm. For 41 of the 42 Sy1, similar positive slopes as those for Sy2 were observed. The Sy1.2 PGC 011706 was the only object showing a positive slope, going from .4 to .64µm.

In the NIR, going from J to H-band, three forms were observed for the Sy2 SED in the sample. Of all 77, 15 (19%) have a SED essentially flat, while 19 (25%) have moderate to large positive slopes with PGC 044167 standing out as the most extreme example. For that Sy2 the value of $\nu \cdot S_\nu$ increased from 3.1418 x 10^{-11} to 1.0974 x 10^{-10}, a factor of about 3.5 between J and H bands. The remaining 43 (56%) had a negative slope. For Sy1, the SEDs show positive slopes between these two bands for 13 objects (31%), a negative slope for 24 (57%), and essentially flat for 5 (12%). So overall the SEDs for the Sy1 and Sy2 are fairly similar.

The positive slope from J-H band noted above (25% of Sy2 and 31% of Sy1) could be explained a couple of different ways. It could be from stellar sources such as young circumnuclear starburst activity (Veilleux et al. 2009). The H-band more than the others "… is severely affected by atmospheric "airglow" emission" and so that could not be appropriately accounted (IPAC 1999).

Also, the total throughput (including atmospheric absorption) is slightly higher for the H-band filters (IPAC 2005).

Going from H to K_s band, all Sy2 SED show a negative slope but for one object, PGC 062134, which shows a positive one, almost as steep as the jumps in its values from J to H bands. For the Sy1 in the sample, similar negative slopes between the H and K_s wavelengths were seen in the SEDs, except for three objects, LEDA 087392 (Sy1.0), LEDA 2793282 (Sy1.5), and CTS 0109 (Sy1.2), all of which showed a decrease/negative slope.

For reasons to be discussed further in Chapter 4, it is worth distinguishing here the results between the general shape of the SEDs between 12 and 25 µm and from 25 to 100 µm. This will also be explored further in the next section when computing various spectral indices.

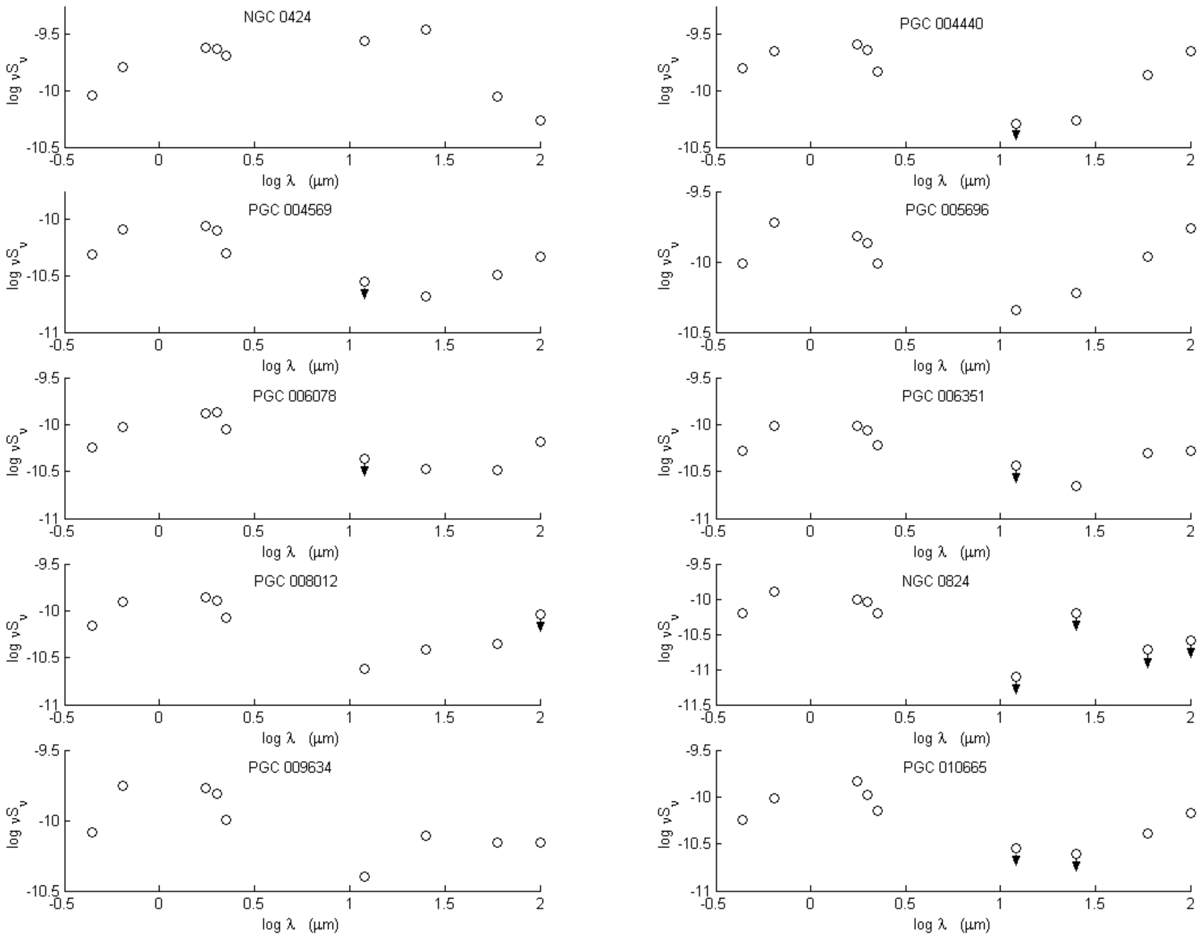

FIG. 3.13. - SEDs for Sy2 with data at all nine covered wavelengths. Arrows indicate values obtained by using the adopted upper limits.

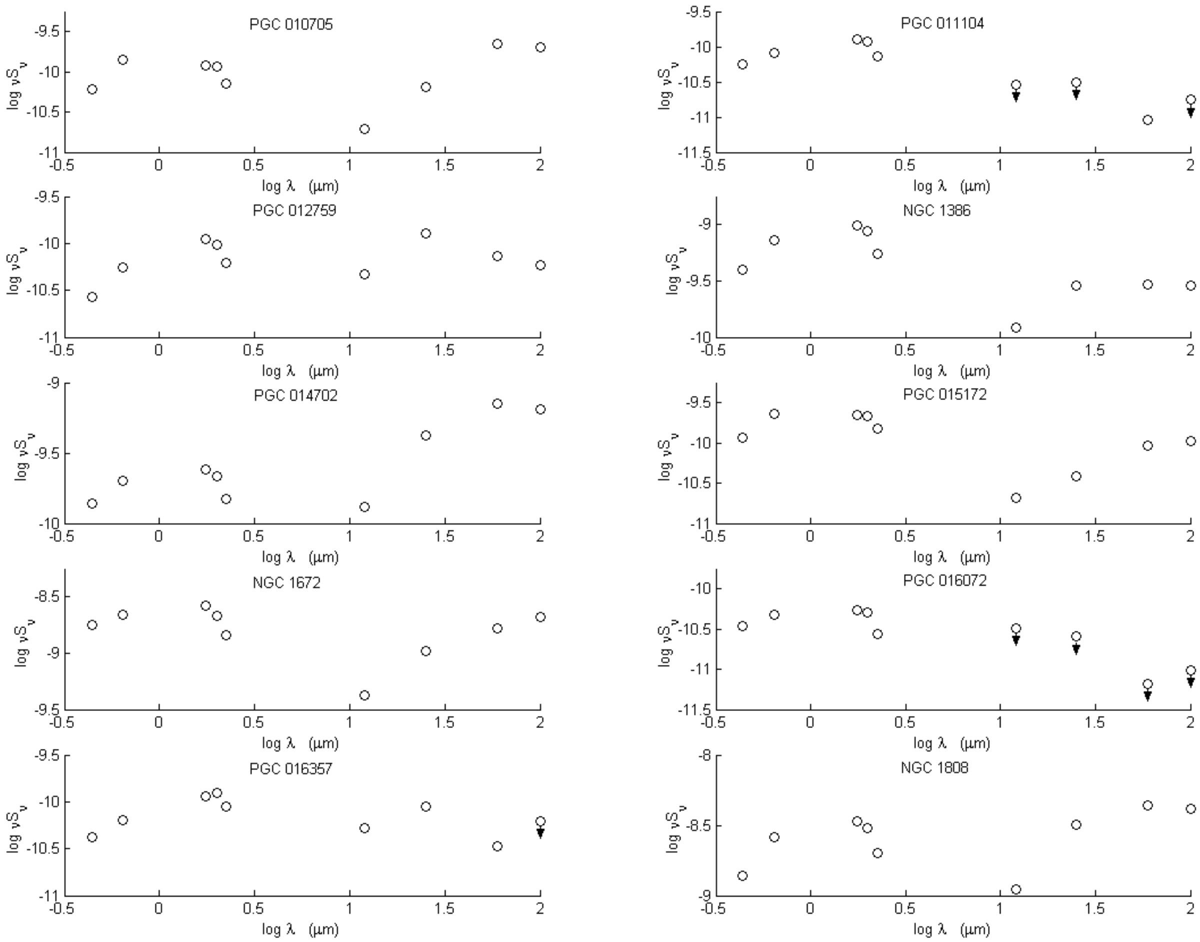

FIG. 3.14. - SEDs for Sy2 with data at all nine covered wavelengths. Arrows indicate values obtained by using the adopted upper limits.

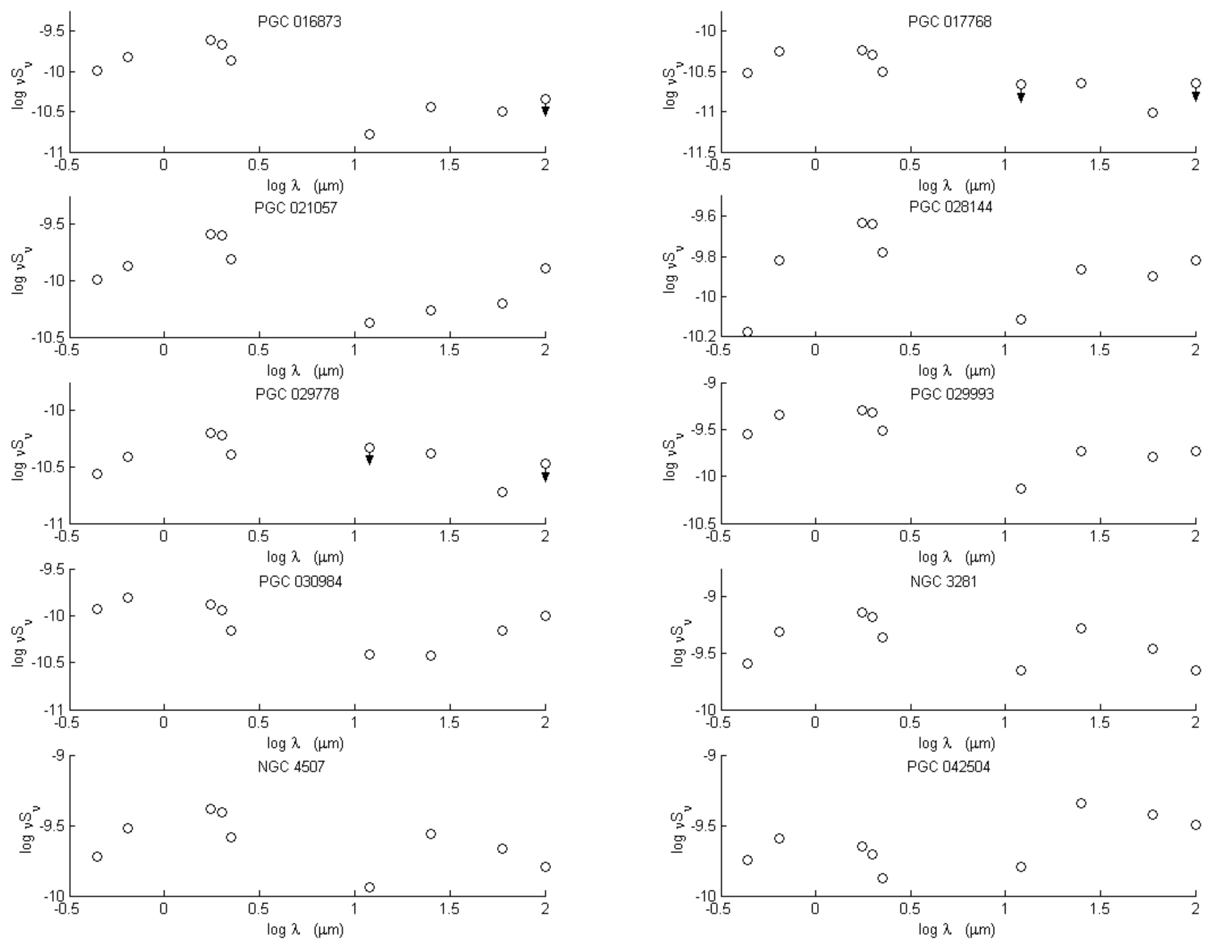

FIG. 3.15. - SEDs for Sy2 with data at all nine covered wavelengths. Arrows indicate values obtained by using the adopted upper limits.

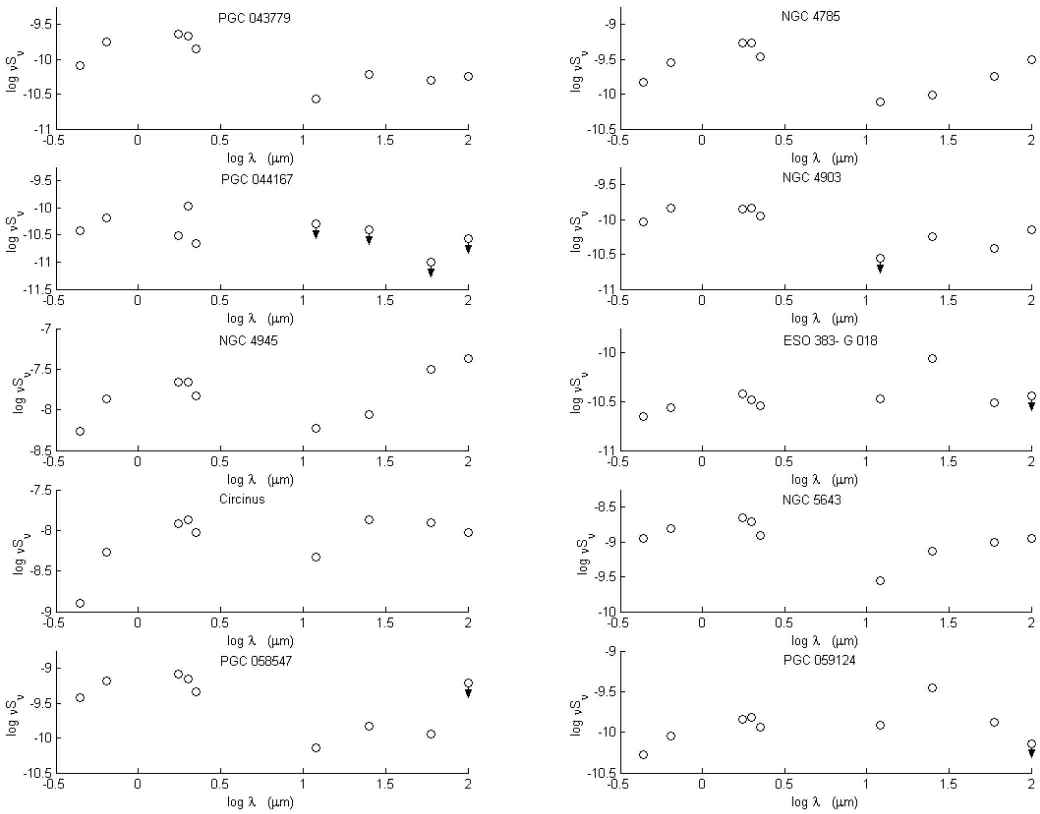

FIG. 3.16. - SEDs for Sy2 with data at all nine covered wavelengths. Arrows indicate values obtained by using the adopted upper limits.

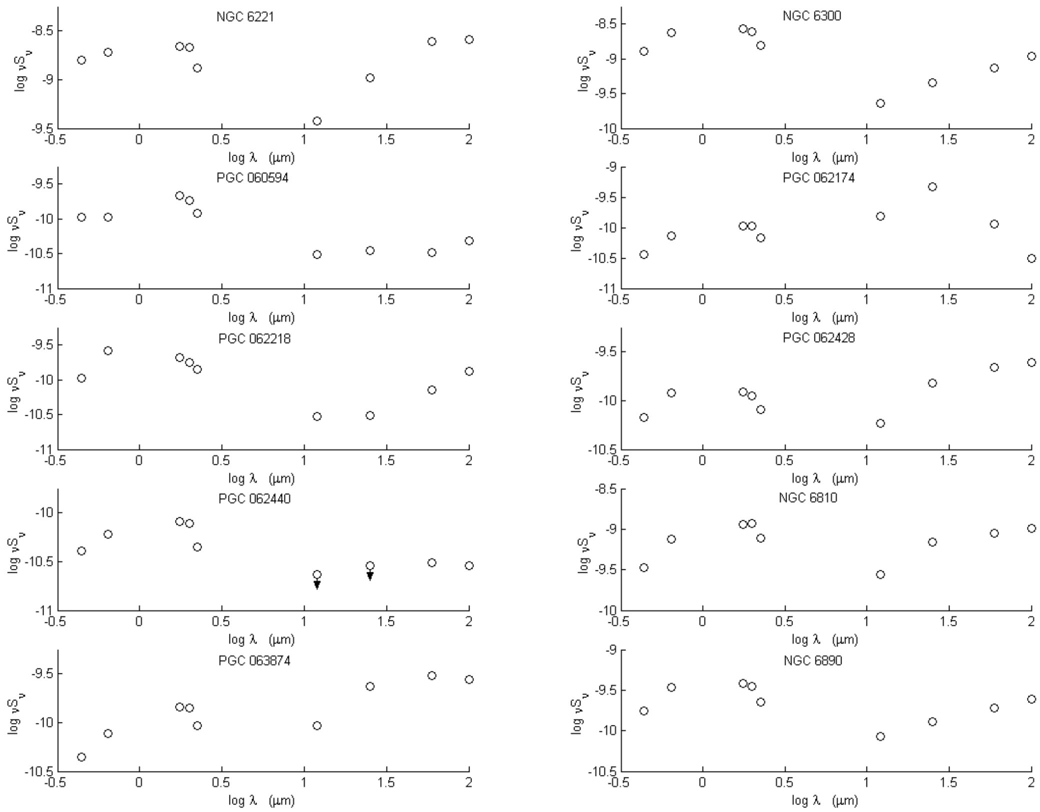

FIG. 3.17. - SEDs for Sy2 with data at all nine covered wavelengths. Arrows indicate values obtained by using the adopted upper limits.

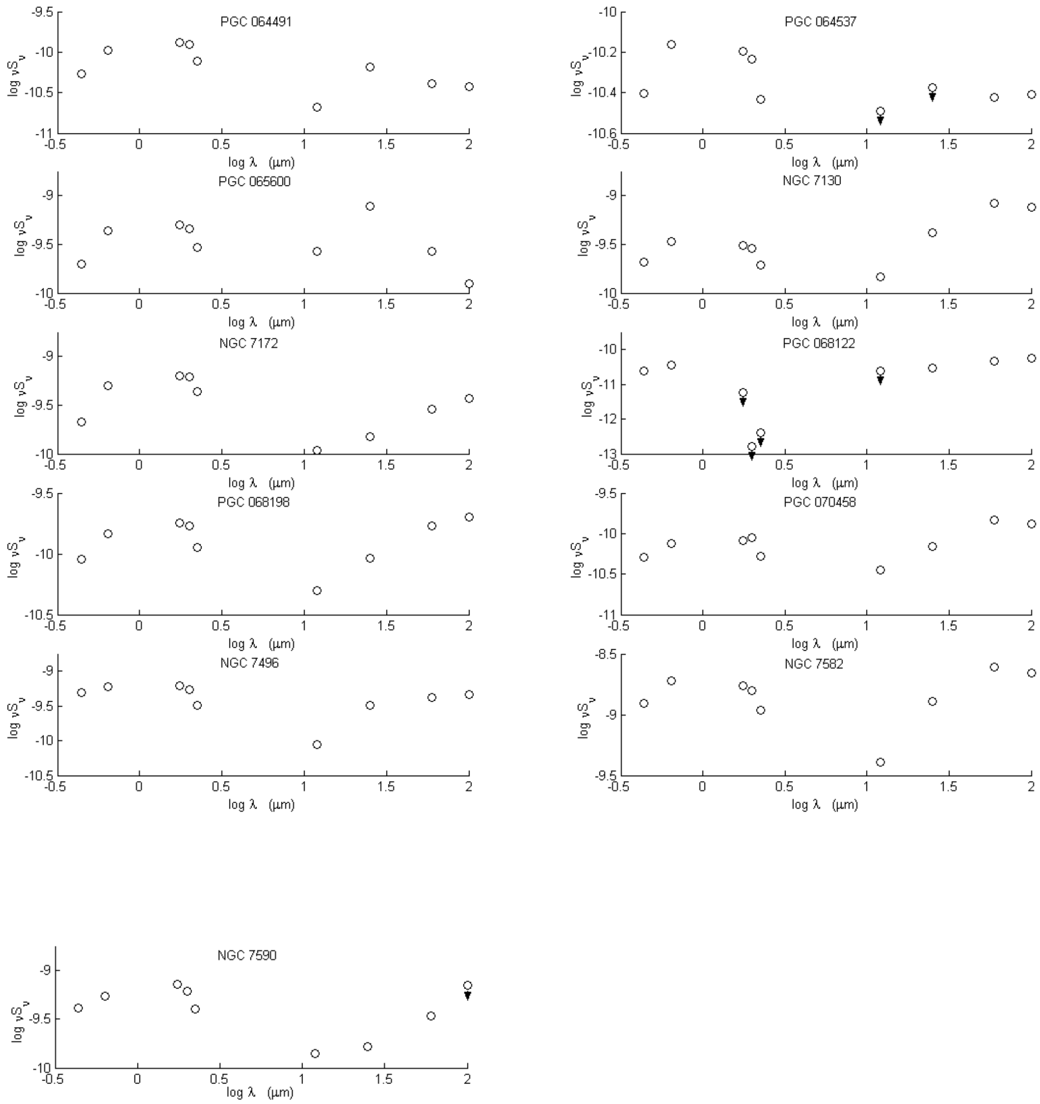

FIG. 3.18. - SEDs for Sy2 with data at all nine covered wavelengths. Arrows indicate values obtained by using the adopted upper limits.

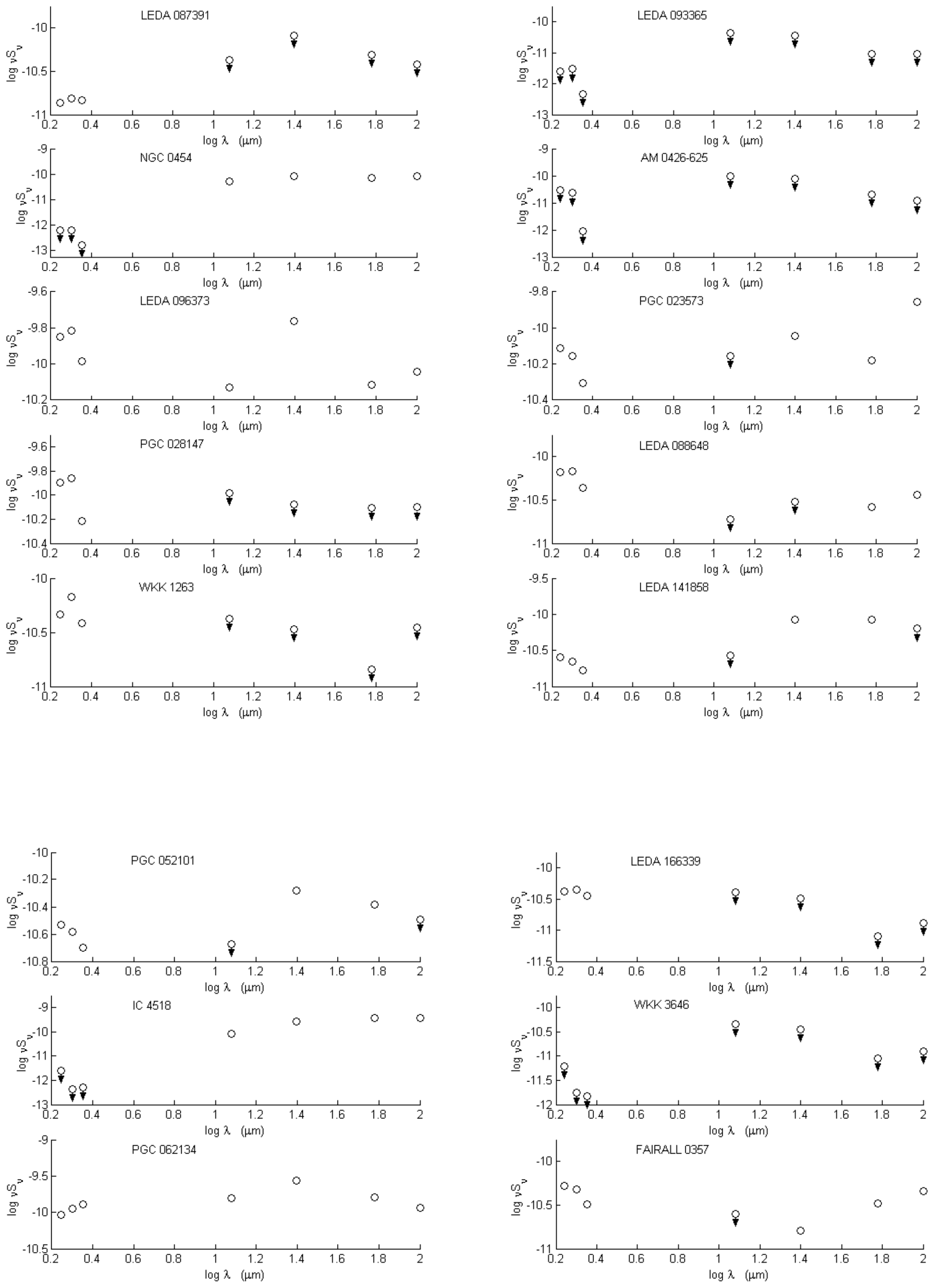

FIG. 3.19. - SEDs for Sy2 with data at just the seven IR bands covered. Arrows indicate values obtained by using the adopted upper limits.

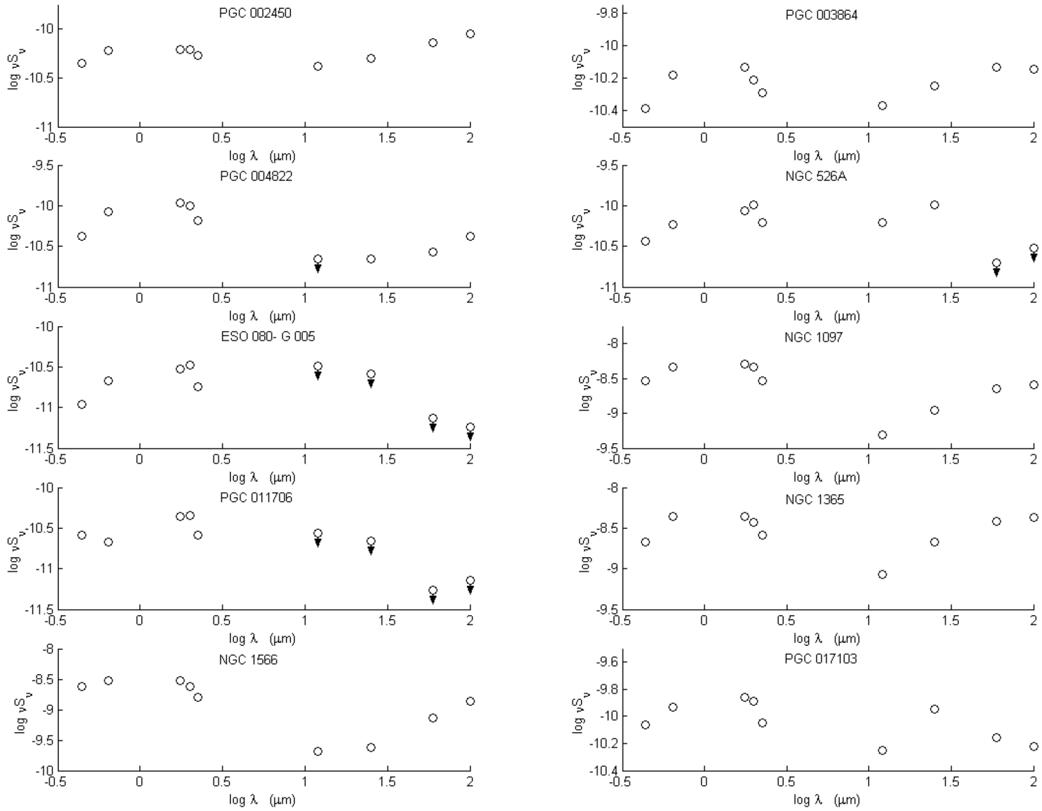

FIG. 3.20. - SEDs for Sy1 with data at all nine covered wavelengths. Arrows indicate values obtained by using the adopted upper limits.

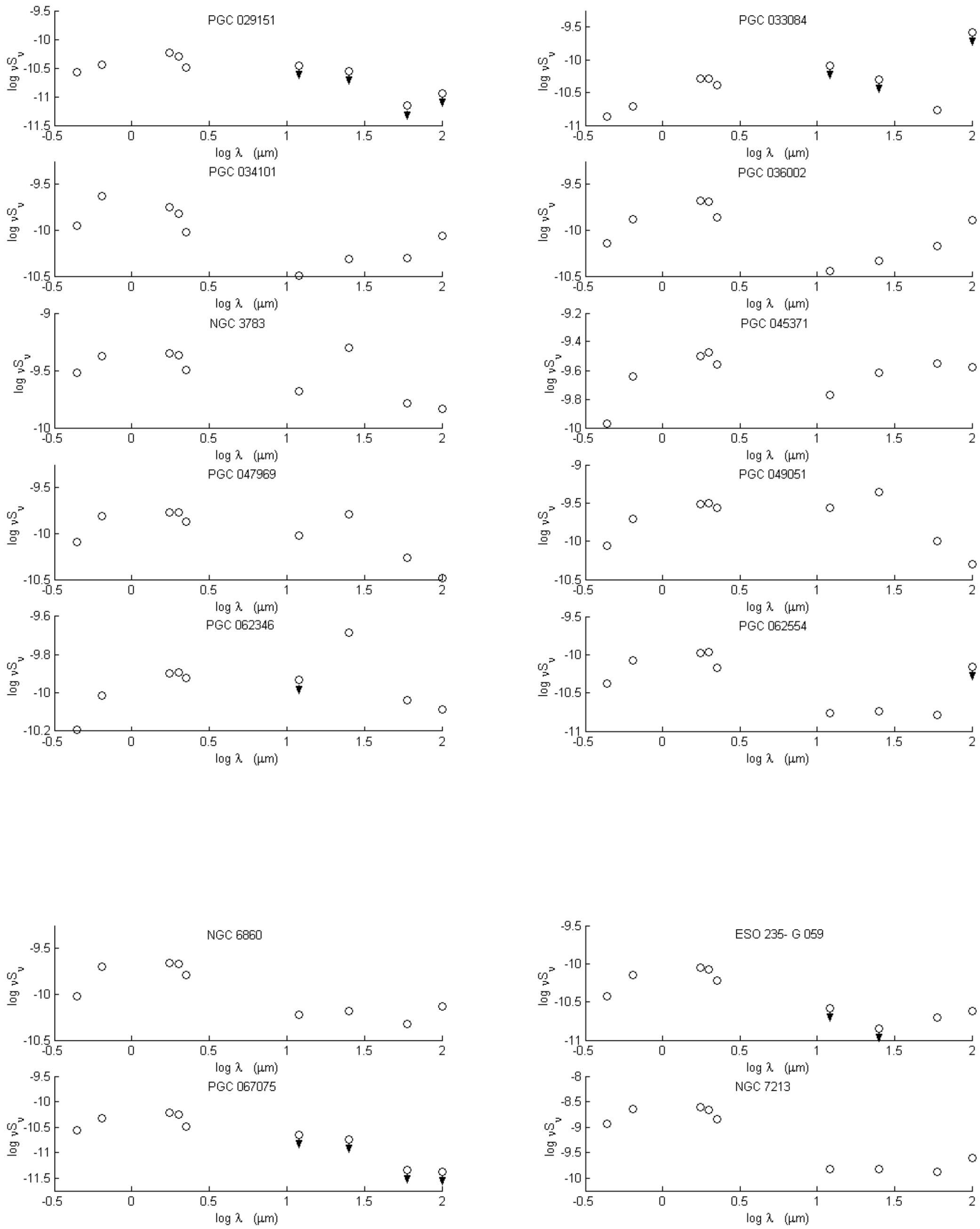

FIG. 3.21. - SEDs for Sy1 with data at all nine covered wavelengths. Arrows indicate values obtained by using the adopted upper limits.

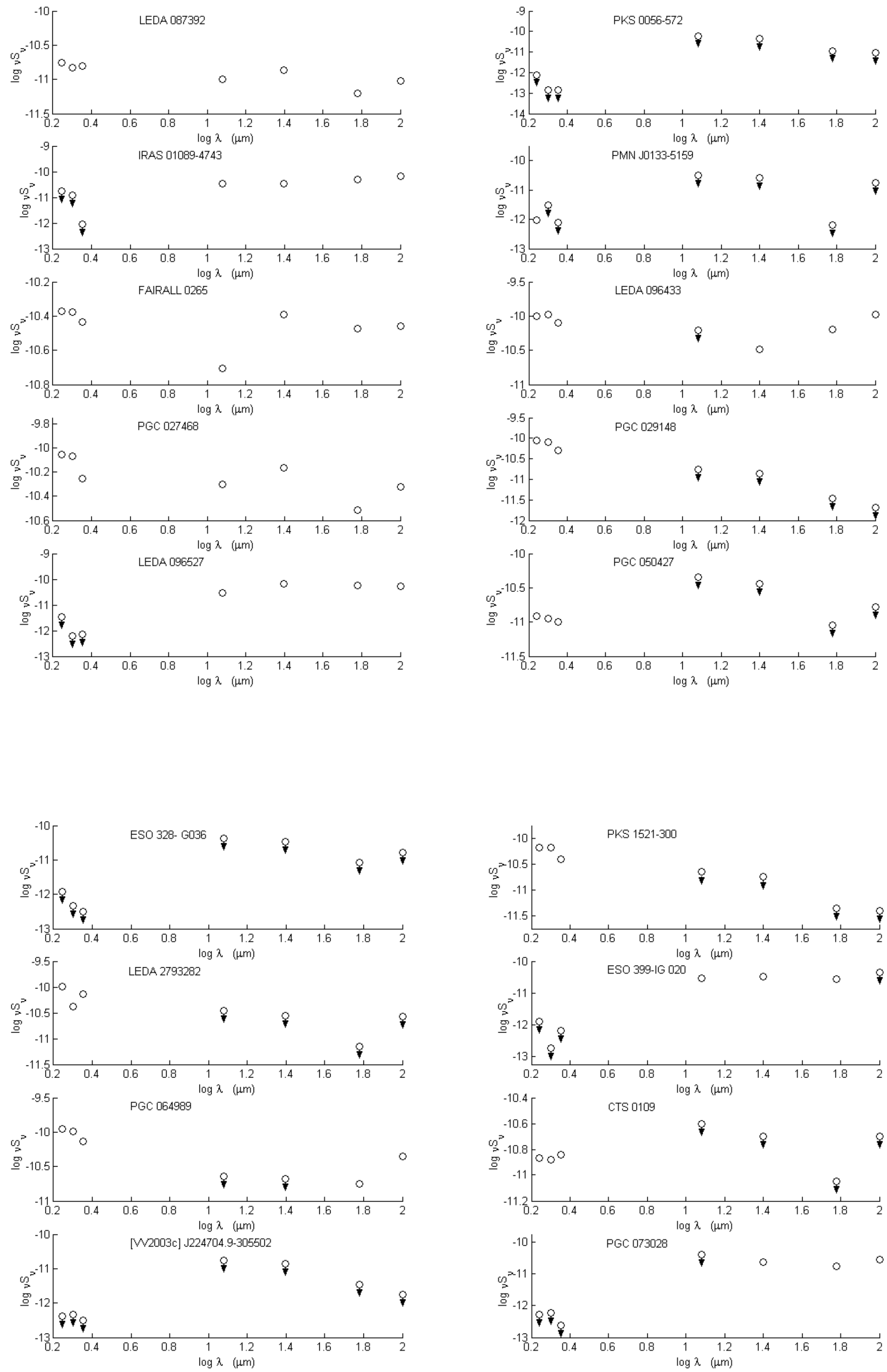

FIG. 3.22. - SEDs for Sy1 with data at just the seven IR bands covered. Arrows indicate values obtained by using the adopted upper limits.

From 12 to 25 µm, among those objects detected in both bands (71 objects, consisting of 49 Sy2 and 22 Sy1), most of the sample objects show a moderate to large increase. However the shape of the SEDs of five objects (7% of total sample) are flat in this wavelength range. The objects are the two Sy2 PGC 030984 and PGC 062218, the two Sy1.0 ESO 399 IG- 020 and *IRAS* 01089-4743, and the Sy1.5 NGC 7213.

From 25 to 60 µm, among those objects detected in both bands or one band in which the shape of the SED was unambiguous (93 objects, consisting of 65 Sy2 and 28 Sy1), there was a mix of shapes observed. For the Sy2, 28 (43%) show a positive slope between these two bands, while 23 (35%) show a decrease or negative slope, while the remaining 14 (22%) display a SED that is essentially flat in this wavelength range.

For the Sy1 in the 25 to 60 µm range the results are fairly similar, with 10 (38%) of the objects with positive slopes and the same number displaying negative slopes, with the remaining 8 (29%) being essentially flat.

From 60 to 100 µm, among those objects detected in both bands or one band in which the shape of the SED was unambiguous (84 objects, consisting of 58 Sy2 and 26 Sy1), there was again a mix of shapes observed. For the Sy2, 22 (38%) show a positive slope between these two bands, while 15 (26%) show a decrease or negative slope, while the remaining 21 (36%) display a SED that is essentially flat in this wavelength range.

For the Sy1 in the 25 to 60 µm range the results are fairly similar with 13 (50%) of the objects with positive slopes, 5 (19%) of the objects with clearly negative slopes, and 8 (31%) of the objects displaying an essentially flat SEDs between these two bands.

3.5.3 SPECTRAL INDICES

As noted in §3.4, the slope of the line between two log-log points [in the form log wavelength vs. log flux density]; ($\log\lambda_1$, $\log S_1$) and ($\log\lambda_1$, $\log S_1$) is given by Equation 3.2,

$$\alpha_{1-2} = \frac{log\left(\frac{S_2}{S_1}\right)}{log\left(\frac{\lambda_2}{\lambda_1}\right)}.$$

Using the 2MASS data, the values of $\alpha_{J\text{-}H}$, $\alpha_{J\text{-}Ks}$, $\alpha_{H\text{-}Ks}$ were computed, the results given below in Table 3.11. Because of the evidence discussed earlier that the upper limits adopted for the censored objects seem to be somewhat high, the indices were computed for all objects, by type, and then the same but for only detected objects.

TABLE 3.11

	Sy2			Sy1			All		
	α_{J-H}	α_{J-Ks}	α_{H-Ks}	α_{J-H}	α_{J-Ks}	α_{H-Ks}	α_{J-H}	α_{J-Ks}	α_{H-Ks}
Mean	0.572	-0.040	-0.660	0.349	0.050	-0.254	0.494	-0.008	-0.517
Median	0.716	0.105	-0.509	0.822	0.226	-0.314	0.763	0.148	-0.474
Mode	0.5907	-	0	-	-	-	0.5907	-	0
S. Deviatio	1.803	0.921	1.654	1.905	0.955	1.911	1.835	0.930	1.752
Min.	-11.974	-5.330	-10.864	-6.007	-4.383	-8.445	17.479	6.911	16.590
Max.	5.505	1.582	4.271	5.126	1.109	5.726	-11.974	-5.330	-10.864
Range	17.479	6.911	15.135	11.133	5.492	14.171	5.505	1.582	5.726
n	77	77	77	42	42	42	119	119	119

	Detected Sy2			Detected Sy1			All Detected Objects		
	α_{J-H}	α_{J-Ks}	α_{H-Ks}	α_{J-H}	α_{J-Ks}	α_{H-Ks}	α_{J-H}	α_{J-Ks}	α_{H-Ks}
Mean	0.873	0.184	-0.514	0.875	0.334	-0.087	0.833	0.233	-0.376
Median	0.760	0.148	-0.509	0.878	0.264	-0.314	0.781	0.174	-0.478
Mode	0.591	-	0.000	-	-	-	0.591	-	0.000
S. Deviation	0.660	0.303	0.696	0.952	0.339	0.851	0.643	0.321	0.772
Min.	-0.157	-0.327	-4.872	-2.232	-0.157	-1.200	-2.232	-0.327	-4.872
Max.	5.505	1.582	1.464	5.126	1.109	3.139	5.505	1.582	3.139
Range	5.662	1.909	6.336	7.358	1.266	4.339	7.737	1.909	8.011
n	71	71	71	35	34	34	105	105	105

As can be seen from Table 3.11, the inclusion of the censored objects changed the arithmetical mean and median in substantial but varying amounts. For the Sy2 in the sample, using the flux density upper limits to compute α_{J-Ks} changed the mean from slightly negative value of -0.040 to a positive value of 0.184. The median values were of course changed less, with the median α_{J-H} values changing from 0.716 (all 77 Sy2) to 0.760 (only 71 detected Sy2). For α_{J-Ks} the median value changes from 0.105 to 0.148, and for α_{H-Ks} the median value remains unchanged at -0.509.

For the Sy1 in the sample the changes in the median values for the indices, when considering only the detected objects, is very small. The largest change being for α_{J-H} going from 0.822 (all 42 Sy1) to 0.878. The (arithmetical) mean values for the Sy1 NIR indices are changed considerably by the inclusion of the indices computed for the censored Sy1 using the adopted upper limits. For α_{J-Ks} the increase in the mean value from 0.050 (all 42 Sy1) to 0.334 (34 detected Sy1), a factor of ~ 6.7, was the largest. For α_{H-Ks} the change was a decrease, going from -0.254 to -0.087, for all Sy1 to just the detected ones, respectively. For α_{J-H} the increase in mean value was the smallest, from 0.349 to 0.875.

The computed NIR indices for only the detected Sy are close to the ones obtained in §3.6 using the Kaplan-Meier product estimator, which as discussed earlier, uses information on the pattern of censoring to estimate the true (parent) population value.

The maximum index values computed for just the detected objects were fairly similar by type, except for α_{H-Ks} in which the value for Sy1 is 3.139 and for the Sy2, 1.464, a factor of ~2 larger. The minimum index values for just the detected objects varied much more by type. For the index α_{J-H} the minimum value (-0.157) for the detected Sy2 is a factor of 14 smaller than the minimum (-2.232) for Sy1. That extreme index value for the Sy1 is for LEDA 2793282 (Sy1.5). This steep drop in flux density values from J to H bands is all the more interesting because it is the *only detected* Sy1 to show a negative slope between those two data points. Only one Sy2 had a negative value, PGC 010665. It is the minimum Sy2 α_{J-H} value of -0.157 just mentioned. All of the other negative values for α_{J-H} computed resulted from using the adopted upper limits, which as discussed in §3.6 strongly suggests the upper limits are outliers, significantly higher than what the true flux density values are likely to be.

The M/FIR spectral indices $\alpha_{12\text{-}25\,\mu m}$ and $\alpha_{25\text{-}60\,\mu m}$ were computed for the detected objects (69 Sy2 and 29 Sy1) only, though the adopted M/FIR upper limit flux density values seem to more in line with the averages computed from the detected objects than the ones for the NIR bands. The results are in Table 3.12.

The (arithmetical) mean and median values of $\alpha_{12\text{-}25\,\mu m}$ for the detected Sy2 were found to be 1.149 and 1.222. For $\alpha_{25\text{-}60\,\mu m}$ the values obtained were 1.615 and 1.620. The mean and median values of $\alpha_{12\text{-}25\,\mu m}$ for the 29 detected Sy1 are less than one-half the value of those, at 0.650 and 0.687, respectively. However for $\alpha_{25\text{-}60\,\mu m}$ the mean and median values for the Sy1 are closer to those of the Sy2, at 1.354 and 1.447, respectively. The mean value for $\alpha_{12\text{-}25\,\mu m}$ for all 98 detected sample objects was 1.002 and the median value 1.036. For $\alpha_{25\text{-}60\,\mu m}$ the mean for all detected objects was found to be 1.538 and median value 1.547.

TABLE 3.12

	Detected Sy2			Detected Sy1			All Detected Objects		
	$\alpha_{12\text{-}25\mu m}$	$\alpha_{25\text{-}60\mu m}$	α_1 / α_2	$\alpha_{12\text{-}25\mu m}$	$\alpha_{25\text{-}60\mu m}$	α_1 / α_2	$\alpha_{12\text{-}25\mu m}$	$\alpha_{25\text{-}60\mu m}$	α_1 / α_2
Mean	1.149	1.615	0.240	0.650	1.354	0.174	1.001	1.538	0.220
Median	1.222	1.620	0.742	0.687	1.447	0.364	1.036	1.547	0.647
Mode	-	-	-	-	-	-	-	-	-
S. Deviation	0.657	0.735	9.823	0.594	0.776	2.342	0.676	0.753	8.320
Range	3.508	3.075	93.796	2.163	3.141	14.735	3.712	3.347	93.796
Min.	-0.371	-0.024	-76.891	-0.574	-0.296	-9.888	-0.574	-0.296	-76.891
Max.	3.137	3.051	16.905	1.588	2.845	4.847	3.137	3.051	16.905
n	69	69	69	29	29	29	98	98	98

Also reported in Table 3.12 are the values of $\alpha_{12\text{-}25\ \mu m} / \alpha_{25\text{-}60\ \mu m}$. This ratio (of slopes) tells us whether the slope of the line from 25 to 60 µm is steeper (ratio < 1) or not (ratio > 1) than the slope of the line going from 12 to 25 µm. This distinction will be of use in the later discussion of the results being reported here, and their comparison with some in the published literature.

The median value of the ratio $\alpha_{12\text{-}25\ \mu m} / \alpha_{25\text{-}60\ \mu m}$ for the Sy2, 0.742, is larger than the median value for the Sy1, 0.364, by a factor of 2. The mean value reported for the Sy2 was 0.240 and for Sy1, 0.174, a factor of 1.4 difference. For all 98 detected objects, the mean and median values of $\alpha_{12\text{-}25\ \mu m} / \alpha_{25\text{-}60\ \mu m}$ was found to be 0.220 and 0.647, respectively.

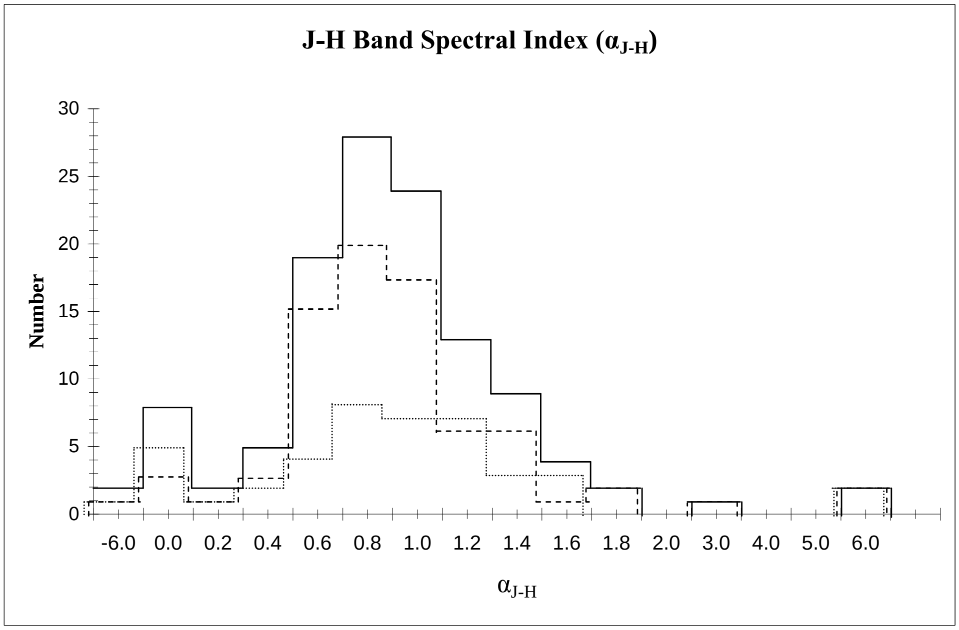

FIG. 3.23. - Spectral Indices computed for J-H bands. *Top*: contains all objects (solid), and by type (dashed Sy2, dotted Sy1). *Bottom*: censored objects; dashed Sy2, dotted Sy1. Vertical lines offset horizontally for clarity.

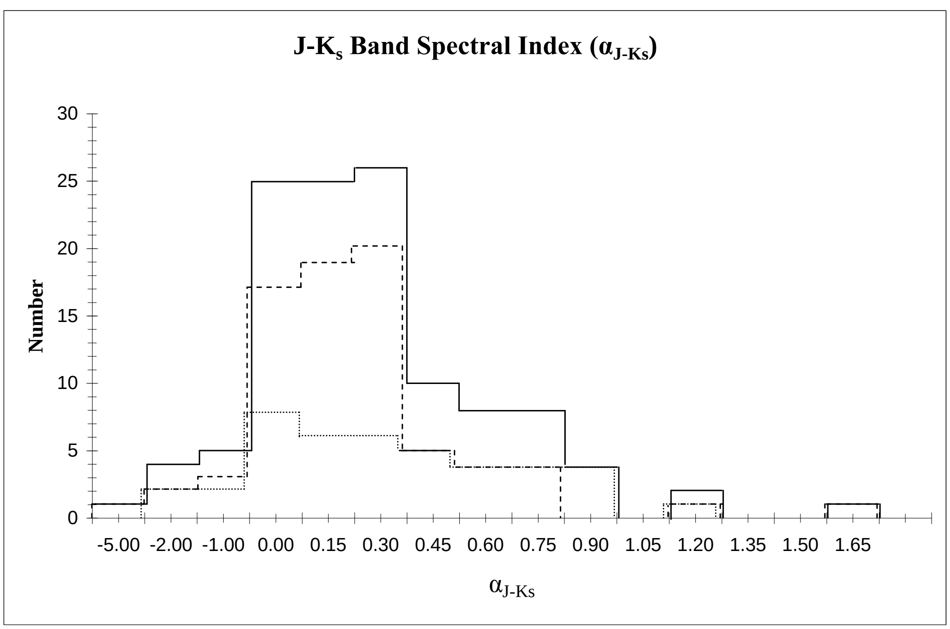

FIG. 3.24. - Spectral Indices computed for J-K_s bands. *Top*: contains all objects (solid), and by type (dashed Sy2, dotted Sy1). *Bottom*: censored objects; dashed Sy2, dotted Sy1. Vertical lines offset horizontally for clarity.

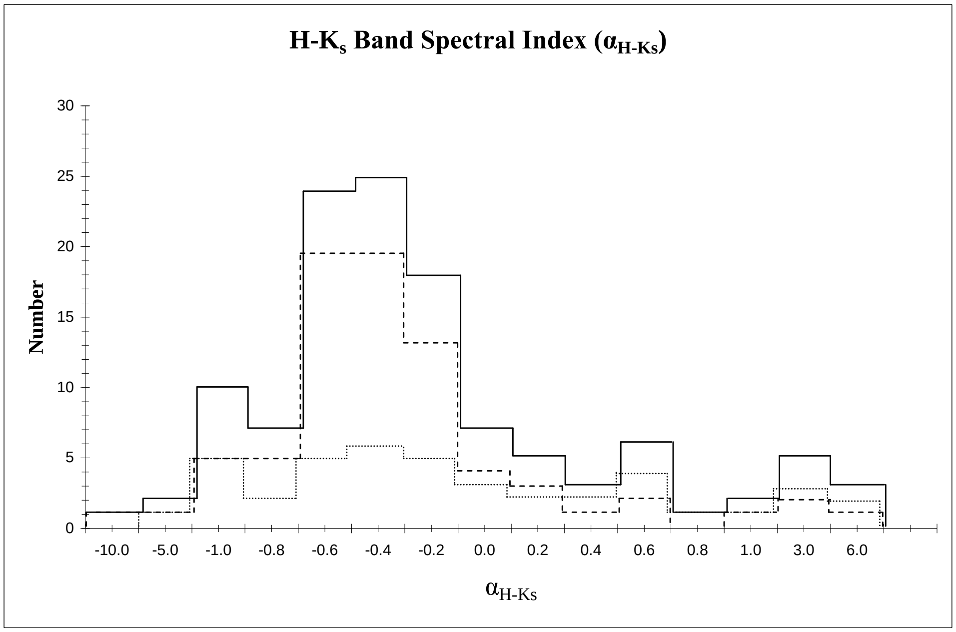

FIG. 3.25. - Spectral Indices computed for H-K_s bands. *Top*: contains all objects (solid), and by type (dashed Sy2, dotted Sy1). *Bottom*: censored objects; dashed Sy2, dotted Sy1. Vertical lines offset horizontally for clarity.

3.6. STATISTICAL TESTS

As in chapter 2 with the radio data, certain two-sample tests were carried out on the IR data of the sample. This includes the NIR and M/FIR luminosities at all seven of the bandwidths investigated, as well as the 12 micron flux values (for a comparison to several other recent, related studies; see §3.1 and 3.9). The package ASURV was used to compute the probability that the Sy1 and Sy2 in this sample are drawn from the same parent population, again testing the unified view of Seyferts. The same tests as in chapter 2 were carried out, and the results are reported in Table 3.13 below. Also reported are the mean and median values of the different parameters under consideration using the Kaplan-Meier product estimator as implemented in ASURV which uses the censored object data to estimate the true distribution of the sample.

Following the same convention as discussed in §2.7, results are considered significant if all of the probabilities are less than 0.05. Further, the results are considered "weakly significant" if all results p(null) are less than 0.10, or if all but one result is less than 0.05.

For the computed NIR luminosities, no significant difference was found between Sy1 and Sy2 as shown in Table 3.13. As with the arithmetical mean and median values of the luminosities reported above in

Table 3.10, the mean and median values increase from J to H band, then decrease for K_s band. This is more clearly seen in the spectral indices computed and reported above.

The results in the M/FIR luminosities are mixed. As shown in Table 3.13, at 60 and 100 µm a significant difference was found between Sy type. The number of censored objects in given by the value of *n* in the table. As discussed in Chapter 4, this is not unexpected based on past research and what we know about the different IR components of an active galaxy.

The Sy1 and Sy2 luminosities at 25 µm show a borderline weakly significant difference. All probabilities are less than 0.10 but two, however they are two similar tests - Gehan's Generalized Wilcoxian tests, with permutation and hypergeometric variances, giving *p* values 0.1213 and 0.1261, respectively.

TABLE 3.13

Variable	*Sy2*			*Sy1*			*All Sy*			*p*				
	n	Mean	Median	*n*	Mean	Median	*n*	Mean	Median	Gehan1	Gehan2	Logrank	PP	PPW
2MASS														
log(L) [J band]	6	22.32 ± 0.08*	22.52	7	21.99 ± 0.17*	22.37	13	22.20 ± 0.09*	22.50	0.226	0.229	0.075	0.224	0.213
log(L) [H band]	6	22.39 ± 0.10*	22.60	8	22.06 ± 0.18*	22.50	14	22.26 ± 0.09*	22.59	0.234	0.236	0.065	0.232	0.215
log(L) [Ks band]	6	22.33 ± 0.10*	22.54	8	22.03 ± 0.18*	22.46	14	22.21 ± 0.09*	22.53	0.471	0.471	0.142	0.471	0.456
IRAS														
log(L) [12µm]	27	22.87 ± 0.05	22.82	20	22.89 ± 0.07*	22.85	47	22.87 ± 0.04	22.84	0.582	0.576	0.957	0.689	0.674
log(S) [12µm]	27	-0.658 ± 0.070*	-0.782	20	-0.858 ± 0.083	-0.985	47	-0.729 ± 0.055*	-0.864	0.063	0.067	0.085	0.061	0.060
log(S) [12µm] +	27	-0.710 ± 0.061*	-0.796	20	-0.858 ± 0.083	-0.985	47	-0.764 ± 0.050*	-0.872	0.101	0.104	0.116	0.095	0.093
log(L) [25µm]	15	23.29 ± 0.05	23.23	16	23.10 ± 0.08*	23.07	31	23.23 ± 0.04*	23.19	0.121	0.126	0.027	0.083	0.079
log(L) [60µm]	10	23.86 ± 0.06*	23.84	14	23.33 ± 0.14*	23.45	24	23.64 ± 0.07*	23.82	0.006	0.007	0.002	0.005	0.005
log(L) [100µm]	22	24.08 ± 0.06	24.13	17	23.55 ± 0.17*	23.81	39	23.82 ± 0.10*	24.07	0.047	0.050	0.023	0.037	0.035
2MASS Spec. Indices														
J-H	6	0.221 ± 0.341*	0.704	7	0.024 ± 0.382*	0.763	13	-0.109 ± 0.328*	0.740	0.894	0.893	0.421	0.891	0.888
J-H - median UL	6	0.848 ± 0.073	0.700	7	0.800 ± 0.151	0.763	13	0.835 ± 0.069	0.732	0.564	0.558	0.738	0.591	0.582
J-K	6	-0.246 ± 0.172*	0.102	8	-0.370 ± 0.275*	0.214	14	-0.324 ± 0.159*	0.137	0.153	0.138	0.860	0.160	0.137
J-K - median UL	6	0.168 ± 0.034	0.104	8	0.304 ± 0.054	0.225	14	0.215 ± 0.030	0.215	0.035	0.026	0.096	0.041	0.032
H-K	6	-0.908 ± 0.244*	-0.536	8	-0.799 ± 0.410*	-0.404	14	-0.905 ± 0.233*	-0.500	0.081	0.067	0.679	0.090	0.069
H-K - median UL	6	-0.541 ± 0.084	-0.543	8	-0.167 ± 0.126	-0.468	14	-0.410 ± 0.074	-0.509	0.030	0.021	0.201	0.042	0.030

At 12 µm there is no significant, or even close to weakly significant, difference found between the Sy by type. As mentioned earlier, it has been known for some time (Sinoglio & Malkin 1989) that at

wavelengths between 7-12 μm there is minimal scatter in the SED between most all AGN types, and so we would expect, if this sample is close to complete out to the redshift cutoff chosen in this study (z < 0.0303), the 12 μm flux density values to be similar in distribution. This is one reason that the 12 μm sample of Rush et al. (1993) continues to be used in Sy research (e.g., Buchanan et al. 2006).

At 60 and 100 μm, all of the statistical tests indicate a significant difference in the (log) luminosities by type. The smallest probabilities were at 60 μm, where the values in the thousandths. At 100 μm all of the probabilities are less than 0.05 except for the Gehan2 test, but it is nearly there at 0.050.

A weakly significant difference in the log of the 12 μm flux density values was found between Sy types. The tests were then run again but with two Sy2 removed (Circinus and NGC 4945) because they are both nearby (in fact the two closest Sy in the sample, at just z ~ 0.0014 and 0.0019, respectively, the next closest Sy being almost twice the distance of these two) and consequently have comparatively large flux density values (18.80 and 23.65 Jy, respectively). The two sample results with those two Sy2 not included are not significant, weakly or otherwise.

The same tests were performed on the spectral indices described in the previous section. As can be seen in Table 3.13, for each of the three NIR indices under study, α_{J-H}, α_{J-Ks}, and α_{H-Ks}, the tests were performed twice. On the first run of the tests the upper limits from Table 3.1 & 3.2, for the censored objects, were used to compute the indices. On the second run of the tests the median values of the indices of the uncensored objects were used instead. For α_{J-H} there were six censored Sy2 and 7 censored Sy1. For α_{J-Ks}, and α_{H-Ks} there were seven censored Sy2 and eight censored Sy1. The reason this was done is because the upper limits used, while at or near the 97% confidence level, are such that the indices computed from them are clear outliers compared to the rest of the sample.

For example, consider the results for α_{J-H}. Only four of the 77 values computed for the Sy2 are negative. Of those, three are censored objects (IC 4518, WKK 3646, and PGC 068122). The values of α_{J-H} for the three censored objects (computed from their upper limits) are -5.294, -3.514, and -11.974, respectively. As a comparison, of the 71 Sy2 that were detected (J band), the minimum value was -0.157 (and was the fourth of the four negative values), the maximum value was 5.126, with arithmetical mean and median values of 0.873 and 0.759, respectively, and a standard deviation of 0.660. So those three negative values for α_{J-H} (censored objects) are outliers. Another reason for these large negative index values is because a ratio of logarithms (Equation. 3.2) was used to compute them and so there is more sensitivity to the larger flux values used derived for the upper limits. These outliers resulted in mean values, using Kaplan-Meier product estimator in ASURV, which are dubious. For example, with the values of α_{J-H} for the Sy1 in the sample, only six are negative, and again the majority, five, are for censored objects. Again they are all outliers and because of the modest size of the number of Sy1 in the sample (42), these cause a mean of 0.024 ± 3.82 to be computed by ASURV which is not very helpful. However, if the median value (which is 0.878, computed from the 34 detected Sy1) was used for α_{J-H} for the censored objects instead of the values computed using their upper limits, the ASURV implementation of the Kaplan-Meier product estimator gives a mean value of 0.800 ± 0.151 which is more realistic (and very close to the arithmetical mean given in Table 3.10).

As can be seen from Table 3.13, there was no significant difference (by Sy type) found for α_{J-H}, with either the median value of the detected objects used for the censored objects, or if the index value is computed using the upper limits. For α_{J-Ks}, no significant (or weakly significant) results were reported when the index values for the censored objects were computed using the upper limits. However, when using the median value for the detected objects instead, a weakly significant result was reported, with all probabilities less than 0.10, in fact all but one less than 0.05. For α_{H-Ks} weakly significant results (all *p* values but one < 0.10) was reported and when using the median values instead, a significant result (all p(null) < 0.05) was found.

3.7 THE RADIO VERSUS INRARED CORRELATION

Nearby spirals demonstrate a correlation between radio continuum emission and Hα emission, which is a measure of the abundance of H II regions (Kennicutt 1983, Dickey & Salpeter 1984), and hence massive star formation. Other correlations, especially between radio and IR emission - since the latter is obscured less than emission at most other wavelengths - have been known for some time and have been investigated widely. Hence, the (presence or absence of) the correlation is a way, for example, of studying the relationship between starburst activity and AGN (e.g., Imanishi & Wada 2004). Seyfert galaxies (which are usually contained in a spiral host galaxy) show this correlation but are more scattered; one indicator of this would then be a lower r^2 value (the square of the Pearson's product-moment correlation coefficient).

The first study to establish a linear correlation between global (that is, including the host galaxy) radio and IR emission in spiral galaxies was by van der Kruit (1971). The sample (eight of which were Seyferts), consisted of all of the galaxies listed in Seyfert (1943) with δ > +10°. The radio observations were made with the Westerbork Synthesis Radio Telescope (WSRT) at 1415 MHz and the resulting data was compared with 10 μm data from Kleinman & Low (1970a,b), which were infrared observations of galaxies between 1 – 25μm using the three Cassegrain telescopes at the Catalina Observing Station of the

University of Arizona. A strong correlation for all of the spiral galaxies in van der Kruit (1971) was observed.

Of the extragalactic sources of far infrared (FIR) radiation of any significance, most are dust clouds opaque to visible light. This includes the dusty torus in the unified model of AGN, as well as large amounts of dust in many host galaxies. Such dust is fairly transparent to radio waves, making such identifications of infrared sources unbiased (Condon & Broderick 1986). A large FIR luminosity observed in an AGN is an indicator of large dust masses (Roy & Norris 1997). The global FIR-radio correlation is seen to hold for many different galaxy types, at large and small scales, and over more than 3 orders of magnitude (Appleton et al. 2004).

As discussed in §1.10, the standard explanation for the observed global FIR-radio correlation is that the FIR and radio emission are both due to star formation and death. In this scenario, the FIR emission is produced by high-mass stars that heats nearby dust, which is then reradiated at FIR wavelengths. The correlation is thought to come about due to the same high-mass stars; when the giant stars end their lives as supernovae they produce relativistic electrons which generate the observed (non-thermal) synchrotron radio emission (Vlahakis et al. 2007). One little understood variable here is the galactic magnetic field and how exactly it influences the process (Thompson et al. 2006). It is still not known with any certainty, however, if the M/FIR emission from Seyferts is dominated by large-scale disk emission or emission by the circumnuclear torus (Thean et al. 2001a and references therein; Vlahakis et al. 2007).

This M/FIR-radio correlation was investigated for this sample using the SUMMS 843MHz data and the four *IRAS* bands that have been under investigation in this paper so far; 12, 25, 60, and 100 µm. The flux density values were taken from Tables 3.1 & 3.2. The results are displayed below in Figures 3.29 - 3.32.

Also investigated here is the extent of any correlation existing between the NIR and 843MHz data. Considering the radio and IR continuum emission mechanisms in active galaxies, some amount of correlation is to be expected. The results are given in Figures 3.26 - 3.28 and Table 3.14, below. As of the time of this writing, there have been no published results on this, that I have been able to find, whether for samples of active or normal galaxies, involving these wavelengths. The results of Peng et al. (2006) does however show a strong correlation in Sy between the (nuclear) K_s -band magnitudes and the [O III] λ5007 and hard X-ray luminosities. The K_s -band emission is thought to primarily originate from graphite grains in the warm, dusty torus in the central regions of the AGN, as discussed earlier, though the significant FIR emission from the host galaxy should also contribute to the detected emission at these lower wavelengths.

Since the flux density values for the objects in this sample are from large surveys, and so global in nature, they are well suited for the study of global FIR-radio correlations. It needs to be kept in mind however that because of the global nature of the results obtained here, they are not directly comparably with many recent ones that are similar, yet focused only on the central regions of the galaxy, the AGN. Many published studies on Sy over the years however have involved the analysis of such global data, that from *IRAS* being probably the most famous, and continue to play an important part in helping to complete our understanding of the nature and evolution of AGN and galaxies in general. That is done precisely by being global in nature, while most modern work is focused on the nuclear regions and use instruments without the unique properties of the MOST.

In Table 3.14 the lines of best fit along with their corresponding r^2 value are given. For each band (column) these values are given by Sy type, both types combined, and by type but considering only detected objects (that is, non-censored in the IR). The later was done, especially for the Sy2 in the sample since this subsample size is fairly large, to try and get a measure on how close the upper limit values for the censored objects might be to the true ones. For the ordinate (843MHz flux value) no distinction was made in the lines of best fit as to whether or not it is an upper limit or detection. This results in 35 lines of best fit and r^2 values in Table 3.14.

In Figures 3.26 - 3.32 the radio vs. IR flux density values are plotted by type and also whether the radio and/or IR flux density values were censored. So this results, for each IR band, in eight different plots (and symbols) per figure. Each figure has a legend showing all eight of the plot combinations. For detected (in both radio and in the IR) objects the plotted points are of the form (Rj, Ij) where j = 1, 2 indicates the Sy type. This results in four of the plots in each figure (each band). The censored (either in the radio, IR, or both) objects result in the other four of the eight total plots per figure, the points being of the form (RjC, IjC) where j = 1, 2 indicates the Sy type and C that the object was censored. So for example, a plot of the 843MHz flux density versus any of the seven N/M/FIR IR flux densities for the Sy2 censored in the radio is written as (R2C, I2). This results in a total of seven figures, each with eight plots, giving 56 total plots. Lines of best fit were not computed with consideration of whether the radio flux density value was censored or not (that is, in the case of the abscissa being of the form RjC for j = 1, 2. Hence there are more plots than lines of best fit computed.

In each of the seven plots of the *log*(radio) vs. *log*(IR) total flux densities below, Figures 3.26 - 3.32, error bars are given on both the radio (x) and IR (y) values. The errors are small and so the error bars are best seen by zooming in on the figure. If an object is censored in either or both x and y, an “uncapped” bar is used to differentiate them from the regular, “capped” bars for uncensored (non-upper-limits) values. The uncapped bars for the SUMSS and 2MASS censored data are set at 10% of the adopted upper-limit value simply to make it easily visible. For the *IRAS* data the uncapped bars are set at 30% of the upper-limit values. These are arbitrary values.

For the logarithmic plots in Figures 3.26 - 3.32, the errors for the error bars were computed using the standard theory of arithmetical error propagation when dealing with logarithms (e.g., ChemWiki, 2012). For a given sample object, the error associated with the total flux density propagates logarithmically as approximately $.434\left(\frac{err}{S}\right)$, where S is the total flux density S_{IR} and *err* the associated error for that measurement (both given in Tables 3.1 and 3.2).

TABLE 3.14

	J	**H**	**K_s**	**12μm**	**25μm**	**60μm**	**100μm**
All Sy slope intercept r^2	0.558 -0.504 0.191	0.564 -0.436 0.162	0.576 -0.479 0.166	0.496 0.133 0.510	0.634 0.602 0.534	0.775 1.295 0.470	0.702 1.516 0.429
All Sy2	0.668 -0.227 0.360	0.678 -0.145 0.300	0.681 -0.236 0.288	0.595 0.290 0.652	0.726 0.804 0.682	0.899 1.611 0.720	0.827 1.805 0.666
All Sy1	0.248 -1.231 0.028	0.238 -1.206 0.022	0.223 -1.261 0.019	0.297 -0.222 0.239	0.399 0.089 0.266	0.420 0.462 0.147	0.371 0.769 0.121
Det. Sy2	0.751 -0.041 0.539	0.753 0.060 0.555	0.759 0.015 0.580	0.695 0.399 0.645	0.826 0.907 0.667	0.907 1.632 0.685	0.855 1.854 0.622
Det. Sy1	-0.301 0.725 0.047	0.653 -0.056 0.309	0648 -0.076 0.329	0.567 0.215 0.374	0.663 0.615 0.394	0.732 1.254 0.378	0.673 1.489 0.308

Note. - The components of the lines of best to the plots in Figures 3.26 - 3.32. The lines are the standard least squares line of the form *log(IR flux density) = a*log(radio flux density) + b* where *a* is the slope and *b* the vertical intercept. A total of 35 lines of best fit were computed, one for each combination containing the radio flux density value (regardless of whether it was an upper limit) and the seven IR bands, by type, types combined, and only detected objects. For all objects, the ordinate for each point plotted is the SUMSS 843MHz flux density value from Table 1.1 & 1.2.

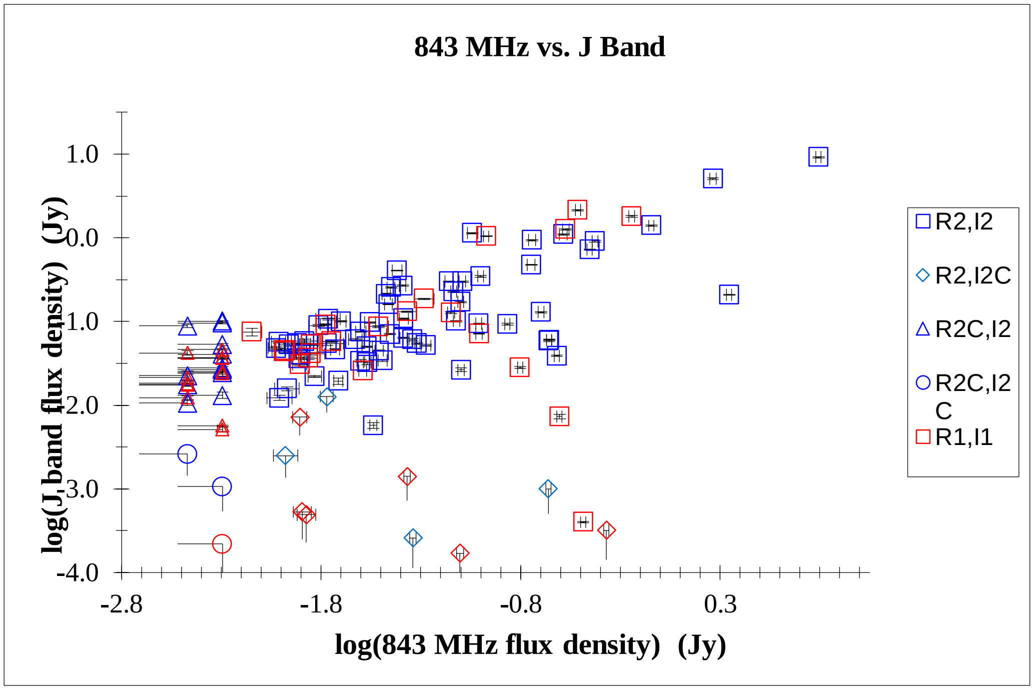

FIG. 3.26.

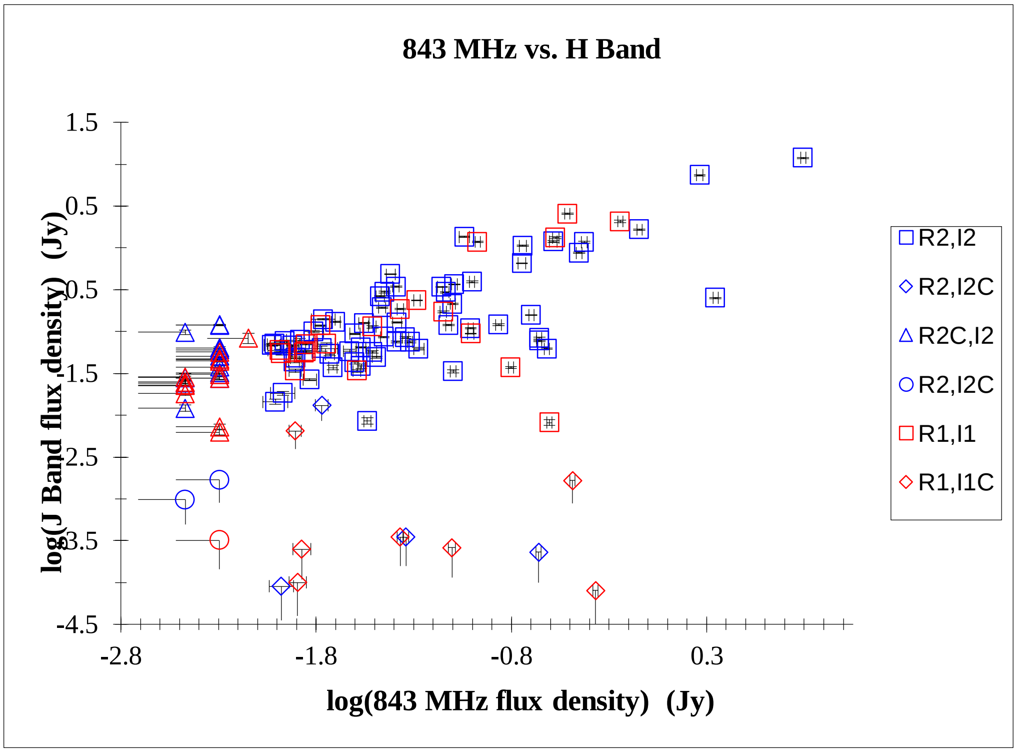

FIG. 3.27.

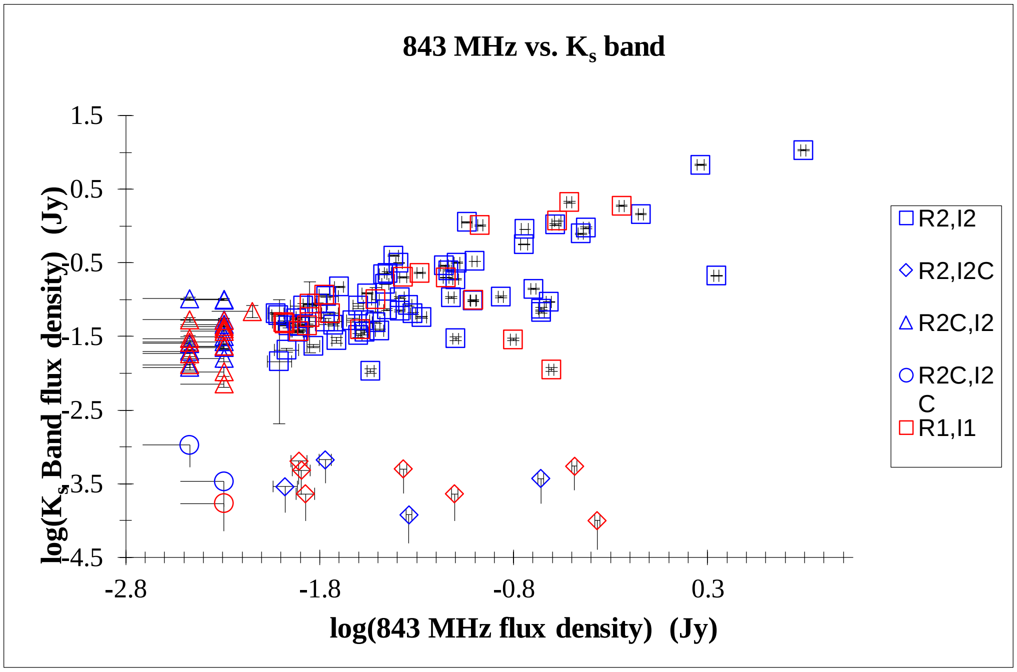

FIG. 3.28.

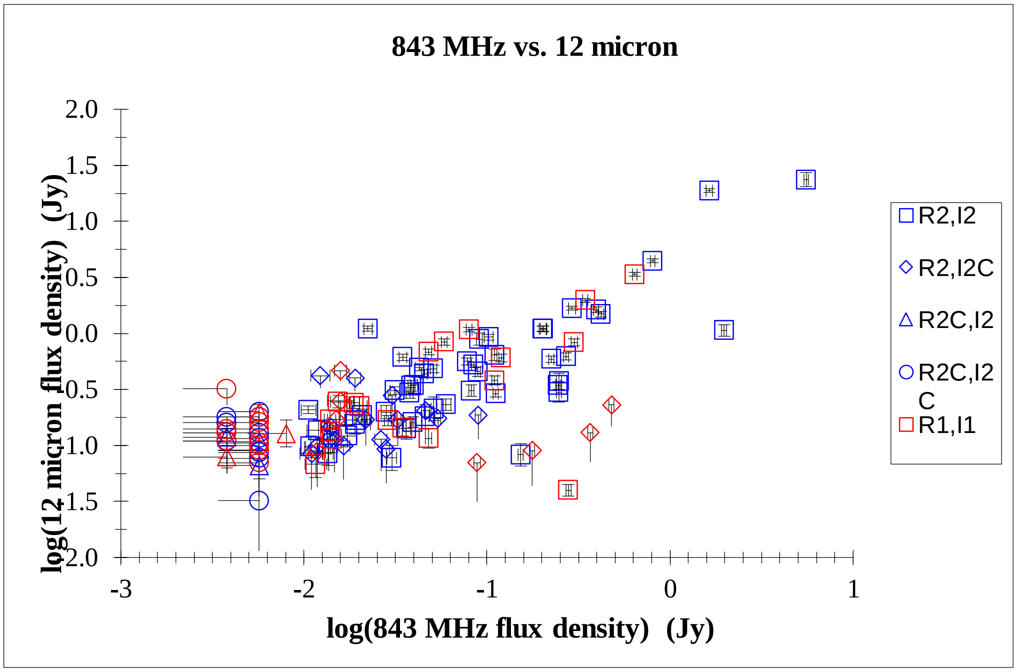

FIG. 3.29.

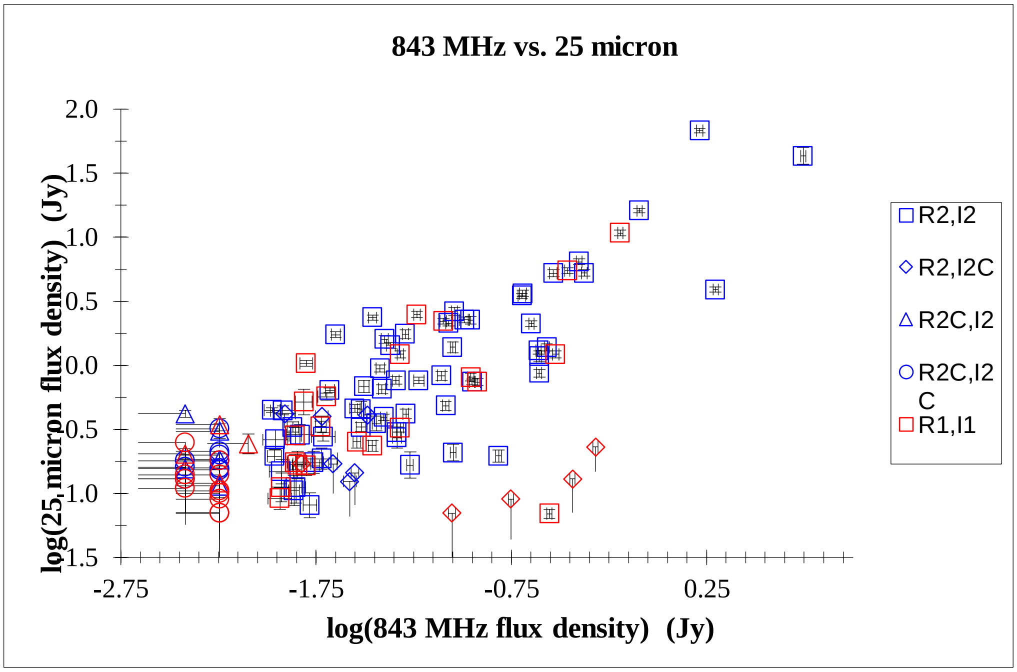

FIG. 3.30.

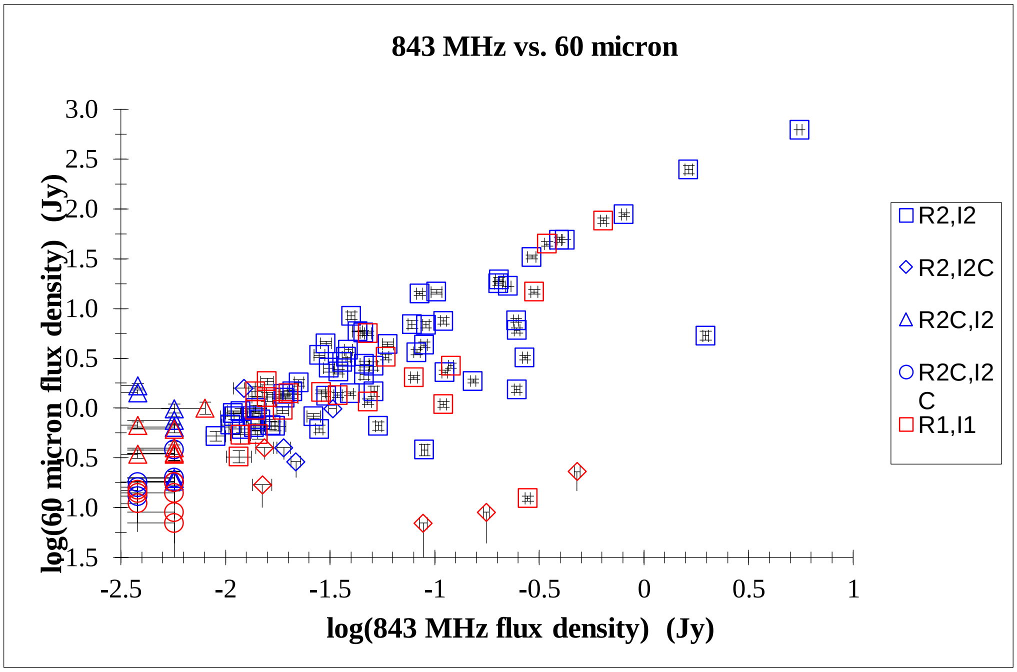

FIG. 3.31.

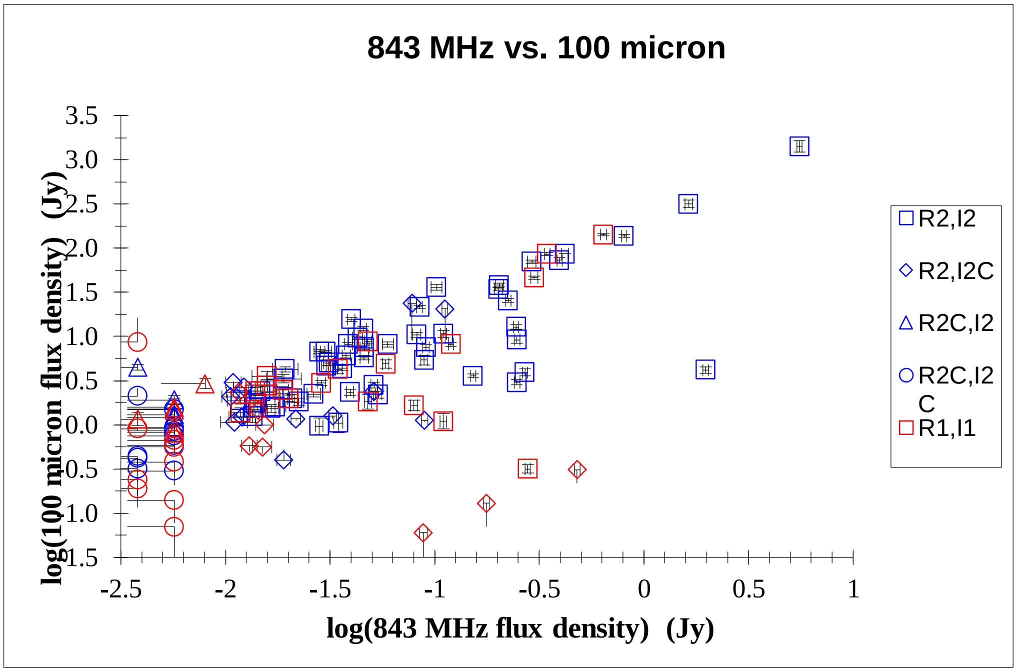

FIG. 3.32.

When comparing all Sy2 to only the detected ones, it is interesting to note that the smallest difference in *r* value was found with *IRAS* data, which has the *most* censored (in the IR) objects. For example, between the radio and J band fluxes (flux understood to mean total flux density from now in this section, unless stated otherwise) there are only six censored Sy2, so the line of best fit was computed for 71 objects. The r^2 value obtained was $r^2 = 0.539$ ($r = 0.734$). Including the six upper limit values for the censored Sy2, 77 points total, the value obtained was $r^2 = 0.360$ (r = 0.600). The amount of scatter induced by just 6/77 < 8% of the Sy2 that were censored indicates that the upper limits adopted are likely to be significantly higher than the true values. This is consistent with the findings above showing that the spectral indices ($\alpha_{J\text{-}H}$, $\alpha_{J\text{-}Ks}$, and $\alpha_{H\text{-}Ks}$) computed using the adopted upper limits were all outliers.

Conversely, between the radio and 100 μm data there were 22 censored Sy2. The line of best fit was computed for the 55 detected objects and $r^2 = 0.622$ ($r = 0.789$) was obtained. The value for all 77 Sy2 (22 upper limits) was close to this, $r^2 = 0.666$ ($r = 0.816$). Similar results were obtained for the Sy2 at all of the *IRAS* bands. For Sy1 the difference was greater at all *IRAS* bands than what was found for the Sy2 but this is not surprising since there are only 42 Sy1 in the sample and a large fraction of them censored (~48% at 12 μm, ~38% at 25 μm, ~33% at 60 μm, and ~40% at 100 μm). The difference is still less than with the 2MASS (and radio) data.

In all the FIR bands, the radio vs. FIR plots show a large difference by type, with a strong correlation for the Sy2 with values in the range $r^2 = 0.622 - 0.720$ ($r = \sim 0.789 - 0.849$). This is true whether looking at all the Sy2 (77 objects) or when omitting the censored ones (27, 15, 10, 22 objects censored at 12, 25, 60, and 100 µm, respectively).

For all 42 Sy1 in the sample, the values $r^2 = 0.121 - 0.239$ ($r = \sim .35 - .49$) were computed. Omitting the censored Sy1 (20, 16, 14, 17 objects censored at 12, 25, 60, and 100 µm, respectively), values in the range of $r^2 = 0.308 - 0.394$ ($r = \sim 0.55 - 0.63$) resulted; not only a smaller range, but also somewhat higher values. These results are, as can also be seen from Table 3.14, significantly lower than is the case with the Sy2.

For the full sample (119 objects) there was fairly strong linear correlation between the radio and FIR fluxes. Values for r^2 range from a low of 0.429 ($r = .655$) at 100 µm, to a high of 0.534 ($r = 0.731$) at 25 µm.

At 12 µm the result was close to that, $r^2 = 0.510$. By type (including censored objects) the Sy2 in the sample show the highest level of linear correlation, $r^2 = 0.720$, at 60 µm. For the Sy1 in the sample the greatest degree of correlation was found at 25 µm, $r^2 = 0.266$).
Overall the Sy1, whether considered all together or just the detected (in the IR), show the least correlation as can be seen in Table 3.14. A large amount of scatter for the Sy1 at the three 2MASS bandwidths result in $r^2 < 0.03$, the lowest being just $r^2 = 0.019$, for K_s-band. Of course since there are fewer Sy1 in the sample, any scatter will more consequential when computing the r^2 value.

The slope values for the lines of best fit of the radio vs. FIR data are all in the range 0.297 (all Sy1 only) to 0.907 (detected Sy2 only), depending on FIR band and Sy type. As with the correlation coefficients, all of the slope results for Sy2 were higher than for just the Sy1. Overall the slopes for the 42 Sy1 were lowest values found, for all four FIR bands; 0.297, 0.399, 0.420, and 0.371 at 12, 25, 60, and 100 µm, respectively. When only detected Sy1 were considered, significantly higher values are found; 0.567, 0.663, 0.732, and 0.673.

For the full sample (119 objects) the slopes of the lines of best fit for the 843MHz radio data with the four FIR bands are 0.496, 0.634, 0.775, and 0.702 at 12-100 µm, respectively.

The results of the radio vs. NIR data was more mixed. The slope values for the lines of best fit for all 119 sample objects in the J, H, and K_s bands are all very similar, increasing slightly going from J to K_s band; 0.558, 0.564, and 0.576.

When considering just the 77 Sy2 in the sample we see similar results - a slight increase in slope value going from J to K_s bands; values 0.668, 0.678, and 0.681 were obtained. Similar but slightly larger slope values were found when considering just the detected Sy2.

As with the radio vs. FIR lines of best fit, the slope values were lowest for the Sy1 in the NIR. In addition, the slope values of the three lines for only the 42 Sy1 *decrease* slightly going from J to K_s bands, with slope values of 0.248, 0.238, and 0.225 obtained. Only in this case were strictly decreasing slope values found.

It is important to note that many authors, when investigating the radio-FIR correlation, have the FIR flux density as the independent variable, whereas above it is the dependent variable. So in comparing slopes one must be sure to compare the same quantities. For example, for all 119 objects in the sample a slope of 0.775 was reported at 60 µm (Table 3.14). The slope of the line of best fit, when the FIR flux density is the independent variable, is computed to be 0.694.

As a way of investigating the scatter observed in the Figures 3.26 - 3.32, a search for radio-excess Sy was undertaken. As mentioned above, Roy & Norris (1997) identified a class of galaxies (not all AGN) that display a much larger radio flux density that would be expected from their observed FIR flux density. The central selection criterion used by Roy & Norris (1997) that identified (indeed defines), radio-excess galaxies is that the ratio of flux densities $S_{6.3\text{cm}}$ / $S_{60\mu\text{m}}$ (for all *detected* objects) is more than 3σ above (or below) those reported in a large, important early study of this correlation between 6.3 cm (4750 MHz radio) and 60 µm (FIR) flux densities among normal galaxies (de Jong et al. 1985). Roy & Norris (1997) uses the 4850 MHz ~ 6.2 cm radio data from the PMN radio survey (Wright 1994) instead. The 3σ values translate into the ratio being > 1/55 or < 1/875, for those objects more than 3σ above or below the correlation reported in de Jong et al. (1985), respectively. The other selection criteria used by Roy & Norris (1997) were related to excluding stars, reflection nebulae, etc.

In the first of a series of papers investigating radio-excess galaxies, Drake et al. (2003) adopt the radio-excess definition of Yun et al. (2001), which is based on the logarithm of the reciprocal of the ratio used in Roy & Norris (1997), given as $u = log\left[\frac{S_{60\mu m}}{S_{4850MHz}}\right]$. A galaxy is considered radio-excess if u < 1.8 (and considered radio-loud if u < 0.0). This is essentially equivalent to the criterion mentioned above but with the cut-off value of 0.016 instead of 1/55 ~ 0.018.

The 843 MHz (~ 35.6 cm) radio data from the SUMSS was used to estimate the 6.3 cm (4750 MHz) flux densities for all of the Sy in the sample that were detected at both 843 MHz and 60 µm. This was done the conventional way of assuming the (radio) power law relation $S \propto \nu^{-0.7}$. In particular $S = b\upsilon^{-0.7}$ was assumed, for the flux density *S*, the frequency υ, and parameter *b*. By using the value of *S* at 843 MHz the value for *b* was computed for each object and then used to estimate its 6.3 cm flux density.

A total of nine Sy (six Sy2 and three Sy1) in the sample met the ratio criterion of being more than 3σ from the correlation as reported in de Jong et al. (1985). The ratio in question for these objects were all > 1/55 ≈ 0.182. The results are shown below in Table 3.15. Note that using the other measure of radio-excess mentioned above (Yun et al. 2001; Drake et al. 2003), the same nine Sy are selected.

Three of the objects, PGC 062134, PGC 065600, and NGC 7213 were part of the sample in Roy & Norris (1997) and the PMN survey 4850 MHz flux density values adopted here were taken from that study. These same three objects, but none of the other six listed above, are also in the sample of Drake et al (2001) mentioned above. PGC 006078, PGC 047969, and PGC 029778 were censored in the PMN survey and so would not have been selected for that sample.

PGC 006078 was censored in the PMN survey. At declination δ ~ -40°, the flux density limit of the survey was approximately 50 mJy. The flux density value estimated for this object, as described above (we only get one significant digit), was 20 mJy.

PGC 015172 was detected in the PMN survey. Wright (1994) gives a 4850 MHz flux density value of 50 mJy, which is not listed in NED. The value estimated, as described above, was also 50 mJy (rounded to one significant figure), showing the method of estimating the flux densities can be quite accurate.

PGC 047969 was censored in the PMN survey. With a declination of δ ~ -34°, the flux density limit of the survey was approximately 72 mJy. The adopted, estimated, value in Table 3.15 is 30 mJy.

For LEDA 096373 the 6.3 cm flux density value estimated as described above was 70 mJy. The 4850 MHz value from the PMN survey (Wright 1994) was 109 mJy, which increased the ratio in question.

PGC 029778 was censored in the PMN survey. With a declination of δ ~ -36°, the flux density limit of the survey was approximately 72 mJy. The adopted, estimated, value in Table 3.15 is 30 mJy.

LEDA 087392, which shows the largest value of the ratio in question among all of the Sy in this sample, has a 4850 MHz flux density of 54 mJy as reported in Wright (1994). The flux density value estimated as described above was 80 mJy. Adopting the PMN survey value of 54 mJy reduced the ratio under investigation here from 0.6 to 0.44, still larger by a factor of approximately 4.5 than the next largest ratio value of 0.098 (for PGC 065600).

Using the radio-loud criterion mentioned above (Drake et al. 2003), *u* < 0.0, none of the Sy in the sample in this paper would be considered radio loud. By those measures LEDA 087392 comes close, with *u* ~ 0.19. As noted below, however, using methods explored in Visnovsky et al. (1992) the newly identified radio-excess PGC 029778 galaxy would be classified as radio-loud.

Four of the objects (PGC 006078, PGC 047969, LEDA 096373, and PGC 029778) were also detected in the NRAO VLA Sky Survey (NVSS). The survey was at 1.4 GHz ~ 21 cm and the primary reference paper is Condon et al. (1998). The flux density values reported from that survey are listed in Table 3.15. They are all consistent with the estimated 6.3 cm flux density value estimated for these objects.

The Sy2 PGC 006078 stands out however as having a reported 4850 MHz flux density (57.8 $\pm$ 1.8 mJy) that is larger than the reported flux density at 843 MHZ (53.9 $\pm$ 2.0 mJy). This is obviously not consistent with a power law relation with a negative exponent. Assuming the power law relation discussed above, the estimated flux density for PGC 006078 based the objects flux density at 843 MHz is, rounded to one significant figure, 40 mJy. As discussed in Chapter 4 this could be explained by variability in the radio emission, a phenomenon that has been well documented for other Sy, including the Sy1.5 NGC 7213 in this sample. In fact the variability of NGC 7213 is evident in Table 3.15. The reported (detected) 6.3 cm flux density value is more than twice the (detected) value at 843 MHz (~36 cm).

None of the Sy had a ratio < 1/875, therefore no Sy in the sample were more than 3σ below the correlation reported in de Jong et al (1985). All nine of these radio-excess candidates are discussed in more detail in Chapter 4.

Table 3.15

Name	$S_{6.3}$ (mJy)	S_{21} (mJy)	S_{36} (mJy)	$S_{6.3}/S_{60\mu m}$	Host Type	AGN Type
PGC 062134*	70	--	270.3	0.022	Sa	Sy2
PGC 006078	20	57.8	53.8	0.03	Sa: sp	Sy2
PGC 015172**	50	--	152.9	0.03	(PR?)SB(rl)	Sy2
PGC 047969	30	47.9	110.1	0.03	E-S0	Sy1.5
LEDA 096373**	109	171.7	247.0	0.071	S	Sy2
PGC 029778	30	78.5	89.5	0.08	(R'_2)SB(s)ab	Sy2
NGC 7213*	247	--	119.6	0.093	SA(s)0^0	Sy1.5
PGC 065600*	524	--	1975	0.098	SA(s)0+:	Sy2
LEDA 087392**	54	--	278.6	0.44	n/a	Sy1.0

Note.- Identified radio-excess Sy. A marking with ** indicates the 6.3 cm flux densities are actually 4850 MHz (~ 6.2 cm) data from the PMN survey (Wright 1994). The asterisk indicates that the object was in Roy & Norris (1997), which also uses the PMN survey data. The remaining 6.3 cm flux densities were estimated as described above.

3.8 DECOMPOSITION OF 2MASS Ks -band IMAGES

In the study of active galaxies using data from all-sky surveys, such as those under discussion here, the flux density values are "global" in that the contribution from the host galaxy is included. That is the benefit of using data from the SUMSS, 2MASS and *IRAS* surveys; much of the data they provide is global in nature, and so all are similar in that way. Such global information plays an important part in our understanding of the birth and evolution of (all types of) galaxies, one example being the radio-IR correlation discussed in §3.7.

In many cases the object appears as a point source (e.g., at radio wavelengths see Figures 2.3 - 2.22 in Chapter 2) so extracting any significant detail is not possible. But for many nearby galaxies much of the structure can be discerned. This allows one to measure the detected IR emission from the different components of a galaxy, by fitting each separately.

The software package GALFIT fits different functions directly to astronomical images, to decompose the image of a nearby galaxy into the disk, bulge, and nuclear components. The 2-D fitting package uses standard, commonly used functions in astronomical research for such purposes. Peng et al. (2004) discusses much of the theory useful in the decomposition of galaxy images in general, as well as the different built-in functions in GALFIT and how to then implement them.

The paper Peng et al. (2006) is, at the time of this writing, the only published paper on Seyfert samples that utilizes 2MASS data. In it the authors use GALFIT to decompose 2MASS (K_s-band) images of 65 nearby ($z < 0.02$) Sy2 into the disk, bulge, and nuclear components. A strong correlation was found between the nuclear K_s-band magnitudes and the [O III] λ5007 and hard X-ray luminosities

To complement the results presented in Peng et al. (2006), all Sy2 with $z < 0.02$ from the sample of Sy2s under investigation in this thesis that were not censored in the 2MASS, and that reside spiral host galaxies, were analyzed using GALFIT. Thirty Sy2 of the 77 in this sample were investigated by Peng et al. (2006). Of the remaining 47, 30 have $z < 0.02$. Of those 30, three are interacting host galaxies and so were excluded (NGC 0454, AM 0426-625, IC 4518; all three of which happened to be censored in the 2MASS as well). Of the remaining 27, two (WKK 3646, PGC 068122) were censored in the 2MASS and so excluded. That left 25 Sy2 that were detected in the 2MASS and have $z < 0.02$. However PGC 030984, while not censored and with z = 0.014 < 0.02, is very faint (nearly point) source, with K_s -band flux density = 50.3 mJy (19.0 mJy at 843 MHz), and so was also excluded. Table 3.16 shows the remaining 24 objects along with some of their properties, reproduced from earlier tables. All are in some type of spiral host galaxy. Eleven of the 24 reside in some type of barred spiral (SB) and the remaining 13 in some type of SA, as can be seen in Table 3.16.

The K_s -band 2MASS images (obtained from NASA/IPAC 2) for the 24 Sy2 in Table 3.16 were fitted so as to obtain the contributions (the output from GALFIT is magnitude) from the AGN, bulge, and disk (of the host galaxy), separately. Following Peng et al. (2006), the 24 Sy2 were fitted in GALFIT with a Point Spread Function (PSF, centered on each image), an inclined exponential disk, and a function to model the bulge. For the latter, the function (built-in GALFIT, as is the exponential disk, among many others) used to model the surface brightness of the bulge was of the form $e^{-(r/r_s)^{1/n}}$ with $0.5 \leq n \leq 5.0$. This is a so-called Sersic function (Sersic 1968), which is a generalization of the so-called de Vaucouleurs profile. These have been widely used for many decades, often in the study of elliptical galaxies (Mazure & Capelato 2002). The exponential disk is of an essentially similar form with $n = 1$.

GALFIT uses the Levenberg-Marquardt algorithm (which I also happened to use in computing the curve of best fit shown in Figure 2.2) to minimize residuals between a given data image and the model chosen for fitting it.

For the PSF, Peng et al. (2006) followed the work of Jarret et al. (2000) and used a radially symmetric exponential function to model the K_s -band images from 2MASS. The function has the form

$$f(r) = f_0 e^{-(r/\alpha)^{1/\beta}}$$

where α and β are free parameters and f_0 is the central surface brightness. I adopted the same parameter values as used in Peng et al. (2006). These are $\alpha = \sqrt{2}\sigma = 1.5''$ and $\beta = 0.5$. The quantity σ is FWHM/2.354, with FHHM, the seeing of the 2MASS images, taken to be 2.5" for the K_s band images (IPAC 1998). The quantities r, r_s, and r_e are the length, the scale length, and the effective radius (the length such that half of the total flux is within r_e), respectively, in pixels.

The PSF must be in a separate file in .fits format. Peng et al. (2006) created one using the analysis software IRAF. To ensure the most directly comparable results with those from that study, I acquired through a private communication with Zhixin Peng, the lead author of Peng et al. (2006), the PSF file (Peng 2009) used in that study.

Each object listed in Table 3.16 was fitted, manually through the GALFIT menu system, for the host galaxy disk, the host galaxy bulge, and a PSF appropriate to the 2MASS instruments in the K_s band as described above. The results are also listed in Table 3.16. GALFIT v.3.0 (compiled to run in Windows) was used, running on an AMD Athlon 7750 Dual-Core processor with Windows XP (SP3).

For the bulge magnitudes, the mean and median values computed for the 24 Sy2 were 10.14 and 10.30, respectively. For the 30 Sy2 in Peng et al. (2006) the values reported were 10.10 and 10.20. For the disk magnitudes, the mean and median values computed for the 24 Sy2 were 10.30 and 10.67, respectively. The corresponding values reported in Peng et al. (2006) were 9.83 and 10.13.

For the AGN magnitudes, the mean and median values computed were 11.77 and 11.85, respectively. For the 30 Sy2 in Peng et al. (2006) the values reported were 11.98 and 12.12.

That the AGN averages for the 24 Sy2 from this sample were both lower, meaning brighter since we are dealing with magnitudes, is explained at least in part by the fact that there were three low outliers. These are Circinus, NGC 1808, and NGC 4945 - the closest of the 24 Sy2 to the Milky Way, all with $z < 0.003$. However the disk magnitude averages computed were noticeable higher (fainter) for the 24 Sy2 in this sample. This is partly explained by several galaxies with very faint disks for which getting a good fit from the bulge was difficult.

Table 3.16

Component Magnitudes (2MASS Ks - band)

Name	Global mag	Bulge mag	Disk mag	AGN mag	Host Classification	z
PGC 005696	9.94	11.17	10.38	12.63	SB(r)bc:	0.016
PGC 008012	10.09	10.88	10.42	11.83	(R'_1)SB(rs)ab	0.020
NGC 0824	10.40	11.26	11.02	13.14	SB(rs)b	0.019
PGC 009634	9.91	10.31	12.37	11.97	(R'L)SA:(s:)a	0.017
PGC 010665	10.27	11.26	10.87	13.14	Sb	0.020
PGC 010705	10.26	10.92	10.77	12.57	(R'_1)SB(rs)a	0.017
PGC 011104	10.24	11.32	10.36	11.87	(R)SA0/a?	0.016
PGC 012759	10.41	10.81	10.57	12.55	(R)SAB(r)0^+	0.019
NGC 1386	8.07	9.88	9.25	10.89	SB(s)0+	0.003
PGC 014702	9.55	10.25	11.99	11.57	SA(r)a?	0.012
PGC 015172	9.47	10.31	10.08	12.11	(PR?)SB(rl)	0.017
PGC 016357	10.03	10.54	12.59	11.69	SB0	0.018
NGC 1808	6.66	6.84	11.20	9.82	(R'_1)SAB(s:)b	0.003
PGC 021057	9.45	10.24	9.82	11.90	SAB(s)bc	0.012
PGC 023573	10.67	11.62	10.99	13.49	SA(s)c	0.018
NGC 4785	8.57	9.78	8.95	12.41	(R')SAB(r)ab	0.012
NGC 4945	4.48	6.48	4.33	10.01	SB(s)cd: sp	0.002
Circinus	4.98	7.63	5.11	9.88	SA(s)b:	0.001
PGC 060594	9.71	10.04	11.67	11.12	(R':)SA(rs)bc	0.017
PGC 062218	9.53	9.77	12.07	11.63	SAB(rs)bc	0.015
NGC 6810	7.70	10.09	8.23	10.87	SA(s)ab:sp	0.007
PGC 063874	9.98	10.16	13.18	11.55	Sb	0.019
PGC 064537	10.99	11.54	11.10	12.01	(R'_1)SB(rl)a	0.019
PGC 068198	9.78	10.28	9.97	11.74	(R_1)SAB(r)0+	0.010

Note.- The Sy2 from the sample with $z < 0.02$, to complement and compare to the results in Peng et al. (2006); GALFIT was used to decompose the 2MASS Ks band images of these objects into the disk, bulge, and nuclear components. The global magnitudes are taken from the 2MASS Extended Source Catalog.

4. DISCUSSION & CONCLUSIONS

One of the primary goals of the research, the results of which are presented in this thesis, was to search for large-scale extended radio emission around Seyfert galaxies in the local universe, using the data from the SUMSS. Because of the good sensitivity and *(u,v)* -plane coverage of the MOST, the SUMSS provided a good opportunity to find any type of unusual emission that might, for example, be a relic from an earlier evolutionary stage of an AGN. Though a *null result* was obtained in that search, the data and analysis provided here nevertheless helps to fill in the wavelength coverage gap for Seyferts. Such a view helps to add to what we know of the global radio properties of this type of AGN in the local universe by carrying out a survey at the little studied frequency of the MOST (843 MHz). In addition, the radio investigation of this sample has resulted in several new, original results worth publishing. Those results include the new identification of six radio-excess Sy, significant radio variability in five Sy, and the designation of radio-loud to one of the Sy, in this newly constructed sample (all discussed below). Also, the results reported in §3.8 add substantially to what has been published on that topic.

The sample of Seyfert galaxies under investigation in this thesis is similar in size to several other Sy samples in the local universe, both northern and southern sky, that have been investigated over the years. However, one must be careful in directly comparing such studies because of the differing characteristics of the samples used.

One important and much studied sample of this kind, mentioned in §3.1, is the 12 µm - selected sample from Rush et al. (1993), derived from the larger galaxy sample of Spinoglio & Malkin (1989), which continues to be used (e.g., Buchanan et al. 2006; Tommasin et al. 2008). Both studies analyze IR data from the *Spitzer Space Telescope*. The sample of Rush et al. (1993) consists of 118 objects, composed of 53 Sy1 and quasars, 63 Sy2, and two blazars. Buchanan et al. (2006) investigates a sample consisting of the 87 Sy from Rush et al. (1993) with *cz* < 10,000 km/s. This is close to the value *cz* < 9,100 km/s for the sample in this thesis. Actually, Buchanan et al. (2006) reports on new *Spitzer* data on 51 of the 87 Sy that were available at the time of that publication. A follow-up paper, Buchanan et al. (2008) includes data on 85 of the 87 of the Rush et al. (1993) sample with the above velocity/distance criterion (two were excluded because of problems with the data). Similar to what was done in this thesis, Sy1.8 and Sy1.9 were considered together with all of the other Sy1, instead of separately as is sometimes done (e.g., Deo et al. 2007, and references therein).

Other notable Sy samples to which the results presented are somewhat comparable include the ones from Meurs & Wilson (1984), Ulvestad & Wilson (1984a), Edelson (1987), Unger et al. (1987a), Ulvestad & Wilson (1989), de Grijp et al. (1987, 1992), Nagar et al. (1999), and Ulvested & Ho (2001). Most of these samples have some problems with completeness. Ulvestad & Ho (2001) and Schmitt et al. (2001a) have a good discussion of the history of such sampling issues. The latter is a study using the sample from de Grijp et al. (1987, 1992) and the former uses the Palomar Seyfert sample derived from Sandage & Tammann 1981). As discussed in Chapter 1, these are issues such as sampling too large volume of space (and so Malmquist bias becomes important), or the selection criteria used excludes weaker sources, as is the case with the UV selected "Markarian Seyferts" (Markarian 1967, 1969a,b; Markarian & Lipovetsky 1971, 1976). Newer evidence (Goulding & Alexander 2009) suggests that samples based on identification in optical spectroscopic surveys could be missing as many as one-half of all local AGN due to host galaxy obscuration (highly inclined disk and/or dust lanes) of the AGN emission. Before this, Keel (1980) similarly showed that there seems to be a deficiency of Sy1 in nearly edge-on host galaxies in the local universe.

Many of these earlier studies (before the mid-1990s) were based on fairly low resolution, global data, so the results in this paper would be more comparable with them, rather than many newer, much higher resolution ones that focus more on just the AGN. The comparison with the latter, though, can still be informative as it can help determine the contribution of each of the components.

The results of the statistical tests for correlation between distance and 843 MHz luminosity for the Sy2 in this sample were reported in Table 2.12 and were seen to be weakly significant. Excluding the few most distant Sy2 in the sample (LEDA 088648, LEDA 087391, and PGC 006351) did not change the results significantly either way. Are there Sy2 that are being missed? This is possible as it has been known for some time that in the local universe Sy2 are observed to be more numerous but that many Sy2 are hard to detect, independent of the intrinsic luminosity of the object (Wagner 1988), as might be expected today considering the unified model of AGN. However, when testing galactocentric recession velocity, instead of distance, the results are much more mixed; the results do not meet the adopted criteria for being considered weakly significant, though were close. So it could be that the volume of space being sampled contains low luminosity Sy2 that for some reason have not yet been identified, but these test results are inconclusive.

As was reported in Table 2.12 the computed V/V_{max} values, measures of the space distribution of the objects in the sample, have an average significantly less than the 0.5 one would expect from a large, complete sample. However because the sample under study here is in the local universe it is not appropriate that a uniform distribution should be assumed. Most Sy within the volume of space sampled in this investigation are luminous enough to be detected. What is observed, for all (detected) Sy2 is an average V/V_{max} value of 0.051. What is observed for all (detected) Sy1 is 0.073.

As an example of a study with published results using a sample not too unlike the one being reported on in this thesis is Schmitt et al. (2001a). Using the 25 & 60 μm *IRAS* data from the de Grijp et al. (1992) sample (29 Sy1 and 59 Sy2 with $z < 0.031$, close to the value of $z = 0.0303$ used in the construction of the sample in this thesis), the researchers reported V/V_{max} values of ~ 0.146 and 0.111 for Sy1 and Sy2, respectively, using the 25 μm data. Using the 60 μm data the values of 0.327 and 0.251 were reported. These values are biased, however, because censored objects were not considered. Additionally, only IR "warm" Sy were selected, that is objects with $-1.5 < \alpha(25/60) < 0$.

As reported in §2.5.2, a median distance of 70 Mpc was computed for the full sample of 119 Sy. The median values by type show larger values for Sy1, with values of 67 and 82 Mpc reported. The results of the two-sample statistical tests reported in Table 2.10 show however no significant differences in the distribution of distances, by type.

The Kaplan-Meier product estimator, which should be more accurate estimate of the distribution of (all) Sy in the volume of space sampled, gives the median distance for Sy2 in the sample (Table 2.2) as 51. For the Sy1 in the sample the value computed was 63 Mpc. For all 119 Sy in this sample the median and mean values computed were 56 and 60 Mpc.

In general, how these average distance values compare to those from other Sy samples depends a great deal on the selection criteria used in the sample construction. The CfA sample (Huchra & Burg 1992) have a median value of 80 Mpc. The sample from Ulvestad & Wilson (1989), based on the sample in Huchra et al. (1983), which is also the one used by Edelson (1987) mentioned earlier, have a much lower median distance value (35 Mpc) because the volume of space sampled is roughly half of the one in this thesis. Similarly, the median distances for the sample of 52 Sy in Ulvestad & Ho (2001) are 17.0 and 20.4 Mpc, for Sy1 and Sy2 respectively. However that sample (from the Palomar survey) includes only bright ($B_T < 12.5$ mag) Sy (with $\delta > 0°$) and so is biased towards mostly closer objects.

The mean and median distances of the objects in the sample used in Buchanan et al. (2006, 2008) were not reported. However, in a paper not quite yet released at the time of this original writing (Gallimore et al. 2010), describing some new results using the same sample as Buchanan et al. (2006, 2008), the computed values of *cz* were reported. Those values were (originally) obtained through private communication with J. Gallimore, one of the authors of Buchanan et al. (2006, 2008). The arithmetical mean and median values were found to be 4152 and 3527 km/s, respectively. The values reported in §2.5.2 for this sample of 119 Sy were found to be 5015 and 4935 km/s, both more than 20% higher than the sample of Gallimore et al. (2010). An arithmetical median value of cz = 3527 km/s ~ 50 Mpc for all

Sy was reported, which is not too dissimilar to the value of ~56 Mpc for this sample obtained using the Kaplan-Meier Product Estimator. The minimum and maximum *cz* values were found to be 700 and 9432 km/s, respectively, for that sample. This compares favorably to the minimum and maximum values of 434 and 9080 km/s for the sample under investigation here (that minimum value is for Circinus at $z \sim 0.014$).

Similarly, for the 12 micron sample of Rush et al. (1993) on which Buchanan (2006, 2008) builds, the mean distance reported was 51 Mpc. This contrasts with the mean value of 60 Mpc for the sample investigated in this thesis, as computed using the Kaplan-Meier product estimator.

The radio flux densities observed and the radio luminosities computed from them agree well, based on the conventional power-law relation $\nu^{-0.7}$ discussed earlier, with what is found in the literature although most of the published radio data on Seyferts are at higher frequencies.

The total flux density measurements reported (in ergs s^{-1}) in Edelson (1987), an early 6 cm study of 25 Sy1 and 23 Sy2 ($z < 0.06$), were used to compute their 6 cm luminosities (in units of W Hz^{-1}, as used in this thesis). The resultant mean and median log luminosities were 21.59 and 21.78 for the Sy1 and 21.77 and 21.67 W Hz^{-1} for the Sy2. As expected, based on the approximate $L \propto \nu^{-0.7}$ power law relation for Seyfert radio luminosity that has been observed in many studies over the years (e.g., Contini & Viegas 1991; Roy & Norris 1998), these values are lower than what is reported here at 843MHz (~ 35.6 cm).

The closest wavelength to the ~36 cm coverage in the SUMSS that has been investigated to any large degree is 20 cm. For example, Nagar et al. (1999) investigated the 20 cm radio emission of a sample, from Mulchaey et al. (1998), similar to the one reported on in this thesis in the volume of space sampled, though too small for a meaningful statistical inferences. The sample consisted of 16 Sy1 and 27 Sy2 Seyferts (note that 2 of the Sy1 are classified as Sy1.9 and considered separately) with $\delta < -40°$ and $z < 0.024$. Mean log luminosities of 22.72 and 22.75 for the Sy1 and Sy2, respectively, were reported. Ulvestad & Wilson (1989), using a sample of all known nearby ($z < 0.016$) Sy with $\delta > -45°$, 57 Sy in all, obtained (with the VLA) 20 cm luminosities that as whole were much lower than the smaller sample of Nagar et al. (1999); more than 60% of the Sy2 in the sample had 20 cm log luminosities < 22.00. The results of that larger sample in Ulvestad & Wilson (1989) are consistent with what was observed in the results being reported in this thesis at 843 MHz (36 cm).

Schmitt et al. (2001) reported mean and median log luminosities of 21.19 and 21.50 for Sy1 and 21.14 and 21.53 for Sy2 Seyferts at 3.6 cm. The sample investigated consisted of 29 Sy1 and 59 Sy2 taken from de Grijp et al. (1987) with $z < 0.031$, a similar sample to the one reported on here. Extrapolated using the conventional power law $v^{-0.7}$, these results are broadly consistent with what was observed in this paper at 843 MHz.

While investigating the observed scatter in the various radio-IR plots in §3.7, a total of nine Sy in this sample have been identified as so-called radio-excess galaxies (§3.7) as defined by Roy & Norris (1997) and Drake et al. (2003), several of them for the first time, it would appear. The three objects PGC 062134, PGC 065600, and NGC 7213 were in both of those papers. PGC 062134 and PGC 065600 are both Sy2 and NGC 7213 is classified as Sy1.5. The (log) 4850 GHz luminosities of the Sy reported in Roy & Norris (1997) were all in the range 22.1 - 25.4, significantly higher than what was reported in the sample of Ulvestad & Wilson (1989) mentioned above.

Compared to the rest of the sample in this paper, PGC 062134 and PGC 065600 (reported 843 MHz log luminosities of 23.39 and 23.74 W/Hz, respectively) are also among the most luminous; only six Sy2 in this sample have a 843 MHz log luminosity > 23.00. However, among the Sy1 in the sample, NGC 7213 has a luminosity of 21.94 which is only ~ 1.5 standard deviations from the mean. In all, 24/42 of the Sy1 in this sample (~ 57%) are more luminous, with their 843 MHz log luminosities > 22.00. As discussed further below, however, NGC 7213 is known to display significant radio variability.

In Figure 3.31 it can be seen that PGC 065600 is one of the most obvious outliers when plotting the radio vs. FIR flux densities; the empty blue box plotting its 843 MHz vs. *IRAS* 60 µm flux density values is isolated in the lower-right of the figure at, approximately, the point (0.3, 0.73). It deviates more than any other Sy in the sample from whatever linear correlation is demonstrated. PGC 062134, shown by the empty blue box in Figure 3.32 at the approximate coordinates of (-0.57, 0.51), is scattered more than most other objects in the sample except PGC 065600. The same is true for NGC 7213.

Among the other six radio-excess Sy (those not in Roy & Norris 1997 and Drake et al. 2003) identified in §3.7, the Sy1 LEDA 087392 has the largest ratio of 6.3 cm and 60 µm flux densities as can be seen from Table 3.16. It is also the most luminous Sy1 in the sample at 843 MHz, with the (log) luminosity ~ 23.69 (W/Hz). It is a little-researched AGN aside from several X-ray studies. It would appear that no host galaxy morphology has been published. In Figure 3.31 it can be clearly seen (empty red box) in the lower-middle of the figure, at the approximate coordinates of (-0.56, -0.91).

The first criterion listed in Roy & Norris (1997) in the search for radio-excess galaxies was that the object be detected at 60 µm. LEDA 087392 however was one of only three Sy in this sample located in the few gaps in the sky not covered of *IRAS*. In §3.4 the 12, 25, 60 and 100 µm upper limits were estimated for the object. At 60 µm a value of ~ 0.12 Jy was adopted. So if the true flux density at 60 µm was significantly higher than this, which does not seem likely based on the 2MASS NIR data, the Sy might not really be classified as a radio-excess galaxy. However, in addition to what we know of the NIR emission for the object, this Sy has such a large radio/FIR flux density ratio (Table 3.15) that it seems likely that it would keep the designation. All of the other sample-selection criteria in Roy & Norris (1997) were related to identifying the type of object, which is not necessary here, or restriction of location in the sky so as to have been detected in the PMN radio survey.

LEDA 087392 is classified as a X-ray transient narrow-line Sy1 (Grupe 2007), and most of the work published on this object have been on its interesting X-ray properties. In Grupe (2007) it was reported that the object is currently (as of that writing) a faint X-ray source though was considered X-ray bright in the ROSAT All-Sky Survey. In addition to the continued X-ray faintness, UV variability has been observed. Grupe et al. (2007) argue that the observed variability in LEDA 087392 "can be caused either by a change in the absorption column density, and therefore the reddening in the UV, or by flux variations of the central engine." There are no other photometric data points available for LEDA 087392 in the IR. The object was detected at 4850 MHz in the PMN survey, with a flux density value of 54 mJy reported (Table 3.15). This value is not listed in NED. The estimated 6.3 cm flux density value (as described in §3.7), which was not adopted here, was 80 mJy. From the SUMSS LEDA 087392 has a reported flux density of 278.6 mJy, which consistent with value at 4850 MHz. However, with such limited wavelength coverage it is not possible to tell what role, if any, significant AGN radio variability might play in the observed FIR-radio correlation for this object. The SUMSS contour map for this Sy (Figure A.13, Appendix A) is that of essentially a point source but with a slight elongation to the east, consistent with the disk of the host galaxy.

Significant radio variability though is a factor with the Sy1.5 NGC 7213 (an object in Roy & Norris 1997, as mentioned above). For example in Harnett (1987) the 843 MHz flux density value obtained (using the MOST) was 170 mJy. In the SUMSS (as reported here), 20 years later, the value of 119.6 mJy was obtained. This translates into log luminosities of approximately 22.10 observed in 1987 and 21.94 observed in the SUMSS. Considering the instrument sensitivity / errors involved this would seem to indicate a variability in detected radio emission. Radio variability in NGC 7213 has been established before, for example as reported by Blank & Harnett (2004) discussed in Chapter 1.

Similarly, the 4850 MHz log luminosity reported in Roy & Norris (1997) for NGC 7213 was 22.05 (W/Hz). Based on the SUMSS data, as reported in Tables 2.6, the 843 MHz log luminosity was computed to be 21.94. This again shows the variable nature of NGC 7213, as one would expect the value at 843 MHz to be larger than at 4850 MHz.

As can be seen in Table 3.15, there is evidence for variability in radio emission of PGC 006078. At 21 cm a value of 57.8 mJy was reported whereas in the SUMSS (~36 cm) a value of 53.8 mJy was obtained, not what is expected based on the power law relation (flux density decreasing with increasing frequency) observed for Sy.

Ueda et al. (2007), an X-ray (0.2 - 700 keV) study using the Suzaku orbiting telescope, included PGC 006078. It was found it had "an extremely small fraction of scattered light from the nucleus, (< 5%), with respect to the intrinsic power-law component." This observation suggests that perhaps the AGN is embedded in a "very geometrically thick" torus that has a small opening angle and so is seen nearly edge-on. In addition to this, or instead of it, the AGN could just have a very low amount of gas involved in the scattering. PGC 006078 is also one of eight AGN found (using the 70 m antennas of NASA's Deep Space Network) to have water maser emission (Kondratko et al. 2007). The observed maser is coincident, to within 0.3", of the host nuclei in this galaxy and the others in that study and so "most likely mark the locations of the embedded central engines." No other radio data has been published on this Sy2 residing in a (Sa) spiral host galaxy. This object would then be a good candidate for further radio observations, to investigate the apparent radio variability. In the SUMMS, PGC 006078 shows up as an isolated point source (Figure A.2, Appendix A).

Another of the six radio-excess Sy identified in this sample, PGC 015172 (alias the Carafe Nebula), is a Sy2 residing in what has been considered a SB(r1) host galaxy. The asymmetric barred structure of the host is clearly discernable in the SUMSS radio maps (Figure A.4, Appendix A). A fairly recent study (Rifatto et al. 2001), however, shows that the traditional morphological classification of this object is likely to be incorrect. Instead it is shown that PGC 015172 is the result of the merging of two galaxies, each containing an AGN. In that study, deep R-band images revealed a knot next to the known nucleus, the Sy2 AGN for which this galaxy is routinely classified. A long slit spectrum analyzed in Rifatto et al. (2001) shows "features typical of a LINER heavily reddened by dust."

As mentioned in §3.7, this object was detected at in the PMN at 4850 MHz, with a flux density value of 50 mJy reported. This value was taken from Wright (1994), as the value is not listed in NED. The ratio of the 6.2 cm radio and the 60 µm flux densities for PGC 015172 is 0.03 > 1/55 (the main radio-excess criterion from Roy & Norris 1997). All of the photometric data points listed in NED, except for a few optical, are at IR wavelengths. The galaxy is a IR warm galaxy (as introduced in de Grijp et al. (1987) assuming the flux power-law relation $S \propto \nu^{\alpha}$, it has a value of the exponent 1.5 < α < 0 between 25 and 60 µm) and many of the 35 published papers on this object are related to this property. This Sy was, similar to PGC 006078 discussed above, one of the eight AGN in which a water maser emission was detected using NASA's Deep Space Network (Kondratko et al. 2007).

Of the three remaining sample objects identified here (PGC 047969, LEDA 096373, and PGC 029778) as radio-excess, PGC 047969 (Sy1.5) is the most studied, with almost 400 references listed in NED. Most of the research on this object has been related to the observed long term X-ray variability of the AGN (host galaxy classified as E-S0). It is a point source in the SUMSS (Figure A.18, Appendix A). As can be seen in Table 3.15 (and this is true for LEDA 096373 and PGC 029778 as well), the limited radio data available from the literature (from 6 to 36 cm) is consistent with the assumed power-law relation between frequency and flux discussed above.

LEDA 096373 (Sy2) is, comparatively, a little researched object with only 10 papers listed in NED, all of the photometric data points listed are in the IR aside from one X-ray and two radio (from PMN and NVSS). As described in §2.4, the object is essentially a point source in the SUMSS (Figure A.5, Appendix A) but with several apparently nearby objects sharing several of the lowest contour lines. The classification of the spiral host galaxy is S.

PGC 029778 (Sy2) is another little studied sample object with just 13 references in NED, with all data points listed in the IR aside from a couple of optical. It was censored in the PMN (upper limit ~ 72 mJy) but detected in the NVSS (78.5 mJy, a value taken from Wright 1994). In the SUMSS (Figure A.18, Appendix A) this object shows up as essentially a point source but with a two contour-level lobe. Host galaxy classification is SB(s)ab. This object, among all nine of the newly identified radio-excess objects in this new sample (Table 3.15), has the third largest ratio (~ 0.08) of 6 cm and 60 µm flux densities. Even though the 6 cm data is estimated as described above, because of the available values at 21 cm (78.5 mJy) and ~36 cm (89.5 mJy) the estimated value at 6.3 cm (30 mJy) seems reasonable. It would take an unusually low (true) flux density value at 6 cm for this object to end up not satisfying the radio-excess criterion discussed above. Considering how little published data exists for this object, further radio studies particularly at frequencies > 4 GHz would be useful.

The nature of radio-excess objects is an active area of research. In Drake et al. (2004), the third in a series of papers, high resolution imaging was done primarily at ~4.8 and 8.5 GHz, of two representative radio-excess objects from their sample. Not all are Seyferts. Some of the important results are that the dominant radio emission is nuclear, usually compact sources. Synchrotron cooling timescales indicate young (~10^4 - 10^5 yr) sources, possibly a burst in accretion of gas and dust into the SMBH. Most of the objects display steep radio spectral energy distributions or turnovers at gigahertz frequencies. The authors suggest that radio-excess objects are likely transient and will fall back more in line with the tighter correlation observed for most galaxies as discussed above. Because of the revealed nature of the radio emission from radio-excess objects, the SUMSS data is of an insufficient resolution to offer anything much more than identification of such objects.

As reported in §3.7, none of the Sy in the sample in this paper were found to be radio-loud using the radio only criterion discussed in Drake (2003). However, using the more "traditional" criterion (e.g., Visnovsky et a. 1992 and references therein), in which those objects with the log of the ratio R (6 cm to optical (blue) luminosities) $\geq$ 10 are considered radio-loud, the newly identified radio-excess PGC 029778 is right at this cut-off value with R = 10.04. This object is one the 79% Sy2 and 57% of the Sy1 in this sample with optical flux density values in the literature (Tables 3.1 & 3.2). There is also reliable 6.3 cm data (NVSS) available for this object so there should be significant confidence in this result. In general then the results are consistent with those from other studies of the radio properties of Sy; historically Sy been classified as radio-quiet. However Ho & Peng (2001) have shown that quite the opposite is the case, at least for Sy1, when only the nuclear component of the Sy1 is measured. Indeed for their sample of 45 nearby Sy1 more than 60% have R values $\geq$ 10. Considering then the global nature of much of the data used in this study, the true fraction of this sample that are radio-loud cannot be determined.

The statistical tests performed on the radio luminosities, distances, velocities, and fitting ratio b/a, by type (Table 2.6) are consistent with the unified view of AGN outlined in Chapter 1; no significant, weakly or otherwise, difference was found by Sy type. The results of the various two-sample tests used suggest that the Sy2 and Sy1 in this full sample of 119 Sy are indeed from the same parent population.

The Kaplan-Meier estimates of the true mean and median of the above mentioned parameters (Table 2.11) are, assuming the method is correctly accounting for the observed censoring patterns, likely more accurate values than the arithmetical averages usually reported. For 843 MHz radio luminosity, both by type and combined, the estimated median and mean values are slightly higher than the computed arithmetical ones. However the Kaplan-Meier estimates of the true (parent) mean and median distances (59.64 and 55.75 Mpc, respectively, Table 2.11) are all significantly *lower* than the arithmetical ones reported here.

Similarly Kaplan-Meier gives the median (log) luminosity is 22.11 and 22.08 (W/Hz) for the Sy2 and Sy1 in the sample, respectively.

As discussed in Chapter 5 below, several of the objects in this sample have been observed with the MOST over the years in earlier, smaller studies. So to investigate radio variability among these Sy, comparisons with the results of the SUMSS can be made. Unfortunately many such observations, from the 1980s in particular, have not made their way to any databases such as SIMBAD or NED.

For example seven of the objects in this sample, as mentioned in §2.4, were observed in the 1980s as described in Subrahmanya & Harnett (1987). Those results using the MOST and the results from the SUMSS (also using the MOST approximately 20 years later) were compared. Two the seven Sy (NGC 1566 and NGC 6221) showed essentially no change (less than 5% difference in reported flux densities). The other five showed significant variation, particularly NGC 4945 with a decrease of approximately 33% in reported flux densities. There have not been many published studies of such long term radio variability, certainly not at this wavelength (see §1.5). The results are summarized in Table 4.1.

TABLE 4.1

	SH87 (mJy)	SUMSS (mJy)	% Change
NGC 7213	100	119.6 ± 3.4	+19.6
NGC 6221	420	420.0 ± 15.0	0
NGC 1566	310	299.5 ± 11.7	-3.4
NGC 6300	116	102.1 ± 6.1	-12.0
NGC 1672	350	291.7 ± 12.8	-16.7
Circinus	2300	1640.0 ± 65.7	-28.7
NGC 4945	8300	5549.0 ± 165.5	-33.1

Note.- Comparison of the results reported in SH87 (Subrahmanya & Harnett 1987) and in the SUMSSCAT v2.1 for seven Sy in this sample

The data from the 2MASS has been used very little in the investigation of AGN and of Sy in particular. Indeed, the results presented here, except for the work of Peng et al. (2006), at least at the time of this writing, are unique. This is likely to change in the future, as the 2MASS survey has provided researchers with a lot of high quality data to explore.

The results in §3.8 using the 2MASS K_s-band data are fairly consistent with those from Peng et al. (2006) however, the mean and median disk magnitudes for the 24 Sy2 in this example investigated using GALFIT were nearly 0.5 mag fainter than the values for the 65 Sy2 reported in Peng et al. Much of this difference may be explained by the fact that several of the 24 Sy2 in this sample have very faint disks in the K_s -band which made disk fitting from the bulge difficult. In future work the component magnitudes reported here can be checked for correlations with data (new or otherwise) at other wavelengths. Of interest also would be to check for any statistically significant differences between Sy1 and Sy2. As mentioned in chapter 1, Peng et al. (2006) showed that a strong correlation was found between the nuclear K_s-band magnitudes and the [O III] λ5007 and hard X-ray luminosities among the Sy2 investigated. This approximately 2μm emission is thought to originate from the emissions of warm graphite grains in the central torus mentioned above and so could then be good indicator of AGN activity.

As was seen (Table 3.13), for $\alpha_{J\text{-}Ks}$, no significant (or weakly significant) results (by Sy type) were reported when the index values for the censored objects were computed using the (seemingly high outlier) upper limits. However, when using the median value for the detected objects instead, a weakly significant result was reported, with all probabilities less than 0.10, in fact all but one less than 0.05. Also it was found that the test results for $\alpha_{H\text{-}Ks}$ were weakly significant (all p values but one < 0.10) and when using the median values instead, a significant result (all $p < 0.05$) was found.

These significant, weakly or otherwise, results, in addition to the average values computed using the Kaplan-Meier product estimator, show that Sy1 have a flatter NIR energy distribution. As discussed for example in Alonzo-Herrero et al. (2003), a study of Seyfert SEDs from 1 - 16 μm, such results have been observed before. This observed IR dichotomy by Sy type is conventionally explained by unified models which contain an optically thick torus with high equatorial opacities. While the NIR data here is very limited in wavelength range, in it the result is clear.

In Buchanan et al. (2006), the results of an important investigation of Seyfert IR SEDS using the *Spitzer* space telescope, three main types of morphology were observed. For approximately 47% of the sample objects a steep, highly red continuum "suggestive of cool dust" is observed. Another 31% of the objects had a broken power law with a flattening in the continuum slope at around 20 μm. The majority of the remaining sample (16%) showed a continuous, power law spectra. In comparison to the (more limited) results presented here (Table 3.12) we can see that the Sy2 show a larger mean and median value of the ratio $\alpha_{12\text{-}25\ \mu m}$ / $\alpha_{25\text{-}60\ \mu m}$ than the Sy1 in the sample. For example, among just the detected objects, the median ratio value for Sy2 is 0.742 and for Sy1, 0.364. Thus the Sy1 in general show more flattening of the continuum slopes in this wavelength range which is broadly consistent with the unified scheme Seyfert galaxies.

5. SUMMARY & FUTURE WORK

In this study a sample of southern-sky Seyferts was constructed for an on-going study of this type of object in the local universe. The sample objects were mapped at 843 MHz in a search for any previously unidentified large-scale radio emission. While none was found, the data from the SUMSS has enabled us to look at the sky at a little explored wavelength with good (u, v) plane coverage and sensitivity, adding to what we know about this type of AGN. The NIR-FIR properties of the sample objects were explored at seven bands, including the FIR-radio correlation, leading to the identification of six radio-excess objects and an identification of radio-loud in one of the sample objects. Evidence for significant radio variability over a span of twenty years was also found for five of the sample objects by comparing data from the SUMSS to that from early studies using the MOST. Relevant statistical tests indicate that both types of Seyferts are drawn from the same parent population, supporting the unified view of AGN. Finally, the NIR contributions from the different galactic components of several of the closest Sy2 in the sample were estimated by decomposing the 2MASS K_s-band images, increasing by nearly 50% the number of Sy2 for which the NIR component magnitudes are known.

Although the SUMSS was unique in that it was an all-sky survey at a little explored wavelength, the MOST has been around for decades. So there are several Sy in the sample discussed in this paper that have been mapped and fitted before, going back more than 20 years (e.g., Harnett 1987), as part of smaller research programs (usually studies of individual galaxies). So it would be possible to more extensively compare the SUMSS total flux density values for several more Sy, with what was measured earlier, using essentially the same instrumentation (as with the objects in Table 4.1), to search for long-term radio variability. More observations of PGC 006078 would be very helpful in measuring the extent of what appears to be moderate radio variability as can be seen in Table 3.15 with the 21 & 36 cm flux densities. Radio flux density measurements for LEDA 087392 would also be useful since it has been studied so little and displays the largest radio/FIR ratio among the identified radio-excess Sy.

As discussed in §3.2, even though the sensitivity and sky-coverage of the 2MASS was very good, some issues in the automated pipeline have been found (Schombert 2007), mostly relating to the fitting of close, large galaxies with a lot of discernable structure. According to Schombert (2007), for some near-by galaxies the 2MASS fits "consistently underestimate the amount of disk light per isophote". This can give rise to an error in the size of the galaxy, underestimating it by up to 50%. A software package such as ARCHANGEL (developed by Schombert) could be used to perhaps get a better fit of the Sy in this sample. Though many other software options to fit the 2MASS images are available, ARCHANGEL is specifically designed for the task and looks to be superior to many of its competitors based on some preliminary testing of it on a few of the objects in this sample. For example GALFIT could be used but would not be a good choice for efficiency, and the application is not designed specifically for the task. Any issues with the automated 2MASS pipeline fitting may not make a large difference for this sample, as most of the objects are mere point sources. However 19/77 of the Sy2 (~ 25%) and 8/42 of the Sy1 (~ 19%) in this sample have $z < 0.009$ and so are close enough so that, depending on their host galaxy morphologies, the automated fitting of the 2MASS data that went into constructing the official 2MASS catalogs could be off by a significant amount. I would also like to use GALFIT to decompose images of local Sy1, to compare with the results known for Sy2. Comparison with other types of AGN in the local universe would also be instructive. Additionally, IR data from the all-sky survey by the Japanese space telescope *AKARI*, the catalog of which was to be released just after the completion of the main parts of this thesis, could be used to supplement much of the IR analysis for the sample constructed in this study. The *AKARI* telescope has higher sensitivity and higher spatial resolution than the *IRAS*, and covers 1.7 - 180 μm.

BIBLIOGRAPHY

Adams, T.F., Weedman, D.W. 1975, ApJ, 199, 19

Alexander, D.M. 2001, MNRAS, 320, L15

Allen, D.A., Norris, R.P., Meadows, V.S., Roche, P.F. 1991 MNRAS, 248, 528

Aller, H.D., Aller, M., Latimer, G.E., Hodge, P.E. 1985, ApJS, 59, 513

Alonso-Herrero, A., Quillen, A.C., Rieke, G.H., Ivanov, V.D., Efstathiou, A. 2003, AJ, 126, 81

Altenhoff, W., Mexger, P.G., Wendker, H., Westerhout, G. 1960, Veröff. Sternwärte, Bonn, No.59, 48

Antonucci, R.R.J., Miller, J.S. 1985, ApJ, 297, 621

Antonucci, R. 1993, ARA&A, 31, 473

Appleton, P.N., et al. 2004, ApJS, 154, 147

Arp, H. 1965. ApJ, 142, 402

Baldwin, J.A., Phillips, M.M., and Terlevich, R. 1981, PASP, 93, 5

Balzano, V.A. 1983, ApJ, 268, 602

Barth, A.J., Greene, J.E., Ho, L.C. 2005, ApJL, 619, L151

Baum, S.A., O'Dea, C.P., Dallacassa, D., De Bruyn, A.G., Pedlar, A. 1993, ApJ, 419, 553

Beckman, V., Soldi, S., Shrader, C.R., Gehrels, N., Produit, N. 2006, ApJ, 652, 126B

Beers, T.C., Flynn, K., Gebhardt, K. 1990, AJ, 100, 32

Begelman, M.C., Blanford, R.D., Rees, M.J. 1984, Reviews of Modern Physics, 56, Issue 2, 225

Beichman, C.A., Neugebauer, G., Habing, H.J., Clegg, P.E., Chester, T.J. eds., 1984, IRAS, Catalogs and Atlases, Explanatory Supplement. JPL Publication D-1855, JPL, Pasadena

Beichman, C.A., Neugebauer, G., Habing, H.J., Clegg, P.E., Chester, T.J. eds., 1988, Washington, DC: GPO

Beichman, C.A., Neugebauer, G., Habing, H.J., Clegg, P.E., Chester, T.J. eds., 2002: http://irsa.ipac.caltech.edu/IRASdocs/exp.sup/

Bekki, K., Shioya, Y. 2000, ApJ, 542, 201

Bian, W., Zhao, Y. 2002, A&A, 395, 465

Bianchi, S. Matt, G., Balestra, I., Guainazzi, M., Perola, G.C. 2004, A&A, 422, 65

Bicknell, G.V., Dopita, M.A., Tsvetanov, Z.I., Sutherland, R.S. 1998, ApJ, 495, 680

Binette, L., Dopita, M.A., Tuohy, I.R. 1985, ApJ, 297, 476

Binette, L., Fosbury, R.A., Parker, D. 1993, PASP, 105, 1150

Blanford, R.D., Rees, M.J. 1974, MNRAS, 169, 395

Blanford, R.D., Königl, A. 1979, ApJ, 20, L15

Blank, D.L., Harnett, J.I., Jones, P.A. 2005, MNRAS, 356, 734

Blank, D.L. (1999), Doctoral Thesis, University of Sydney

Bock, D.C.-J., Large, M.I., Sadler, M. 1999, ApJ, 117, 1578

Bonato, C. J., Pastoriza, M. G. 1997, ApJ, 486, 132

Boyce, E. 2000, thesis, Sydney University

Bransford, M.A., Appleton, P.N., Heisler, C.A., Norris, R.P., Marston, A.P. 1998, ApJ, 497, 133

Brindle, C., Hough, J.H., Bailey, J.A., Axon, D.J., Ward, M.J., Sparks, W.B., McLean, I.S. 1990, MNRAS, 244, 577

Bromley, B.C., Press, W.H., Lin, H., Kirshner, R.P. 1998, ApJ, 505, 25

Brunthaler, A., Falcke, H., Bower, G.C., Aller, M.F., Aller, H.D., Teräsranta, H. 2005, A&A, 435, 497

Buchanan, C.L., et al. 2007, preprint, arXiv:astro-ph/0604222v1

Buchanan, C.L., et al. 2007, preprint, arXiv:0807.3993v1

Burbidge, E.M., Burbidge, G.R., Hoyle, F. 1963, ApJ, 138, 873

Burgarella, D., Livio, M., O'Dea, C.P., eds., Astrophysical Jets, Cambridge University Press, 1993.

Cappi, M., et al. 1999, Advances in Space Research, Proceedings of 32nd Sci. Ass. of COSPAR, Broad-Band X-ray Spectroscopy of Cosmic Sources

Chi, X., Wolfendale, A.W. 1990, MNRAS, 245, 101

ChemWiki, 2012; http://chemwiki.ucdavis.edu/Analytical_Chemistry/Quantifying_Nature/Propagation_of_Error#Arithmetic_Error_Propagation

Clarke, C.J., Kinney, A.L., Pringle, J.E. 1998, ApJ, 495, 189

Clements, S.D., Smith, A.G., Aller, H.D., Aller, M.F. 1995, AJ, 110, 529

Colbert, E.J., et al. 1996a, ApJS, 105, 75

Colbert, E.J., Baum, S.A., Gallimore, J.F., O’Dea, Christensen, J.A. 1996b, ApJ, 467, 551

Colbert, E.J., Baum, S.A., Gallimore, J.F., O’Dea, Veilleux, S. 1998, ApJ, 496, 786

Colina, L., Arribas, S. 1999, ApJ, 514, 637

Condon, J.J., Condon, M.A., Gisler, G., Puschell, J.J. 1982, ApJ, 252, 102

Condon, J.J., Broderick, J.J. 1986, AJ, 92, 94

Condon, J.J. 1992a. AIP Conf. Series, 254, 629

Condon, J.J. 1992b, ARAA, 30, 575

Condon, J.J. 1997, PASP, 109, 166

Condon, J. J., Cotton, W. D., Greisen, E. W., Yin, Q. F., Perley, R. A., Taylor, G. B., & Broderick, J. J. 1998, AJ, 115, 1693

Condon, J.J., Cotton, W.D., Yin, Q.F., Shupe, D.L., Storrie-Lombardi, J., Helou, G., Soifer, B.T. 2003, ApJ, 125, 2411

Connolly, A.J., Szalay, A.S., Bershady, M.A., 1995, AJ, 110, 1071

Contini, M. & Viegas, S.M. 1991, A&A, 251, 27

Dale, D.A., Helou. G., Contursi, A., Silbermann, N.A., Kolhatkar, S. 2001, ApJ, 549, 215

Dale, D.A., et al. 2005, ApJ, 633, 857

de Bruyn, A.G., Wilson, A.S. 1976, A&A, 53, 93

de Bruyn, A.G., Wilson, A.S. 1978, A&A, 64, 433

de Jong, T., Klein, U., Wielebinski, R., Wunderlich, E. 1985, A&A, 147, L6

de Grijp, M.H.K., Miley, G.K., Lub, J., de Jong, T. 1985, Nature, 314, 240

de Grijp, M.H.K., Miley, G.K., Lub, J. 1987, A&AS, 70, 95, [3]

de Grijp, M.H.K., Keel, W.C., Miley, G.K., Goudfrooij, P., Lub, J. 1992, A&AS, 96, 389

de Vaucouleurs, G., de Vaucouleurs, A., Corwin, JR, H.G., Buta, R.J., Paturel, G., Fouque, P. 1991, Third Reference Catalog of Bright Galxies (RC3), New York: Springer-Verlag.

Delgado, R.M.G. 2002, ASP Conference Proceedings, 258, 101

Deluit, S., Courvoisier, T.J.-L. 2003, A&A, 399, 77

Dent, W.A. 1965, Science, 148, 1458

Deo, R.P., Crenshaw, D.M., Kraemer, S.B., Dietrich, Elitzur, M., Teplitz, H., Turner, T.J. 2007, ApJ, 671, 124

Désert, F.X., Boulanger, F., Puget, J.L. 1990, A&A, 237, 215

Dickey, J.M., Salpeter, E.E. 1984, ApJ, 284, 461

Dopita, M.A., Koratkar, A.P., Allen, M.G., Tsvetanov, Z.I., Ford, H.C., Bicknell, G.V., Sutherland, R.S. 1997, ApJ, 490, 202

Dopita, M.A., Groves, B.A., Fischera, J., Sutherland, R.S. 2005, ApJ, 619, 755

Drake, C.L., McGregor, P.J., Dopita, M.A., van Breugel, W.J.M. 2003, preprint, astro/ph/0306573v1

Drake, C.L., Bicknell, G.V., McGregor, P.J., Dopita, M.A. 2004, AJ, 128, 969

Dreyer, J. L. E. 1888, MNRAS, 49, 1

Dultzin-Hacyan, D., Krongold, Y., Fuentes-Guridi, I., Marziani, P. 1999, ApJ, 513, L111

Edelson, R.A. 1987, ApJ, 313, 651

Enya, K., Yoshii, Y., Kobayashi, Y., Minezaki, T., Suganuma, M., Tomita, H., Peterson, B. 2002, ApJS, 141, 45

Evans, I.N., Ford, H.C., Kinney, A.L., Antonucci, R.R.J., Armus, L., Caganoff, S. 1991, ApJ, 369. L27

Faber, S.M., Jackson, R.E. 1976, ApJ, 204, 668

Fairall A.P., Woudt P.A., Kraan-Korteweg R.C. 1998, A&AS, 127, 463F

Falcke, H., Wilson, A.S., Simpson, C. 1998, ApJ, 502, 199

Falcke, H., et al. 1999, ApJ, 514, L17

Fanaroff, B.L., Riley, J.M. 1974, MNRAS, 167, 31

Feigelson, E. D., Nelson, P. I. 1985, ApJ, 293, 192

Ferland, G.J., Netzer, H. 1983, ApJ, 264,105

Ferrarese, L., Merritt, D. 2000, ApJ, 539, L9

Floyd, D.J.E., et al. 2004, MNRAS, 355, 196

Forbes, D.A., Norris, R.P. 1998, MNRAS, 300, 757

Francis, P.L., Hewitt, P.C., Foltz, C.B., Chaffee, F.H. 1992, ApJ, 398, 476

Fraquelli , H.A., Storchi-Bergmann, T., Levenson, N.A. 2003, MNRAS, 341, 449

French, H.B. 1980, ApJ, 240, 41

Gallimore, J.F., Baum, S.A., O'Dea, C.P. 1996, ApJ, 464, 198

Gallimore, J.F., Baum, S.A., O'Dea, C.P. 2004, ApJ, 613, 794

Gallimore et al. 2010, ApJS, 187, 172

Gator: http://irsa.ipac.caltech.edu/applications/Gator/

Giuricin, G., Mardirossian, F., Mezzetti, M. 1990, ApJS, 72, 551

Giuricin, G., Mardirossian, F., Mezzetti, M., 1995, ApJ, 446, 550

Giuricin, G., Fadda, D., Mezzetti, M. 1996, ApJS, 468, 475

Gondek, D., Zdziarski, A.A., Johnson, W.N., George, I.M., McNaron-Brown, K., Magdziarz, P., Smith, D., Gruber, D.E. 2004, MNRAS, submitted, astro-ph /9607016

Goulding, A.D., Alexander, D.M. 2009, MNRAS, Early View Online: http://dx.doi.org/10.1111/j.1365-2966.2009.15194.x

Green, R.F., Schmidt, M., Liebert, J. 1986, ApJS, 61, 305

Greene, J.E., Ho, L.C. 2004, ApJ, 610, 722

Greene, J.E., Ho, L.C. 2004, ApJ, 641, 117

Grupe, D., Schady, P., Leighly, K.M., Komossa, S., O'Brien, P.T., Nousek, J.A. 2007, AJ, 133, 1988G

Hardcastle, M.J. 2005: http://hercules.herts.ac.uk/~mjh/radio-flux.html

Hargrave, P.J., Ryle, M. 1974, MNRAS, 166, 305

Harned, N., Harned, R., Melugin, R. 1981, Optical Engineering, 20, 195

Haro, G. 1956, Bol. Obs. Tonantzintla y Tacubaya, No. 14, 2, 8

Heckman, T.M., Ptak, A., Hornschemeir, A., Kaufmann, G. 2005, ApJ, 634, 161

Hill, T.L., Heisler, C.A., Norris, R.P., Reynolds, J.E. 2001, ApJ, 121, 128

Ho, L.C., Filippenko, A.V., Sargent, W.L.W. 1997, ApJS, 112, 315

Ho, L.C. 1999, Supermassive Black Holes in Galactic Nuclei. On Observational Evidence for Black Holes in the Universe, Publication of Conference held in Calcutta, January 11-17th , Page 157

Ho, L.C., Peng, C.Y. 2001, ApJ, 555, 650

Ho, L.C., Ulvestad, J.S. 2001, ApJS, 133, 77

Hoopes, C.G., Sembach, K.R., Heckman, T.M., Meurer, G.R., Aloisi, A., Calzetti, D., Leitherer, C., Martin, C.L. 2004, ApJ, 612, 825.

Huchra, J., Sargent, W.L.W. 1973, ApJ, 186, 433

Huchra, J., Burg, R. 1992, ApJ, 393, 90

Hughes, P.A. ed., 1991, Beams and jets in Astrophysics, Cambridge University Press

Humason, M.L. 1932, PASP, 44, 267

Imanishi, M., Wada, K. 2004, ApJ, 617, 214

IPAC, 1998: http://web.ipac.caltech.edu/staff/roc/2mass/seeing/seesum.html

IPAC, 1999: http://www.ipac.caltech.edu/2mass/releases/spr99/doc/test/jarrett2/appendix_sampler.html

IPAC, 2005: http://www.ipac.caltech.edu/2mass/releases/allsky/doc/sec3_1b1.html#s9

Isobe, T., Feigelson, E. D., Nelson, P. I. 1986, ApJ, 306, 490

Jones, P.A., McAdam, W.B. 1992, ApJS, 80, 137

Joguet, B., Kunth, D., Melnick, J., Terlevich, R., Terlevich, E. 2001, A&A, 380, 19J

Kaastra, J.S., de Korte, P.A.J. 1988, A&A, 198, 16

Karma/kvis (v. 1.7.25): http://www.atnf.csiro.au/computing/software/karma/

Kawakatu, N., Nagao, T., Woo, J-H. 2008, preprint, arXiv:0812.1329v1

Kennicutt, R. 1983, A&A, 120, 219

Kewley, J.L., Dopita, M.A., Sutherland, R.S., Heisler, C.A., Trevena, J. 2001, ApJ, 556, 121

Khachikyan, E.Y., Weedman, D.W. 1971, Astrophysics, 7, 389

Khachikyan, E.Y., Weedman, D.W. 1974, ApJ, 192, 581

Kinman, T.D. 1965, ApJ, 179, L61

Kinney, A.L., Antonucci, R.R.J., Ward, M.J., Wilson, A.S., Whittle, M. 1991, ApJ, 377, 100

Kinney, A.L., Schmitt, H.R., Clarke, C.J., Pringle, J.E., Ulvestad, J.S., Antonucci, R.R.J. 2000, ApJ, 537, 152

Kirhakos, S.D., Steiner, J.E. 1990, AJ, 99, 1722

Klein, U., Wielebonski, R., Thuan, T.X. 1984, A&A, 141, 241

Kleinman, D.E., Low, F.J. 1970a, ApJ, 159, 165

Kleinman, D.E., Low, F.J. 1970b, ApJ, 161, 203

Kormendy, J., Richstone, D. 1995, ARA&A, 33, 581

Kondratko, P.T. et al. 2006, ApJ, 638, 100

Koski, A.T. 1978, ApJ, 223, 56

Krabbe, A., Sternberg, A., Genzel, R. 1994, ApJ, 425, 72

Kukula, M.J., Pedlar, A., Baum, S.A., O'Dea, C.P. 1995, MNRAS, 276, 1262

Kukula, M.J., Ghosh, T., Pedlar, A. 1999, ApJ, 518, 117

Kumar, S., Pringle, J.E. 1985, MNRAS, 213, 435

Laing, R.A. 1993, Radio Observations of Jets: Large Scales. Pages 95-119 of Astrophysical Jets, STScI Symposium, no. 6, Cambridge University Press

Lal, D.V. 2002, BASI, 30, 777

Lal, D.V., Shastri, P., Gabuzda, D.C. 2004, A&A, 425, 99

Laor, A. 2001, ApJ, 553, 677

Latta, R. 1981, JASA, 76, 713

Lauberts, A., Valentijn, E.A. 1989, The Surface Photometry Catalog of the ESO-Uppsala Galaxies, Garching Bei Munchen: European Southern Observatory

LaValley, M., Isobe, T., Feigelson, E.D. 1990, BAAS (Software Reports), 22, 917

Lawless, J. F. 1982, Statistical Models and Methods for Lifetime Data. Monograph, Wiley: New York

Lawrence, A. 1987, PASP, 99, 309L

Leitherer, C., Furguson, H.C. 1995, ApJ, 454, L19

Levenson, N.A., Fernandes, R.C., Weaver, K.A., Heckman, T.M., Storchi-Bergman, T. 2001, ApJ, 557, 54L

Li, A. 2008, preprint, arXiv:0808.4117

Lipovetsky, V.A., Neizvestny, S.I., Neizvestny, O.M. 1988, SByuO, 55, 5L [1]

Liu, Ji-Feng, and Bregman, J.N. 2005, ApJS, 157, 59L

Lloyd, C. 1984, MNRAS, 209, 697

Longair, M.S., Ryle, M., Scheuer, P.A.G. 1973, MNRAS, 164, 243

Lubinski, P., Zdziarski, A.A. 2001, MNRAS, 323, L37

Lutz, D. Maiolino, R., Moorwood, A.F.M., Netzer, H., Wagner, S.J., Sturm E., Genzel, R. 2002, A&A, 396, 439

Madgwick, D.S., et al. 2003, ApJ, 599, 997

Magorrian, J., et al. 1998, AJ, 115, 2285.

Maia, M. A. G., Machado, R. S., Willmer, C. N. A. 2003, AJ, 126, 1750M [5]

Maloney, P.R., Begelman, M.C., Pringle, J.E. 1996, ApJ, 473, 582

Markarian, B.E. 1969a, Astrofizika, 5, 443

Markarian, B.E. 1969b, Astrofizika, 5, 581

Markarian, B.E., Lipovetsky, V.A. 1971, Astrofizika, 7, 511

Markarian, B.E., Lipovetsky, V.A. 1973, Astrofizika, 9, 487

Marquardt, D. 1963, SIAM J. Appl. Math. 11, 431

Martini, P., Pogge, R.W., Ravindranath, S., An, J.H. 2001, ApJ, 562, 139

Matt, G. 2000, A&A, 355, L31

Mattson, B.J., Weaver, K.A. 2004, AJ, 601, 771

Mauch. T., Murphy, T., Buttery, H.J., Curran, J., Hunstead, R.W., Piestrzynski, B., Robertson, J.G., Sadler, E.M. 2003, MRAS, 342, 1117

McKernan, B., Reynolds, C.S. 2004, 8th HEAD meeting, Session 26

Meurs, E.J.A., 1982, Ph.D. thesis, University of Leiden

Meurs, E.J.A., Wilson, A.S. 1984, A&A, 136, 206

Mezger, P.G., Henderson, A.P. 1967, ApJ, 147, 471

MGPSCAT: MGPS-2, 2007: http://www.astrop.physics.usyd.edu.au/mgpscat/mgpscat.Aug-15-2007

Middelberg, E., et al. 2004, A&A, 417, 925

Miller, J.S., Goodrich, R.W. 1990, ApJ, 355, 456

Mittaz, J.P.D., Penston, M.V., Snijders, M.A.J. 1990, MNRAS, 242, 370

Morganti, R., Tsvetanov, Z.I., Gallimore, J., Allen, M.G. 1999, A&AS, 137, 457

Morrison, P. 1969, ApJ, 157, L73

Mouri, H., Taniguchi, Y. 1992, ApJ, 386, 68

Mouri, H., Taniguchi, Y. 2000, ApJ, 545, L103

Mouri, H., Taniguchi, Y. 2004, ApJ, 605, 144

Mulchaey, J.S., Wilson, A.S., Tsvetanov, Z. 1996, ApJS, 102, 309

Mundell, C.G., Wilson, A.S., Ulvestad, J.S., Roy, A.L. 2000, ApJ, 529, 816

Mundell, C. G., Wilson, A. S., Ulvestad, J. S., Roy, A. L. 2001, The Nature of Flat-spectrum Nuclear Radio Emission in Seyfert Galaxies, In Galaxies and their Constituents at the Highest Angular Resolutions, IAU Symposium 205, eds. Schilizzi, R.T, Vogel, S.N., Paresce, F., Elvis, M.S., San Francisco, ASP, 72-73

Murphy, E.J, et al. 2005, ApJ, submitted, astro-ph /0510227

Murphy, T., Mauch, T., Green, A., Hunstead, R.W., Piestrzynska, B., Kels, A.P., Sztajer, P. 2007, preprint, arXiv:0708.3092v1

Nagar, N.M., Wilson, A.S., Mulchaey, J.S., Gallimore, J.F. 1999, ApJS, 120, 209

Nagar, N.M., Wilson, A.S. 1999, ApJ, 516, 97

Nagar, M., Wilson, A.S., Mulchaey, J.S., Gallimore, J.F. 1999, ApJS, 120, 209

Nagar, N.M., Falcke, H., Wilson, A.S, Ho, L.C. 2000, ApJ, 542, 186

Nagar, N.M, Wilson, A.S., Falcke, H. 2001, ApJ, 559, L87

Nagar, N.M., Falcke, H., Wilson, A.S, Ulvestad, J.S. 2002, A&A, 392, 53

Nagar, N.M., Falcke, H., Wilson, A.S. 2004, October 12th-15th, Radio Luminosity Function, Importance of Jet Power, and Radio Properties of Nearby LLAGN, Proceedings of the 17th European VLBI Network Symposium, Toledo, Spain

Nagar, N.M., Falcke, H., Wilson, A.S, Ho, L.C. 2005, A&A, 435, 521

Nandra, K., George, I.M., Mushotzky, R.F., Turner, T.J., Yaqoob, T. 1997, ApJ, 477, 602

NASA/IPAC: http://nedwww.ipac.caltech.edu/forms/vel_correction.html

NASA/IPAC 2: http://irsa.ipac.caltech.edu/applications/2MASS/IM/interactive.html

NED: http://nedwww.ipac.caltech.edu/index.html

Neff, S.G., de Bruyn, A.G. 1983, A&A, 128, 318

Neff, S.G., Ulvestad, J.S. 1988, AJ, 96, 841

Nelson, C.H., Green, R.F., Bower, G., Gebhardt, K., Weistrop, D. 2004, ApJ, 615, 652

Nishiura, S., Taniguchi, Y. 1998, ApJ, 499, 134

Norris, R.P., Allen, D.A., Sramek, R.A., Kesteven, M.J., Troup, E.R. 1990, ApJ, 359, 291

Norris, R.P., Roy, A.L., Allen, D.A., Kesteven, M.J., Troup, E.R., Reynolds, J.E. 1992, ASP Conf. Series, 31, 71

Ogle, P.M., Brookings, T., Canizares, C.R., Lee, J.C., Marshall, H.L. 2003, A&A, 402, 849,

Oster, L. 1961, Rev. Modern Physics, 33, 525

Osterbrock, D.E., Koski, A.T., Phillips, M.M. 1976a, ApJ, 206, 898

Osterbrock, D.E. 1976b, PASP, 88, 589

Osterbrock, D.E. 1977, ApJ, 215, 733

Osterbrock, D.E. 1981, ApJ, 249, 462

Pacholczyk, A.G., Weymann, R. 1968, AJ, 73, 836

Paturel, G., Vauglin, I., Petit, C., Borsenberger, J., Epchtein, N., Fouque, P., Mamon, G. 2005, A&A, 430, 751P [4]

Pedlar, A., Booler, R.V., Spencer, R.E., Stewart, O.J. 1983, MNRAS, 202, 647

Pedlar, A., Dyson, J.E., Unger, S.W. 1985, MNRAS, 214, 463

Peng, C.Y., Ho, L. C., Impey, C.D., Rix, H-W. 2002, AJ, 124, 266

Peng, C.Y. 2004, GALFIT Quick Start Guide 2.0: http://users.ociw.edu/peng/work/galfit/galfit.html

Peng, Z., Gu, Q., Melnick, J., Zhao, Y. 2006, A&A, 453, 3, 863

Peng, Z., 2009: File archived online: http://ifnia.org/JCU/files

Penston, M.V., Fosbury, R.A.E. 1978, MNRAS, 183, 479

Pier, E.A, Krolik, J.H. 1992, ApJ, 401, 99

Pier, E.A, Krolik, J.H. 1993, ApJ, 418, 673

Pier, E.A, Voit, G.M. 1995, ApJ, 450, 628

Pogge, R.W., Martini, P. 2002, ApJ, 569, 624

Poggianti, B.M., Bressan, A., Franceschini, A. 2001, ApJ, 550, 195

Polletta, M., Bassani, L., Malaguti, G., Palumbo, G.G.C., Carola, E. 1996, ApJS, 106, 399

Prentice, R., Marek, P. 1979, Biometrics, 35, 861

Prieto, M.A. 2000, MNRAS, 316, 442

Pringle, J.E. 1996, MNRAS, 281, 357

Pringle, J.E. 1997, MNRAS, 292, 136

Pringle, J.E., Antonucci, R.R.J., Clarke, C.J., Kinney, A.L., Schmitt, H.R., Ulvestad, J.S. 1999, ApJ, 526, L9

Quillen, A.C., Alonzo-Herrero, A., Rieke, M.J., McDonald, C., Falcke, H., Rieke, G.H. 1999, ApJ, 525, 685

Rhee, J.H., Larkin, J.E. 2005, ApJ, 620, 151

Rickard, L.J., Harvey, P.M. 1984, AJ, 89, 1520

Rieke, G.H., Low, F.J. 1972, ApJ, 176, L95

Rieke, G.H., Lebofsky, M.J. 1979, Ann. Rev. Astron. Astrophys., 17, 477

Rifatto, A., Rafanelli, P., Ciroi, S., Radovich, M., Vennik, J., Richter, G., Birkle, K. 2001, AJ, 122, 2301

Robertson, B., Hernquist, L., Cox, T.J., Tiziana Di Matteo, T., Hopkins, P.E., Martini, P., Springel, V. 2006, ApJ, 641, 90

Rodríguez-Espinosa, J.M., Rudy, R.J., Jones, B. 1987, ApJ, 312, 555

Roy, A.L., Norris, R.P., Kesteven, M.J., Troup, E.R., Reynolds, J.E. 1994, ApJ, 432, 496

Roy, A.L., Norris, R.P. 1997, MNRAS, 289, 824

Roy, A.L., Colbert, E.J.M., Wilson, A.S., Ulvestad, J.S. 1998a, ApJ, 504, 147

Roy, A.L., Norris, R.P., Kesteven, M.J., Troup, E.R., Reynolds, J.E. 1998b, MNRAS, 301, 1019

Rush, B., Malkan, M.A., Spinoglio, L. 1993, ApJS, 89, 1

Rush, B., Malkan, M.A., Edelson, R.A. 1996, ApJ, 473, 130

Sahayanathan, S., Misra, R. 2005, ApJ, 628, 611

Sanders, D.B., Mirabel, I.F. 1985, ApJ, 298, L31

Scanpi: http://scanpiops.ipac.caltech.edu:9000/applications/Scanpi/docs/overview.html

Scheuer, P.A.G. 1974, MNRAS, 166, 513

Schmitt. H.R., Kinney, A.L., Storchi-Bergmann, T., Antonucci, R. 1997, ApJ, 477, 623

Schmitt, H.R., Storchi-Berman, T., Fernandes, R.C. 1999, MNRAS, 303, 173

Schmitt, H.R., Kinney, A.L. 2000, ApJS, 128, 479

Schmitt, H.R., Antonucci, R.R.J., Ulvestad, J.S., Kinney, A.L., Clarke, C.J., Pringle, J.E. 2001a, ApJ, 555, 663

Schmitt, H.R., Ulvestad, J.S., Antonucci, R.R.J., Kinney, A.L. 2001b, ApJS, 132, 199

Schmitt, H.R., Donley, J.L., Antonucci, R.R.J., Hutchings, J.B., Kinney, A.L. 2003a, ApJS, 148, 327

Schmitt, H.R., Donley, J.L., Antonucci, R.R.J., Hutchings, J.B., Kinney, A.L., Pringle, J.E. 2003b, ApJ, 597, 768

Schmidt, M. 1968, ApJS, 158, 393

Schombert, J. 2007: http://abyss.uoregon.edu/~js/archangel/

Schwartz, C.M., Martin, C.L. 2004, ApJ, 610, 201

Sersic, J.-L. 1968, Atlas de Galaxies Australes, Observatorio Astronomico de Cordoba

Seyfert, Carl K. 1943, ApJ, 97, 288

Shu, X.M., Wang, J.X., Jiang, P., Fan, L.L., Wang, T.G. 2007, ApJ, 657, 167 [6]

Shuder, J.M. 1981, ApJ, 244, 12

Skrutskie, M.F., et al. 2006, AJ, 131, 1163

Smith, D.A., Herter, T., Haynes, M.P. 1998, ApJ, 494, 150

Spinoglio, L., Malkan, M.A. 1989, ApJ, 342, 83

Spinoglio, L., Malkan, M. A., Rush, B., Carrasco, L., Recillas-Cruz, E. 1995, ApJ, 453, 616

Spinoglio et al. 2008, preprint, arXiv:0902.3341 v1

Sramek, R.A., Weedman, D.W. 1980, ApJ, 238, 435

Steffen, W., Gómez, J.L., Raga, A.C., Williams, R.J.R. 1997, ApJ, 491, L73

Storchi-Bergmann, T., Winge, C., Ward, M.J., Wilson, A.S. 1999, MNRAS, 304, 35

Sosa-Brito, R.M., Tacconi-Garman, L.E., Lehnert, M.D. 2001, ApJS, 136, 61

Subrahmanya, C.R., Harnett, J.I. 1987, MNRAS, 225, 297.

SUMSS Catalogue, ver. 2.1. 2008: http://www.astrop.physics.usyd.edu.au/sumsscat/

Sutherland, R.S., Bicknell, G.V., Dopita, M.A. 1993, ApJ, 414, 510

Taniguchi, Y. 1999, ApJ, 524, 65

Taniguchi, Y., Murayama, T., Nagao, T. 2003, ApJ, submitted, arXiv:astro-ph /9910036 v1

Thean, A., Pedlar, A., Kukula, M.J., Baum, S.A., O'Dea, C.P. 2000, MNRAS, 314, 573

Thean, A., Pedlar, A., Kukula, M.J., Baum, S.A., O'Dea, C.P. 2001a, MNRAS, 325, 737

Thean, A.H.C., Gillibrand, T.I., Pedlar, A., Kukula, M.J. 2001b, MNRAS, 327, 369

Thompson, T.A., Quataert, E., Waxman, E., Murray, N., Martin, C. 2006, ApJ, 645, 186

Tran, H.D. 2003a, AGN: From Central Engine to Host Galaxies, ASP Conf. Series

Tran, H.D. 2003b, ApJ, 583, 632

Turner, T.J., George, I.M., Nandra, K., Mushotzky, R.F. 1998, ApJ, 493, 91

Ueda, Yoshihiro et al. 2007, ApJ, 664L, 79

Ulvestad, J.S., Wilson, A.S. 1984a, ApJ, 278, 544

Ulvestad, J.S., Wilson, A.S. 1984b, ApJ, 285, 439

Ulvestad, J.S., Neff, S.G., Wilson, A.S. 1987, AJ, 93, 22

Ulvestad, J.S., Wilson, A.S. 1989, ApJ, 343, 659

Ulvestad, J.S., Roy, A.L., Cobert, J.M., Wilson, A.S. 1998, ApJ, 496, 196

Ulvestad, J.S., Wrobel, J.M., Roy, A.L., Wilson, A.S., Flacke, H., Krichbaum, T.P. 1999a, ApJ, 517, L81

Ulvestad, J.S., Wrobel, J.M., Carilli, C.L. 1999b, ApJ, 516, 127

Ulvestad, J.S., Ho, L.C. 2001, ApJ, 558, 561

Unger, S.W., Pedlar, A., Booler, R.V., Harrison, B.A. 1986, MNRAS, 219, 387

Unger, S.W., Lawrence, A., Wilson, A.S., Elvis, M., Wright, A.E. 1987a, MNRAS, 228, 521

Unger, S.W., Pedlar, A., Axon, D.J., Whittle, M., Meurs, E.J.A., Ward, M.J. 1987b, MNRAS, 228, 671

van der Kruit, P.C. 1971, A&A, 15, 110

van der Kruit, P.C. 1973, A&A, 29, 263

Veilleux, S., Osterbrock, D.E. 1987, ApJS, 63, 295

Veilleux et al. 2009, ApJ, 701(1), 587

Véron, M.P., Veron, P., Zuiderwijk, E.J. 1981, A&A, 98, 34

Véron-Cetty, M.P., Woltier, L. 1990, A&A, 236, 69

Veron-Cetty, M.-P., Veron,P. 2001, A&A, 374, 92V [2]

Visnovsky, K.L., Impey, C.D., Foltz, C.B., Hewitt, P.C., Weyman, R.J., Morris, S.L. 1992, ApJ, 391, 560

Vlahakis, C., Eales, S., Dunne, L. 2007, MNRAS, 379, 1042

Weaver, K.A., Reynolds, C.S. 1998, ApJ, 503, L39

Weedman, D.W. 1976, ApJ, 208, 30

Weedman, D.W. 1977, ApJ, 15, 69

Weedman, D.W., Feldman, F.R., Balzano, V.A., Sramek, R.A. 1981, ApJ, 248, 105

West, R.M., Schuster, H.-E., 1982, A&AS, 49, 577

Whittle, M., Pedlar, A., Meur, E.J.A., Unger, S.W., Axon, D.J., Ward, M.J. 1988, ApJ, 326, 125

Wilson, A.S., Willis, A.G. 1980, ApJ, 240, 429

Wilson, A.S. 1981, Proceedings of Second ESO/ESA Workshop, ESA SP-162, 125

Wilson, A.S. 1982, IAU Symposium No. 97, 179

Wilson, A.S., Ulvestad, J.S. 1987, ApJ, 319, 105

Wilson, A.S. 1991, ASPC, 18, 227

Wilson, A.S., Raymond, J.C. 1999, ApJ, 513, L115

Winge, C., Storchi-Berman, T., Ward, M.J., Wilson, A.S. 2000, MNRAS, 316, 1

Witta, P.J. 1991, Production of Jets: Relation to AGN. In Beams and Jets in Astrophysics, Cambridge University Press

Wright, A.E., Griffith, M.R., Burke, B.F., Ekers, R.D. 1994, ApJS, 91, 111

Wright, N. 2006, PASP, 118, 1711, available at http://www.astro.ucla.edu/~wright/CosmoCalc.html

Wrobel, J.M. 2000, ApJ, 531, 716

Wu, X-B., Han, J.L. 2001, A&A, 380, 31

Wu, W., Clayton, G.C., Gordon, K.D., Misselt, K.A. 2002, ApJS, 143, 377

Wunderlich, E., Klein, U., Wielebinski, R. 1987, A&AS 69, 487

Yee, H.K.C., Oke, J.B. 1978, ApJ, 226, 753

Yee, H.K.C. 1980, ApJ, 241, 894

Yoshida, M., Yagi, M., Okamura, S. 2002, ApJ, 567, 118

Young, E., et al. 1984, ApJ, 278, L75

Yun, M.S., Carilli, C.L. 2002, ApJ, 568, 88

Yun, M.S., Reddy, N.A., Condon, J.J. 2001, ApJ, 554, 803

Zdziarski, A.A. 1999, High Energy Processes in Accreting Black Holes, ASP Conf. Series, 161

Zwicky, F. 1966, ApJ, 143, 192

Zwicky, F. 1967, Adv. A&Ap, 5, 267

APPENDIX A - Radio Contour Maps

TABLE A.1
843 MHz Radio Map Contours for the Sy2

Fig. Num. (1)	Name (2)	Contours (Multiples of rms error) (3)	kpc / " (4)
A.1	LEDA 087391	-2,2,4,8,12,16,20,24: 1.27	0.579
A.1	NGC 0424	-1,-2,2,4,6,8,10,12: 1.9	0.237
A.1	LEDA 093365	-1,1: 1.9	0.516
A.1	PGC 004440	-2,2,4,8,12,16,18,20,21: 1.9	0.241
A.1	NGC 0454	-2,2,4,6,8,12,16,20,26,30,34,36: 1.27	0.245
A.1	PGC 004569	-2,2,4,6,8,9: 1.27	0.484
A.2	PGC 005696	-4,-2,2,4,8,12,16,20: 1.9	0.332
A.2	PGC 006078	-2,2,4,8,12,18,22,25: 1.9	0.501
A.2	PGC 006351	-2,2,4,6,7,8: 1.9	0.584
A.2	PGC 008012	-2,2,4,6,8,9: 1.27	0.395
A.2	NGC 0824	-2,2: 1.9	0.389
A.2	PGC 009634	-2,2,4,8,12,16,19,20: 1.9	0.340
A.3	PGC 010665	-2,2,4,6,8,10,12,13,14: 1.9	0.391
A.3	PGC 010705	-2,2,4,6,8,10,12,13,14: 1.9	0.334
A.3	PGC 011104	-2,2: 1.9	0.327
A.3	PGC 012759	-2,2,4,6,8,10,12,14,16: 1.27	0.370
A.3	NGC 1386	-4,-2,2,4,8,12,18,22,24: 1.9	0.059
A.3	PGC 014702	-4,-2,2,4,8,12,18,24,30,36,40,44,46: 1.9	0.240
A.4	AM 0426-625	-2,2,3,5,8,11,13,14: 1.27	0.367
A.4	PGC 015172	-1,2,4,8,12,16,22,30,40,50,64,74: 1.9	0.331
A.4	NGC 1672	-4,-2,2,4,8,12,16,22,30,40,60,90,120,140,150: 1.27	0.090
A.4	PGC 016072	-2,2: 1.27	0.457
A.4	PGC 016357	-2,2,4,6,8: 1.27	0.363
A.4	NGC 1808	-1,2,4,8,12,16,22,32,48,68,100,180,280,340,360: 1.9	0.068
A.5	PGC 016873	-2,2,4: 1.9	0.321
A.5	PGC 017768	-1,2,4: 1.9	0.497
A.5	LEDA 096373	-2,2,3,4,8,16,32,64,100,122: 1.9	0.581
A.5	PGC 021057	-2,2,4,6,8,9: 1.27	0.242
A.5	PGC 023573	-2,2,4,6,8,12,16,20,22: 1.27	0.357
A.5	PGC 028144	-2,2,4,8,12,14: 1.9	0.172
A.6	PGC 028147	-2,2,4,5: 1.9	0.189
A.6	PGC 029778	-4,-2,2,4,8,16,30,42,46: 1.9	0.563
A.6	PGC 029993	-2,2,4,8,12,16,19: 1.9	0.197
A.6	PGC 030984	-2,2,3,4,5,6,7: 1.9	0.276
A.6	NGC 3281	-4,-2,2,8,12,16,28,40,46: 1.9	0.216
A.6	LEDA 088648	-1,2,4: 1.9	0.596
A.7	NGC 4507	-2,2,4,8,12,18,26,30,34: 1.9	0.238
A.7	PGC 042504	-2,2,4,8,16,28,42,50: 1.9	0.222
A.7	WKK 1263	-2,2,4,8,12,15: 1.27	0.486
A.7	PGC 043779	-2,1: 1.9	0.321
A.7	NGC 4785	-2,2,4,8,16,24,28: 1.9	0.247
A.7	PGC 044167	-2,2,4: 1.9	0.336
A.8	NGC 4903	-2,2,4,6: 1.9	0.330
A.8	NGC 4945	-12,-8,-2,2,6,12,18,36,48,64,84,124,324,824,1648,2600: 1.9	0.038
A.8	ESO 383- G 018	-2,2,4,5: 1.9	0.250
A.8	Circinus	-4,-2,2,4,8,12,16,22,30,40,60,120,240,480,800: 1.27	0.030
A.8	LEDA 141858	-2,-1,1,2: 1.9	0.520
A.8	NGC 5643	-2,2,4,8,12,18,30,36: 1.9	0.081

TABLE A.1 - Continued
843 MHz Radio Map Contours for the Sy2

Fig. Num. (1)	Name (2)	Contours (Multiples of rms error) (3)	kpc / " (4)
A.9	PGC 052101	-4,-2,2,3,4,5,6: 1.9	0.504
A.9	LEDA 166339	-2,-1,2,4: 1.27	0.513
A.9	IC 4518	-2,2,4,8,18,30,44,64,84,104: 1.9	0.316
A.9	WKK 3646	-2,-1,2: 1.27	0.298
A.9	PGC 058547	-2,2,4,8,16,32,48,64,76: 1.27	0.185
A.9	PGC 059124	-6,-4,-2,2,3,4,8,16,26,34: 1.27	0.185
A.10	NGC 6221	-2,2,4,8,16,32,64,100,136: 1.27	0.102
A.10	NGC 6300	-2,2,4,6,8,10,12,18,22: 1.27	0.075
A.10	PGC 060594	-4,-2,2,3,4,6,8,9: 1.27	0.341
A.10	PGC 062134	-2,2,3,4,16,48,96,148,196: 1.27	0.404
A.10	PGC 062174	-2,2,4,8,16,22,26: 1.27	0.268
A.10	PGC 062218	-2,2: 1.27	0.298
A.11	PGC 062428	-2,2,4,8,16,28,36: 1.27	0.304
A.11	PGC 062440	-2,2,4,8,16,21: 1.27	0.371
A.11	NGC 6810	-2,2,4,8,16,32,64,98,112: 1.27	0.138
A.11	PGC 063874	-2,2,4,8,18,30,44,64,84,104,112: 1.9	0.384
A.11	NGC 6890	-1,2,4,8,14,16: 1.9	0.164
A.11	PGC 064491	-2,2,4,6,8,10,11: 1.27	0.323
A.12	PGC 064537	-2,2: 1.9	0.386
A.12	PGC 065600	-16,-12,-8,-6,-4,-2,2,4,8,16,48,100,200,400,800,1200,1500: 1.27	0.229
A.12	NGC 7130	-2,2,4,8,16,32,64,90,102: 1.9	0.324
A.12	NGC 7172	-2,2,4,8,14,20,23: 1.9	0.176
A.12	PGC 068122	-4,-2,2,3,4,5,6: 1.9	0.295
A.12	PGC 068198	-2,2,3,4,6,8,10,12,14: 1.9	0.210
A.13	FAIRALL 0357	-2,2,3,4,6,8,10: 1.27	0.571
A.13	PGC 070458	-4,-2,2,4,8,12,16,19: 1.9	0.561
A.13	NGC 7496	-2,2,4,8,13,15: 1.9	0.112
A.13	NGC 7582	-2,2,4,8,18,30,44,64,104,140,166: 1.9	0.107
A.13	NGC 7590	-4,-2,2,8,14,20,24,26: 1.9	0.107

Note. - Contour levels for the Sy2 radio maps in multiples of the rms noise of the processed SUMSS mosaics. The figure containing the map for a particular object is given in column (1). The primary object names (from Table 1.1) are listed in column (2). Following the contour levels in column (3) the rms for each object is listed.

TABLE A.2
843 MHz Radio Map Contours for the Sy1

Fig. Num. (1)	Name (2)	Contours (Multiples of rms error) (3)	kpc / " (4)
A.13	LEDA 087392	-4,-2,2,4,8,16,32,64,100,148,184,202: 1.27	0.554
A.14	PGC 002450	-2,2,4,8,12,16,20: 1.27	0.593
A.14	PKS 0056-572	-4,-2,2,4,8,12,22,40,80,160,240,320,348: 1.27	0.361
A.14	PGC 003864	-2,2,4,6,8,10,11: 1.27	0.510
A.14	IRAS 01089-4743	-1,2,3,4,5: 1.9	0.483
A.14	PGC 004822	-2,2,3,4,5: 1.9	0.468
A.14	NGC 526A	-2,2,4,5,6: 1.9	0.382
A.15	PMN J0133-5159	-4,-2,2,4,8,16,32,64,100,170,220,250: 1.27	0.400
A.15	ESO 080- G 005	-2,1,2: 1.27	0.534
A.15	NGC 1097	-4,-2,2,4,6,12,18,36,48,64,84,104,124,140,148: 1.9	0.086
A.15	PGC 011706	-2,2: 1.27	0.554
A.15	NGC 1365	-4,-2,2,4,6,12,18,36,64,104,148,196,240,270: 1.9	0.111
A.15	NGC 1566	-2,2,4,8,12,18,24,28,34,40,48: 1.27	0.102
A.16	PGC 017103	-4,-2,2,4,6,8,10,11: 1.9	0.251
A.16	FAIRALL 0265	-2,-1,2,4,8: 1.27	0.583
A.16	LEDA 096433	-2,2,4,5,6,7: 1.9	0.322
A.16	PGC 027468	-2,2: 1.9	0.182
A.16	PGC 029148	-2,2: 1.9	0.470
A.16	PGC 029151	-2,1,2: 1.9	0.471
A.17	PGC 033084	-2,2: 1.27	0.380
A.17	PGC 034101	-2,-1,1,2,3,4: 1.9	0.198
A.17	PGC 036002	-1,2,4,8,12,14: 1.9	0.339
A.17	NGC 3783	-2,2,4,8,12,16,20,25,27: 1.9	0.197
A.17	LEDA 096527	-1,-2,2,4,8,12,16,19: 1.9	0.548
A.17	PGC 045371	-2,2,4,8,12,16,20,24,26: 1.9	0.302
A.18	PGC 047969	-4,-2,2,4,8,12,18,24,30,40,50,55: 1.9	0.157
A.18	PGC 049051	-4,-2,2,4,8,12,18,24,30,36,39: 1.9	0.322
A.18	PGC 050427	-2,2: 1.9	0.469
A.18	ESO 328- G036	-2,2,3,4,5,6: 1.9	0.472
A.18	PKS 1521-300	-2,2,6,12,24,46,68,84,90: 1.9	0.392
A.18	LEDA 2793282	-2,-1,1,2: 1.27	0.314
A.19	PGC 062346	-4,-2,2,2,4,6,8,10,11: 1.27	0.285
A.19	PGC 062554	-2,2,2,4,6,7: 1.27	0.571
A.19	ESO 399-IG 020	-2,2,3,4,5,6,7: 1.9	0.496
A.19	NGC 6860	-2,2,4,6,9,11,13: 1.27	0.299
A.19	PGC 064989	-2,2,3: 1.9	0.380
A.19	ESO 235- G 059	-2,-1,1,2: 1.9	0.495
A.20	CTS 0109	-2,-1,1,2: 1.9	0.579
A.20	PGC 067075	-2,-1,1,2: 1.9	0.374
A.20	NGC 7213	-1,2,4,8,12,18,24,30,36,42,48: 1.9	0.119
A.20	[VV2003c] J224704.9-305502	-8,-4,-2,2,4,8,12,18,24,30,36,42,45: 1.9	0.202
A.20	PGC 073028	-2,-1,2,3: 1.9	0.598

Note. - Contour levels for the Sy1 radio maps in multiples of the processed SUMSS mosaics. The figure containing the map for a particular object is given in column (1). The primary object names (from Table 1.2) are listed in column (2). Following the contour levels in column (3) the rms for each object is listed.

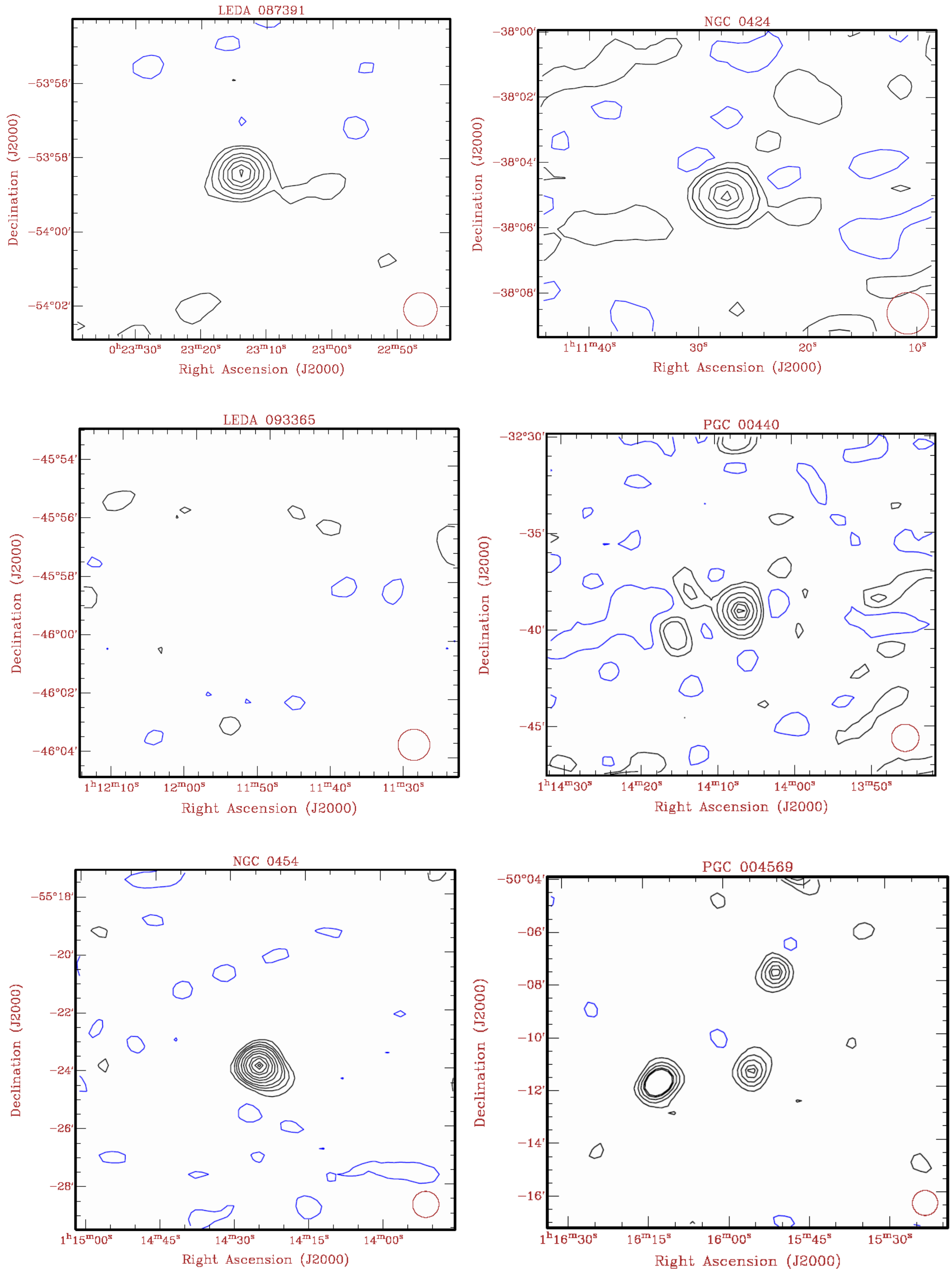

FIG. A.1. - 843 MHz maps from SUMSS. See Table A.1 for contour levels.

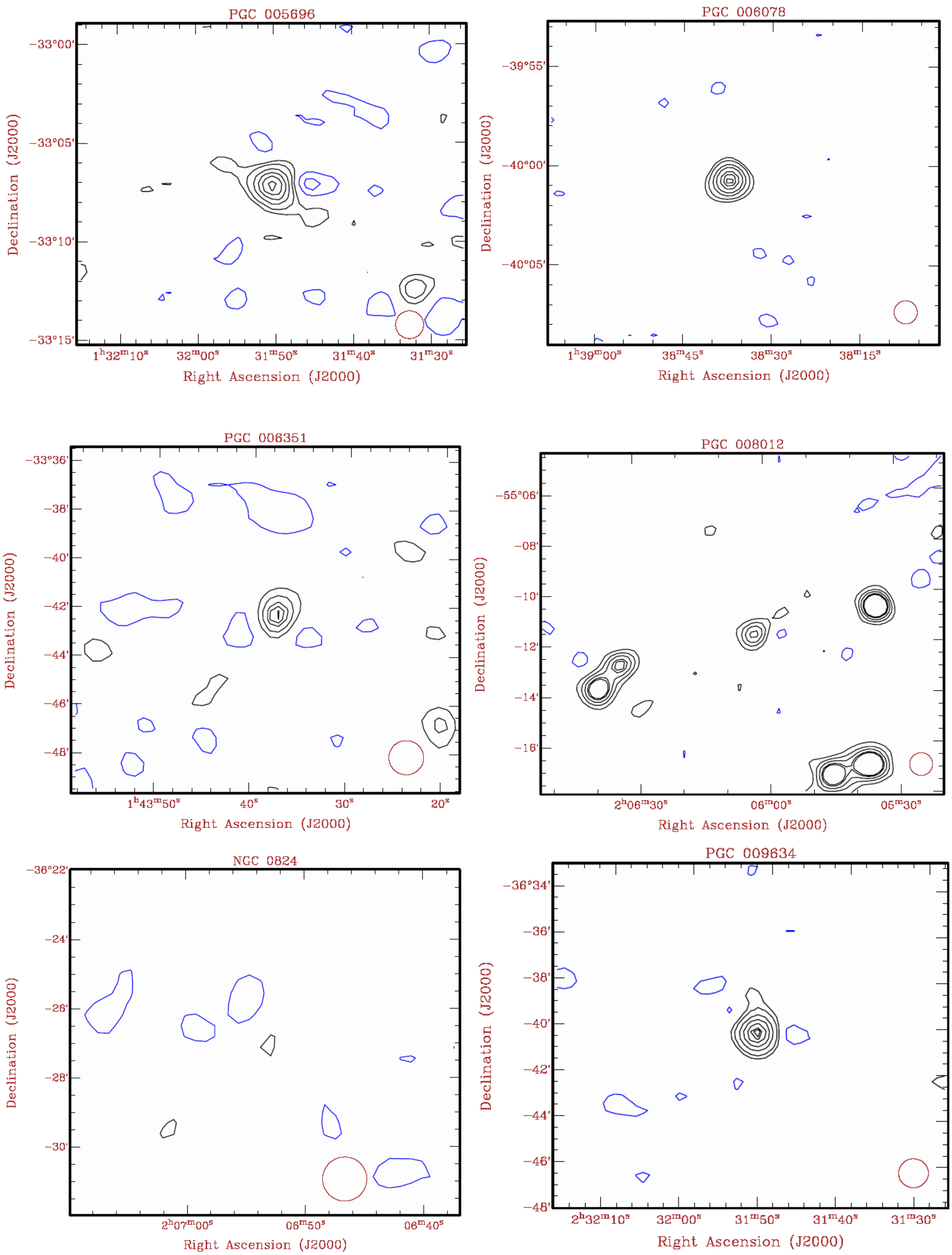

FIG. A.2. - 843 MHz maps from SUMSS. See Table A.1 for contour levels.

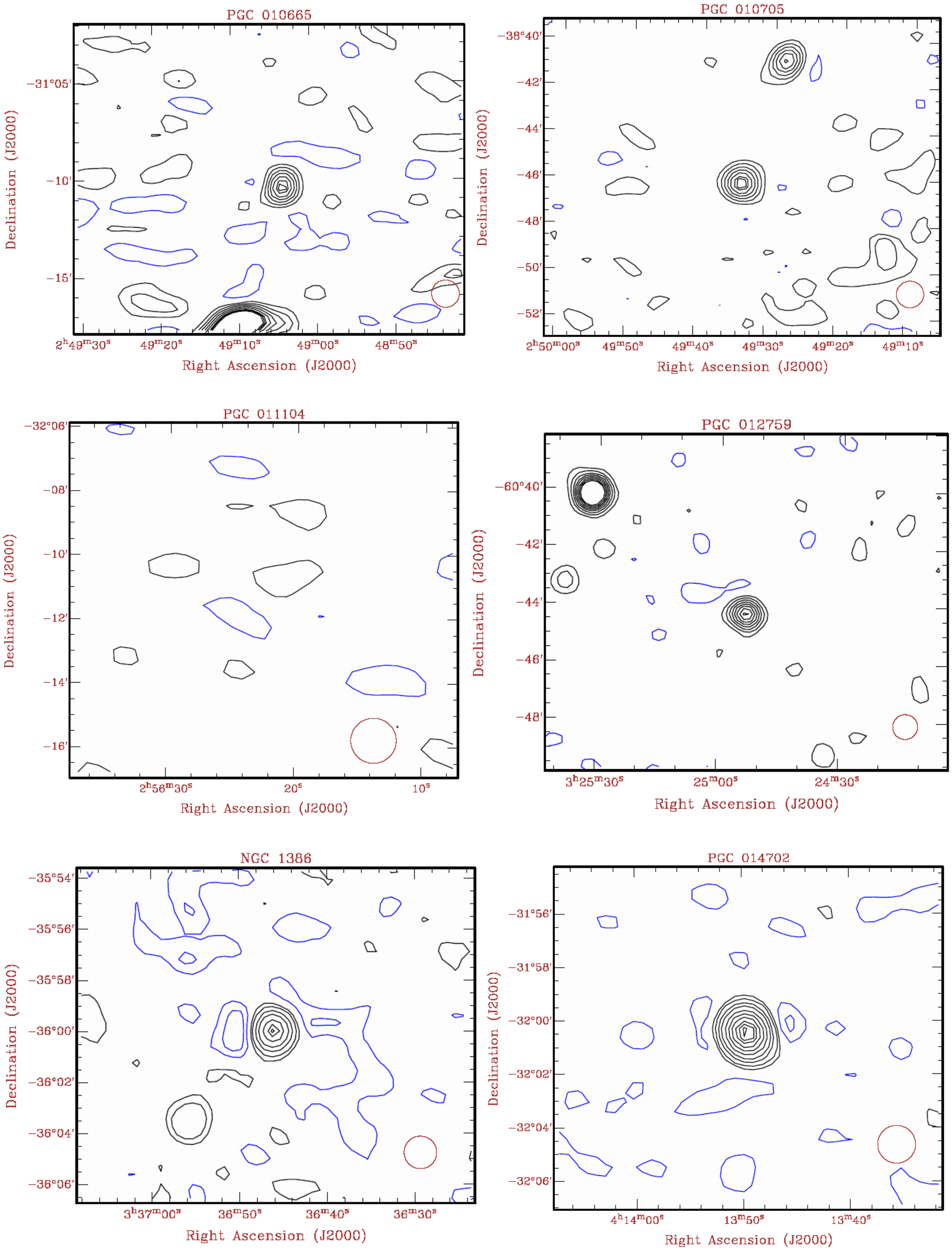

FIG. A.3. - 843 MHz maps from SUMSS. See Table A.1 for contour levels.

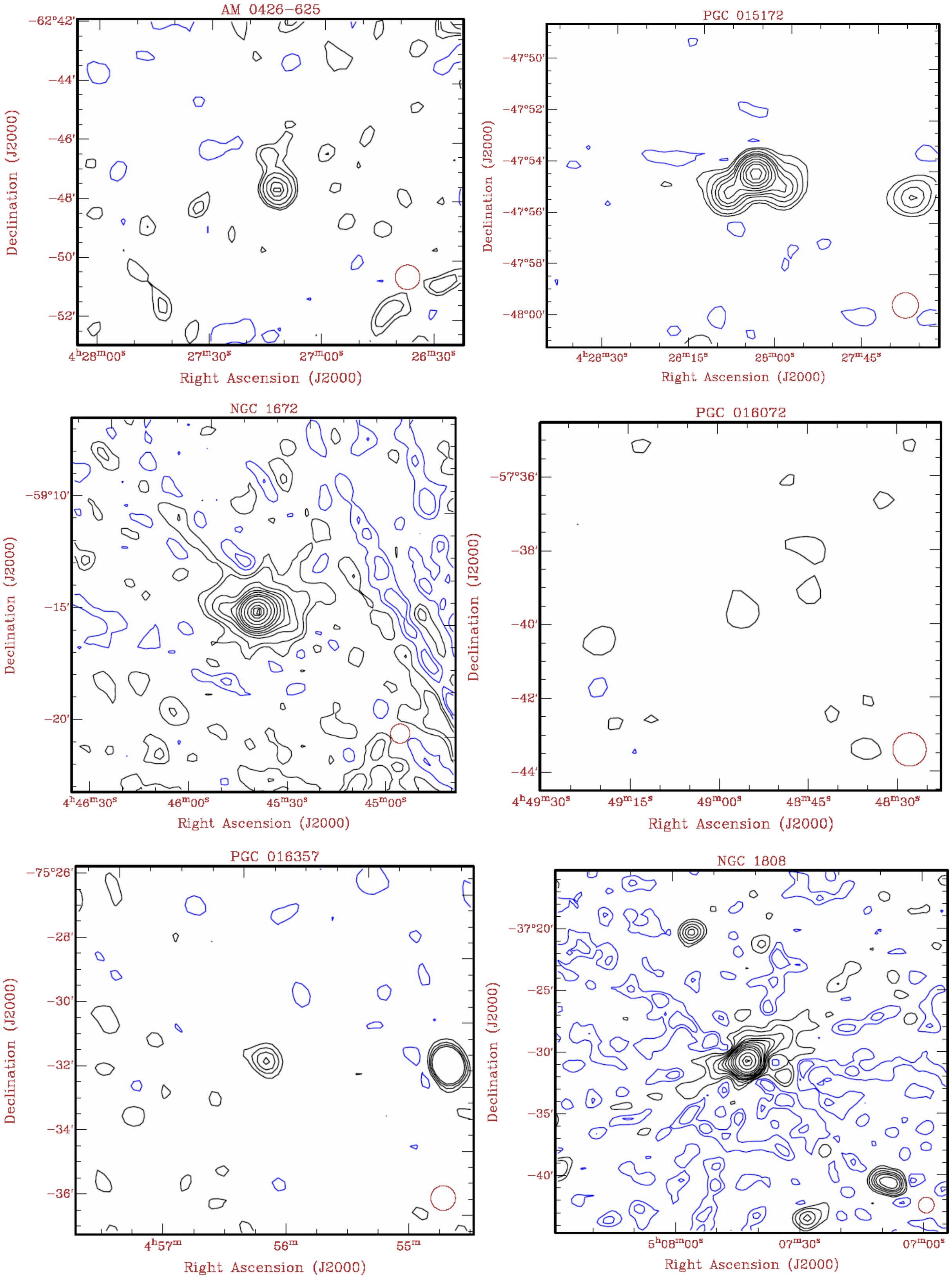

FIG. A.4. - 843 MHz maps from SUMSS. See Table A.1 for contour levels.

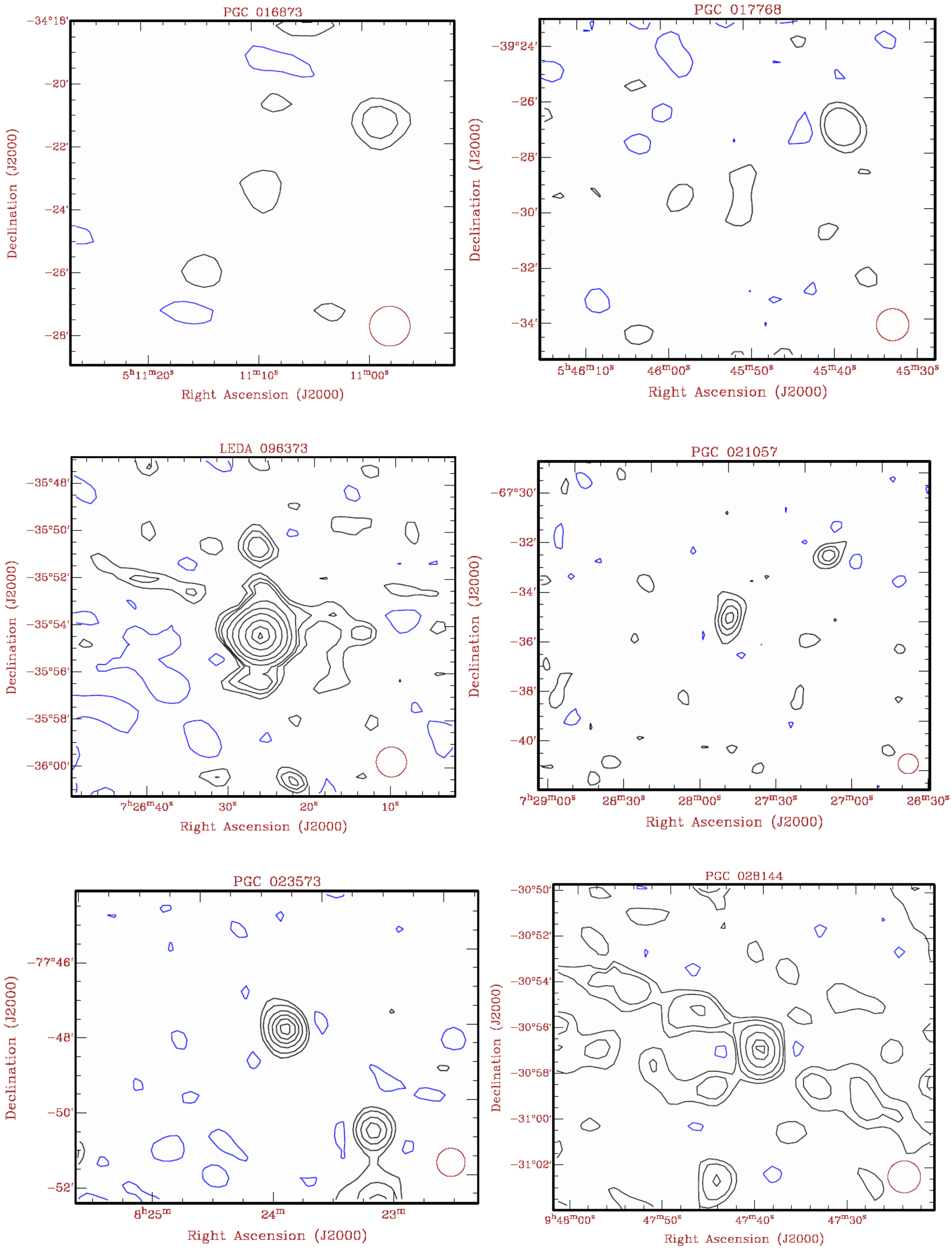

FIG. A.5. - 843 MHz maps from SUMSS. See Table A.1 for contour levels.

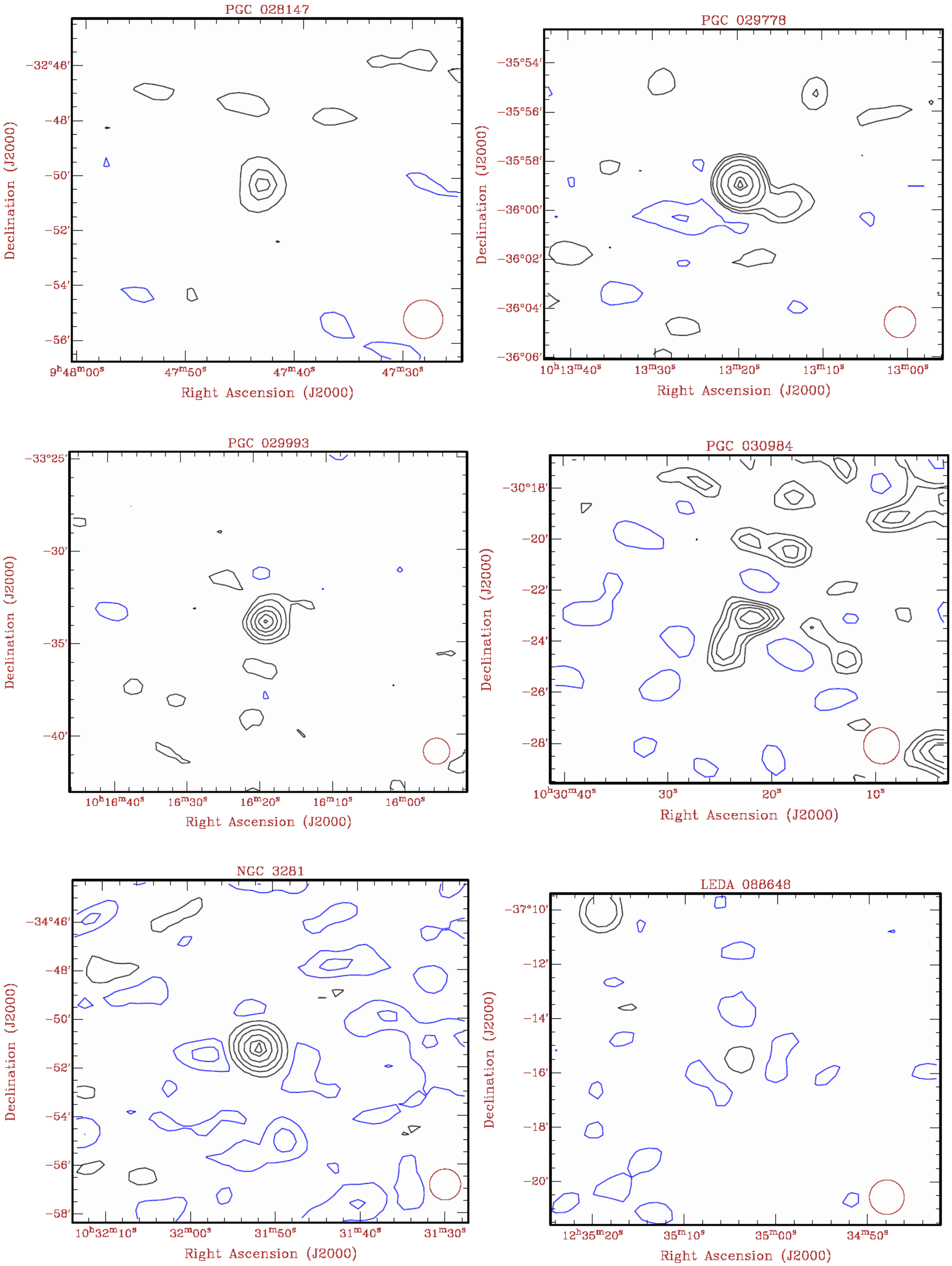

FIG. A.6. - 843 MHz maps from SUMSS. See Table A.1 for contour levels.

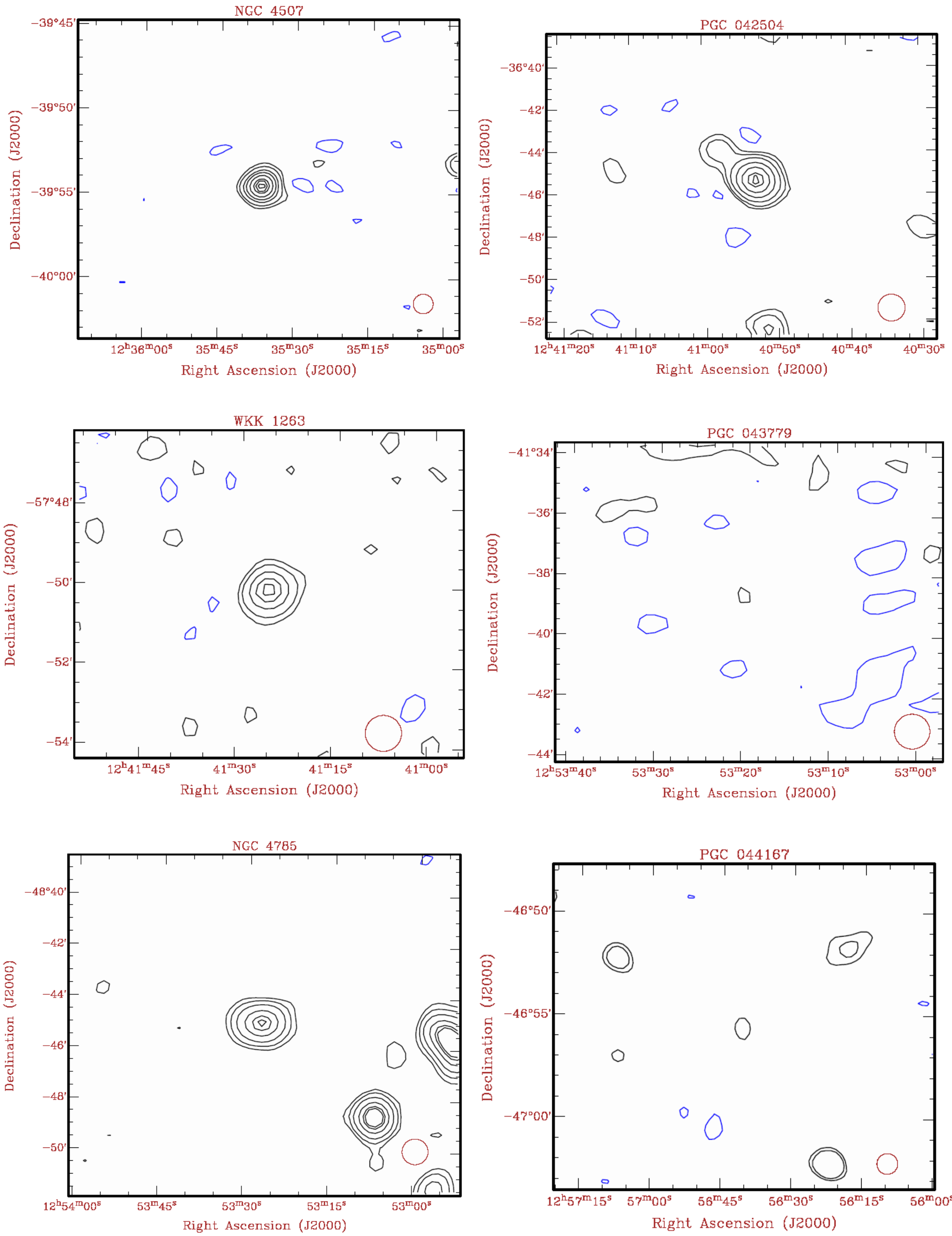

FIG. A.7. - 843 MHz maps from SUMSS. See Table A.1 for contour levels.

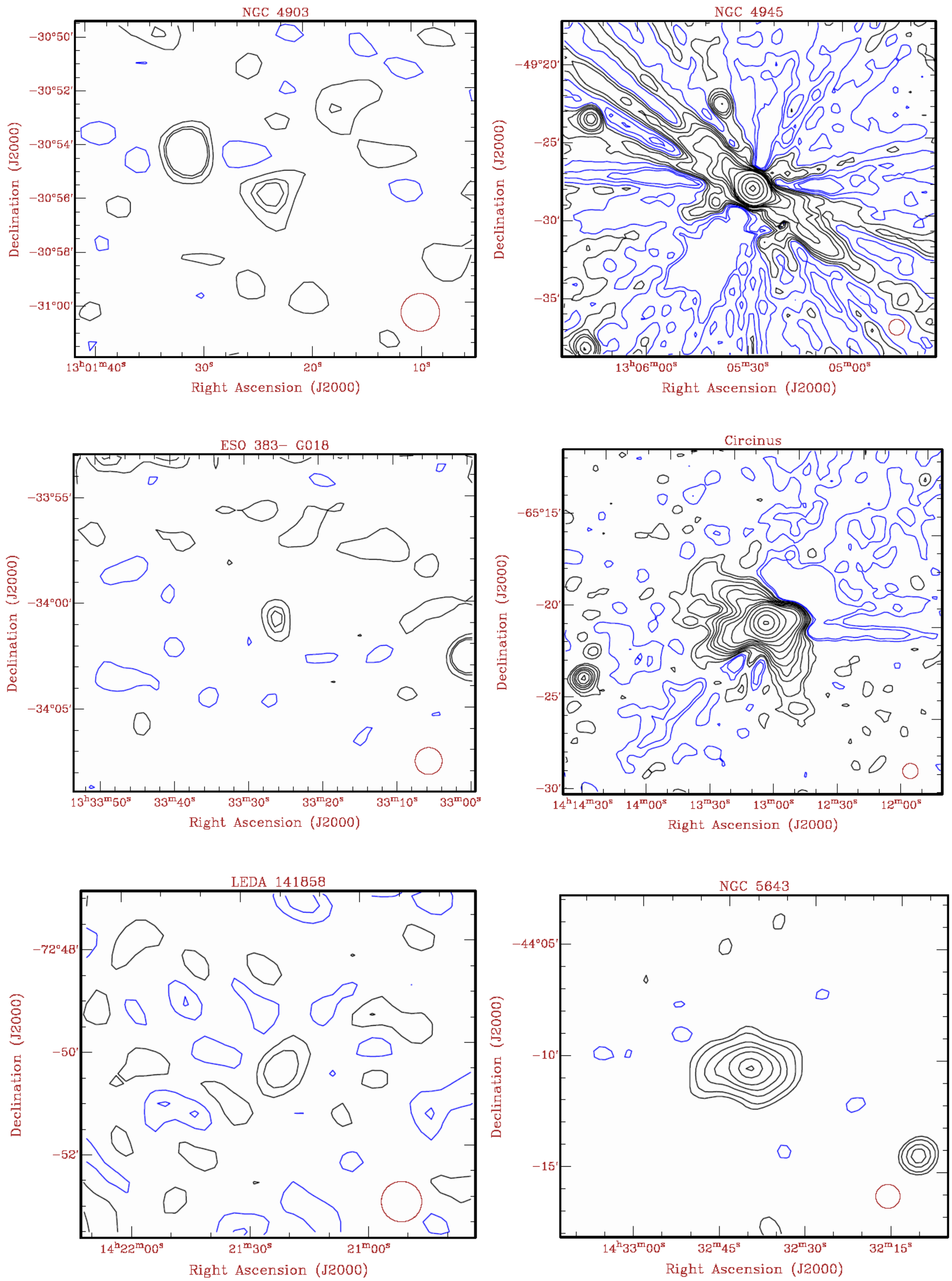

FIG. A.8. - 843 MHz maps from SUMSS. See Table A.1 for contour levels.

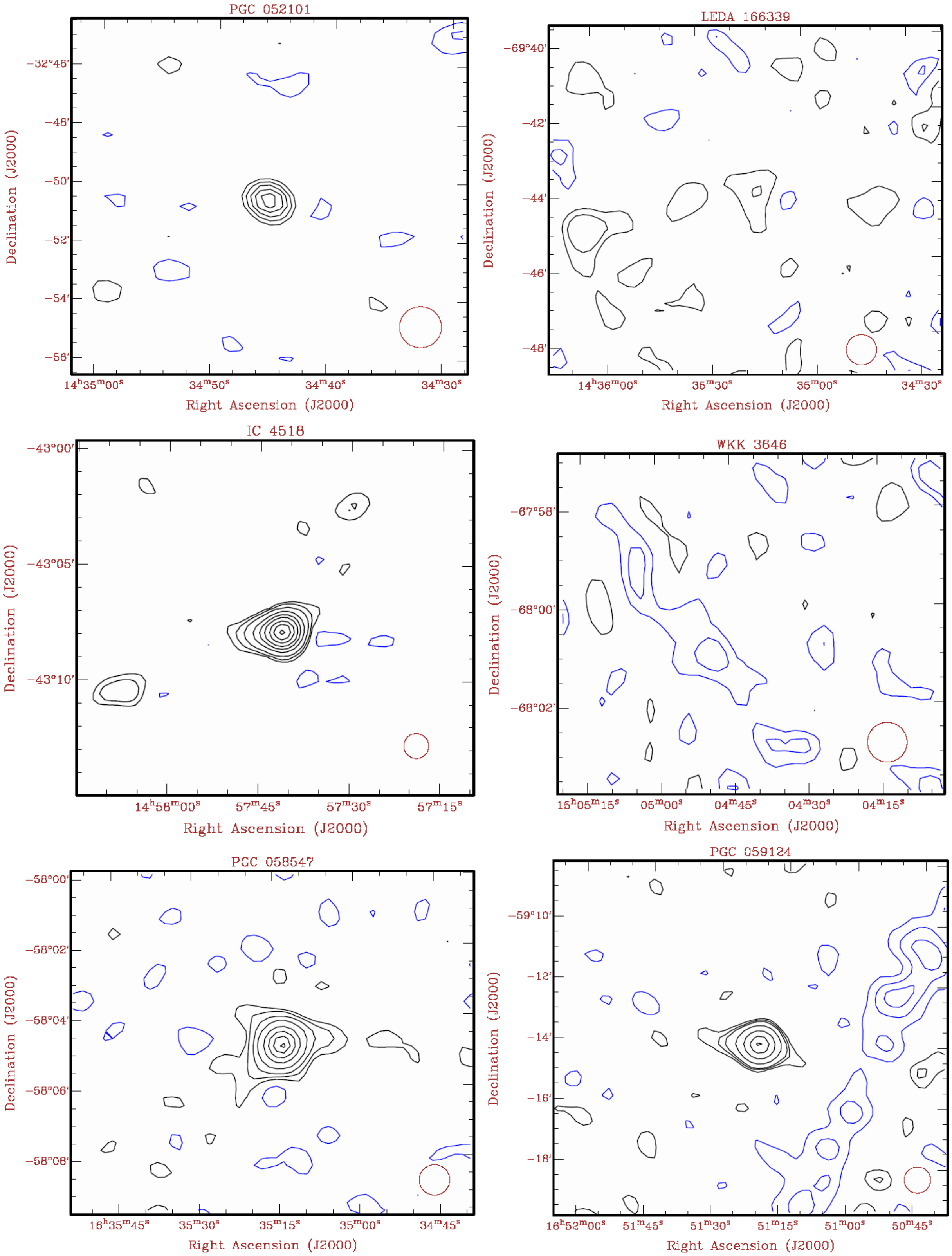

FIG. A.9. - 843 MHz maps from SUMSS. See Table A.1 for contour levels.

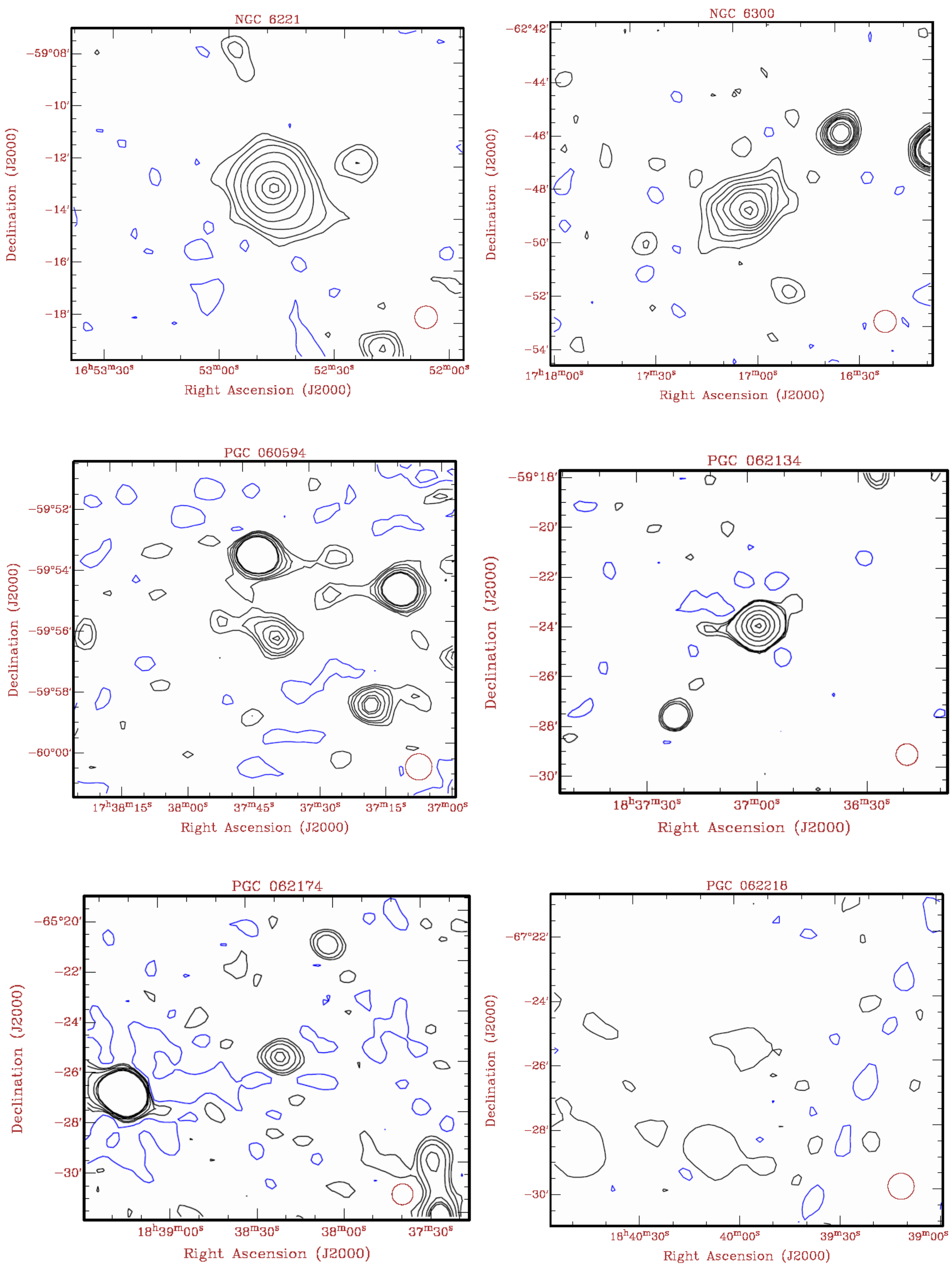

FIG. A.10. - 843 MHz maps from SUMSS. See Table A.1 for contour levels.

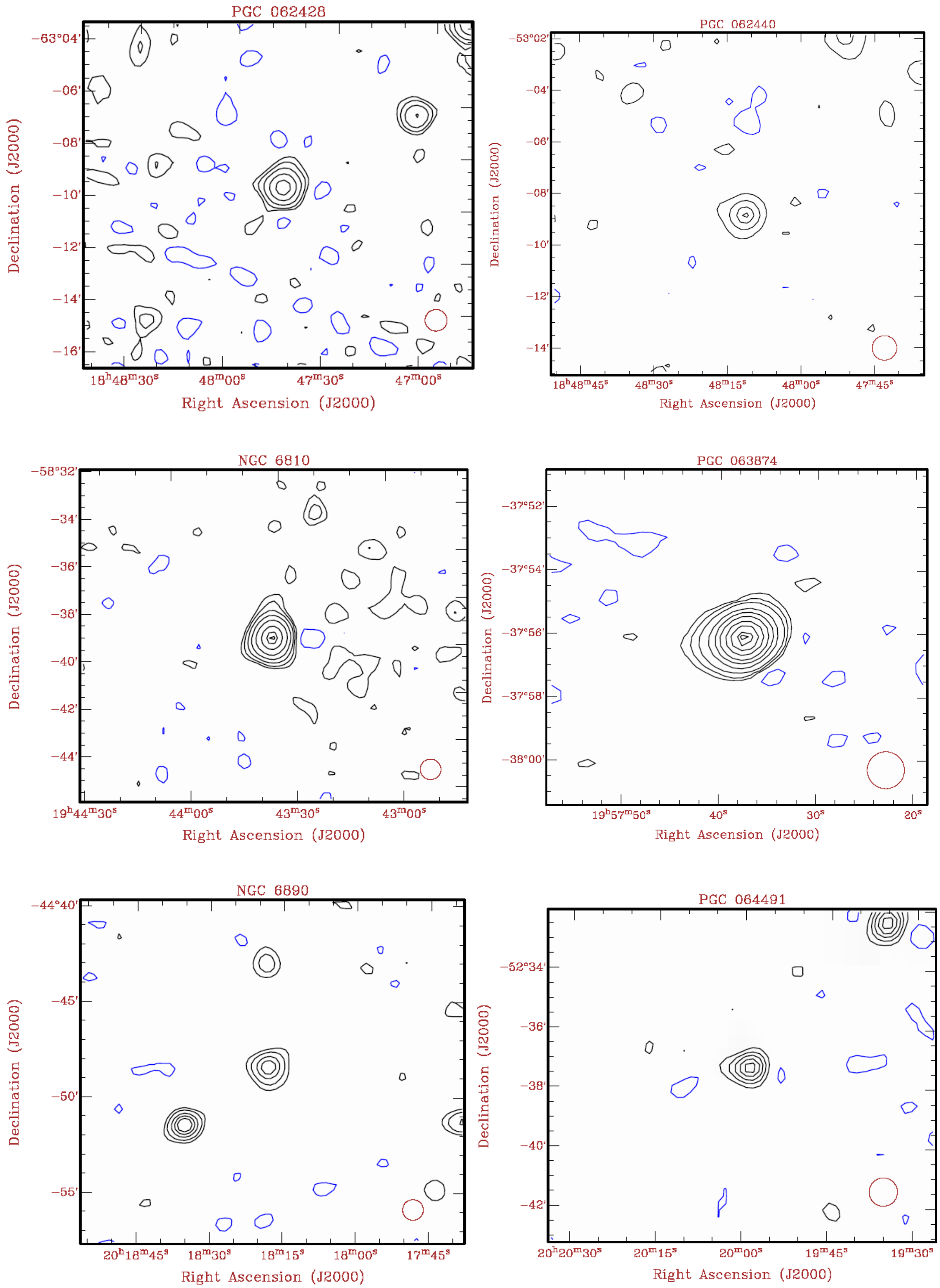

FIG. A.11. - 843 MHz maps from SUMSS. See Table A.1 for contour levels.

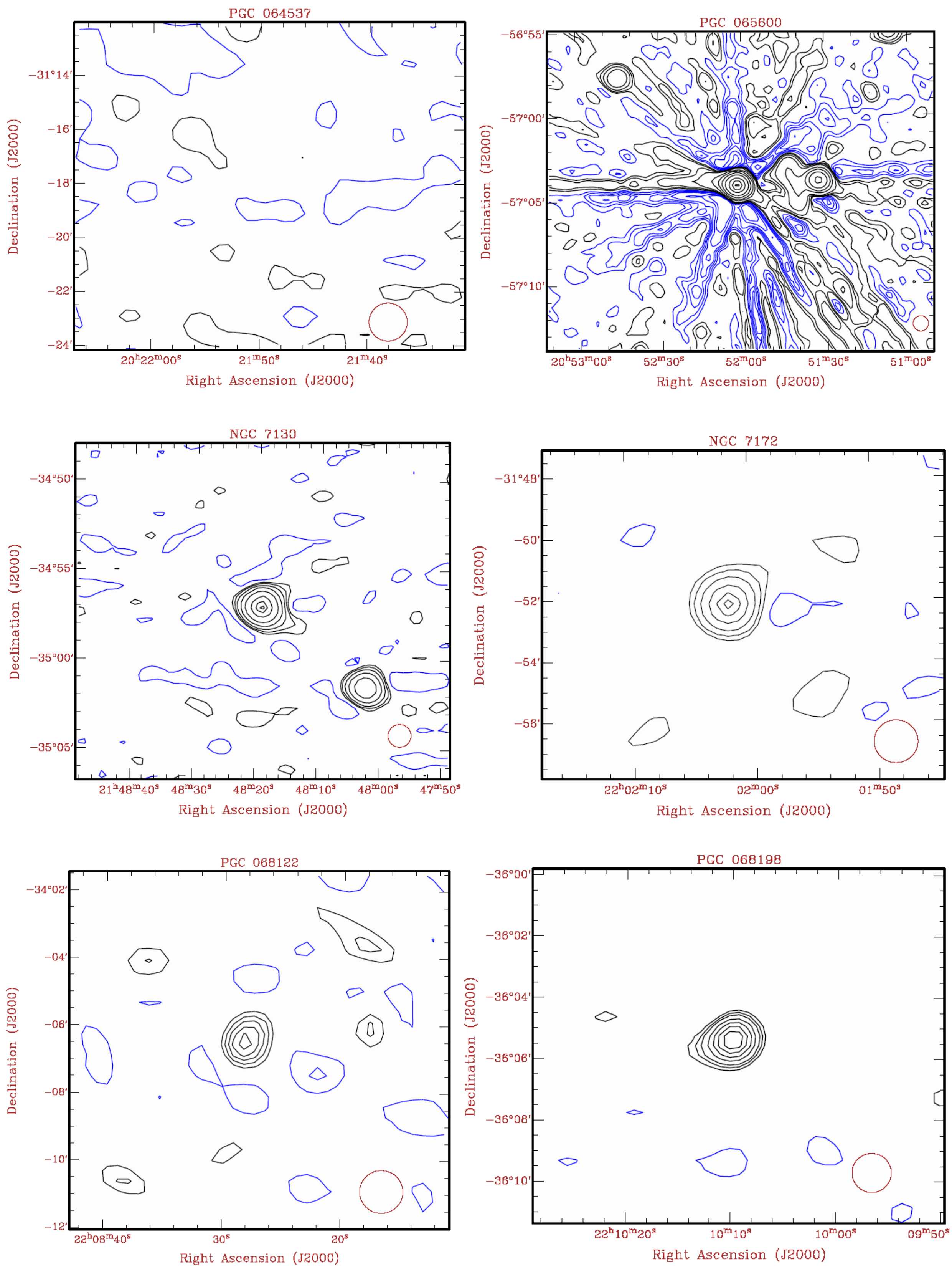

FIG. A.12. - 843 MHz maps from SUMSS. See Table A.1 for contour levels.

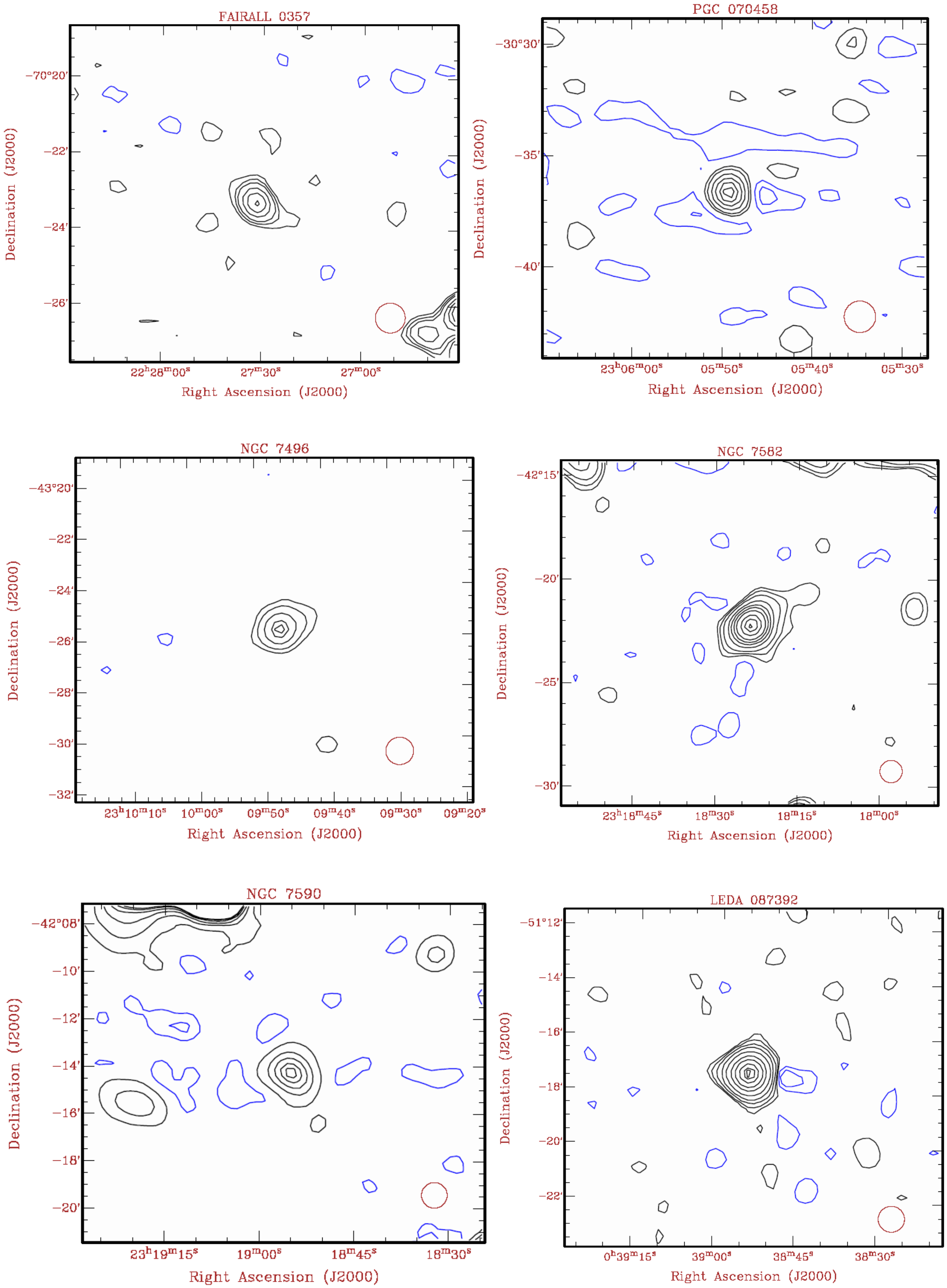

FIG. A.13. - 843 MHz maps from SUMSS. See Table A.1 for contour levels.

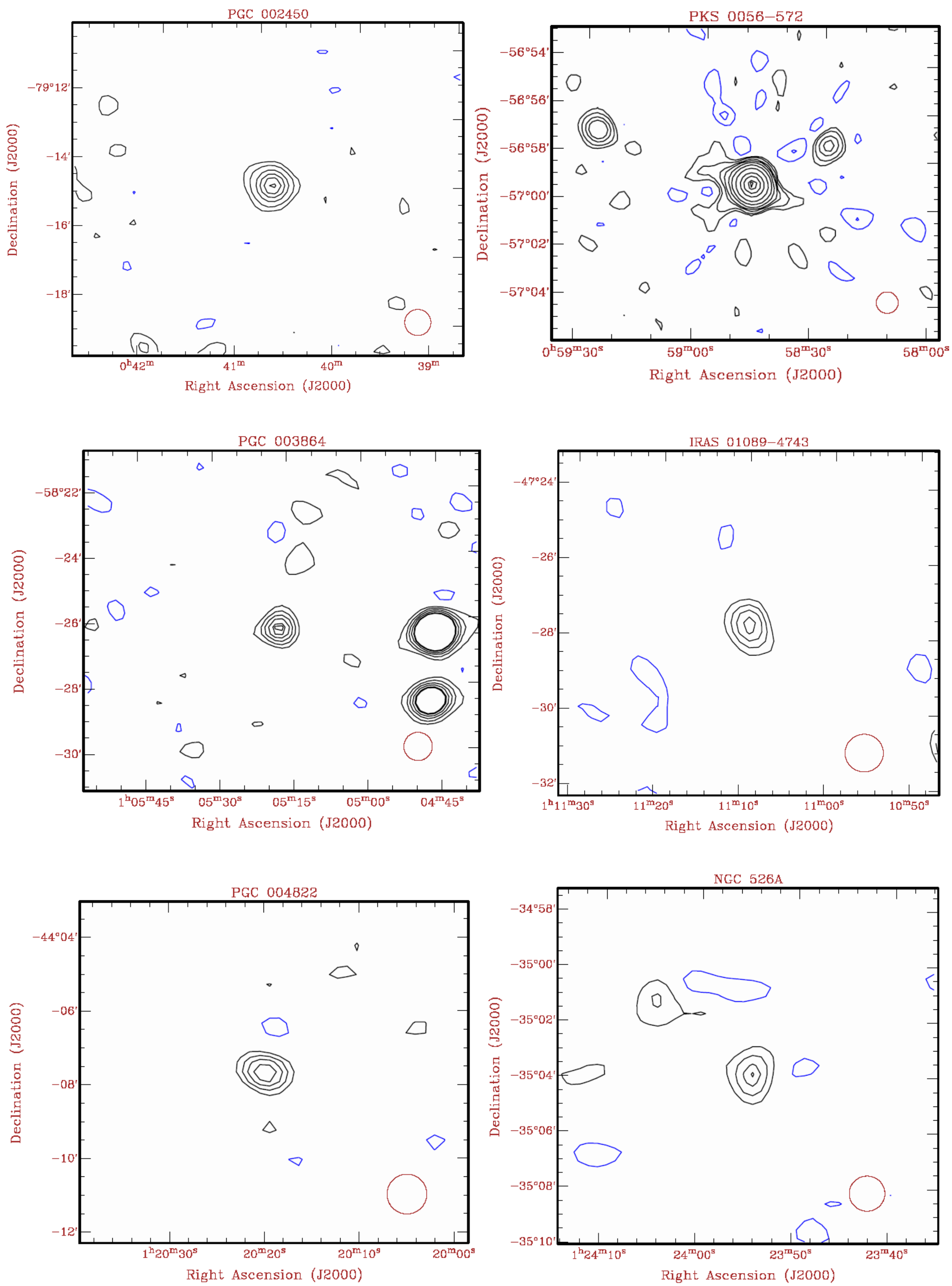

FIG. A.14. - 843 MHz maps from SUMSS. See Table A.2 for contour levels.

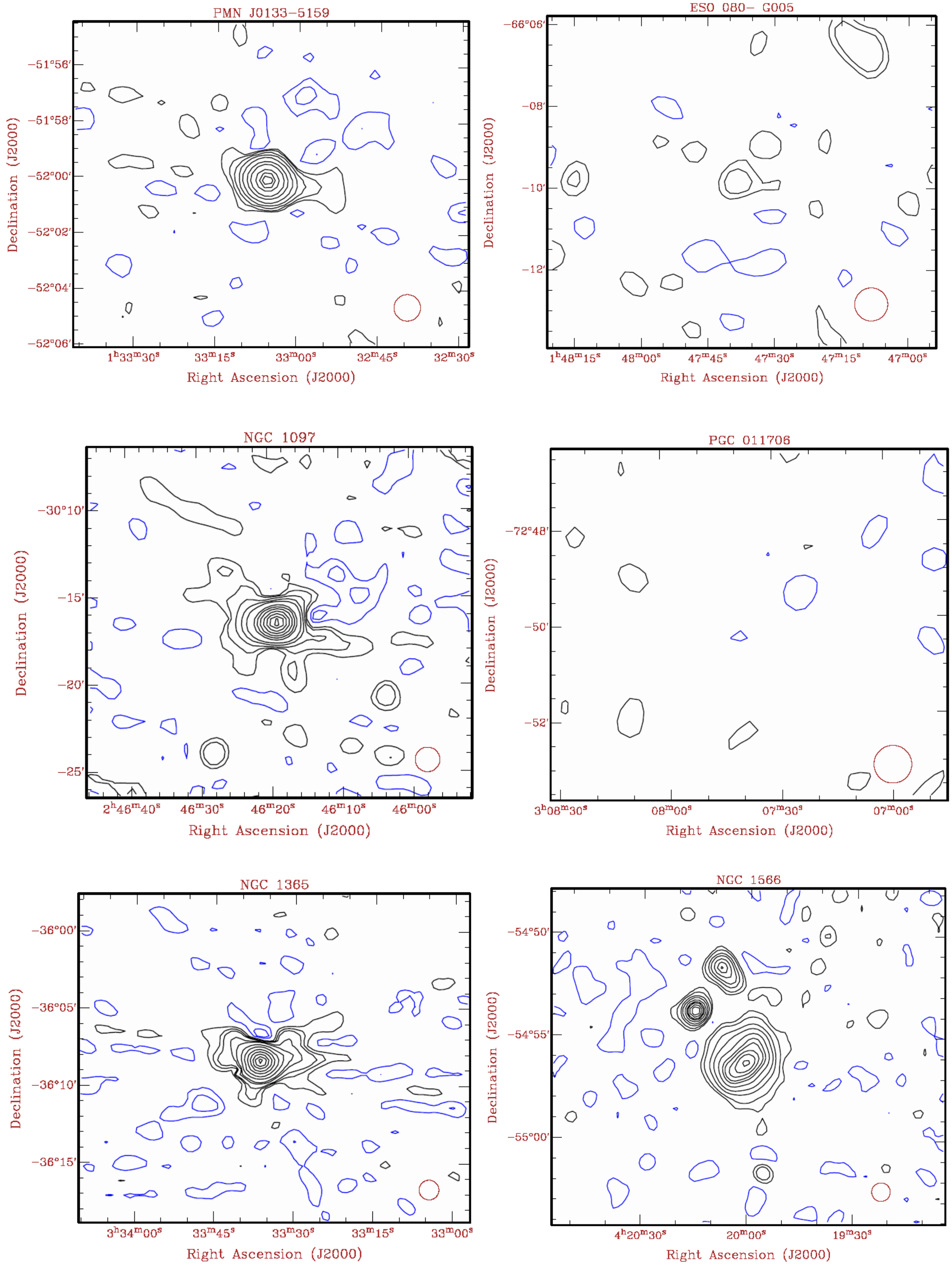

FIG. A.15. - 843 MHz maps from SUMSS. See Table A.2 for contour levels.

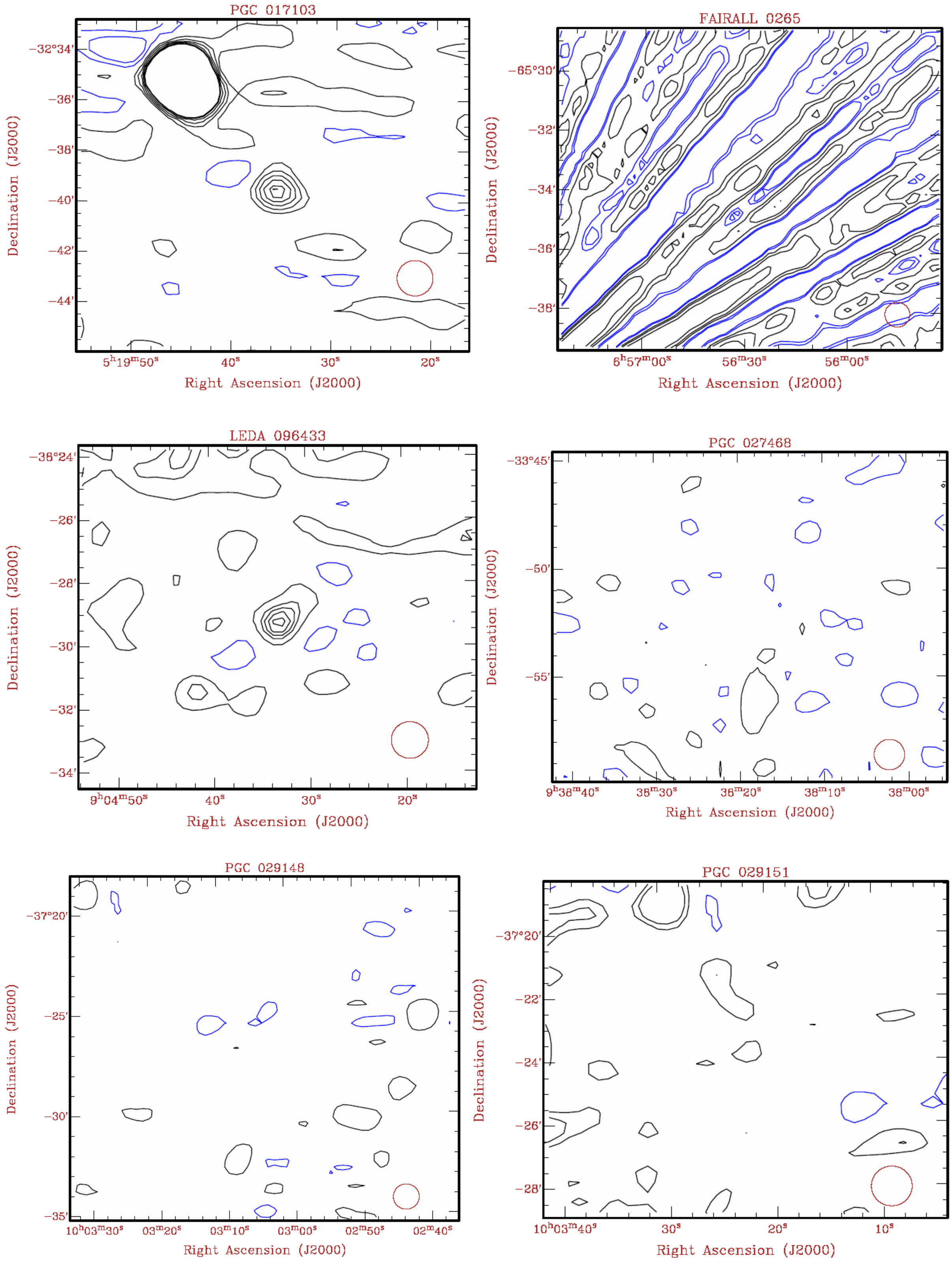

FIG. A.16. - 843 MHz maps from SUMSS. See Table A.2 for contour levels.

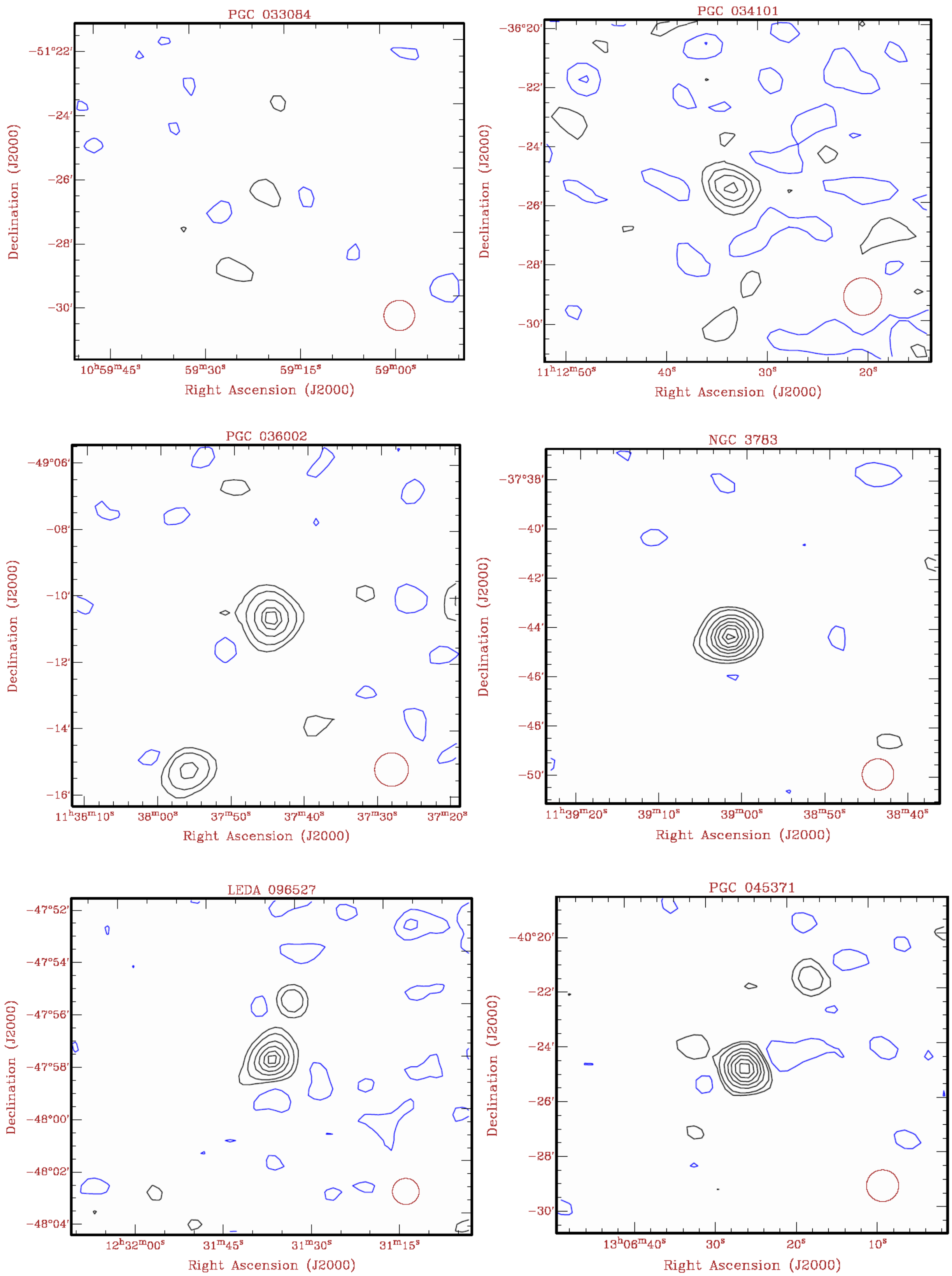

FIG. A.17. - 843 MHz maps from SUMSS. See Table A.2 for contour levels.

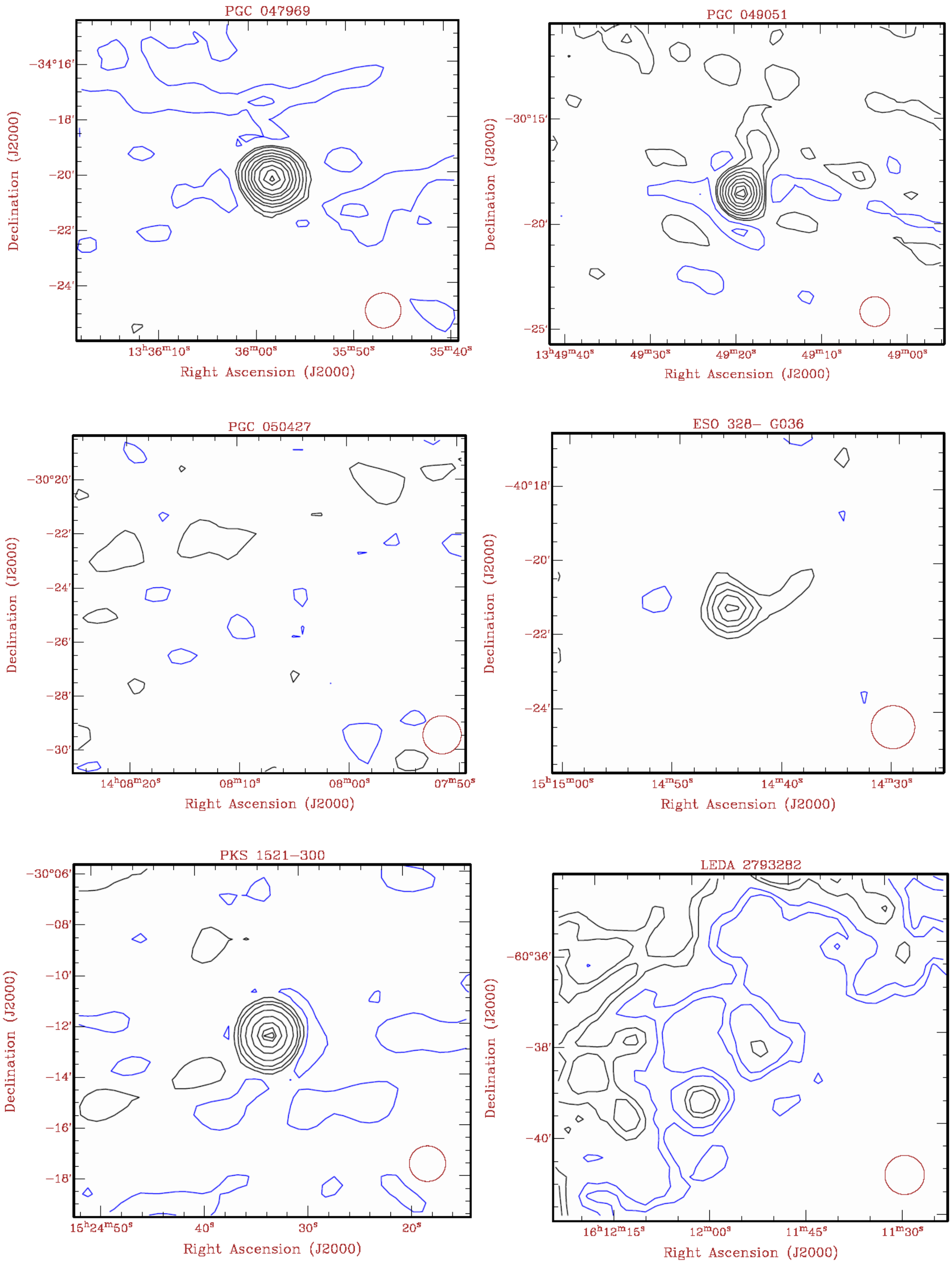

FIG. A.18. - 843 MHz maps from SUMSS. See Table A.2 for contour levels.

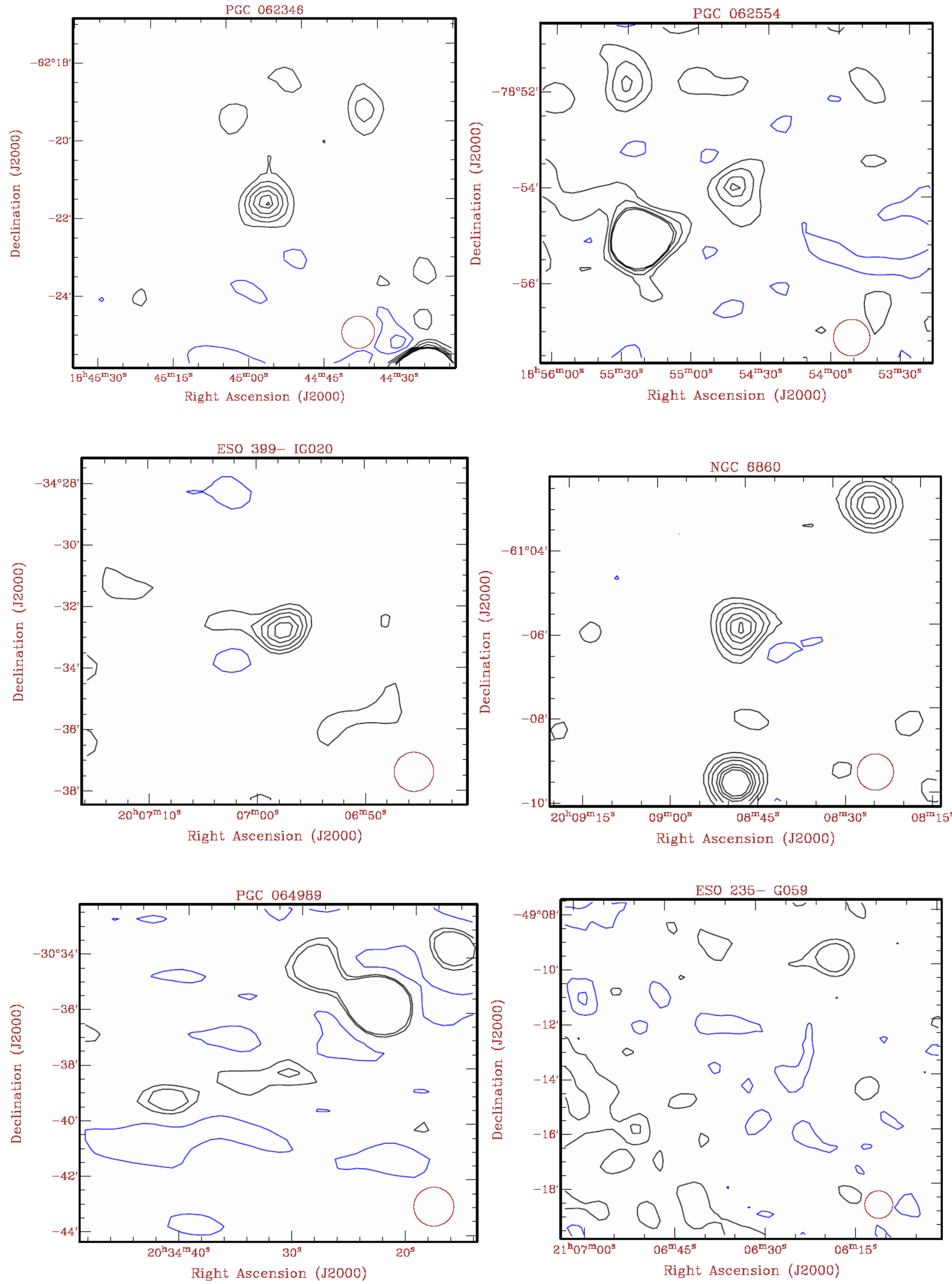

FIG. A.19. - 843 MHz maps from SUMSS. See Table A.2 for contour levels.

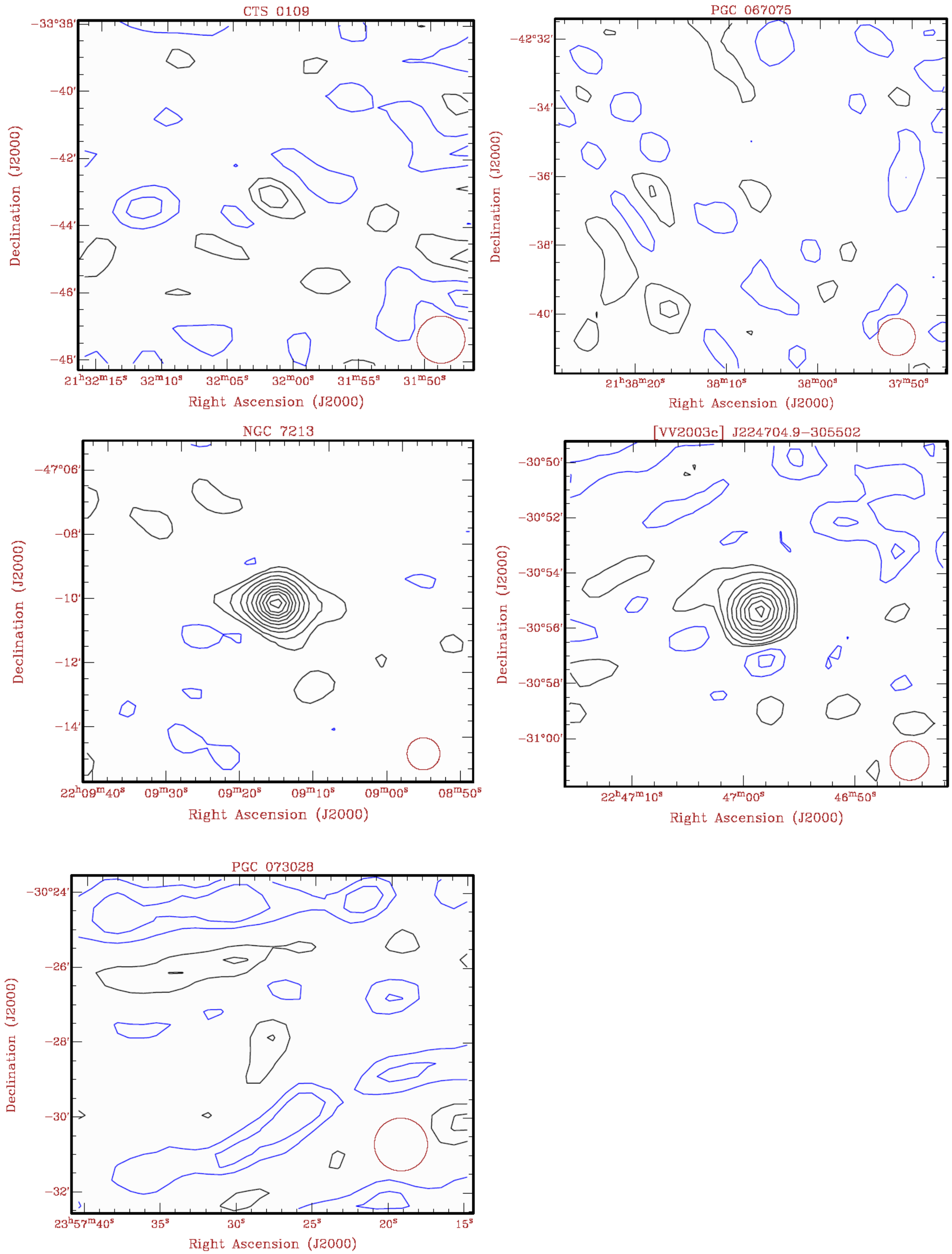

FIG. A.20. - 843 MHz maps from SUMSS. See Table A.2 for contour level

APPENDIX B - Scanpi Results for *IRAS* Upper Limits

Scanpi Results for Sy2

	kpc/"	µm	SFR	LBFR	SERLBF	Scan	Sigma	SNR	Peak	Miss	Amp	S (Jy)	Corr.		
LEDA 087391	0.579	12	1.00	5	1.05	1001	14.27	9.86	0.18	-0.05	0.17	0.17	0.9715		
		25	1.00	5	1.05	1001	36.21	8.88	0.41	-0.01	0.38	0.41	0.9954		
		60	1.00	5	1.05	1002	67.79	13.94	1.00	-0.02	1.01	0.99	0.9984		
		100	1.90	10	1.95	1002	24.25	66.82	1.59	0.22	1.72	1.26	0.9746		
LEDA 093365	0.516	12	1.00	30	1.05	1003	26.71	4.60	0.16	0.62	0.05	0.12	0.6987		
		25	1.00	5	1.05	1003	11.13	2.62	0.04	-0.23	0.02	0.02	0.5299		
		60	1.20	10	1.25	1001	38.77	2.42	0.10	0.74	0.18	0.13	0.9822	^	
		100	1.50	30	1.6	1001	133.96	2.32	0.30	1.33	0.30	0.41	0.9947		
NGC 0824	0.389	12	1.00	10	1.05	1002	29.82	3.25	0.13	-0.23	0.10	0.23	0.8840		
		25	1.00	5	1.05	1001	27.20	8.41	0.29	0.07	0.23	0.32	0.9675	^	
		60	1.20	5	1.25	1002	104.05	3.33	0.37	0.29	-0.25	0.38	0.9742		
		100	2.25	10	2.3	1001	108.47	8.44	0.90	-0.27	0.85	0.81	0.9975		
AM 0426-625	0.367	12	1.00	20	1.05	1001	33.85	2.20	0.10	0.12	0.10	0.15	0.9152		
		25	1.00	8	1.05	999	27.06	3.76	0.13	-0.8	0.06	0.19	0.8009		
		60	2.00	8	2.1	1002	45.04	2.76	0.13	2.24	0.17	0.08	0.7485		
		100	2.25	5	2.3	1002	81.80	5.73	0.46	0.94	0.40	0.32	0.9842	^	
PGC 016072	0.457	12	1.00	30	1.1	1003	20.46	4.51	0.12	0.54	0.11	0.12	0.9426		
		25	1.00	5	1.05	1003	7.08	3.93	0.04	0.81	0.02	0.04	0.6756		
		60	1.00	5	1.05	1001	33.00	4.59	0.16	0.09	0.22	0.13	0.9551	^	
		100	2.50	5	2.6	1003	23.85	12.97	0.30	-0.49	0.27	0.32	0.9720		
PGC 028147	0.189	12	1.00	2	1.05	1001	24.85	5.89	0.19	0.3	0.19	0.21	0.8770		
		25	1.25	20	1.3	1002	64.81	4.60	0.38	0.06	0.42	0.35	0.9661	^	
		60	2.25	20	2.3	1002	78.09	18.97	1.57	0.07	1.58	1.59	0.9974		
		100	2.75	5	2.8	1003	273.55	10.55	2.83	0.04	2.66	2.52	0.9954		
WKK 1263	0.486	12	1.00	3	1.05	1002	26.11	3.21	0.11	-0.28	0.06	0.05	0.6855		
		25	1.00	3	1.05	1003	17.65	8.96	0.20	0.1	0.21	0.17	0.9665	^	
		60	1.10	4	1.2	1003	168.76	2.07	0.37	0.15	0.36	0.29	0.9973		
		100	1.50	6	1.55	1002	1934.48	0.00	1.82	-99	-99.00	1.17	-99.0000		*
PGC 044167	0.336	12	1.00	20	1.05	1002	29.67	3.82	0.15	0.36	0.08	0.25	0.8332		
		25	1.25	20	1.3	1002	42.57	2.34	0.13	-0.08	0.06	0.13	0.6612		
		60	1.20	4	1.25	1002	47.51	3.31	0.17	0	0.20	0.14	0.9573	^	
		100	1.50	5	1.6	1003	320.66	2.22	0.70	0.1	0.92	0.44	0.9767		
LEDA 166339	0.513	12	1.00	3	1.05	1003	17.23	4.47	0.10	-0.02	0.08	0.11	0.9415		
		25	1.00	20	1.05	1003	30.45	4.30	0.17	0.01	0.14	0.21	0.9315		
		60	1.25	3	1.3	1002	35.87	4.30	0.16	0.04	0.16	0.12	0.9761	^	
		100	1.50	1.75	1.55	1002	13.83	33.38	0.45	0.26	0.44	0.20	0.9255		*
WKK 3646	0.298	12	1.25	10	1.3	999	31.38	3.37	0.14	1.01	0.09	0.24	0.9249		
		25	1.00	18	1.05	1003	37.32	2.89	0.14	-0.06	0.05	0.20	0.7717		
		60	1.25	2	1.3	1001	27.48	5.69	0.17	0.18	0.18	0.18	0.9696	^	
		100	1.75	4	1.8	1002	195.57	3.57	0.68	0.67	0.42	0.28	0.9579		

Scanpi Results for Sy1

	kpc/"	µm	SFR	LBFR	SERLBF	Scan	Sigma	SNR	Peak	Miss	Amp	S (Jy)	Corr.		
PKS 0056-572	0.361	12	1.00	1.25	1	1002	8.56	12.35	0.14	-0.43	0.08	0.10	0.8538		
		25	1.00	3	1	1001	39.09	3.67	0.18	0.41	0.12	0.20	0.8679		
		60	1.00	16	1.05	1001	48.40	4.77	0.24	0.12	0.24	0.23	0.9856	^	
		100	1.30	3	1.35	1003	107.01	4.94	0.52	0.34	0.49	0.31	0.9739		
PMN J0133-5159	0.4	12	1.00			1002	34.20	2.95	0.13	0.44	0.10	0.17	0.7752		
		25	1.00	8	1.05	1002	33.21	2.27	0.10	-0.58	0.08	0.03	0.7672		
		60	1.25	20	1.3	1003	52.77	2.77	0.16	-0.25	0.13	0.13	0.9537	^	
		100	1.80	5	1.85	1001	105.38	6.74	0.70	-0.12	0.75	0.58	0.9968		
ESO 080- G 005	0.534	12	1.00	5	1.05	1003	20.60	0.00	0.03	-99	-99.00	0.03	-99.0000		
		25	1.00	3	1.05	1001	17.29	7.00	0.15	-0.16	0.13	0.13	0.9780	^	
		60	1.00	5	1.05	1003	43.50	2.65	0.12	0.08	0.09	0.15	0.9560		
		100	1.75	5	1.8	1003	91.45	3.51	0.31	0.09	0.42	0.19	0.9729		
PGC 011706	0.554	12	1.00	2	1.05	1003	9.62	4.03	0.05	0	0.05	0.03	0.7135		
		25	1.00	5	1.05	999	23.51	4.31	0.13	0.89	0.11	0.09	0.9085		
		60	1.00	2	1.05	1001	16.48	6.64	0.12	-0.08	0.11	0.10	0.9930	^	
		100	1.50	10	1.55	1001	98.38	2.79	0.27	-0.24	0.24	0.21	0.9970		
PGC 029148	0.47	12	1.00	3	1.05	1003	31.51	2.41	0.10	0.89	0.03	0.17	0.6108		
		25	1.00	2	1.05	1001	16.96	3.41	0.07	-0.17	0.05	0.01	0.5559		
		60	1.00	2	1.05	1001	20.96	7.98	0.18	0.8	0.24	0.15	0.9181		
		100	1.75	3	1.8	1002	39.85	3.84	0.15	1.25	0.19	0.07	0.9478	^	*
PGC 029151	0.471	12	1.00	2	1.05	1001	13.61	4.33	0.08	0.06	0.04	0.05	0.6008		
		25				1001	13.98	4.05	0.07	-0.36	0.04	0.07	0.7886		
		60	1.20	4	1.25	1001	31.24	3.80	0.13	-0.27	0.14	0.12	0.9951	^	
		100	2.00	8	2.05	1001	44.95	9.19	0.40	-0.38	0.38	0.27	0.9794		
PGC 050427	0.469	12	1.00	2	1.05	1003	25.41	3.67	0.12	0.09	0.07	0.10	0.6967		
		25	1.00	2	1.05	1001	28.32	3.44	0.12	0.13	0.08	0.11	0.9040		
		60	1.00	4	1.05	1003	24.50	4.02	0.10	0.02	0.10	0.18	0.9438	^	
		100	1.95	14	2	1003	134.87	5.85	0.77	0.79	0.94	0.56	0.9682		
ESO 328- G036	0.472	12	1.00	20	1.05	1002	95.33	3.93	0.49	-0.91	0.18	0.97	0.7716		
		25	1.00	1.3	1.05	1003	18.22	4.66	0.11	0.28	0.06	0.06	0.6658		
		60	1.00	3	1.05	1003	28.92	6.10	0.19	0.04	0.18	0.17	0.9949	^	
		100	1.50	5	1.55	1003	348.51	2.58	0.88	0.29	0.92	0.56	0.9973		
PKS 1521-300	0.392	12	1.00	1.3	1.05	999	2.71	24.59	0.09	0.33	0.06	0.08	0.8689		
		25	1.00	3	1.05	1002	21.01	5.02	0.13	-0.64	0.10	0.05	0.8383		
		60	1.00	2.5	1.05	1001	9.72	9.65	0.10	-0.16	0.07	0.09	0.9615	^	
		100	1.50	20	1.55	1002	1.53	21.38	0.33	-0.3	0.50	0.13	0.8805		*
LEDA 2793282	0.314	12	1.00	3.15	1.05	1003	19.25	4.67	0.12	0.15	0.11	0.11	0.9764		
		25	1.00	2.75	1.05	1001	27.88	3.58	0.13	-0.13	0.09	0.09	0.9410		
		60	1.25	2	1.3	1001	11.42	12.85	0.16	0.06	0.17	0.14	0.9971	^	
		100	2.00	9	2.1	1003	455.90	2.15	0.96	1.59	0.94	0.90	0.9983		
CTS 0109	0.579	12	1.00	30	1	1001	29.50	4.14	0.16	0.02	0.13	0.13	0.9520		
		25	1.00	30	1	1003	21.89	4.36	0.12	0.05	0.11	0.10	0.9673	^	
		60	1.30	5	1.35	1001	39.35	4.67	0.20	0.31	0.22	0.18	0.9955		
		100	2.25	7	2.3	1003	96.75	8.77	0.83	0.7	0.72	0.67	0.9848		
PGC 067075	0.374	12	1.00	1.5	1.05	1001	22.45	6.97	0.20	-0.02	0.15	0.18	0.9643		
		25	1.00	1.5	1.05	1002	24.81	4.09	0.13	-0.45	0.10	0.12	0.9166		
		60	1.00	1.35	1.05	1001	7.96	15.16	0.13	0	0.14	0.09	0.9750	^	
		100	1.50	30	1.55	1003	109.44	2.02	0.22	-0.56	0.58	0.14	0.8917		
[VV2003c] J224704.9-305502	0.202	12	1.00	5	1.05	1001	21.54	2.76	0.08	-0.39	0.07	0.02	0.7762		
		25	1.00	4	1.05	999	28.55	2.06	0.08	0.7	-0.21	0.01	0.6486		
		60	1.00	5	1.05	1001	34.71	3.89	0.14	-0.15	0.20	0.07	0.9176	^	
		100	1.00	1.4	1.05	1003	6.57	26.21	0.17	-1.39	0.75	0.06	0.8112		

APPENDIX C – IR luminosities, errors, and log errors for sample objects

	Seyfert 2 - IR Luminosity Values by Band with Associated Errors (W/Hz)																				
Name	J	error δ	log(δ)	H	error δ	log(δ)	K	error δ	log(δ)	12 µm	error δ	log(δ)	25 µm	error δ	log(δ)	60 µm	error δ	log(δ)	100 µm	error δ	log(δ)
LEDA 087391	1.10E+22	8.75E+20	0.03	1.63E+22	1.41E+21	0.04	2.05E+22	1.56E+21	0.03	3.25E+23	<		7.85E+23	<		1.90E+24	<		2.41E+24	<	
NGC 0424	3.00E+22	4.75E+20	0.01	3.90E+22	7.30E+20	0.01	4.47E+22	8.71E+20	0.01	3.31E+23	1.65E+22	0.02	5.22E+23	2.61E+22	0.02	5.39E+23	3.78E+22	0.03	5.47E+23	4.93E+22	0.04
LEDA 093365	1.59E+21	<		2.54E+21	<		5.11E+20	<		2.71E+23	<		2.71E+23	<		2.71E+23	<		4.51E+23	<	
PGC 004440	3.35E+22	4.65E+20	0.01	3.97E+22	6.63E+20	0.01	3.32E+22	8.37E+20	0.01	6.36E+22	<		8.45E+22	1.61E+22	0.08	8.58E+23	6.01E+22	0.03	2.32E+24	1.39E+23	0.03
NGC 0454	8.35E+19	<		1.12E+20	<		3.85E+19	<		6.84E+22	1.64E+22	0.10	1.34E+23	1.21E+22	0.04	4.74E+23	5.69E+22	0.05	9.06E+23	7.25E+22	0.03
PGC 004569	4.76E+22	1.06E+21	0.01	5.74E+22	1.34E+21	0.01	4.82E+22	1.72E+21	0.02	1.49E+23	<		1.38E+23	3.73E+22	0.12	8.44E+23	6.75E+22	0.03	2.07E+24	2.07E+23	0.04
PGC 005696	3.76E+22	7.02E+20	0.01	4.48E+22	1.13E+21	0.01	4.20E+22	1.21E+21	0.01	1.08E+23	2.69E+22	0.11	1.78E+23	3.03E+22	0.07	1.29E+24	1.41E+23	0.05	3.43E+24	2.06E+23	0.03
PGC 006078	7.70E+22	1.44E+21	0.01	1.05E+23	2.55E+21	0.01	9.09E+22	2.80E+21	0.01	2.44E+23	<		2.34E+23	5.63E+22	0.10	9.32E+23	9.32E+22	0.04	3.11E+24	2.80E+23	0.04
PGC 006351	7.86E+22	1.90E+21	0.01	9.39E+22	2.46E+21	0.01	8.57E+22	3.22E+21	0.02	2.85E+23	<		2.17E+23	6.07E+22	0.12	1.93E+24	1.55E+23	0.03	3.46E+24	3.46E+23	0.04
PGC 008012	4.90E+22	1.46E+21	0.01	6.05E+22	1.70E+21	0.01	5.27E+22	2.23E+21	0.02	8.32E+22	1.91E+22	0.10	1.67E+23	1.84E+22	0.05	7.62E+23	3.81E+22	0.02	2.58E+24	<	
NGC 0824	3.34E+22	1.45E+21	0.02	4.21E+22	1.66E+21	0.02	3.81E+22	2.28E+21	0.03	2.64E+22	<		2.64E+23	<		3.14E+23	<		7.02E+23	<	
PGC 009634	4.44E+22	8.24E+20	0.01	5.40E+22	1.06E+21	0.01	4.57E+22	1.28E+21	0.01	1.01E+23	1.11E+22	0.05	2.47E+23	1.48E+22	0.03	8.77E+23	3.51E+22	0.02	1.47E+24	1.17E+23	0.03
PGC 010665	5.12E+22	1.48E+21	0.01	4.90E+22	2.22E+21	0.02	4.40E+22	2.67E+21	0.03	9.53E+22	<		1.04E+23	<		6.97E+23	4.18E+22	0.03	1.87E+24	1.31E+23	0.03
PGC 010705	3.05E+22	5.66E+20	0.01	3.92E+22	8.03E+20	0.01	3.18E+22	8.33E+20	0.01	4.69E+22	1.22E+22	0.11	2.00E+23	1.60E+22	0.03	2.72E+24	1.09E+23	0.02	4.06E+24	1.62E+23	0.02
PGC 011104	3.10E+22	7.50E+20	0.01	3.72E+22	1.19E+21	0.01	3.12E+22	1.26E+21	0.02	6.73E+22	<		9.17E+22	<		1.07E+23	2.36E+22	0.10	3.41E+23	<	
PGC 012759	3.48E+22	9.10E+20	0.01	4.02E+22	1.32E+21	0.01	3.42E+22	1.22E+21	0.02	1.40E+23	1.82E+22	0.06	4.80E+23	1.92E+22	0.02	1.10E+24	4.39E+22	0.02	1.49E+24	1.64E+23	0.05
NGC 1386	7.40E+21	6.17E+19	0.004	8.73E+21	8.07E+19	0.004	7.17E+21	9.30E+19	0.01	8.92E+21	5.35E+20	0.03	2.59E+22	1.30E+21	0.02	1.07E+23	6.43E+20	0.00	1.75E+23	6.98E+21	0.02
PGC 014702	3.12E+22	4.60E+20	0.01	3.67E+22	6.48E+20	0.01	3.30E+22	7.72E+20	0.01	1.62E+23	9.72E+21	0.03	6.59E+23	3.30E+22	0.02	4.38E+24	1.75E+23	0.02	6.67E+24	2.67E+23	0.02
AM 0426-625	9.32E+21	<		9.66E+21	<		4.93E+20	<		2.94E+23	<		2.94E+23	<		2.94E+23	<		2.94E+23	<	
PGC 015172	5.52E+22	1.23E+21	0.01	7.16E+22	1.80E+21	0.01	6.50E+22	2.43E+21	0.02	4.92E+22	1.13E+22	0.10	1.17E+23	1.29E+22	0.05	1.11E+24	4.46E+22	0.02	2.13E+24	1.07E+23	0.02
NGC 1672	4.65E+22	9.13E+20	0.01	5.03E+22	1.17E+21	0.01	4.40E+22	1.23E+21	0.01	7.08E+22	2.83E+21	0.02	2.22E+23	1.33E+21	0.003	1.39E+24	5.58E+22	0.02	2.96E+24	1.18E+23	0.02
PGC 016072	2.63E+22	8.12E+20	0.01	3.27E+22	1.35E+21	0.02	2.30E+22	1.47E+21	0.03	1.51E+23	<		1.51E+23	<		1.51E+23	<		3.72E+23	<	
PGC 016357	3.46E+22	1.03E+21	0.01	4.97E+22	1.72E+21	0.02	4.67E+22	1.80E+21	0.02	1.49E+23	1.19E+22	0.03	3.21E+23	1.28E+22	0.02	4.87E+23	2.44E+22	0.02	1.49E+24	<	
NGC 1808	3.33E+22	5.26E+20	0.01	3.92E+22	6.57E+20	0.01	3.45E+22	6.73E+20	0.01	1.05E+23	4.22E+21	0.02	3.84E+23	1.54E+22	0.02	2.09E+24	8.36E+22	0.02	3.26E+24	1.31E+23	0.02
PGC 016873	5.47E+22	7.10E+20	0.01	6.45E+22	8.94E+20	0.01	5.38E+22	1.20E+21	0.01	3.58E+22	9.66E+21	0.12	9.93E+22	1.09E+22	0.05	3.49E+23	2.10E+22	0.03	8.13E+23	<	
PGC 017768	3.37E+22	1.04E+21	0.01	3.84E+22	1.44E+21	0.02	3.10E+22	1.81E+21	0.03	1.20E+23	<		1.58E+23	2.69E+22	0.07	2.73E+23	4.63E+22	0.07	1.04E+24	<	
LEDA 096373	1.14E+23	2.99E+21	0.01	1.62E+23	4.38E+21	0.01	1.45E+23	5.58E+21	0.02	5.73E+23	1.15E+23	0.09	1.68E+24	1.18E+23	0.03	2.97E+24	2.08E+23	0.03	5.84E+24	4.09E+23	0.03
PGC 021057	3.36E+22	6.56E+20	0.01	4.39E+22	8.97E+20	0.01	3.48E+22	1.11E+21	0.01	5.27E+22	4.74E+21	0.04	8.66E+22	6.93E+21	0.03	3.96E+23	1.98E+22	0.02	1.33E+24	9.34E+22	0.03
PGC 023573	2.25E+22	1.13E+21	0.02	2.68E+22	1.79E+21	0.03	2.51E+22	2.09E+21	0.04	1.94E+23	<		3.16E+23	4.42E+22	0.06	9.17E+23	9.17E+22	0.04	3.24E+24	5.18E+23	0.07
PGC 028144	1.52E+22	2.26E+20	0.01	1.96E+22	3.46E+20	0.01	1.89E+22	3.70E+20	0.01	4.82E+22	<		1.06E+23	<		3.93E+23	<		7.85E+23	<	
PGC 028147	9.99E+21	3.18E+20	0.01	1.44E+22	4.45E+20	0.01	8.34E+21	5.06E+20	0.03	7.96E+22	<		7.96E+22	<		2.99E+23	<		5.04E+23	<	
PGC 029778	4.76E+22	2.29E+21	0.02	6.04E+22	2.80E+21	0.02	5.32E+22	3.45E+21	0.03	3.37E+23	<		3.76E+23	5.64E+22	0.07	6.86E+23	8.91E+22	0.06	2.02E+24	<	
PGC 029993	4.39E+22	6.12E+20	0.01	5.42E+22	8.57E+20	0.01	4.57E+22	1.07E+21	0.01	6.10E+22	6.71E+21	0.05	1.94E+23	1.17E+22	0.03	6.68E+23	6.68E+22	0.04	1.26E+24	7.55E+22	0.03
PGC 030984	2.23E+22	1.27E+21	0.02	2.58E+22	1.79E+21	0.03	2.06E+22	2.07E+21	0.04	6.31E+22	1.26E+22	0.09	7.64E+22	1.45E+22	0.08	5.64E+23	3.95E+22	0.03	1.36E+24	1.50E+23	0.05
NGC 3281	7.43E+22	1.03E+21	0.01	9.07E+22	1.52E+21	0.01	7.85E+22	1.83E+21	0.01	2.20E+23	2.86E+22	0.06	6.52E+23	4.57E+22	0.03	1.70E+24	1.19E+23	0.03	1.86E+24	1.30E+23	0.03
LEDA 088648	5.65E+22	2.01E+21	0.02	7.65E+22	2.29E+21	0.01	6.41E+22	2.78E+21	0.02	1.56E+23	<		3.10E+23	<		1.07E+24	1.17E+23	0.05	2.49E+24	4.97E+23	0.09
NGC 4507	5.18E+22	7.17E+20	0.01	6.48E+22	9.63E+20	0.01	5.72E+22	1.17E+21	0.01	1.38E+23	1.38E+22	0.04	4.20E+23	4.20E+22	0.04	1.30E+24	9.13E+22	0.03	1.63E+24	1.96E+23	0.05
PGC 042504	2.48E+22	3.90E+20	0.01	2.87E+22	4.79E+20	0.01	2.54E+22	6.16E+20	0.01	1.69E+23	2.03E+22	0.05	5.95E+23	4.17E+22	0.03	1.98E+24	1.38E+23	0.03	2.82E+24	2.54E+23	0.04
WKK 1263	2.56E+22	2.37E+21	0.04	4.90E+22	3.08E+21	0.03	3.67E+22	3.32E+21	0.04	2.25E+23	<		2.25E+23	<		3.83E+23	<		1.55E+24	<	
PGC 043779	5.37E+22	9.52E+20	0.01	6.72E+22	1.12E+21	0.01	5.65E+22	1.53E+21	0.01	6.05E+22	1.57E+22	0.11	1.71E+23	2.22E+22	0.06	5.55E+23	5.55E+22	0.04	1.07E+24	2.14E+23	0.09
NGC 4785	7.40E+22	9.59E+20	0.01	9.65E+22	1.25E+21	0.01	8.18E+22	1.52E+21	0.01	1.01E+23	1.21E+22	0.05	1.58E+23	1.27E+22	0.03	1.19E+24	7.15E+22	0.03	3.43E+24	2.40E+23	0.03
PGC 044167	8.04E+21	7.12E+20	0.04	3.70E+22	1.21E+21	0.01	9.75E+21	1.06E+21	0.05	1.23E+23	<		1.23E+23	<		1.23E+23	<		5.64E+23	<	
NGC 4903	3.46E+22	1.96E+21	0.02	4.70E+22	2.44E+21	0.02	4.87E+22	3.20E+21	0.03	6.59E+22	<		1.70E+23	3.07E+22	0.08	4.56E+23	5.93E+22	0.06	1.42E+24	1.71E+23	0.05
NGC 4945	6.86E+22	1.02E+21	0.01	8.89E+22	1.40E+21	0.01	7.99E+22	1.26E+21	0.01	1.77E+23	2.65E+22	0.07	3.23E+23	4.85E+22	0.07	4.67E+24	9.34E+20	0.000	1.06E+25	1.59E+24	0.07
ESO 383- G 018	5.26E+21	2.52E+20	0.02	6.13E+21	3.31E+20	0.02	6.93E+21	4.12E+20	0.03	4.55E+22	9.56E+21	0.09	1.49E+23	1.19E+22	0.03	2.06E+23	1.86E+22	0.04	4.09E+23	<	
Circinus	2.27E+22	5.52E+20	0.01	3.29E+22	7.03E+20	0.01	3.01E+22	7.03E+20	0.01	8.37E+22	3.35E+21	0.02	3.05E+23	1.22E+22	0.02	1.11E+24	1.11E+23	0.04	1.41E+24	1.41E+23	0.04
LEDA 141858	1.62E+22	1.11E+21	0.03	1.85E+22	1.60E+21	0.04	1.85E+22	1.78E+21	0.04	1.66E+23	<		6.38E+23	3.83E+22	0.03	2.56E+24	1.28E+23	0.02	3.21E+24	<	
NGC 5643	3.21E+22	6.25E+20	0.01	3.62E+22	8.13E+20	0.01	3.10E+22	9.57E+20	0.01	3.75E+22	2.25E+21	0.03	1.25E+23	7.48E+21	0.03	6.66E+23	3.33E+22	0.02	1.30E+24	6.52E+22	0.02
PGC 052101	1.75E+22	1.20E+21	0.03	2.06E+22	1.46E+21	0.03	2.06E+22	2.41E+21	0.05	1.21E+23	<		3.76E+23	6.39E+22	0.07	1.18E+24	8.28E+22	0.03	1.53E+24	<	
LEDA 166339	2.60E+22	1.25E+21	0.02	3.59E+22	1.77E+21	0.02	3.79E+22	1.90E+21	0.02	2.38E+23	<		2.38E+23	<		2.38E+23	<		6.53E+23	<	
IC 4518	5.40E+20	<		1.24E+20	<		2.00E+20	<		1.86E+23	1.49E+22	0.03	7.07E+23	4.24E+22	0.03	4.11E+24	1.64E+23	0.02	6.89E+24	4.14E+23	0.03
WKK 3646	1.24E+21	<		4.68E+20	<		5.07E+20	<		8.60E+22	<		8.60E+22	<		8.60E+22	<		2.01E+23	<	
PGC 058547	6.25E+22	1.51E+21	0.01	7.08E+22	1.92E+21	0.01	6.01E+22	2.03E+21	0.01	5.25E+22	3.68E+21	0.03	1.35E+23	6.73E+21	0.02	4.12E+23	2.06E+22	0.02	3.73E+24	<	
PGC 059124	1.10E+22	3.39E+20	0.01	1.54E+22	4.31E+20	0.01	1.52E+22	4.56E+20	0.01	8.74E+22	7.00E+21	0.03	3.18E+23	2.55E+22	0.03	4.79E+23	4.79E+22	0.04	4.34E+23	<	
NGC 6221	4.91E+22	1.05E+21	0.01	6.29E+22	1.40E+21	0.01	5.08E+22	1.38E+21	0.01	8.03E+22	4.82E+21	0.03	2.83E+23	1.70E+22	0.03	2.64E+24	2.64E+21	0.04	4.63E+24	8.70E+21	0.001
NGC 6300	3.36E+22	5.31E+20	0.01	3.98E+22	7.05E+20	0.01	3.33E+22	6.16E+20	0.01	2.73E+22	1.64E+21	0.03	6.70E+22	3.35E+21	0.02	4.32E+23	2.16E+22	0.02	1.06E+24	7.44E+22	0.03
PGC 060594	5.69E+22	1.48E+21	0.01	6.33E+22	2.07E+21	0.01	5.53E+22	2.02E+21	0.02	7.72E+22	1.70E+22	0.10	1.10E+23	2.20E+22	0.09	4.16E+23	4.16E+22	0.04	1.02E+24	2.35E+23	0.10
PGC 062134	3.49E+22	6.16E+20	0.01	5.59E+22	9.38E+20	0.01	8.35E+22	1.16E+21	0.01	5.62E+23	3.93E+22	0.03	1.25E+24	7.49E+22	0.03	2.91E+24	1.45E+23	0.02	3.52E+24	3.17E+23	0.04
PGC 062174	1.72E+22	3.85E+20	0.01	2.20E+22	5.96E+20	0.01	1.90E+22	6.19E+20	0.01	2.35E+23	1.65E+22	0.03	9.09E+23	4.54E+22	0.02	8.90E+23	4.45E+22	0.02	4.05E+23	1.01E+23	0.11
PGC 062218	4.23E+22	1.71E+21	0.02	4.69E+22	2.57E+21	0.02	4.94E+22	2.47E+21	0.02	5.69E+22	1.02E+22	0.08	7.47E+22	1.94E+22	0.11	6.85E+23	4.11E+22	0.03	2.15E+24	1.51E+23	0.03
PGC 062428	2.58E+22	6.49E+20	0.01	3.11E+22	9.29E+20	0.01	2.90E+22	9.19E+20	0.01	1.16E+23	1.39E+22	0.05	3.81E+23	2.28E+22	0.03	2.19E+24	1.09E+23	0.02	4.07E+24	2.85E+23	0.03
PGC 062440	2.54E+22	9.28E+20	0.02	3.24E+22	1.40E+21	0.02	2.47E+22	1.38E+21	0.02	7.04E+22	<		1.09E+23	<		4.63E+23	4.17E+22	0.04	7.28E+23	1.60E+23	0.10
NGC 6810	4.73E+22	3.94E+20	0.004	6.51E+22	4.81E+20	0.003	5.61E+22	4.66E+20	0.00	1.09E+23	5.46E+21	0.02	3.46E+23	1.73E+22	0.02	1.77E+24	8.83E+22	0.02	3.42E+24	1.37E+23	0.02
PGC 063874	4.89E+22	8.67E+20	0.01	6.26E+22	1.52E+21	0.01	5.49E+22	1.54E+21	0.01	3.03E+23	4.84E+22	0.07	9.52E+23	9.52E+22	0.04	4.90E+24	2.94E+23	0.03	7.41E+24	6.67E+23	0.04
NGC 6890	2.27E+22	2.51E+20	0.005	2.72E+22	3.28E+20	0.01	2.29E+22	4.05E+20	0.01	4.82E+22	5.30E+21	0.05	9.21E+22	7.37E+21	0.03	5.43E+23	3.26E+22	0.03	1.15E+24	5.74E+22	0.02
PGC 064491	3.09E+22	7.48E+20	0.01	3.83E+22	1.22E+21	0.01	3.15E+22	1.18E+21	0.02	4.80E+22	1.20E+22	0.11	1.87E+23	1.68E+22	0.04	4.69E+23	3.28E+22	0.03	7.10E+23	1.14E+23	0.07
PGC 064537	2.18E+22	7.77E+20	0.02	2.62E+22	1.18E+21	0.02	2.19E+22	1.24E+21	0.02	1.05E+23	<		1.73E+23	<		6.13E+23	4.91E+22	0.03	1.06E+24	2.77E+23	0.11
PGC 065600	5.83E+22	7.56E+20	0.01	7.03E+22	1.04E+21	0.01	5.89E+22	1.09E+21	0.01	2.98E+23	3.57E+22	0.05	1.09E+24	5.46E+22	0.02	1.49E+24	1.49E+23	0.04	1.16E+24	9.31E+22	0.03
NGC 7130	7.37E+22	8.91E+20	0.01	8.97E+22	1.08E+21	0.01	8.00E+22	1.41E+21	0.01	3.36E+23	2.02E+22	0.03	1.21E+24	6.05E+22	0.02	9.55E+24	2.86E+22	0.001	1.46E+25	7.30E+23	0.02
NGC 7172	4.35E+22	7.67E+20	0.01	5.60E+22	1.09E+21	0.01	5.12E+22	1.10E+21	0.01	7.12E+22	5.70E+21	0.03	1.24E+23	8.68E+21	0.03	9.31E+23	5.58E+22	0.03	2.00E+24	1.00E+23	0.02
PGC 068122	1.17E+21	<		4.22E+19	<		1.36E+20	<		4.56E+22	<		6.93E+22	1.52E+22	0.10	4.38E+23	2.63E+22	0.03	8.81E+23	7.04E+22	0.03
PGC 068198	1.75E+22	1.62E+20	0.004	2.20E+22	3.06E+20	0.01	1.92E+22	2.66E+20	0.01	4.63E+22	6.49E+21	0.06	1.08E+23	7.54E+21	0.03	7.96E+23	3.98E+22	0.02	1.57E+24	7.87E+22	0.02
FAIRALL 0357	4.09E+22	1.03E+21	0.01	4.94E+22	1.48E+21	0.01	4.35E+22	1.97E+21	0.02	1.84E+23	<		1.50E+23	4.05E+22	0.12	1.24E+24	1.24E+23	0.04	2.86E+24	2.86E+23	0.04
PGC 070458	6.14E+22	1.43E+21	0.01	8.91E+22	2.50E+21	0.01	6.82E+22	2.50E+21	0.02	2.54E+23	5.59E+22	0.10	6.31E+23	8.20E+22	0.06	5.23E+24	4.18E+23	0.03	7.84E+24	5.49E+23	0.03
NGC 7496	1.66E+22	3.40E+20	0.01	1.94E+22	4.51E+20	0.01	1.50E+22	6.07E+20	0.02	2.26E+22	3.84E+21	0.07	1.04E+23	7.28E+21	0.03	5.49E+23	4.94E+22	0.04	1.01E+24	5.05E+22	0.02
NGC 7582	4.31E+22	6.78E+20	0.01	5.18E+22	8.69E+20	0.01	4.70E+22	9.16E+20	0.01	9.64E+22	5.78E+21	0.03	3.83E+23	1.91E+22	0.02	2.92E+24	1.75E+23	0.03	4.34E+24	3.04E+23	0.03
NGC 7590	1.79E+22	1.66E+20	0.004	2.03E+22	2.26E+20	0.005	1.72E+22	2.71E+20	0.01	3.35E+22	2.34E+21	0.03	4.95E+22	3.96E+21	0.03	4.11E+23	4.11E+22	0.04	1.41E+24	<	

Seyfert 1 - IR Luminosity Values by Band with Associated Errors (W/Hz)

Name	J	error δ	log(δ)	H	error δ	log(δ)	K	error δ	log(δ)
LEDA 087392	1.28E+22	7.75E+20	0.03	1.43E+22	1.23E+21	0.04	1.96E+22	1.21E+21	0.03
PGC 002450	5.22E+22	1.26E+21	0.01	6.81E+22	1.98E+21	0.01	7.86E+22	2.20E+21	0.01
PKS 0056-572	2.28E+20	<		5.69E+19	<		7.11E+19	<	
PGC 003864	4.47E+22	1.42E+21	0.01	4.97E+22	1.96E+21	0.02	5.45E+22	2.26E+21	0.02
IRAS 01089-4743	9.40E+21	<		8.47E+21	<		8.38E+20		0.00
PGC 004822	5.55E+22	1.82E+21	0.01	6.73E+22	3.17E+21	0.02	5.78E+22	3.12E+21	0.02
NGC 526A	2.93E+22	9.31E+20	0.01	4.49E+22	1.47E+21	0.01	3.58E+22	1.69E+21	0.02
PMN J0133-5159	3.52E+20	<		1.46E+21	<		4.84E+20	<	
ESO 080- G 005	1.99E+22	9.77E+20	0.02	2.94E+22	1.70E+21	0.03	2.12E+22	1.65E+21	0.03
NGC 1097	8.30E+22	1.70E+21	0.01	9.92E+22	2.31E+21	0.01	8.14E+22	2.60E+21	0.01
PGC 011706	3.20E+22	1.51E+21	0.02	4.34E+22	2.26E+21	0.02	3.24E+22	2.62E+21	0.04
NGC 1365	1.16E+23	2.80E+21	0.01	1.32E+23	3.82E+21	0.01	1.20E+23	4.05E+21	0.01
NGC 1566	6.84E+22	1.46E+21	0.01	7.22E+22	1.96E+21	0.01	6.35E+22	2.02E+21	0.01
PGC 017103	1.94E+22	3.44E+20	0.01	2.40E+22	4.69E+20	0.01	2.20E+22	6.78E+20	0.01
FAIRALL 0265	3.44E+22	1.13E+21	0.01	4.47E+22	1.81E+21	0.02	5.15E+22	1.98E+21	0.02
LEDA 096433	2.31E+22	6.91E+20	0.01	3.26E+22	8.20E+20	0.01	3.22E+22	9.60E+20	0.01
PGC 027468	6.41E+21	2.70E+20	0.02	8.21E+21	3.32E+20	0.02	7.04E+21	3.65E+20	0.02
PGC 029148	4.49E+22	1.04E+21	0.01	5.50E+22	1.59E+21	0.01	4.61E+22	1.86E+21	0.02
PGC 029151	2.99E+22	1.07E+21	0.02	3.43E+22	1.51E+21	0.02	2.89E+22	1.86E+21	0.03
PGC 033084	1.70E+22	1.47E+21	0.04	2.27E+22	1.99E+21	0.04	2.34E+22	2.00E+21	0.04
PGC 034101	1.55E+22	1.60E+21	0.04	1.72E+22	2.30E+21	0.06	1.43E+22	2.22E+21	0.07
PGC 036002	5.46E+22	1.63E+21	0.01	7.15E+22	2.41E+21	0.01	6.27E+22	2.48E+21	0.02
NGC 3783	3.81E+22	4.96E+20	0.01	4.84E+22	7.18E+20	0.01	4.74E+22	8.82E+20	0.01
LEDA 096527	2.40E+21	<		5.96E+20	<		8.51E+20	<	
PGC 045371	6.46E+22	1.02E+21	0.01	9.12E+22	1.36E+21	0.01	9.91E+22	1.56E+21	0.01
PGC 047969	9.26E+21	1.12E+20	0.01	1.22E+22	1.81E+20	0.01	1.27E+22	2.01E+20	0.01
PGC 049051	7.23E+22	1.68E+21	0.01	9.66E+22	2.33E+21	0.01	1.13E+23	1.36E+21	0.01
PGC 050427	6.29E+21	3.88E+20	0.03	7.65E+21	5.70E+20	0.03	8.82E+21	7.10E+20	0.03
ESO 328- G036	6.09E+20	<		3.11E+20	<		2.86E+20	<	
PKS 1521-300	2.36E+22	6.39E+20	0.01	3.13E+22	1.02E+21	0.01	2.43E+22	1.06E+21	0.02
LEDA 2793282	2.24E+22	1.45E+21	0.03	1.21E+22	2.35E+20	0.01	2.85E+22	1.62E+21	0.02
PGC 062346	2.32E+22	4.73E+20	0.01	3.08E+22	6.57E+20	0.01	3.81E+22	7.09E+20	0.01
PGC 062554	8.15E+22	2.75E+21	0.01	1.11E+23	4.24E+21	0.02	9.08E+22	4.28E+21	0.02
ESO 399-IG 020	7.31E+20	<		1.38E+20	<		6.62E+20	<	
NGC 6860	4.45E+22	5.76E+20	0.01	5.71E+22	9.58E+20	0.01	5.66E+22	1.10E+21	0.01
PGC 064989	3.66E+22	6.12E+20	0.01	4.52E+22	1.09E+21	0.01	4.15E+22	1.17E+21	0.01
ESO 235- G 059	5.13E+22	1.10E+21	0.01	6.38E+22	1.73E+21	0.01	5.97E+22	1.61E+21	0.01
CTS 0109	1.09E+22	<		1.39E+22	<		2.01E+22	<	
PGC 067075	1.94E+22	4.70E+20	0.01	2.36E+22	6.38E+20	0.01	1.78E+22	7.51E+20	0.02
NGC 7213	7.65E+22	6.34E+20	0.00	8.68E+22	8.83E+20	0.004	7.51E+22	1.12E+21	0.01
[VV2003c] J224704.9-	3.69E+19	<		5.65E+19	<		4.99E+19	<	
PGC 073028	4.51E+20	<		6.56E+20	<		3.49E+20	<	

Name	12 μm	error δ	log(δ)	25 μm	error δ	log(δ)	60 μm	error δ	log(δ)	100 μm	error δ	log(δ)
LEDA 087392	6.97E+22	<		1.21E+23	<		2.16E+23	<		5.54E+23	<	
PGC 002450	3.36E+23	3.69E+22	0.0477	5.10E+23	3.57E+22	0.0304	2.93E+24	1.17E+23	0.0174	6.01E+24	3.61E+23	0.03
PKS 0056-572	1.64E+23	<		1.64E+23	<		1.64E+23	<		2.20E+23	<	
PGC 003864	2.49E+23	5.23E+22	0.0911	4.12E+23	6.18E+22	0.0651	2.16E+24	2.37E+23	0.0477	3.50E+24	3.85E+23	0.05
IRAS 01089-4743	1.74E+23	3.13E+22	0.0781	2.29E+23	3.21E+22	0.0608	1.25E+24	8.77E+22	0.0304	2.88E+24	2.59E+23	0.04
PGC 004822	1.08E+23	<		1.36E+23	3.55E+22	0.1128	6.57E+23	1.45E+23	0.0955	1.70E+24	2.03E+23	0.05
NGC 526A	1.97E+23	2.36E+22	0.0521	4.16E+23	9.57E+22	0.0998	3.21E+23	<		8.03E+23	<	
PMN J0133-5159	1.15E+23	<		1.15E+23	<		1.15E+22	<		5.11E+23	<	
ESO 080- G 005	2.10E+23	<		2.10E+23	<		2.42E+23	<		3.07E+23	<	
NGC 1097	7.68E+22	3.07E+21	0.0174	2.14E+23	1.07E+22	0.0217	1.73E+24	8.63E+22	0.0217	3.31E+24	1.32E+23	0.02
PGC 011706	1.92E+23	<		1.92E+23	<		1.92E+23	<		4.20E+23	<	
NGC 1365	2.15E+23	8.61E+21	0.0174	6.91E+23	3.45E+22	0.0217	4.86E+24	2.92E+23	0.026	9.10E+24	3.64E+23	0.02
NGC 1566	4.51E+22	3.16E+21	0.0304	6.62E+22	3.97E+21	0.026	7.99E+23	3.99E+22	0.0217	2.52E+24	1.01E+23	0.02
PGC 017103	7.55E+22	1.43E+22	0.0825	1.92E+23	1.15E+22	0.026	4.71E+23	3.30E+22	0.0304	6.72E+23	5.38E+22	0.03
FAIRALL 0265	1.53E+23	3.37E+22	0.0955	3.95E+23	3.56E+22	0.0391	1.31E+24	9.16E+22	0.0304	2.26E+24	4.07E+23	0.08
LEDA 096433	1.40E+23	<		9.21E+22	1.66E+22	0.0781	7.24E+23	7.24E+22	0.0434	2.00E+24	2.40E+23	0.05
PGC 027468	3.49E+22	<		6.06E+22	<		1.08E+23	<		2.78E+23	<	
PGC 029148	8.63E+22	<		8.63E+22	<		8.63E+22	<		8.63E+22	<	
PGC 029151	1.74E+23	<		1.74E+23	<		1.74E+23	<		4.71E+23	<	
PGC 033084	2.55E+23	<		1.99E+23	<		2.73E+23	2.73E+22	0.0434	6.84E+24	<	
PGC 034101	2.65E+22	7.41E+21	0.1215	5.05E+22	9.09E+21	0.0781	2.07E+23	2.89E+22	0.0608	6.06E+23	7.88E+22	0.06
PGC 036002	8.97E+22	1.43E+22	0.0694	1.48E+23	1.48E+22	0.0434	8.43E+23	5.06E+22	0.026	2.67E+24	2.93E+23	0.05
NGC 3783	1.72E+23	1.21E+22	0.0304	5.11E+23	3.07E+22	0.026	6.68E+23	4.01E+22	0.026	1.00E+24	1.11E+23	0.05
LEDA 096527	1.97E+23	3.94E+22	0.0868	5.55E+23	4.44E+22	0.0347	1.97E+24	1.18E+23	0.026	3.11E+24	5.91E+23	0.08
PGC 045371	3.37E+23	2.02E+22	0.026	6.02E+23	3.61E+22	0.026	2.79E+24	1.40E+23	0.0217	4.33E+24	2.60E+23	0.03
PGC 047969	4.93E+22	4.43E+21	0.0391	1.05E+23	7.33E+21	0.0304	1.41E+23	9.85E+21	0.0304	1.42E+23	2.84E+22	0.09
PGC 049051	6.11E+23	3.06E+22	0.0217	1.25E+24	6.25E+22	0.0217	1.15E+24	5.73E+22	0.0217	9.38E+23	1.22E+23	0.06
PGC 050427	2.21E+23	<		2.21E+23	<		2.21E+23	<		6.88E+23	<	
ESO 328- G036	2.11E+23	<		2.11E+23	<		2.11E+23	<		6.96E+23	<	
PKS 1521-300	7.60E+22	<		7.60E+22	<		7.60E+22	<		1.10E+23	<	
LEDA 2793282	7.47E+22	<		7.47E+22	<		7.47E+22	<		4.81E+23	<	
PGC 062346	2.05E+23	<		4.53E+23	2.27E+22	0.0217	8.08E+23	6.46E+22	0.0347	1.20E+24	2.05E+23	0.07
PGC 062554	1.27E+23	3.54E+22	0.1215	1.69E+23	3.39E+22	0.0868	6.02E+23	8.43E+22	0.0608	4.33E+24	<	
ESO 399-IG 020	1.58E+23	4.42E+22	0.1215	2.30E+23	5.75E+22	0.1085	7.48E+23	7.48E+22	0.0434	2.04E+24	<	
NGC 6860	1.16E+23	1.39E+22	0.0521	1.61E+23	1.61E+22	0.0434	4.62E+23	3.69E+22	0.0347	1.19E+24	1.08E+23	0.04
PGC 064989	7.16E+22	<		8.32E+22	<		2.81E+23	5.33E+22	0.0825	1.17E+24	3.28E+23	0.12
ESO 235- G 059	1.45E+23	<		9.70E+22	<		5.45E+23	8.17E+22	0.0651	1.12E+24	2.45E+23	0.10
CTS 0109	1.91E+23	<		1.91E+23	<		3.45E+23	<		1.28E+24	<	
PGC 067075	6.89E+22	<		6.89E+22	<		6.89E+22	<		1.07E+23	<	
NGC 7213	4.46E+22	3.57E+21	0.0347	5.46E+22	3.28E+21	0.026	1.96E+23	1.18E+22	0.026	6.02E+23	3.01E+22	0.02
[VV2003c] J224704.9-	1.52E+22	<		1.52E+22	<		1.52E+22	<		1.30E+22	<	
PGC 073028	3.30E+23	<		2.46E+23	8.86E+22	0.1562	7.10E+23	9.94E+22	0.0608	1.91E+24	4.01E+23	0.09